

## INFORMATION TO USERS

This manuscript has been reproduced from the microfilm master. UMI films the text directly from the original or copy submitted. Thus, some thesis and dissertation copies are in typewriter face, while others may be from any type of computer printer.

**The quality of this reproduction is dependent upon the quality of the copy submitted.** Broken or indistinct print, colored or poor quality illustrations and photographs, print bleedthrough, substandard margins, and improper alignment can adversely affect reproduction.

In the unlikely event that the author did not send UMI a complete manuscript and there are missing pages, these will be noted. Also, if unauthorized copyright material had to be removed, a note will indicate the deletion.

Oversize materials (e.g., maps, drawings, charts) are reproduced by sectioning the original, beginning at the upper left-hand corner and continuing from left to right in equal sections with small overlaps.

ProQuest Information and Learning  
300 North Zeeb Road, Ann Arbor, MI 48106-1346 USA  
800-521-0600

UMI<sup>®</sup>



**Theoretical, Experimental and Numerical Investigation  
of Flow and Solute Transport in Saturated Porous Media  
Subjected to Violation to the Continuum Hypothesis**

**By**

**Amgad Salama**

**A Thesis presented to the Faculty of Graduate Studies and Research in  
partial fulfillment of the requirements for the degree  
Of Doctor of Philosophy in Engineering\*  
Department of Environmental Engineering  
Carleton University  
Ottawa, Ontario  
Canada**

**May 2005**

**\* The Doctor of Philosophy in Engineering Program is a joint program  
with the University of Ottawa administered by the Ottawa-Carleton  
Institute for Environmental Engineering**

**© Amgad Salama, May 2005**



Library and  
Archives Canada

Bibliothèque et  
Archives Canada

Published Heritage  
Branch

Direction du  
Patrimoine de l'édition

0-494-08348-4

395 Wellington Street  
Ottawa ON K1A 0N4  
Canada

395, rue Wellington  
Ottawa ON K1A 0N4  
Canada

*Your file* *Votre référence*

*ISBN:*

*Our file* *Notre référence*

*ISBN:*

**NOTICE:**

The author has granted a non-exclusive license allowing Library and Archives Canada to reproduce, publish, archive, preserve, conserve, communicate to the public by telecommunication or on the Internet, loan, distribute and sell theses worldwide, for commercial or non-commercial purposes, in microform, paper, electronic and/or any other formats.

The author retains copyright ownership and moral rights in this thesis. Neither the thesis nor substantial extracts from it may be printed or otherwise reproduced without the author's permission.

**AVIS:**

L'auteur a accordé une licence non exclusive permettant à la Bibliothèque et Archives Canada de reproduire, publier, archiver, sauvegarder, conserver, transmettre au public par télécommunication ou par l'Internet, prêter, distribuer et vendre des thèses partout dans le monde, à des fins commerciales ou autres, sur support microforme, papier, électronique et/ou autres formats.

L'auteur conserve la propriété du droit d'auteur et des droits moraux qui protègent cette thèse. Ni la thèse ni des extraits substantiels de celle-ci ne doivent être imprimés ou autrement reproduits sans son autorisation.

---

In compliance with the Canadian Privacy Act some supporting forms may have been removed from this thesis.

Conformément à la loi canadienne sur la protection de la vie privée, quelques formulaires secondaires ont été enlevés de cette thèse.

While these forms may be included in the document page count, their removal does not represent any loss of content from the thesis.

Bien que ces formulaires aient inclus dans la pagination, il n'y aura aucun contenu manquant.

  
**Canada**

## ABSTRACT

The partial differential equations typically used to solve flow and solute transport in porous media are based on the continuum approach for which the pores and soil grains are replaced by a continuum with averaged macroscopic parameters. However, in order to validate the use of the continuum approach over the domain of interest certain length scale constraints need to be satisfied. Three main criteria for length scale constraints were defined in the literature. Justification for the third length scale constraint was further defined in this work as a requirement for proper averaging rather than a consequence of certain mathematical manipulations.

In cases when these length scale constraints are not satisfied, the continuum approach may not be adapted and other sophisticated approaches need to be devised. This work attempts to experimentally shed light on the behavior of such systems and show how this violation impacts our ability to simulate such systems.

The motive for this work arose when modeling the pervious surround concept at uranium Tailings Management Facilities (TMF) in Northern Saskatchewan, Canada. The pervious surround concept provides a path of low resistance so that groundwater will move around rather than through the tailings. Typically, the pervious surround is a 1 m thick permeable layer constructed with crushed rock with grain sizes of up to 20 cm. Thus, the length scale constraints

may not be satisfied in this region and hence the use of traditional groundwater flow and solute transport equations questioned.

A parametric study was conducted to highlight the influence of the pervious surround parameters on the performance of this system. This study demonstrated the impact of the permeability contrast on the effectiveness of the pervious surround and the impact of the sand layer between the surround and tailings on the downgradient concentrations and mass flux.

An experimental study was conducted to illustrate the impact of violating the length scale constraints on model simulations through a comparison of experimental and simulation data. The study demonstrated that there are indeed differences between measurements and simulations based on the assumption of the validity of the continuum hypothesis in this system. The condition of the interface between the different zones was shown to significantly impact the comparisons. Unfortunately, the condition of the interface is case dependent and hence no sharp conclusion may be drawn on its influence. However, the experimental work indicated that the downgradient peak concentrations were not significantly different from simulation, which will certainly help for design and licensing purposes.

## ACKNOWLEDGMENTS

I would like first to express my sincere gratitude and deep thanks to ALLAH SWT, the lord of the universe, the creator, the almighty for supporting me with help and patience to complete this work.

Secondly my deepest appreciations and great thanks go to my parents who spent every precious thing they have for the education and welfare of their children.

I have been very fortunate to have the guidance of my advisor and friend, Paul Van Geel. Words cannot describe how beneficial Paul's mentorship has been over the last four years. I thank him for his interest, effort, and enthusiasm with respect to my life and research.

I would also like to thank all the staff of the civil engineering laboratory here at Carleton University, particularly Pierre Trudel, for their help and patience during the course of this research.

My deep thanks and appreciations also go to the Canadian Nuclear Safety Commission, CNSC, for providing this project with all sorts of financial support.

I would also like to acknowledge with appreciation Carleton University and the Department of Civil and Environmental Engineering for providing me with all kind of help and financial support.

Many thanks also go to my family for their patience and continual support.

## **DEDICATION**

To the soul of my father and grandmother  
May ALLAH SWT forgive them and grant them paradise...Ameen

To my mother for her endless love and concern.

To my brother, sisters and their children for their sincere love.

To my wife and great children.

# TABLE OF CONTENTS

<b>ABSTRACT</b> .....	i
<b>ACKNOWLEDGMENTS</b> .....	iii
<b>DEDICATION</b> .....	iv
<b>TABLE OF CONTENTS</b> .....	v
<b>LIST OF FIGURES</b> .....	xi
<b>CHAPTER 1: INTRODUCTION</b> .....	1
1. General.....	1
1.1 Power, Progress and the Environment.....	1
1.2 Nuclear Fuel. ....	3
1.2.1 Uranium mines.....	4
1.3 Milling of the Ore and the Hazardous Potential of its Wastes.....	6
1.3.1 Uranium waste deposits.....	7
1.3.2 Concepts for tailings disposal.....	10
1.4 Uranium Mining in Northern Saskatchewan.....	11
1.5 Uranium Mine Tailings Disposal in Northern Saskatchewan.....	12
1.5.1 General.....	12
1.5.2 Tailings management facility in northern Saskatchewan.....	13
1.5.3 Performance Criteria.....	17
1.6 Simulation of this System.....	19
1.6.1 Problems related to the simulation of this system.....	20
1.7 Objectives.....	21



3.3.1 Historical background.....	93
3.3.2 Approaches applied to derive Darcy's law.....	98
3.3.2.1 The method of geometric modeling.....	98
3.3.2.2 Statistical methods.....	99
3.3.2.3 Method of homogenization. ....	99
3.3.2.4 Method of local volume averaging.....	101
3.3.2.4.1 History of the development of the method of volume averaging.....	101
3.4 Elements of the Theory of Volume Averaging.....	104
3.4.1 Transport partial differential equations.....	104
3.4.2 Averaging processes.....	106
3.5 Proper Averaging Processes and Length Scale Constraints.....	110
3.5.1 General.....	110
3.5.2 The choice of an averaging volume.....	112
3.6 On the Length Scale Constraints in Porous Media.....	116
3.6.1 Length scale constraints due to the heterogeneity of porous media.....	117
3.6.2 A new requirement.....	118
3.6.3 Length scale constraints arising during averaging processes..	121
3.8 Problems Associated with the Interface Boundary.....	128
3.8.1 The interface between a porous medium and a fluid body.....	130
3.8.1.1 The Beavers and Joseph boundary condition.....	130
3.8.1.2 Volume averaging techniques as applied to momentum transfer at the boundary between a porous medium and a homogeneous fluid.....	132

3.8.2 The interface between a porous medium and a solid surface..	135
3.8.3 The interface between a porous medium and another porous medium. ....	137
3.9 Conclusions.....	146
3.10 Length Scale Constraints as Applied to the Pervious Surround Concept.....	148
<b>CHAPTER 4: METHODOLOGY</b> .....	158
4.1 General.....	158
4.2 Methodology.....	159
<b>CHAPTER 5: EXPERIMENTAL WORK</b> .....	165
5.1 Macroscopic Porous Media Properties Measurements.....	165
5.2 Containers and constant-head reservoirs.....	165
5.3 Material testing and Emplacement.....	166
5.3.1 Sand.....	166
5.3.2 Gravel.....	174
5.4 Sand-Gravel System.....	179
5.4.1 Instrumentation.....	180
5.4.2 Water supply and flow rate measurements.....	181
5.4.3 Experiment operation.....	181
<b>CHAPTER 6: NUMERICAL INVESTIGATIONS OF THE EXPERIMENTAL     WORK</b> .....	201
6.1 General.....	201
6.2 Numerical Difficulties.....	202
6.2.1 Hyperbolic first-order equations.....	204

6.2.2 Propagation of discontinuities in first order equations.....	205
6.3 Discontinuities and Numerical Methods.....	206
6.3.1 Discontinuities and finite difference methods.....	206
6.4 Modified Equations and Consistency.....	208
6.5 Stability.....	211
6.6 The CFL Condition.....	213
6.7 Experimental Results and Numerical Simulations.....	214
6.7.1 The base scenario (gravel width 50 cm).....	215
6.7.1.1 Hydraulic heads.....	216
6.7.1.2 Solute transport.....	216
6.7.2 The 30 cm scenario.....	217
6.7.2.1 Hydraulic heads.....	217
6.7.2.2 Solute transport.....	218
6.7.3 The 20 cm scenario.....	220
6.7.3.1 Hydraulic heads.....	220
6.7.3.2 Solute transport.....	221
6.7.4 The 15 cm scenario.....	222
6.7.4.1 Hydraulic heads.....	223
6.7.4.2 Solute transport.....	223
6.7.5 The 10 cm scenario.....	225
6.7.5.1 Hydraulic heads.....	225
6.7.5.2 Solute transport.....	225
6.7.6 The 5 cm scenario.....	227

6.7.6.1 Hydraulic heads.....	227
6.7.6.2 Solute transport.....	228
6.8 Summary of the Main Findings out of the Experimental Work.....	228
6.9 Implications on the TMF in Northern Saskatchewan.....	233
<b>CHAPTER 7: CONCLUSIONS.....</b>	<b>298</b>
7.1 On the Parametric Study.....	298
7.2 On the Continuum Hypothesis.....	299
7.2.1 Conclusions related to the TMFs in Northern Saskatchewan.	304
7.3 Contributions.....	306
<b>CHAPTER 8: RECOMMENDATIONS FOR FUTURE WORK.....</b>	<b>309</b>
<b>APPENDIX A.....</b>	<b>311</b>
<b>APPENDIX B.....</b>	<b>326</b>
<b>REFERENCES.....</b>	<b>341</b>

## LIST OF FIGURES

Fig. 1.1 Projected world primary energy demand (World Energy Outlook 1998).....	24
Fig. 1.2 Uranium production and reactor-related requirements (Nuclear Energy Agency 2001).....	25
Fig.1.3 Uranium pit mine at Rabbit Lake, Saskatchewan, Canada.....	26
Fig. 1.4 Locations of northern Saskatchewan in-pit tailings management facilities, from West (2000).....	27
Fig.1.5 Conceptualization of three northern Saskatchewan tailings management facilities, from West (2000).....	28
Fig. 1.5 Schematic of the operational and the post decommissioning phases, from West (2000).....	29
Fig. 2.1 The 2D Conceptual Model.....	59
Fig. 2.2 Initial concentration at the sand-tailings interface for a one-dimensional element.....	60
Fig. 2.3 Two blocks in the pervious surround.....	60
Fig. 2.4 Eight blocks in the pervious surround.....	60
Fig. 2.5 Sixteen block in the pervious surround.....	60
Fig. 2.6 Concentration history at the point (700, 500) for different discretization scenarios.....	61
Fig. 2.7 Comparisons of the mass remaining and the rate of solute mass leaving the domain for different discretization scenarios.....	62
Fig. 2.8 Flow nets for the scenario E-8-4-2-5.....	63
Fig. 2.9 Flow nets for the scenario E-8-4-2.25-5.....	63
Fig. 2.10 Flow nets for the scenario E-8-4-2.5-5.....	63
Fig. 2.11 Flow nets for the scenario E-8-4-2.75-5.....	63

Fig. 2.12 Flow nets for the scenario E-8-4-3-5.....	64
Fig. 2.13 Flow nets for the scenario E-8-4-4-5.....	64
Fig. 2.14 Flow lines through the sand layer for the scenario E-8-4-2-5.....	64
Fig. 2.15 Flow lines through the sand layer for the scenario E-8-4-2.5-5....	64
Fig. 2.16 Flow lines through the sand layer for the scenario E-8-4-3-5.....	65
Fig. 2.17 Flow lines through the sand layer for the scenario E-8-4-4-5.....	65
Fig. 2.18 Hydraulic head profiles across the TMF for all the scenarios.....	66
Fig. 2.19 X-component velocity profiles for the different scenarios at the plan x=450, a closer look.....	67
Fig. 2.20 Concentration profiles for the E-8-4-2-5 scenario at the plan y=500.....	68
Fig. 2.21 Concentration profiles for the E-8-4-2-5 scenario at the plan x=450.....	68
Fig. 2.22 Concentration profiles for the E-8-4-3-5 scenario at the plan y=500.....	68
Fig. 2.23 Concentration profiles for the E-8-4-3-5 scenario at the plan x=450.....	68
Fig. 2.24 Concentration profiles for the E-8-4-4-5 scenario at the plan y=500.....	69
Fig. 2.25 Concentration profiles for the E-8-4-4-5 scenario at the plan x=450.....	69
Fig. 2.26 Comparison of concentration profiles for all the scenarios at the plan y=500 after 6342 years.....	69
Fig. 2.27 Comparison of concentration profiles for all the scenarios at the plan y=500 after 31710 years.....	69
Fig. 2.28 Concentration profiles at the plane y=500 after 95129 years for the different scenarios.....	70
Fig. 2.29 Concentration history at the point (700, 500) for the different scenarios.....	70

Fig. 2.30 Mass remaining in the domain for the different scenarios.....	71
Fig. 2.31 Concentration history at the point (700, 500) for different dispersivity scenarios.....	72
Fig. 2.32 Flow nets for the scenario E-8-4-2-5.....	73
Fig. 2.33 Flow nets for the scenario E-8-5-2-5.....	73
Fig. 2.34 Flow nets for the scenario E-8-6-2-5.....	73
Fig. 2.35 Flow nets for the scenario E-8-7-2-5.....	73
Fig. 2.36 Flow nets for the scenario E-8-8-2-5.....	74
Fig. 2.37 Behavior of flow lines that cross the tailings as they release to the sand for the scenario E-8-4-2-5, a closer look.....	74
Fig. 2.38 Behavior of flow lines that cross the tailings as they release to the sand for the scenario E-8-5-2-5, a closer look.....	74
Fig. 2.39 Behavior of flow lines that cross the tailings as they release to the sand for the scenario E-8-6-2-5, a closer look.....	74
Fig. 2.40 Behaviour of flow lines that cross the tailings as they release to the sand for the scenario E-8-7-2-5, a closer look.....	75
Fig. 2.41 Behaviour of flow lines that cross the tailings as they release to the sand for the scenario E-8-8-2-5, a closer look.....	75
Fig. 2.42 Flow lines at the top of the tailings for different hydraulic conductivity of the sand.....	76
Fig. 2.43 Hydraulic head profiles for the different scenarios at the plane $y=500$ .....	77
Fig. 2.44 X-component velocity profiles at the plane $x=450$ for the different hydraulic conductivity of the sand.....	77
Fig. 2.45 Concentration profiles for the scenario E-8-5-2-5 at the plane $y=500$ .....	78
Fig. 2.46 Concentration profiles for the scenario E-8-6-2-5 at the plane $y=500$ .....	78
Fig. 2.47 Concentration profiles for the scenario E-8-7-2-5 at the plane	

y=500.....	78
Fig. 2.48 Concentration profiles for the scenario E-8-8-2-5 at the plane y=500.....	78
Fig. 2.49 Comparison of concentration profiles for the different scenarios at the plane y=500.....	79
Fig. 2.50 Comparison of concentration profiles for the scenarios E-8-4-2-5 and E-8-8-2-5 at the plane y=500.....	79
Fig. 2.51 Comparison of concentration profiles for the different scenarios at the plane x=450 after 951 years.....	79
Fig.2.52 Comparison of concentration profiles for the different scenarios at the plane x=450 after 12684 years.....	79
Fig. 2.53 Concentration history for the different scenarios at the point (700, 500).....	80
Fig. 2.54 The rate of leaving for the scenarios E-8-4-2-5 and E-8-8-2-5 on a linear scale.....	80
Fig. 2.55 Mass remaining and the solute mass flow rate leaving the boundary for the different scenarios.....	81
Fig. 2.56 Concentration profiles at the plane y=500 for the scenario E-8-4-2-5 with the sand layer initial concentration $0.25 \text{ kg/m}^3$ .....	82
Fig.2.57 Concentration profiles at the plane y=500 for the scenario E-8-4-2-5 with the sand layer initial concentration $0.5 \text{ kg/m}^3$ .....	82
Fig.2.58 Concentration profiles at the plane y=500 for the scenario E-8-4-2-5 with the sand layer initial concentration $1.0 \text{ kg/m}^3$ .....	82
Fig. 2.59 Comparisons of concentration profiles for different sand initial concentration at the plane y=500 after 951 year.....	83
Fig. 2.60 Concentration profiles for the scenario E-8-4-2-5 with the sand initial concentration of $0.25 \text{ kg/m}^3$ at the plane x=450.....	83
Fig. 2.61 Concentration profiles for the scenario E-8-4-2-5 with the sand initial concentration of $0.5 \text{ kg/m}^3$ at the plane x=450.....	83
Fig. 2.62 Concentration profiles for the scenario E-8-4-2-5 with the sand initial concentration of $1.0 \text{ kg/m}^3$ at the plane x=450.....	84

Fig. 2.63 Comparison of concentration profiles for the different scenarios after 63 year at the plane $x=450$ .....	84
Fig. 2.64 Concentration history for different solute initial concentration in the sand at the point (700, 500).....	84
Fig. 2.65 Mass remaining and solute mass flow rate leaving the boundary for the different scenarios.....	85
Fig. 2.66 Concentration history for different solute initial concentration in the sand at the point (700, 500).....	86
Fig. 2.67 Mass remaining and solute mass flow rate leaving the boundary for the different scenarios.....	86
Fig.3.1 Homogenization limit.....	150
Fig.3.2 Representative region of a porous medium domain.....	150
Fig.3.3 One-dimensional presentation of piece wise continuous function (indicator function).....	151
Fig. 3.4 Selecting an REV.....	151
Fig. 3.5 Fluid-solid system.....	152
Fig. 3.6 Larger scale description.....	152
Fig. 3.7 Schematic of material viewed on different scales of observation (from Cushman). ....	153
Fig. 3.8 Porosity variations at the interface region due to averaging process.....	154
Fig. 3.9 Fluctuations in local porosity in the vicinity of a confining wall.....	154
Fig. 3.10 Interface boundary between a porous layer and a liquid body.....	155
Fig. 3.11 Averaging volume at the interface boundary.....	155
Fig. 3.12 Jump condition at the interface between porous medium and homogeneous fluid.....	156
Fig. 3.13 Simple and nonsimple interfaces.....	157

Fig. 3.14 Averaging volume for a nonsimple interface.....	157
Fig. 4.1 Schematic of the proposed experimental set up.....	164
Fig. 5.1 Schematic of the steel boxes.....	183
Fig. 5.2 Schematic of sand experiment.....	184
Fig. 5.3 Effect of lowering upgradient reservoir water level on plume arrival time.....	185
Fig 5.4 Injection and measuring ports in the instantaneous point source experiment in sand.....	186
Fig. 5.5 Instantaneous point source experiments in sand, set up #1.....	187
Fig. 5.6 Instantaneous point source experiments in sand, set up #2.....	188
Fig. 5.7 Concentration measurements at level "0", 117 cm downstream from the well, point B.....	189
Fig. 5.8 Concentration measurements at level "0", 117 cm downstream from the well, points A,B,C.....	190
Fig. 5.9 Concentration measurements at level "-1", 117 cm downstream from the well.....	191
Fig. 5.10 Comparison of measured and numerically calculated line source experiments.....	192
Fig. 5.11 Hydraulic conductivity estimation for the gravel.....	193
Fig. 5.12 Tracer test in gravel, #1.....	194
Fig. 5.13 Tracer test in gravel, #2.....	195
Fig. 5.14 Schematic of Mariot bottle set up.....	196
Fig. 5.15 Dye flow restriction for the continuous point source experiment.....	197
Fig. 5.16 Continuous point source analytical solution.....	198
Fig. 5.17 Concentration contours at the measuring ports.....	198
Fig. 5.18 3-D schematic of the sand-gravel system.....	199

Fig. 5.19 Location of the manometers.....	200
Fig. 6.1 Propagation of discontinuity along characteristics.....	238
Fig. 6.2 Illustration of CFL criterion.....	238
Fig. 6.3 Comparison of simulated concentration history downgradient using different numerical techniques.....	239
Fig. 6.4 Deactivated region for solute transport for numerical runs.....	240
Fig. 6.5 Hydraulic heads distribution for the 50 cm sand-gravel system.....	241
Fig. 6.6 Simulated flow lines for the 50 cm sand-gravel system.....	242
Fig. 6.7 Plume contours for the 50 cm sand-gravel system after 15 hrs.....	243
Fig. 6.8 Plume contours for the 50 cm sand-gravel system after 20 hrs.....	244
Fig. 6.9 Plume contours for the 50 cm sand-gravel system after 25 hrs.....	245
Fig. 6.10 Simulated concentration profiles with time at different measuring points for the 50 cm sand-gravel system.....	246
Fig. 6.11 Concentration profiles with time at different measuring points with the simulated at the center for the 50 cm sand-gravel system.....	247
Fig. 6.12 Transverse concentration profile shows the plume is sifted to the left for the 50 cm sand-gravel system.....	248
Fig. 6.13 Transverse concentration profile with plume adjusted to the center for the 50 cm sand-gravel system. ....	248
Fig. 6.14 Comparison of measured and simulated transverse concentration profile after 27.9 hours for the 50 cm sand-gravel system.....	249
Fig. 6.15 Comparison of measured and simulated transverse concentration profile after 29.2 hours for the 50 cm sand-gravel system.....	249
Fig. 6.16 Comparison of measured and simulated transverse concentration profile after 31.5 hours for the 50 cm sand-gravel system.....	250
Fig. 6.17 Comparison of measured and simulated transverse concentration profile after 33.3 hours for the 50 cm sand-gravel system.....	250

Fig. 6.18 Hydraulic heads distribution for the 30 cm sand-gravel system.....	251
Fig. 6.19 Simulated flow lines for the 30 cm sand-gravel system.....	252
Fig. 6.20 Plume contours for the 30 cm sand-gravel system after 15 hrs.....	253
Fig. 6.21 Plume contours for the 30 cm sand-gravel system after 20 hrs.....	254
Fig. 6.22 Plume contours for the 30 cm sand-gravel system after 30 hrs....	255
Fig. 6.23 Simulated transverse concentration profile with time for the 30 cm sand-gravel system.....	256
Fig. 6.24 Measured transverse concentration profile after 28.2 hours for the 30 cm sand-gravel system.....	256
Fig. 6.25 Measured transverse concentration profile after 29.7 hours for the 30 cm sand-gravel system.....	257
Fig. 6.26 Measured transverse concentration profile after 31.6 hours for the 30 cm sand-gravel system.....	257
Fig. 6.27 Measured transverse concentration profile after 33 hours for the 30 cm sand-gravel system.....	258
Fig. 6.28 Measured transverse concentration profile after 34.5 hours for the 30 cm sand-gravel system.....	258
Fig. 6.29 Calculated concentration history at measuring ports for the 30 cm sand-gravel system.....	259
Fig. 6.30 Hydraulic heads distribution for the 20 cm sand-gravel system....	260
Fig. 6.31 Simulated flow lines for the 20 cm sand-gravel system.....	261
Fig. 6.32 Plume contours for the 20 cm sand-gravel system after 12 hrs....	262
Fig. 6.33 Plume contours for the 20 cm sand-gravel system after 15 hrs....	263
Fig. 6.34 Plume contours for the 20 cm sand-gravel system after 20 hrs....	264
Fig. 6.35 Plume contours for the 20 cm sand-gravel system after 25 hrs....	265
Fig. 6.36 Comparison of measured and simulated transverse concentration profile after 22.1 hours for the 20 cm sand-gravel system.....	266

Fig. 6.37 Comparison of measured and simulated transverse concentration profile after 23.4 hours for the 20 cm sand-gravel system.....	266
Fig. 6.38 Comparison of measured and simulated transverse concentration profile after 24.8 hours for the 20 cm sand-gravel system.....	267
Fig. 6.39 Comparison of measured and simulated transverse concentration profile after 26 hours for the 20 cm sand-gravel system.....	267
Fig. 6.40 Plume history at the measuring ports as well as that calculated at the center for the 20 cm sand-gravel system.....	268
Fig. 6.41 Hydraulic heads distribution for the 15 cm sand-gravel system.....	269
Fig. 6.42 Simulated flow lines for the 15 cm sand-gravel system.....	270
Fig. 6.43 Plume contours for the 15 cm sand-gravel system after 12 hrs.....	271
Fig. 6.44 Plume contours for the 15 cm sand-gravel system after 15 hrs.....	272
Fig. 6.45 Plume contours for the 15 cm sand-gravel system after 20 hrs.....	273
Fig. 6.46 Plume contours for the 15 cm sand-gravel system after 25 hrs.....	274
Fig. 6.47 Comparison of measured and simulated transverse concentration profile after 18.7 hours for the 15 cm sand-gravel system.....	275
Fig. 6.48 Comparison of measured and simulated transverse concentration profile after 19.7 hours for the 15 cm sand-gravel system.....	275
Fig. 6.49 Comparison of measured and simulated transverse concentration profile after 20.8 hours for the 15 cm sand-gravel system.....	276
Fig. 6.50 Measured concentration history at some measuring ports and the calculated at the center for the 15 cm sand-gravel system. ....	276
Fig. 6.51 Hydraulic heads distribution for the 10 cm sand-gravel system.....	277
Fig. 6.52 Simulated flow lines for the 10 cm sand-gravel system.....	278
Fig. 6.53 Plume contours for the 10 cm sand-gravel system after 12 hrs.....	279
Fig. 6.54 Plume contours for the 10 cm sand-gravel system after 15 hrs.....	280
Fig. 6.55 Plume contours for the 10 cm sand-gravel system after 20 hrs.....	281

Fig. 6.56 Plume contours for the 10 cm sand-gravel system after 25 hrs.....	282
Fig. 6.57 Comparison of measured and simulated transverse concentration profile after 19.9 hours for the 10 cm sand-gravel system.....	283
Fig. 6.58 Comparison of measured and simulated transverse concentration profile after 22.9 hours for the 10 cm sand-gravel system.....	283
Fig. 6.59 Comparison of measured and calculated transverse concentration profile after 24.7 hours for the 10 cm sand-gravel system....	284
Fig. 6.60 Comparison of measured and simulated transverse concentration profile after 22.75 hours for the 5 cm sand-gravel system.....	284
Fig. 6.61 Calculated concentration history at measuring ports for the 10 cm sand-gravel system.....	285
Fig. 6. 62 Measured concentration history at measuring ports as well as that calculated at center for the 10 cm sand-gravel system.....	286
Fig. 6.63 Hydraulic heads distribution for the 5 cm sand-gravel system.....	287
Fig. 6.64 Simulated flow lines for the 5 cm sand-gravel system.....	288
Fig. 6.65 Plume contours for the 5 cm sand-gravel system after 10 hrs.....	289
Fig. 6.66 Plume contours for the 5 cm sand-gravel system after 12 hrs.....	290
Fig. 6.67 Plume contours for the 5 cm sand-gravel system after 13 hrs.....	291
Fig. 6.68 Plume contours for the 5 cm sand-gravel system after 15 hrs.....	292
Fig. 6.69 Plume contours for the 5 cm sand-gravel system after 20 hrs.....	293
Fig. 6.70 Plume contours for the 5 cm sand-gravel system after 25 hrs.....	294
Fig.6.71 Comparison of measured and simulated concentration history at center for the 5 cm sand-gravel system.....	295
Fig. 6.72 Comparison of measured and simulated transverse concentration profile after 18.6 hours for the 5 cm sand-gravel system.....	295
Fig. 6.73 Comparison of measured and simulated transverse concentration profile after 19.7 hours for the 5 cm sand-gravel system.....	296
Fig. 6.74 Comparison of measured and simulated transverse	

concentration profile after 23.5 hours for the 5 cm sand-gravel system.....	296
Fig. 6.75 Comparison of measured and simulated transverse concentration profile after 24.6 hours for the 5 cm sand-gravel system.....	297
Fig. 6.76 Comparison of measured and simulated transverse concentration profile after 25.8 hours for the 5 cm sand-gravel system.....	297

## CHAPTER 1

### INTRODUCTION

#### 1. General

##### 1.1 Power, Progress and the Environment

Electricity represents the most useful form of energy that virtually can fulfil most of mankind's needs. It is the form of energy that can easily flow from place to place over long distances and thereby provide mankind with his needs of power wherever he may be. Once there, all our communications, transport, food supplies, offices and factories can function and life may conveniently establish. However, the establishment of a sustainable growing economy requires the existence of reliable supply of electric power at reasonable cost. In other words, large scale generation of electricity requires the existence of undepleted or long term reserves of energy supply. Unfortunately, renewable sources of energy (solar, wind, waves, etc.) provide only a small portion of the required power around the world in addition to the fact that there are large uncertainties associated with these sources. Thus most of the world's need of electric power is largely satisfied from depleting sources of energy (fossil and nuclear fuels). The consumption of electric power is increasing rapidly nowadays. In the IAEA booklet (2000) it is stated that "worldwide energy consumption has multiplied twenty-five fold since the last century. Average per capita consumption of electricity is about ten times higher in industrial countries than in the developing

world. But with the economies in many developing nations now expanding rapidly, electricity demand is expected to grow at over 5% annually during the next fifteen years. Meeting this demand will require a dramatic rise in electricity output". The problems, however, associated with generating electric power from the burning of fossil fuels (coal, oil and gas) is the production of large amounts of polluting gases including carbon dioxide (CO<sub>2</sub>), sulphur dioxide (SO<sub>2</sub>), nitrogen oxide (NO<sub>x</sub>) etc., which have proven to be harmful to the environment. Carbon dioxide (one of what are called greenhouse gases) is believed to be the principal reason for global warming. Greenhouse gases allow sunlight to freely pass through earth's atmosphere and thereby heat its surface. When earth's surface is heated it radiates back this heat as infrared radiation, which is then absorbed by these gases and trap the heat within the atmosphere. On the other hand, sulphur dioxide (mainly from coal burning plants), is largely responsible for what is called "acid rain".

These negative impacts of burning fossil fuels have raised the awareness of the importance of nuclear power in generating electricity. Nuclear power plants produce neither greenhouse gases nor acid rain gases; they practically produce no carbon dioxide, sulphur dioxide, nitrogen oxide or particulate matter emissions. The nuclear radiation that results from the fission of uranium in nuclear reactors is largely confined within the reactor and does not constitute a threat to the environment as long as the system is operating properly. The fear of nuclear accidents after the Chernobyl tragedy has also raised the awareness of the devastating environmental impact that may result upon the occurrence of a

serious nuclear power plant accident. Nowadays, however, the design of nuclear reactors has been such that the risk of using nuclear power plants is minimized. Nuclear power now provides many countries (like France, Sweden and Belgium) with more than 50% of their total electrical supplies. It also provides other countries (including Finland, Japan, Republic of Korea, Spain and Switzerland) with more than 30% of their total need of electricity (IAEA report 2000). Worldwide there are more than 438 reactors currently in operation (World Nuclear Association 2005).

## 1.2 Nuclear Fuel

Figure 1.1 depicts the projected world primary energy demand (WEO 1998). Although the current trend in energy consumption as depicted in this figure shows more dependence on energy from fossil fuel, nuclear energy will still be the solution given the fact that the world reserves of fossil fuel are estimated to be in the order of hundred years and the recent increases in oil prices that are expected to last.

Nuclear power plants (NPP) rely on fissionable  $^{235}\text{U}$  and  $^{238}\text{U}$  as their fuel. This has made uranium deposits of intrinsic economic importance because of its use as a fuel feeding nuclear power plants. Since the commissioning of the world's first NPP in 1954, uranium has been very valuable and exploration all over the world to estimate its reserves and to provide economical as well as efficient ways of extraction has been enormous. In comparison with other substances found on earth's crust, uranium is now considered to be more

plentiful than many substances including mercury, antimony, silver, or cadmium, and is about as abundant as molybdenum or arsenic ([www.uic.com.au](http://www.uic.com.au)). It is believed that approximately five percent of all known minerals contain uranium as an essential structural constituent (Finch et al. 1999). Now it is estimated that with the current uranium reserves and extraction technologies the world production of uranium can extend 60-fold if demand requires it ([http://www.uic.com.au/](http://www.uic.com.au)). Worldwide, the yearly uranium mine production is estimated to be about 35,000 tones ([http://www.uic.com.au/](http://www.uic.com.au)). Canada stands as one of the largest producers of uranium ore in the world. It produces about one third of the world's uranium mine output ([http://www.uic.com.au/](http://www.uic.com.au)). Fig. 1.2 shows world wide Uranium production and reactor-related requirements in the year 2001 (Nuclear Energy Agency 2001).

### **1.2.1 Uranium mines**

This section is intended to provide an overview on uranium deposits, their chemical states while underground and upon mining as well as highlighting some facts regarding its radiological hazardous effects.

As stated previously, minerals containing uranium are numerous. Examples include pitchblende, uraninite, carnotite, autunite, etc. In the WISE project (2002) it is stated that “most uranium ore is mined in open pit or underground mines. The uranium content of the ore is often between only 0.1 and 0.2%. Therefore, large amounts of ore have to be mined to get at the uranium. In the early years up until the 1960s, uranium was predominantly mined

in open pit mines from ore deposits located near the surface. Later, mining was continued in underground mines. After the decrease of uranium prices on the world market since the 1980s, underground mines became too expensive for most deposits; therefore, many mines were shut down. In a uranium ore deposit, equilibrium obtains between U-238 and its decay products, and between U-235 and its decay products. The equilibrium may be somewhat disturbed by geochemical migration processes in the ore deposit. In case of an undisturbed uranium deposit, the activity of all decay products remains constant for hundreds of millions of years. The radiation is virtually trapped underground; exposures are only possible if contaminated groundwater that is circulating through the deposit is used for drinking. Radon gas, a prime source of alpha radiation, is of no concern for deep deposits since it decays before it can reach the surface. The situation changes completely, when the deposit is mined: Radon gas can escape into the air, ore dust can be blown by the wind, and contaminants can be leached and seep into surface water bodies and groundwater. Radon gas released during mining, milling and from tailings can travel hundreds of miles at low concentrations. The wastes therefore become a source of radioactive contamination much more severe than the unmined ore body". Given the half-lives of many of the radioactive elements (Table 1.1), WISE project (2002) commented that "they [tailings] are hazardous virtually forever".

Table 1.1 The Uranium decay chain (WISE 2002).

<b>Uranium-238 Decay Series</b>		
<b>Nuclide</b>	<b>Half-Life</b>	<b>Radiation</b>
U-238	4.468.10 <sup>9</sup> years	alpha
Th-234	24.1 days	beta
Pa-234m	1.17 minutes	beta
U-234	244,500 years	alpha
Th-230	77,000 years	alpha
Ra-226	1,600 years	alpha
Rn-222	3.8235 days	alpha
Po-218	3.05 minutes	alpha
Pb-214	26.8 minutes	beta
Bi-214	19.9 minutes	beta
Po-214	63.7 microseconds	alpha
Pb-210	22.26 years	beta
Bi-210	5.013 days	beta
Po-210	138.378 days	alpha
Pb-206	stable	-

### 1.3 Milling of the Ore and the Hazardous Potential of its Wastes.

The extraction of uranium from the ore depends to a large extent on its relative abundance in the deposits. If a uranium site is found in which the percentage of uranium deposits are economically feasible, the mining industry establishes a mining site as well as a mill to recover uranium from minerals. A uranium mill (a chemical plant) is usually located near the mines to limit

transportation and therefore reduce the potential of spreading hazardous materials into the environment. Uranium ore is crushed and leached in the mill using sulfuric acid, in most cases, as the leaching agent (WISE 2002). The extracted uranium in the form of yellow powder (called the yellow cake,  $U_3O_8$ ) is packed and shipped in casks. The waste produced during the milling processes is called tailings (WISE 2002).

During the extraction of the uranium ore as well as during the leaching process to prepare a uranium concentrate, large amounts of solids and liquid residues in which heavy metals are readily leachable are produced. These elements, including arsenic, molybdenum, vanadium, selenium, iron, lead, and uranium and its daughter products are hazardous and may occur in groundwater at levels exceeding drinking water standards. While the hazard per gram of mill tailings is low relative to most other radioactive wastes (e.g. from nuclear reactors), it is now evident that the large volume of uranium mill tailings may have resulted in widespread environmental contamination (Dominique-Janine 1993). Recently, uranium mine tailings have been the subject of extensive research to characterize its sources, estimate its impact to the environment and to propose safe containment facilities.

### **1.3.1 Uranium waste deposits**

It is important while designing tailings management facilities to realize the fact that TMFs are built to confine radioactive contaminants for tens of thousand of years before they will cease to present a radiological hazard. On the other

hand, the nonradioactive toxic metals (such as those mentioned earlier) will persist, virtually, forever (Dominique-Janine 1993). Thus, the long term storage of these harmful substances needs to be studied carefully. Mainly two kinds of waste are produced at mining sites, and these include:

### **I. Waste Rock**

A large volume of rock materials are usually mined in order to gain access to the uranium (i.e., rock with uranium concentrations that make it economical to remove or extract). However, due to technical difficulties as well as economic infeasibility, not all the rocks containing the ore are fed into the mill. Only those with anticipated higher uranium deposits are fed for further milling processes. Two types of rock materials (called waste rock) are produced during mining of the ore. The first represents the rock materials that are removed to arrive at uranium deposits. They often are clean rocks and are usually used as filling materials (e.g. pervious surround), in roads constructions, etc. The second represent those rocks contain the ore with too low a grade for processing. They often contain elevated concentrations of radioisotopes compared to normal rock.

### **II. Uranium Mill Tailings.**

In WISE (2002) it is indicated that at a mill feed grade of 0.1% uranium, 99.9% of the material is left over as sludge called mill tailings. Because tailings sludge contains long-lived decay products such as thorium-230 (approximately 80,000 years half life) and radium-226 (1600 years half life), it therefore contains

approximately 85% of the initial radioactivity of the ore (Abdelouas et al. 1999). Moreover, not all of the uranium present in the ore can be economically extracted due to technical difficulties and limitations. Therefore, 5 to 10% of the uranium initially present in the ore is usually contained in the sludge (WISE 2002). On the other hand, heavy metals originally contained within the ore, as indicated earlier, are also released from their relatively safe underground location resulting in these hazardous materials becoming more susceptible to dispersion in the environment (WISE 2002). In addition, uranium mine tailings contain chemical reagents that were used during the milling process (e.g., sulfuric acid). Most importantly, the constituents inside the tailings have been undergoing several chemical processes and are therefore in a state of geochemical inequilibrium. The result is that they become more susceptible to mobility to the environment. It is thus important to confine these contaminants and prevent their release to the environment. In contrast to the high level radioactive wastes (usually from nuclear reactors) which are collectively of smaller volume; uranium mill tailings are large in volume such that a 0% release of contaminants from its containment may not be achievable at economical costs. The criterion for uranium mill tailings containment facilities therefore is to minimize the release of its hazardous constituents to the environment such that the standard acceptable levels are not compromised.

### 1.3.2 Concepts for tailings disposal.

As a result of the high level of potential threat to the environment contained within the uranium mill tailings, careful disposal techniques needed to be devised. Two methods have been proposed and used to dispose uranium mine tailings; in the first, mill tailings are dumped as a pile above the ground surface. Concerns related to the possible spreading of radionuclides into the environment through the atmosphere as well as seepage into groundwater has resulted in the search for an efficient containment alternative. Several alternatives were investigated to determine the best way to store uranium mill tailings and to confine them in such a way as to minimize their impact to the environment in an economic way. One of these alternatives was to bring the tailings back to where the ore has been taken from ([www.uic.com.au](http://www.uic.com.au)). Although this idea is appealing, it does not in most cases lead to an acceptable solution for tailings disposal. This may be because most of the contaminants (85% of the total radioactivity and all the chemical contaminants) are still present (Abdelouas et al. 1999). Moreover, as explained earlier, the materials' original stable states have been altered by mechanical and chemical processes resulting in increasing the degree of mobility of the contaminants and hence increase the possibility of its migration into the environment. Therefore, dumping the tailings in an underground mine or in former open pit mines may not be appropriate. There, they would be in direct contact with groundwater (for former underground mines after halting the pumps) or seep into groundwater (for former open pit mines). The only solution that could be appealing may be the construction of man-made

impermeable layers to confine the contaminant and minimize the risk to groundwater.

The concept of disposing the tailings in former open pits has been pursued in France and in Canada at several sites in recent years (WISE 2002). Fig.1.3 shows one of these pits in northern Saskatchewan, Canada. It has been proposed that if the tailings were made in such a way that its permeability upon consolidation becomes very low and was enveloped with a highly permeable layer (called the pervious surround) it is anticipated that groundwater will move around rather than through the tailings and the exchange of contaminants between tailings and groundwater will largely be limited by diffusion processes only. Recent proposals even deny the necessity of an artificial permeable layer around the tailings in the sense that the surrounding rock would (in some cases) provide a high enough permeability. To highlight the role of the pervious surround in connection with tailings management facilities in northern Saskatchewan, Canada, a parametric study was performed during the course of this work as will be discussed later. In cases where tailings have to be disposed of or stored on the surface for lack of other options, additional measures have to be performed to assure protection from erosion.

#### **1.4 Uranium Mining in Northern Saskatchewan, Canada.**

Saskatchewan, Canada holds significant portion of the world's known uranium resources. It is currently the largest uranium-producing region in the world and accounts for more than 25 percent of annual world uranium production

([www.nuclearsafety.gc.ca](http://www.nuclearsafety.gc.ca)). Uranium has been produced from two main areas in Saskatchewan of which the richest uranium deposits in the world occur at or near the base of the Athabasca Basin sandstone sequence ([www.gov.sk.ca](http://www.gov.sk.ca)). Figure 1.4 highlights these places in Saskatchewan where most of the deposits were found. Uranium deposits in Saskatchewan are large and can economically be extracted at costs far below that in many other places in the world. Saskatchewan's uranium resources are expected to remain competitive and sufficient for more than 40 years at current rates of production ([www.gov.sk.ca](http://www.gov.sk.ca)). Uranium deposits in Saskatchewan are found near the surface as well as deep in the earth's crust; therefore the ore is mined by both underground and open pit mining methods. There are currently four uranium mining operations in the province; Rabbit Lake, Cluff Lake, Key Lake and McClean Lake ([www.nuclearsafety.gc.ca](http://www.nuclearsafety.gc.ca)). Most of the extracted uranium is sold by the mining companies to electric power utilities in Canada, the United States, Europe and the Far East ([www.gov.sk.ca](http://www.gov.sk.ca)).

## **1.5 Uranium Mine Tailings Disposal in Northern Saskatchewan.**

### **1.5.1 General**

In Canada, about 200 million tonnes of uranium mine and mill tailings have been generated since the mid-1950s ([www.nuclearsafety.gc.ca](http://www.nuclearsafety.gc.ca)). A total of 24 tailings sites exist in the provinces of Ontario, Saskatchewan and in the Northwest Territories, twenty of them no longer receive waste material. Currently,

in Canada, only the four, previously mentioned, sites in Saskatchewan are active ([www-pub.iaea.org](http://www-pub.iaea.org)).

### 1.5.2 Tailings management facility (TMF) in northern Saskatchewan.

As of 1998, uranium mining in Saskatchewan has resulted in the production of approximately 33 M tones of tailings (Inventory of Radioactive Waste in Canada 1999). Table 1.2 provides an inventory of the uranium tailings in storage at operational mine sites in Saskatchewan ([www.nuclearsafety.gc.ca](http://www.nuclearsafety.gc.ca)).

Table 1.2: Uranium tailings accumulation at operational mines as of December 31, 2001 ([www.nuclearsafety.gc.ca](http://www.nuclearsafety.gc.ca)).

Site	Method of storage	Accumulation (tonnes)
Cluff Lake	Surface	3,840,000
Key Lake	Open pit	2,465,588
Rabbit Lake	Open pit	5,140,000
McClellan Lake	Open pit	257,922

Geochemical characterization of uranium tailings pore water and solids in many sites in northern Saskatchewan proved that, in addition to the radioactive materials, heavy metals like nickel and metalloids like arsenic are present (Cameco 1998; Donahue 2000). Arsenic contained within the tailings is one of the primary contaminants of concern because of its potential to affect downstream receptors. For example, the tailings body in the Rabbit Lake tailings management facility (TMF) is approximately 425 m long, 300 m wide and 91 m

thick at its center (Cameco 1998). The analysis of mill records indicates that the TMF contains over 17,000 tonnes of As (Cameco 1994). The physico-chemical conditions and the chemical distribution of As in TMFs have been investigated by Donahue and others (Donahue 2000; Donahue et al. 2000). They concluded that 88% of the As is present as arsenates and the remaining 12% in the form of primary minerals.

Since the exploration of uranium in northern Saskatchewan began in early forties of the last century ([www.gov.sk.ca](http://www.gov.sk.ca)) when the awareness of the hazardous effects of uranium mine tailings was largely unknown, tailings were initially disposed of as a slurry into topographic low or natural lakes (Donahue 2000). As it, later, becomes evident the potential environmental and health impacts of uranium mill tailings, a second generation of engineered above ground TMFs were developed. However, as indicated earlier, problems associated with above ground tailings storage facilities regarding the possibility of contaminants spreading to the environment as well as operational problems, such as freezing, grain size segregation etc., led to the proposal and implementation of a third generation of disposal facilities: the engineered in-pit TMFs in which the tailings are permanently placed below the water table in a mined-out open pit (Donahue 2000). As stated in Donahue (2000), three designs of in-pit TMFs were implemented in Saskatchewan: The Rabbit Lake TMF (pervious surround design), The Key Lake Deilmann TMF (side drain and subaqueous discharge design), and the McClean Lake Jeb pit TMF (natural surround and subaqueous discharge design), Fig.1.5. The common feature of these three designs is the

utilization of contrast in permeability between the consolidated tailings and the adjacent materials to alter groundwater movement and direct it around rather than through the tailings, (Donahue 2000).

One may be able to distinguish three phases during the lifespan of an in-pit TMF: the preparatory phase, the operational phase, and the post-decommissioning phase (West 2000).

In the preparatory phase, the pit is mined out of the host rock, which is then stored on the surface for further use during the construction of the pervious surround (West 2000). A drainage system is constructed at the bottom of the TMF to collect contaminated water released during the life span of the TMF and help consolidate the tailings. The drainage system is composed of a shaft that is placed in an excavated drift at the bottom of the pit and is connected to the ground surface through piping system. Drainage of the pit can subsequently commence by pumping water out of the bottom of the pit via the drift shaft (West 2000). For TMFs utilizing the pervious surround technique a layer of crushed rocks (approximately 1 m thick) is constructed at the edge of the TMF adjacent to the host rock followed by a sand layer (approximately 4 m thick) to prevent tailings' fine from migrating to the pervious layer. These layers are constructed as the tailings level rise, hence it continues during the next phase.

The second phase, "the operational phase", of the life of an in-pit TMF begins as soon the uranium mill is operated. During this phase, tailings in the form of a slurry are piped from the milling plant and deposited on top of the

bottom drain. Figure 1.6a describes schematically an operational TMF. As the tailings are deposited, their own self weight causes them to compact thereby releasing pore water (West 2000). During this process, known as consolidation, the contaminated water is drained and pumped up to a nearby treatment facility. This is an important process in a sense as it helps minimize the permeability of the tailings. Pumping the released contaminated water that results during the consolidation process to a treatment plant not only reduces the risk of mixing the contaminated water with fresh clean groundwater but also creates a capture zone by drawing groundwater inwards from the host rock, therefore, minimizing the migration of solute out of the pit and into the groundwater (West 2000).

The third phase, “decommissioning of the facility”, may commence when the milling processes finish or when the capacity of the pit has been reached (West 2000). Figure 1.6b shows a schematic of a decommissioned facility in which the facility is capped, the surface is cleaned and graded, and the pumps are shut down. Capping of the facility will also help in the consolidation process of the tailings as a result of the extra weight obtained by the capping materials. Moreover, shutting off the pumps would result in groundwater to establish its new natural level, in which the flow direction and velocity is impacted by the presence of the TMF in addition to the regional topography and hydrogeology (West 2000). On the other hand, as regional groundwater flow past and through the TMF, it becomes contaminated by solute contained within the tailings. Hence, a solute plume is expected to form downgradient of the facility (West 2000). To minimize early time release of contaminants, flushing of the system was proposed to

release one pore volume of the water saturating the sand and the pervious surround.

### **1.5.3 Performance criteria.**

A successful in-pit TMF should meet the following objectives

- Minimize advection of groundwater through the tailings. This may be achieved by both or either of two ways. The first would be through minimizing the tailings' hydraulic conductivity by disposing of the tailings as a slurry of fine grains and allowing sufficient time for dewatering or consolidation. Mine tailings generally have a uniform particle size  $<125 \mu\text{m}$ . It has been proposed by the mining industry that the hydraulic conductivity of the tailings will be on the order of  $10^{-8} \text{ m/s}$  (West 2000). The second method to minimize advection through the tailings would be through constructing a highly permeable envelop around the tailings to provide groundwater with a preferential path of low resistance to move around rather than through the tailings (pervious surround concept). It has also been proposed as a design criterion that the minimum hydraulic conductivity of the pervious surround be on the order of  $10^{-2} \text{ m/s}$  (West 2000).
- Minimize diffusion of contaminants out of the tailings by minimizing concentration gradients.
- Minimize surface infiltration through conditioning of the surface.
- Prevention of freezing to maximize the consolidation of the tailings.

- Promote uniformity during tailings deposition to assure homogeneity in tailings properties. Segregation may promote heterogeneity, leading to preferential flow paths and non-uniform consolidation characteristics.

The pervious surround, by acting as a bottom and side drain during the operational phase of the TMF, will also help consolidate the tailings. However, more recently, researchers have raised the concern of a possible detrimental effect of the high groundwater velocities in the pervious surround (West 2000). They argue that the high groundwater velocities in the pervious surround maintain a lower solute concentration adjacent to the tailings and therefore result in large concentration gradients which may eventually cause an enhanced solute mass flux via diffusion. To explore this concern, extensive research has been conducted during the design of TMFs and recently, as will be discussed later.

To maintain the high permeability of the pervious layer after the decommissioning of these sites, it is important to prevent fines from migrating into the pervious layer and deteriorating its role. Migration of fines will occur under a strong hydraulic gradient (from the fine to coarse material) if the smallest pore size in the adjoining coarse material is large enough to pass the smallest particles of the finer material (Cameco 1994). This may result in plugging of the coarse material. During the operational phase, flow in the overburden is directed vertically downward due to dewatering activities. Thus there would be no tendency for the migration of fines from the overburden to the pervious surround during operation. However, a strong hydraulic gradient may be established if it is

decided that back flushing of the pervious surround is necessary after initial flooding of the pit. Back washing may be conducted to remove one pore volume of contaminated water in the pervious surround immediately after the system is allowed to flood. This would be accomplished by a rapid drawdown of the water in the pervious surround, thereby causing strong hydraulic gradients from the surrounding materials towards the crushed rock (Cameco 1994). A filter sand zone (approximately 4 m wide) was thus proposed between the tailings and the pervious surround. The basic criterion for design of the filter sand in this case has been proposed as:

$$\frac{D_{15}(\text{of the rocks})}{D_{85}(\text{of the sand})} < 4 \text{ to } 5 \quad (1.1)$$

This criterion may be stated as the 15% (passing) size of crushed rock must not be more than 4-5 times greater than the 85% (passing) size of the sand. This ensures that migration of fine particles will not occur (Cameco 1994).

### **1.6 Simulation of this System.**

Groundwater flow and solute transport within this system has been studied in relation to the design and licensing of different TMF in northern Saskatchewan (Gulf Minerals 1981; Total and Minatco 1991; Cameco Corporation 1994; Donahue 2000; Donahue et al. 2000; West 2000; Lautermilch 2000, West et al. 2003; Lange et al. 2003). These studies were mainly aimed at studying the given TMFs with all their geometric complexities and geochemical processes. Little emphases were made to show the exact role of the pervious surround concept

as opposed to the natural surround concept. Misfeldt et al. (1999) have numerically studied this system assuming a two-dimensional conceptual model. They assumed a continuous source in the tailings (i.e., a prescribed concentration) and showed that the simulated mass flux from the tailings mass in the case of pervious surround scenario is always higher than that predicted in the case of natural surround scenario. However, the assumption that the concentration within the tailings is constant may be inappropriate and may lead to an erroneous conclusion. Perhaps the most comprehensive study on this issue has been done by West et al. (2003) and Lange et al. (2003). West et al. have proposed a three-dimensional conceptual model and simulated groundwater flow and solute transport within this system both numerically and experimentally. They assumed the equivalent porous medium (EPM) and discrete fracture scenarios for the host rock. They also assumed an initial concentration condition in the tailings, and simulated the concentration downgradient and mass flux with time. Lange et al. (2003) simulated the system numerically and experimentally assuming a dual porosity model for the host rock. No previous work, to my knowledge, has addressed the significance of the sand layer on flow and transport in this system as well as the effect of the initial mass that may exist in the sand after decommissioning of the facility.

#### **1.6.1 Problems related to the simulation of this system.**

Two problems have shown to be common in the simulation of this system. The first of which is inherent to the numerical technique used to simulate the

problem. This is related to the presence of discontinuities in porous media parameters at the interface boundaries between different zones as well as to the initial sharp concentration front at the tailings interface. This imposes difficulties to any numerical scheme in the sense that unrealistic contaminant quantities may be introduced due to the inherent characteristics of the numerical scheme and not due to the physical problem under study. For example, an additional mass is introduced into the zone adjacent to the tailings as the concentration is assumed to vary linearly between nodes at the tailings interface and the adjacent nodes in the neighboring zone. Hence, this increases the early time concentration and mass flux leaving the simulated TMF. To minimize this effect, fine discretization in the vicinity of this sharp interface is needed or alternatively higher order formulation may be needed as will be discussed in the next chapter.

The second, and probably the most serious, is related to the possible violation of the length scale constraints defined for the continuum hypothesis to be used for this system. This violation in fact may leave the system insolvable with the type of equations currently available and alternatives may need to be devised.

## **1.7 Objectives**

The objectives of this work may be summarized as follows:

1. To conduct a parametric study to illustrate the effects of the pervious surround parameters on its expected role to divert groundwater around rather than through the tailings.
2. To illustrate the effects of the sand layer, which exists between the pervious surround and the tailings to minimize the migration the tailings to the pervious surround, on system hydrodynamics and solute transport.
3. To explore the behavior of the system with the sand layer having different initial solute concentrations ranging from zero, if completely flushed upon decommissioning, to concentrations equal to the tailings water concentrations.
4. To provide a thorough investigation of the continuum hypothesis as well as the length scale constraints and apply them to the pervious surround used in TMFs in northern Saskatchewan.
5. To look for alternatives to dealing with systems when the continuum hypothesis may not be adopted.
6. To conduct a set of experiments to study the behavior of systems when violating the continuum hypothesis and to model them numerically to address the significance of this violation in the pervious region on our ability to model this system.
7. To provide criteria that may help when designing similar systems.

The next chapter explains the impact of discretization in the vicinity of the sharp interface between the different zones on the solute transport and mass flux from a TMF. It also provides a sensitivity or parametric analysis to illustrate the

effect of different permeability contrasts between the different zones on groundwater flow and solute transport. This study also highlights the impact of the sand layer on the peak downgradient concentrations and mass flux.

In chapter 3, a review of different length scale constraints identified for the continuum approach to be adopted is introduced. Also different methods proposed in the literature to deal with the violation of these length scale constraints are discussed. Moreover, the applicability of these length scale constraints to the pervious surround system will be shown to indicate whether this system is violating the continuum approach or not.

In chapter 4 a methodology to deal with systems that violate the continuum approach is introduced and in chapter 5 the experimental set up used to verify and support the hypothesized methodology is explained, together with the measurement techniques. In addition, the numerical technique used in conjunction with the experimental work is explained.

Chapter 6 discusses and analyzes the gathered data and checks the validity of the hypothesis, and chapter 7 provides the conclusions and the main contributions of this research. Chapter 8 provides recommendations for future work.

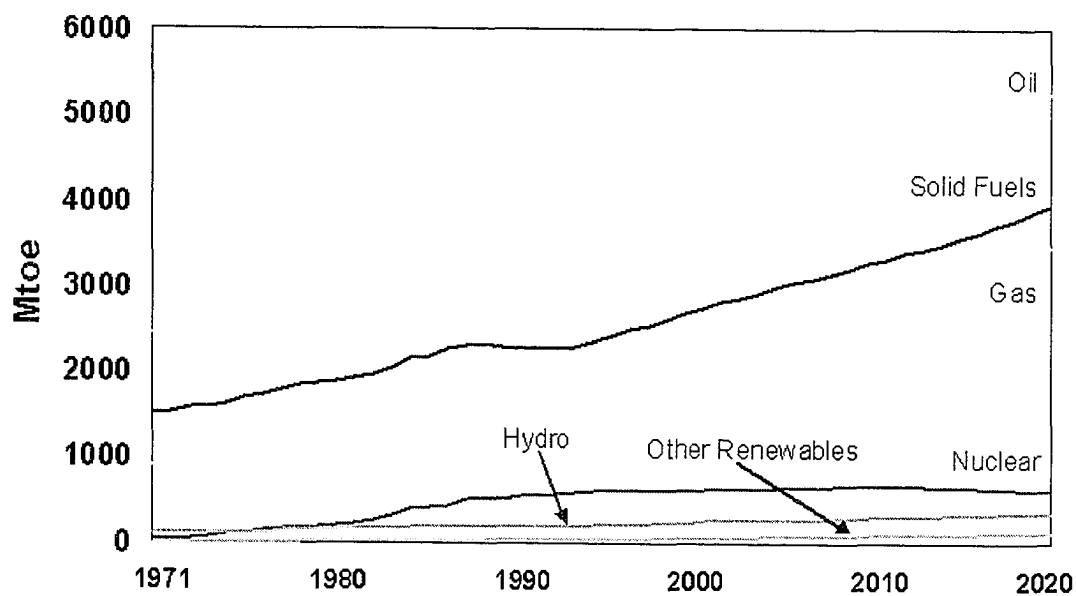
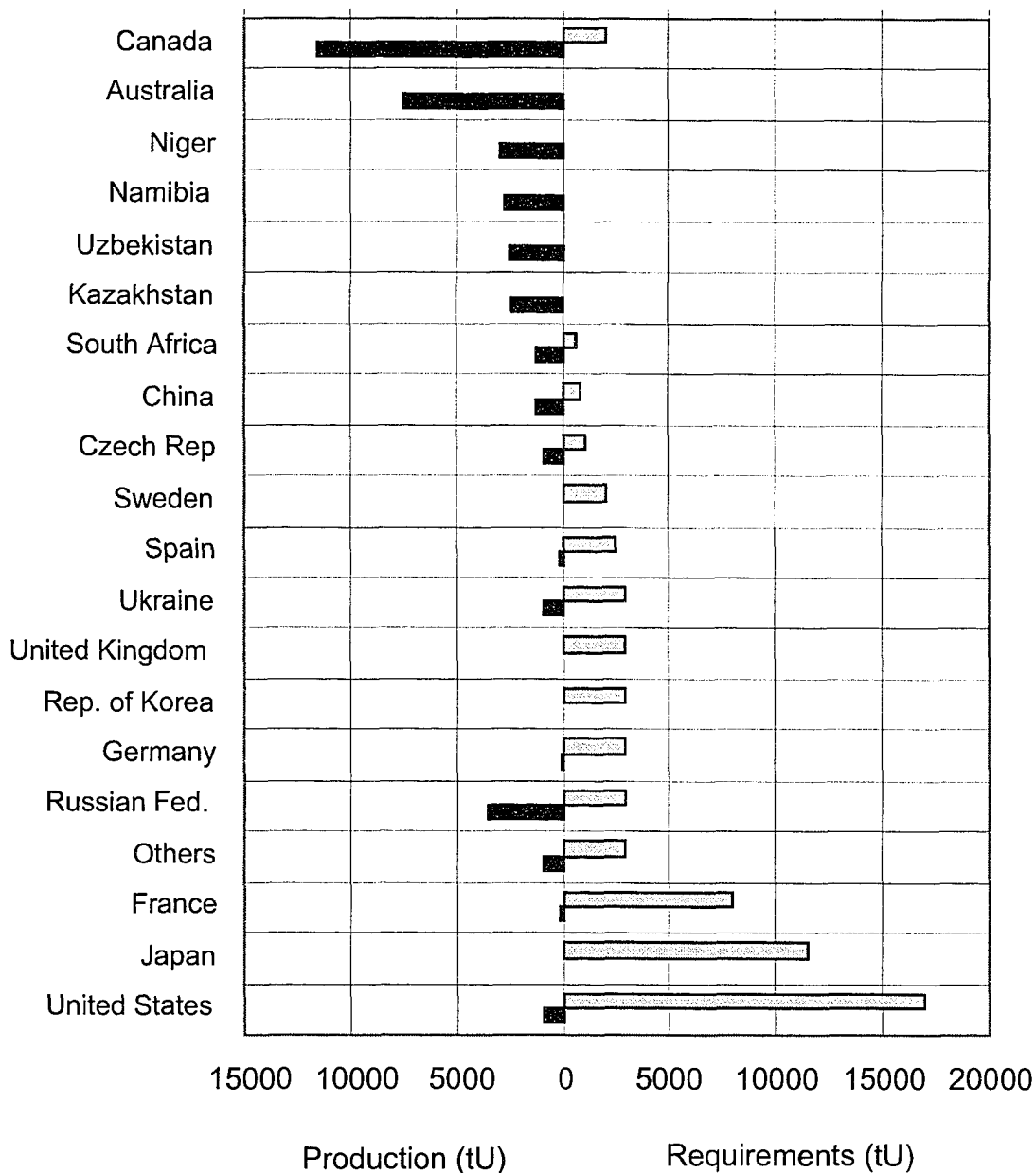


Fig. 1.1 Projected world primary energy demand (World Energy Outlook 1998).



“Others” producers include: Brazil, Hungary, India, Pakistan, Portugal, Romania.

“Others” consumers include: Argentina, Armenia, Belgium, Brazil, Bulgaria, Finland, Hungary, India, Lithuania, Mexico, the Netherlands, Pakistan, Romania, the Slovak Republic, Slovenia, Switzerland.

Fig. 1.2 Uranium production and reactor-related requirements (Nuclear Energy Agency 2001).



Fig.1.3 Uranium pit mine at Rabbit Lake, Saskatchewan, Canada.

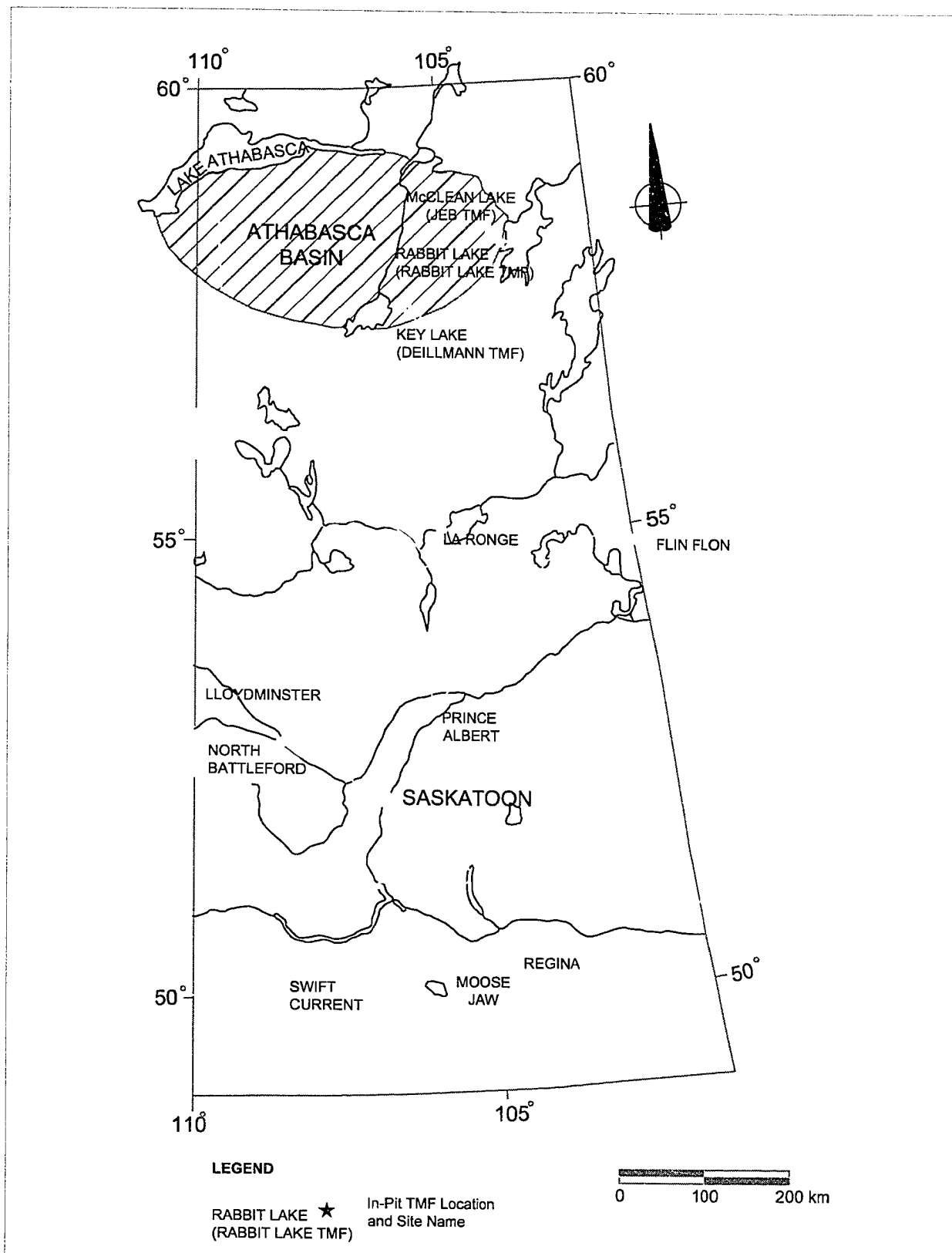


Fig. 1.4 Locations of northern Saskatchewan in-pit TMFs, from West (2000)

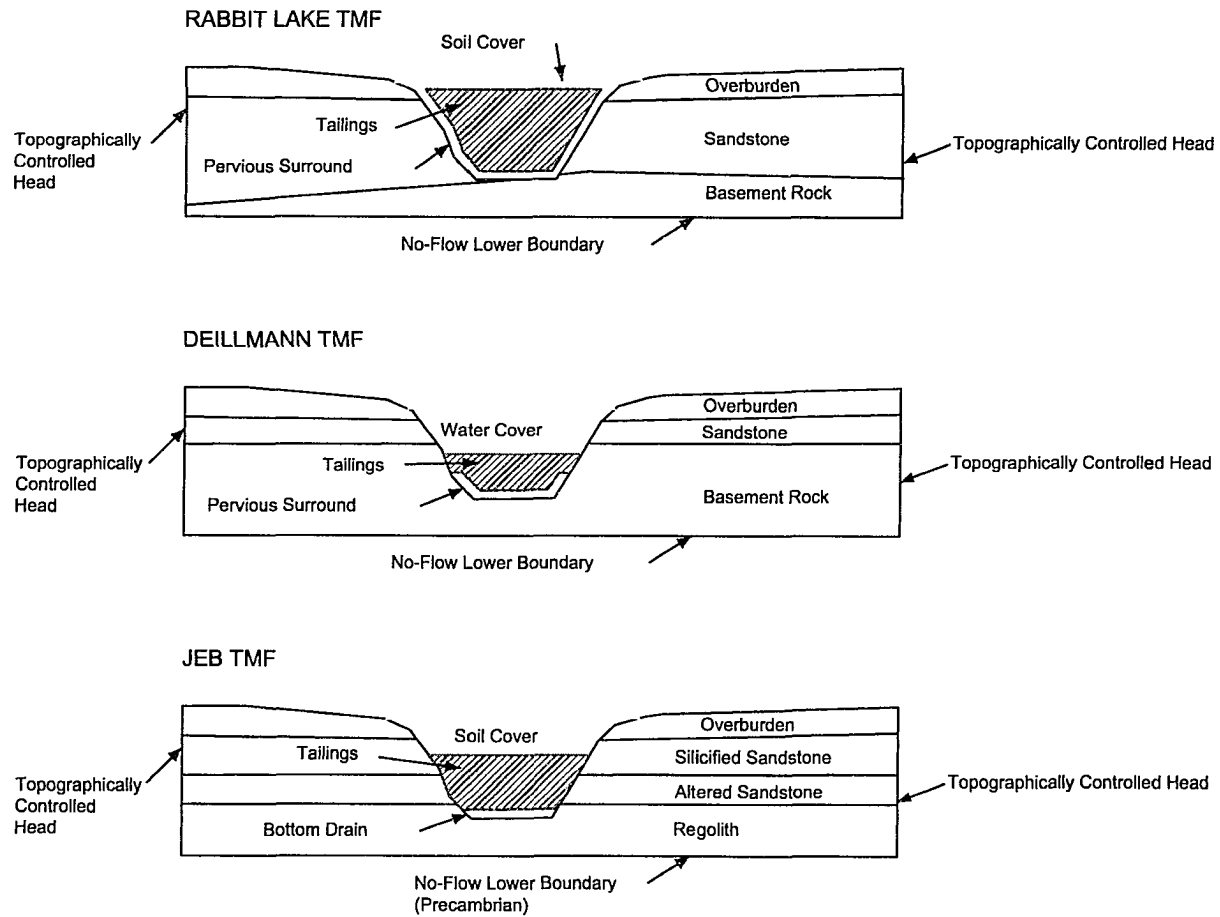
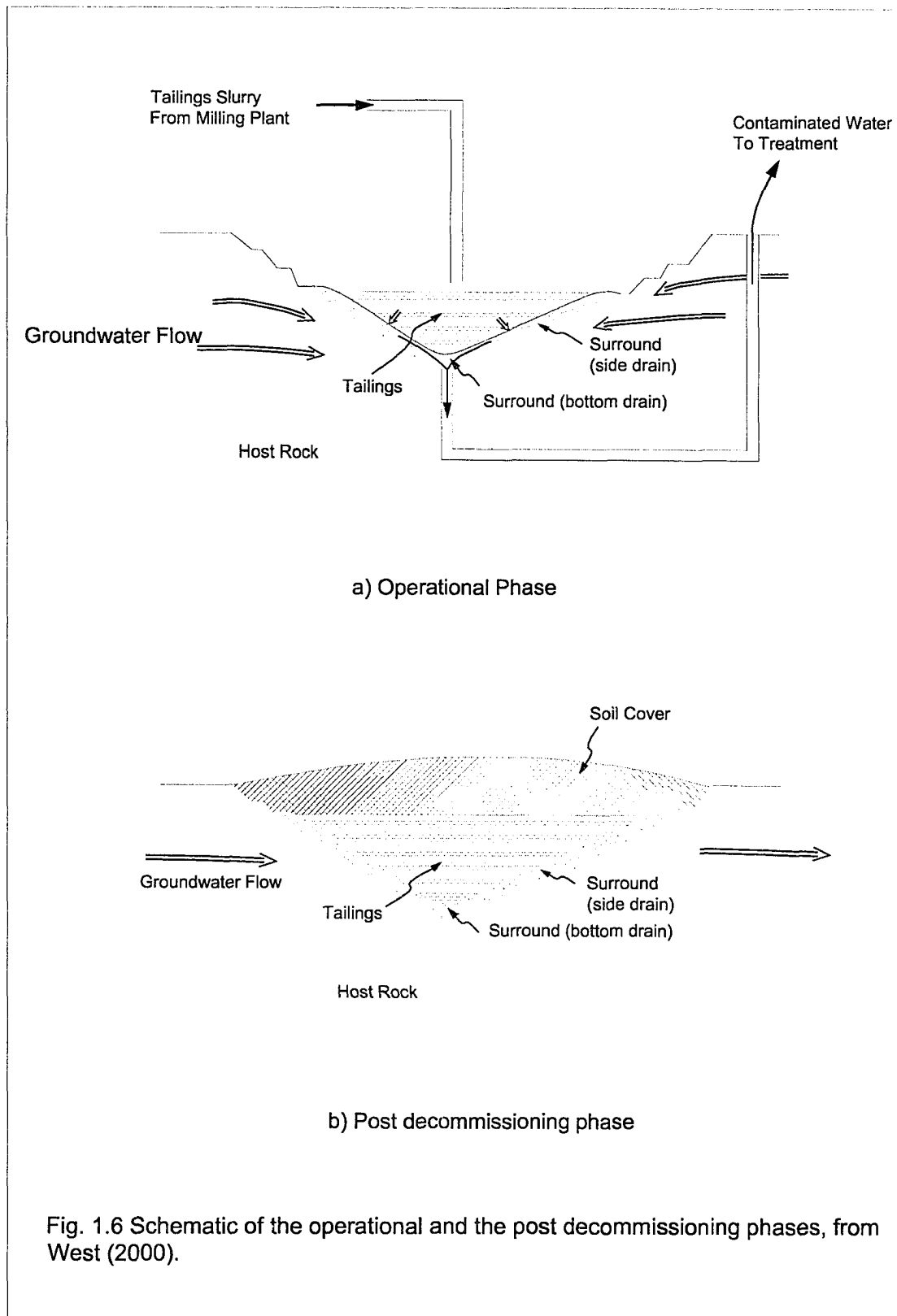


Fig. 1.5 Conceptualization of three northern Saskatchewan tailings management facilities, from West (2000).



## CHAPTER 2

### PARAMETRIC STUDY

The pervious surround concept in TMFs aims at reducing the potential risk of groundwater contamination after decommissioning. By providing groundwater with a path of low resistance, it is hoped that minimal amounts of groundwater will move through the tailings and the release of contaminants from the facilities will mainly be via diffusion which is a slower mechanism. As indicated in chapter 1, previous work has demonstrated this role via numerical as well as experimental work. However, no detailed study has been conducted to highlight the effect of various permeability contrasts between the pervious surround and the host rock. Moreover, the role of the sand layer that is constructed between the tailings and the pervious surround was not included in any previous study.

On the other hand, the geometry of the region and the presence of sharp contrasts in soil properties and in the initial concentration profile at the tailings/surround interface suggest that the selection of an appropriate numerical technique is critical. This is apparent in the sense that misuse of a numerical technique may introduce errors due to the inherent characteristics of the numerical formulation, which need to be identified and minimized.

It may, thus, be important to conduct a parametric numerical study to illustrate how the magnitudes of the properties of the pervious surround impact both the hydraulic head distribution and the migration of contaminants, and to

look at the discretization in the vicinity of the interface boundaries. It is also important to recognize the potential sources of possible errors due to the numerical methods used to simulate these systems. The results of the parametric study are discussed in this chapter.

It is also important to indicate at this stage that, the pervious surround in the Rabbit Lake TMF is filled with crushed rock mainly from excavating activities and is approximately 1 m in thickness. The crushed rock has grain sizes ranging from approximately 1 to 20 cm and hence a 1 m surround is approximately 5 to 10 grain sizes in width. This definitely violates the representative elementary volume (REV) length scale constraints and thus questions the applicability of the continuum approach in this region (as will be detailed in next chapter). Since we do not have the mathematical machinery to deal microscopically with systems in cases when the continuum hypothesis may not be adapted, such a system virtually has no solution. No solution in the sense that both groundwater flow and solute transport equations may not be used in regions where the continuum approach is violated. The questions that may now arise are as follows: If one modeled the system assuming the applicability of the continuum hypothesis everywhere in the region including those subregions where the continuum approach is violated, can one still match the hydraulic head distribution and the contaminant release downgradient of the TMF? Can one still use the properties measured at the macroscopic scale and apply them to regions that may not be dealt with macroscopically? How will this impact our ability to accurately predict

the behavior of the system and its evolution? How much error will be introduced in modeling the system under these circumstances?

Unfortunately, no direct answers may be given to these and similar questions. The only way to explore if there is a possibility to model this system may be through experimentation. The discussion on this issue will be delayed to the next chapters where more thorough analysis is carried out.

## **2.1 Objectives.**

The parametric study was conducted using a two-dimensional conceptual model to study the effects of different pervious surround parameters on groundwater flow and solute transport in a conceptualized in-pit TMF. The study assumed that continuum approach within the pervious layer was valid and thus allowed the use of the usual macroscopic transport equations. The study was conducted numerically using Frac3dvs, which is a robust three-dimensional finite element/finite difference flow and transport model (Therrien et al. 1996). The objectives of the parametric study were to:

- Vary the contrast in permeability between the sand, surround and host rock by changing that of the pervious surround to illustrate the impact of the permeability contrast on the effectiveness of the pervious surround.
- Vary the permeability of the sand to study its role in this system.
- Vary the initial concentration in the sand layer to illustrate the impact of the initial concentration at decommissioning on the downgradient peak concentration and mass flux.

- Vary the value of dispersivities of the pervious surround to assess its significance in solute transport in this system.
- To evaluate the impact of the numerical discretization in the vicinity of the interface boundaries on the predicted concentrations and mass flux downgradient from the TMF.

## **2.2 The Two Dimensional Conceptual Model and Boundary Conditions.**

The model domain was chosen to be 900 m long and 1000 m wide. Only half of the domain was modeled because of the existence of a plane of symmetry, as shown in Fig. 2.1. The pit diameter was assumed to be 300 m in which an initial solute concentration of 1.0 was assigned. The thickness of the sand layer and pervious surround were assumed to be 6 m and 2 m, respectively. The left boundary was assigned a constant head of 6 m and the right boundary was assigned a constant head of zero. The top and bottom boundaries were assumed as no flow boundaries.

## **2.3 Solution Techniques.**

Many numerical methods are available to solve groundwater flow and solute transport problems in porous media as well as many commercial codes. Finite element was chosen as the numerical technique because it has shown to be superior in dealing with irregular geometries. Frac3dvs, a code developed at the University of Waterloo, was used for two reasons; the first one is that it is equipped with grid builder, which allows the users to easily build, change and

refine the mesh; the second is that this code has been shown to be efficient in solving fluid flow and solute transport in variably saturated porous media and discretely fractured rock (Therrien et al. 1996).

## **2.4 Mesh Choice.**

Different mesh scenarios were simulated to:

1. Determine the extent of the artificial top boundary beyond which the TMF had little to no impact on the flow field.
2. Determine the size of the mesh in the pervious surround and sand layers that would correctly:
  - Reflect the initial mass of pollutant in the pit.
  - Reflect the large contrast in permeabilities between the different zones.
  - Approximate the governing equations such that the mesh size did not impact model predictions.

The need for a better representation of the initial mass distribution at the tailings-sand interface as well as the large contrast in permeability between the different zones required that a finer mesh be used in the vicinity of the interface boundaries. These concerns occur for any numerical scheme for which the domain is discretized into a series of nodes or blocks. Finite element, which is the technique chosen for this study, as formulated in Frac3dvs, assumes piece wise linear interpolation functions. This means that the initial sharp contrast in concentration at the sand-tailings interface is not maintained as such when

represented using finite elements. Nodes located at the tailings sand interface are assigned an initial concentration of 1.0 and nodes located in the sand adjacent to the interface are assigned an initial concentration of 0.0. The linear interpolation basis function used assumes the concentration between these nodes varies linearly between 0.0 and 1.0 and hence an initial mass exists in these elements. Fig. 2.2 shows the initial concentration distribution for a one-dimensional element, as an example. As the discretization becomes coarser, the model calculates a slightly larger initial mass within the domain. Although the initial mass contained in the elements adjacent to the tailings/sand interface is very small in comparison to the total mass in the tailings, this initial mass is contained in the higher permeability sand layer in which there is a relatively higher advective flux. Hence the simulated initial mass flux from the TMF as well as the concentration downgradient is increased as the grid size is increased. To minimize this effect, one may make the size of the mesh at the tailings-sand interface very small. However, the problem that arises when considering the 3D scenario is the restrictions related to the aspect ratio. In order to maintain a stable solution, an enormous number of nodes would be required which may generate memory requirements that exceed those typically found on a personal computer today. Alternatively, one may use higher order elements.

To determine the impact of the numerical discretization, five different discretization scenarios were considered: namely: one block, two blocks, four blocks, eight blocks and sixteen blocks within the 2 m pervious surround and correspondingly in the sand layer. Figures 2.3-5 show different refinements of the

mesh in the vicinity of the pervious surround (between  $x=292$  m and 294 m). The analysis shows that the largest grid size in the pervious surround region that would not have a significant impact on the initial mass in the system as well as the concentration profiles is 8 blocks of 25 cm width.

Figure 2.6 shows the concentration history at a point 100 m directly downgradient from the downgradient edge of the TMF. From this figure it is apparent that as the number of blocks increases, the concentration versus time graphs asymptotically approach a similar profile and that the concentration profile for the scenario with 8 blocks is very similar to the 16-block scenario. This is also demonstrated on comparing the mass remaining in the model domain and the solute mass flow rate leaving the downgradient boundary with time for the different scenarios, as shown in Fig. 2.7. It can be seen that the mass flow rates leaving the domain for all the scenarios converge after approximately 150 years. The difference in the total mass that has left the domain after 150 years is equal to the difference in the initial mass in the system. This is clearly supported by the plot of the mass remaining with time. Thus for the parametric study that follows, the pervious surround discretization with 8 blocks was used.

## **2.5 Results of the Parametric Study.**

The parametric study as has been discussed earlier was mainly aimed at studying the effects of different permeability contrast between the pervious surround and both sand and host rock regions on both groundwater flow and

solute transport. Moreover, effects of dispersivities of the pervious surround were also included.

### **2.5.1 Performance criteria.**

In order to compare and discuss the simulation data generated for the parametric study, a set of defined performance variables was identified. For groundwater risk assessment, the contaminant concentrations downgradient from the source as well as the overall contaminant fluxes (emission) from the source are important (Grathwohl 1998). The conceptual model identified an in-pit TMF and a downgradient receptor (e.g., a lake). The TMF should be designed to minimize the downgradient concentrations and to minimize the contaminant mass flux to the downgradient receptor. Hence, for this study, the performance variables selected for comparison were:

- Contaminant concentration at the centerline, 100 m downgradient from the downgradient edge of the TMF ( $x=700$ ,  $y=500$ ).
- Evolution of the mass remaining in the domain.
- Evolution of solute mass flow rate out of the domain (i.e., flux to a downgradient receptor or lake).

Based on these three conditions, one could compare the different scenarios.

### 2.5.2 Impact of pervious surround permeability.

As has been mentioned earlier, the permeability of the different zones plays a key role in groundwater flow and consequently on solute transport in this system. Understanding of groundwater flow through the different zones is vital in order to understand the way solute is likely going to behave upon release from the tailings. A base scenario was defined based on the typical design values of permeability of the different zones as determined in the field. The hydraulic conductivity values used were  $10^{-8}$  m/s for the tailings,  $10^{-4}$  m/s for the sand,  $10^{-2}$  m/s for the pervious surround, and  $10^{-5}$  m/s for the host rock. The different scenarios that were considered aimed at studying the impact of pervious surround permeability on flow and transport.

The following parameters of the pervious surround region were used for all the scenarios that evaluate the role of permeability in flow hydrodynamics and solute transport: Longitudinal dispersivity ( $\alpha_L$ ) of 1.0 m, transverse dispersivity ( $\alpha_T$ ) of 0.1 m, porosity of 0.4 and tortuosity of 0.6.

Six simulations were conducted to study the effects of permeability of the pervious surround on groundwater flow and solute transport. The values of the hydraulic conductivity of the pervious surround that were considered are  $10^{-2}$ ,  $10^{-2.25}$ ,  $10^{-2.5}$ ,  $10^{-2.75}$ ,  $10^{-3}$ , and  $10^{-4}$  m/s, respectively. The permeability of the sand, tailings, and host rock remained the same as for the base scenario. The role of the pervious surround can be viewed in terms of both groundwater flow and solute transport.

### 2.5.2.1 Flow hydrodynamics.

The presence of the TMF in the flow field has, generally, shown to impact groundwater flow. Moreover, varying the hydraulic conductivity of the pervious surround from  $10^{-2}$  m/s to  $10^{-4}$  m/s (the latter being equivalent to the permeability of the sand layer) has significant impact on the flow field for the system. Figures 2.8-2.13 show flow nets for the different scenarios. Scenario E-8-4-2-5 refers to the base scenario with hydraulic conductivities of the tailings, sand, surround and host rock equal to  $10^{-8}$ ,  $10^{-4}$ ,  $10^{-2}$  and  $10^{-5}$  m/s, respectively. This designation system is used throughout this chapter to aid in presenting and comparing the results of the various simulations. Comparisons of these figures indicate that the role of the pervious surround is to give groundwater a preferential path of low resistance around the tailings. This is obvious as more flowlines are concentrating within the pervious layer. The effect of the pervious surround on the flow field is more pronounced when the permeability is higher and its effect extends more towards the far boundary. This is obvious as more flow lines are drawn towards the pervious surround when the permeability is high. As the permeability of the pervious surround decreases, less flow is drawn towards the pervious surround. Figures 2.14-2.17 show flow lines within the sand layer. These figures were generated using reverse particle tracking. A series of particles were placed across the width of the sand layer at the centre of the TMF (plane defined by  $x=450$ ). The particle tracks illustrate the hydraulic capture zone of the sand layer. At  $x=250$  m, the width of the capture zone for the sand layer for the base scenario (E-8-4-2-5) is approximately 5 m in comparison to a width of

almost 100 m for scenario (E-8-4-4-5). Hence, as the hydraulic conductivity decreases in the pervious surround layer, a larger portion of the upgradient flow travels through the sand layer. It may be possible to approximately express the impact of the pervious surround permeability on the percentage distribution of groundwater flow as shown in Table 2.1. Table 2.1 illustrates the effect of the pervious surround permeability on the percentage of upgradient groundwater flow drawn into the TMF and the percentage of the upgradient groundwater flow drawn into the sand and tailings. The difference is the percentage flowing through the pervious surround.

Table 2.1 Percentage flow distribution through the TMF system.

Pervious surround Hydraulic conductivity	Approximate percentage of flow drawn into the TMF	Approximate percentage of flow drawn into the sand and the tailings
$10^{-2}$	51	1.6
$10^{-2.5}$	46	4.4
$10^{-3}$	37	7.2
$10^{-4}$	23	17

Figure 2.18 shows the hydraulic head distribution along the centre line of TMF (plane  $y=500$ ) for the different scenarios. The impact of the TMF on the hydraulic head distribution is apparent from this figure. The distribution of the hydraulic head for a homogeneous medium (i.e., at the far boundary) would be a

straight line. For all scenarios except E-8-4-4-5, the hydraulic head upgradient of the TMF is lower than the hydraulic head at the far boundary indicating that flow is drawn towards the TMF. The corresponding flow nets in Figures 2.8 through 2.12 also illustrate this. For the scenario in which the permeability of the surround and sand are equal (E-8-4-4-5) the head upgradient of the TMF is greater than the heads at the far boundary indicating that flow is diverted around the TMF and this is also illustrated in Figure 2.13. These behaviors reverse downgradient the TMF. It may be concluded that the net effective permeability of the TMF (surround, sand and tailings) was higher than the host rock for all the scenarios except E-8-4-4-5. Moreover, the hydraulic head difference across the tailings was shown to be smaller the higher the pervious surround permeability. This, in fact, achieves the role of the pervious surround as to reduce the advection through the tailings by making the hydraulic head difference across the tailings small.

Understanding seepage velocity profiles in the different layers was shown to be important in explaining some of the issues related to solute transport as will be discussed later. Figure 2.19 show the x-component velocity profiles for the six different scenarios at the plane defined by the equation  $x=450$ . The following points may be noticed on examining these graphs:

- As the permeability in the pervious surround decreases, the seepage velocity in the tailings increases and hence more solute would transport via advection.

- As the contrast in the permeability of the sand and pervious surround media decrease, the velocity in the sand layer increases. This also impacts the rate at which solute leaves the TMF as will be discussed later.

### **2.5.2. 2 Solute transport.**

Figures 2.20-2.25 show the concentration profiles for the scenarios E-8-4-2-5, E-8-4-3-5, and E-8-4-4-5 at the planes  $y=500$  and  $x=450$ . Inspection of concentration profiles at the plane  $y=500$  indicate that diffusion is the most significant mechanism contributing to solute transport when the pervious surround permeability was the highest. As the permeability of the pervious surround decreases, advection becomes a more significant process within the tailings, and the centre of mass within the tailings advances more towards the downgradient tailings boundary. The pervious surround acts to reduce advection within the tailings and hence reduce the release of solute via advection. This in fact has been demonstrated on studying the seepage velocity profiles for the different scenarios at the plane  $x=450$ , which illustrated that as the permeability of the pervious surround decreased, advection within the tailings increased. Although it might be difficult to accurately determine the contribution of different mechanisms to solute transport, it may be possible to indicate that the contribution of advection to solute transport for the scenario E-8-4-4-5 is almost 8 times as much as that for the scenario E-8-4-2-5.

Figures 2.26, 2.27 and 2.28 provide a comparison of concentration profiles for the three scenarios after 6342, 31710 and 95129 years at the plane

y=500. An additional scenario (the so called natural surround scenario where the TMF is surrounded by the host rock materials with the properties of the sand and the pervious layers set equal to that of the host rock, E-8-5-5-5) was included in the comparisons. One may notice that the mass left in the tailings is larger when the permeability of the pervious surround is higher while it was the least for the natural surround scenario.

The solute concentration history at the downgradient observation point (700, 500) is shown in Fig. 2.29 on logarithmic scale. The following points may be inferred from this figure:

- It is clear that the lowest peak solute concentration has been achieved when the permeability of the pervious surround is the highest. This may be explained in light of the argument presented earlier. That is, the advection in the tailings is less when the permeability of the pervious surround is high and hence the rate of contaminant release out of the tailings due to advection is slower. It should be noted that a significant portion of the peak concentration may be attributed to the initial mass present in the sand layer due to the discretization and linear interpolation used by the finite element method (discussed in section 2.4). Since the seepage velocity in the sand is lower when the pervious surround permeability is higher, it takes a greater amount of time to flush out the initial solute mass in the sand layer resulting in a lower peak concentration since this mass is released over a longer period of time.

- The time at which the peak solute concentration has reached the observation point is seen to be shifted to an earlier time, compared with the E-8-4-2-5 scenario, as the permeability of the pervious surround is lowered. This trend then reverses as the permeability of the pervious surround continues to decrease. The dashed line connects the peak solute concentration points for the different scenarios that confirm this observation. This behavior may be understood in light of three time intervals. The first time interval is the time during which solute concentration is going to build up in the sand layer and reach its maximum at the downgradient edge of the tailings. The second time is the time which the solute will take to cross both the sand and the pervious surround layers to reach the downgradient host rock. And the third time interval is the time to reach the observation point (700, 500) in the host rock. Since the thicknesses of the different layers are the same for the six scenarios, it is the magnitude of the velocity that should explain the aforementioned behavior. Velocity profiles and flow net diagrams give an explanation to the relative duration of each interval for the different scenarios. As has been mentioned earlier, when the pervious surround permeability is higher, and hence the velocity in the sand layer is lower, it will take a greater time for the solute to reach the downgradient edge of the tailings. So, it may be concluded that the higher the pervious surround permeability the longer this duration will be. The second interval is relatively small because the distance the solute will travel is small. The

third time interval, the travel time in the host rock, is shorter the higher the pervious surround permeability. This is obvious as the average x-component velocity in the host rock is higher the higher the pervious surround permeability. Hence, the observed behavior in the time to reach the peak concentrations at (700, 500) can be explained based on these three time intervals.

### **2.5.2.3 Evolution of mass remaining in the domain.**

Figure 2.30 shows the evolution of the mass remaining in the domain for the different scenarios. From this figure it is apparent that while all the mass has been flushed away from the domain in approximately 70,000 years for the scenario E-8-4-4-5 almost 50% of the mass still remains in the domain for the scenario E-8-4-2-5.

### **2.5.3 Impact of dispersivity.**

All the previous discussions have been made on the assumption that the values of dispersivity of the pervious surround in all the scenarios are the same. Dispersivity, despite the fact that it is a scale dependent property, is a macroscopic property of porous media, which means that its values should depend on the characteristics of the medium. The effects of dispersivity would result in the concentration profiles to be more dispersed or concentrated, and also impact the value of the maximum solute concentration as the plume moves. In this study, dispersivity effects will be discussed only in reference to the base

scenario, (E-8-4-2-5). No flow variations will result upon changing the dispersion coefficients. So, the effects of dispersivity will only impact solute transport. Five combinations of longitudinal and transverse dispersivities have been tested, as identified in Table 2.2.

It is expected that no differences in concentration profiles will occur in the tailings for the different dispersivities, because of the small magnitude of the velocities. However, on examining the concentration history at the point (700, 500), Fig. 2.31, it may be noticed that the maximum concentration has dropped from approximately 0.028 to 0.017 for scenarios with the lowest and higher dispersivities, respectively. The higher dispersivities cause the solute to disperse in the x and y direction and hence reduce the peak concentration.

Table 2.2 Values of dispersivities of the different cases.

	Case I, Base case	Case II	Case III	Case IV	Case V
$\alpha_x, m$	1.0	0.5	2.0	5.0	10.0
$\alpha_y, m$	0.1	0.05	0.2	0.5	1.0
$\alpha_z, m$	0.1	0.05	0.2	0.5	1.0

#### 2.5.4 Impact of sand layer permeability.

The values of the hydraulic conductivity of the sand layer that were considered are  $10^{-4}$ ,  $10^{-5}$ ,  $10^{-6}$ ,  $10^{-7}$ , and  $10^{-8}$  m/s, with the latter equal to that of

the tailings. It is important to mention that the values of hydraulic conductivity assigned to this layer may be smaller than that of typical sand, so in these cases, sand refers only to the name of the layer. The study on the effects of the sand layer permeability has shown interesting results in both fluid flow and solute transport as follows:

#### **2.5.4.1 Flow hydrodynamics.**

Figures 2.32-36 show flow nets for the five scenarios. They appear to be identical and this is justified given the hydraulic gradient is similar for all the scenarios as will be discussed later. They also indicate that groundwater flow is drawn towards the TMF for all scenarios with the bulk flow through the pervious surround and very little entering the tailings. Figures 2.37-41 depict the behavior of those flow lines moving through the tailings as they exit the tailings into the sand layer. They show, however, that the flow patterns within the sand and the pervious surround layers vary considerably as the permeability of the sand layer is altered. This was shown to impact solute transport as will be explained later.

Consider the flow line passing through the lower boundary of the domain. For reference, consider another flow line that follows the sand/tailings interface at the upper most point. The flow lines between these two reference flow lines are those moving through the tailings. Figure 2.37 shows the flow lines as they exit the tailings for the scenario E-8-4-2-5. This figure indicates that groundwater flow exiting the tailings remains largely close to the tailings-sand interface due to the fact that most of the flows are taking place in the pervious surround as well as

the sand layer and are bypassing the tailings. As a result, the flow lines leaving the tailings do not move across the sand layer until they approach the lower boundary on the downgradient edge of the TMF. As the permeability of the sand layer is decreased and approaches the permeability of the tailings, a greater fraction of the flow within the sand layer has migrated through the tailings. For the scenario in which the sand layer has a permeability equal to that of the tailings (E-8-8-2-5, Fig. 2.41) the flow lines within the tailings continue straight through the sand layer, since there is no permeability contrast, and enter the pervious surround layer where they closely follow the sand/surround interface. These flow characteristics impact the peak concentrations in the downgradient host rock and the mass flux exiting the downgradient boundary. Figure 2.42 collects the above-mentioned arguments.

As mentioned earlier, the hydraulic head profiles for all the scenarios at the plane  $y=500$  show identical behavior, as shown in Fig.2.43. Moreover, the seepage velocity in the sand layer for the different scenarios is directly related to the hydraulic conductivity of the sand. Fig. 2.44 shows a comparison between the x-component of the velocity at the plane  $x=450$ . As expected, the seepage velocity for the scenario E-8-4-2-5 is four orders of magnitude greater than for the scenario E-8-8-2-5.

#### **2.5.4.2 Solute transport.**

Again interesting results have been noticed. Figures 2.45–2.48 show the concentration profiles for the different scenarios at different times at the plane

$y=500$ . It may be noticed that the concentration profiles in the tailings are almost identical for all the scenarios. This is because the seepage velocities in the tailings are similar for all the scenarios. However, on comparing these profiles after 95129 years was elapsed, one may notice that there are slight differences as shown in Fig. 2.49. The same figure has been reproduced for the two extreme scenarios (E-8-4-2-5 and E-8-8-2-4) in Fig. 2.50. The small difference in the concentration profile indicates that slightly more mass was released from the tailings for the scenario E-8-4-2-5. However, since the seepage velocities in the tailings appear identical, Fig 2.44, this difference in solute mass in the tailings may be attributed to the diffusion mechanism, which is controlled by the gradient in concentrations at the tailing-sand interface. When the sand layer permeability is high, greater flow occurs in this layer in comparison to lower permeability scenarios, Fig.2.44. This increased flow causes the solute to be transported out of this layer more quickly and hence maintains a lower concentration adjacent to the tailings. This increases the diffusive flux out of the tailings, which also explains the results presented in Figs. 2.51 and 2.52. Figures 2.51 and 2.52 show the concentration profiles for the different scenarios at the plane  $x=450$  after 951 and 12684 years, respectively. It is apparent from these figures that solute concentration in the sand layer is higher for the lower permeability sand scenarios, which may, again, be attributed to the diffusion mechanism.

However, the solute concentration history at a point downgradient of the pit, (700,500), Fig. 2.53, shows different patterns for the different scenarios, and the following points may be noticed:

- The time at which the observation point will begin to detect the solute is different, being late when the permeability is small. This may be explained in light of the seepage velocity in the sand layer, which is smaller the smaller the permeability. Hence we expect the solute to take more time to pass through the sand layer when the permeability is small than it takes when the permeability is high.
- The maximum concentration at the observation point (700, 500) is higher the higher the sand layer permeability. This is interesting in light of the almost identical behavior of solute concentration profiles for all the scenarios in the tailings due to the identical seepage velocity. The reason for this is largely attributed to the initial mass in the sand layer due to discretization discussed earlier in section 2.4, and the groundwater flow in the sand layer. It has been shown that the seepage velocity in the sand layer increases with an increase in the sand layer permeability and hence the flushing effect of this initial mass in the sand would be more pronounced when the sand layer permeability is higher. Moreover, more mass will be released from the tailings via diffusion when the sand layer permeability is higher as explained earlier. This mass, though small, contributes largely to the maximum concentration behavior at the observation point. Also, the way the contaminant is going to behave as it is released from the tailings is expected to affect the peak concentration at the observation point (700, 500). In light of the argument presented previously; for the high sand permeability scenario, example is E-8-4-2-5,

as the solute is released from the tailings it will be carried directly away by the relatively higher groundwater flow in the sand compared with that in the tailings. The two mechanisms of solute transport, advection and dispersion, are now significant. Most of the solute will continue moving within the sand layer and hence the concentration will continue to build up in the sand layer until it reaches the maximum at the downgradient edge of the tailings. As the permeability of the sand layer decreases, more streamlines are likely going to leave the sand layer to the pervious surround earlier resulting in more mass to migrate to the pervious surround and hence the solute will not build up in the sand layer to the same extent, and the concentration at the downgradient edge is likely going to be lower. For the scenario E-8-8-2-5, as the solute is released from the tailings it will first penetrate the sand layer until it reaches the pervious surround where it will encounter a large dilution in this layer resulting in the lowest maximum concentration at the observation point.

#### **2.5.4.3 Mass remaining and the rate of solute mass leaving the boundary.**

Figure 2.54 shows comparisons between the rate of solute release out of the domain for the scenarios E-8-4-2-5 and E-8-8-2-5 on a linear scale with time and Fig. 2.55 shows that comparison for the different scenarios on a logarithmic scale as well as the change with time of the mass remaining within the domain. Inspections of these figures indicate the initial jump in the rate of solute mass leaving the boundary when the permeability of the sand is higher. This may be

attributed to the initial mass in the sand due to discretization, which is a common problem in any numerical technique as discussed earlier in section 2.4. This mass, though small (a rough estimation of this mass indicates around 50 kg of solute initially in the sand), is largely responsible for the increased rate of mass leaving the boundary. Although this same initial mass would be present in the sand for all scenarios, the way this initial mass moves is responsible for the differences in the rate of solute mass leaving the boundary for the different scenarios. When this additional initial mass in the sand layer is flushed out, results from all the scenarios approach each other. However, because more mass has been released through diffusion when the sand layer permeability was higher, the mass flow rate curves apparently cross at a later time.

Based on the performance criteria mentioned in section 2.5.1, one may be able to state that the best scenario is the one where the sand layer permeability is very small, of the same order of magnitude as that of the tailings. This assumes that the initial concentrations within the sand layer are zero. The impact of nonzero scenarios is provided in the following section. The assumed initial concentration in the sand layer will impact the maximum concentration and solute flux. If the sand layer were to have permeability close to that of the tailings, the sand layer would act as a low permeability barrier, which would delay the consolidation of the tailings.

#### 2.5.4.4 Initial solute concentration in the sand layer.

The initial solute concentration in the sand layer has been assumed to be equal to zero for all previous simulations. However, in reality, and based on the post decommissioning intentions, the initial concentration in the sand layer might not be zero. The decommissioning processes involve stopping of dewatering pumps and allowing the water table to rise to its normal level. During this process, the initial solute concentration in the sand layer is likely going to be greater than zero. Three scenarios have been simulated in addition to the base scenario. These include simulations with the initial solute concentrations in the sand layer equal to 0.25, 0.5, and 1.0 kg/m<sup>3</sup>.

- Figures 2.56-2.58 show concentration profiles for the different scenarios at the plane  $y=500$ . It may be noticed that, at early times, the higher seepage velocity in the sand layer acts to flush the contaminant out of this layer so that at later times, the concentration profiles are similar for all three scenarios after all the initial mass in the sand was flushed out, as shown in Fig. 2.59.

Figures 2.60-2.62 shows concentration profiles at the plane  $x=450$ . One may notice the following:

- The concentration in the sand layer drops with time due to the flushing that results from the high seepage velocities.

- The concentration adjacent to the tailings at this plane is higher than the initial concentration at early time due to the mass release into the sand mainly via diffusion.

A comparison of concentration profiles at the plane  $x=450$  is shown in Fig. 2.63. The concentration profiles for the different scenarios coincide with the zero initial concentration scenario after approximately 60 years when all the initial mass in the sand layer has flushed out.

Figure 2.64 shows the concentration history at the point (700, 500) for the different scenarios. It is apparent that the maximum concentration at the observation point will be for the case when the initial solute concentration in the sand layer is set to 1.0. Moreover, the time at which this maximum concentration is achieved is almost the same for the three cases where the initial concentration in the sand is greater than zero, while it is shifted to a later time for the zero initial concentration scenario. There may be two reasons that explain this behavior; the first is that for the scenarios where the initial solute concentration in the sand is not zero, an initial mass is introduced into the high permeability gravel layer as a result of the numerical formulation (as explained earlier) and hence solute reaches the downgradient point earlier than the zero initial concentration scenario which does not have such an initial mass in the gravel. Secondly, solute in the sand layer will instantly utilize the higher flow in the pervious surround as compared with the zero initial concentration scenario in which the solute would need to cross the sand layer.

Figure 2.65 shows mass remaining and the rate of mass leaving the boundary. It is apparent that the initial mass is different because of the additional mass in the sand layer. Moreover, the mass of solute in the sand layer drops rapidly, leaving the mass in the tailings the same as that in the zero initial concentration scenario after approximately 500 years. The rate of solute mass leaving the boundary shows a maximum when the initial concentration in the sand was  $1.0 \text{ kg/m}^3$ , as expected.

#### **2.5.4.5 Sand versus no sand.**

It is interesting to compare the scenario where the sand layer permeability is the same as that of the tailings, i.e.,  $10^{-8} \text{ m/s}$ , with an initial solute concentration of 1.0, which may be regarded as the no sand scenario, with the base scenario, E-8-4-2-5, with different initial solute concentrations in the sand layer.

Figure 2.66 shows the concentration history at the point (700, 500) for the different initial solute concentration in the sand (E-8-4-2-5) and the no-sand scenarios (E-8-8-2-5). The following points may be noticed:

- It is apparent that the peak solute concentration for the no-sand scenario at the observation point is a little higher than the zero initial concentration scenario. This is attributed again to the flushing of the initial mass due to discretization, which will be flushed out at a higher rate for the no-sand scenario compared with the zero initial concentration scenario. It is,

however, less than the non-zero initial concentration scenarios because of the larger mass in the sand layer.

- Moreover, the time at which the concentration at the observation point is maximum is now earlier than the zero initial concentration scenario due to the fact that for the no sand scenario, solute is released instantly utilizing the higher flow in the pervious surround region and hence reaches the downgradient point earlier.
- On comparing the mass remaining and the rate of mass leaving the boundary, Fig. 2.67, one may be able to notice that no flushing effect is encountered for the no-sand scenario. Moreover, one may notice that the maximum mass flow rate for the no-sand scenario is a little higher than the zero initial concentration scenario. This, as explained earlier, is due to the initial solute mass due to desorption, which this time is in the pervious surround rather than in the sand layer that would be flushed out at a higher rate because of the higher seepage velocity in the pervious surround compared with that in the sand layer. It is, however, lower than the scenarios where the initial concentration in the sand was not zero. This is because of the large initial mass in the sand layer.

This could lead us to the conclusion that the sand layer would be effective in reducing the rate of solute mass leaving the tailings only when the initial concentration is close to zero. On the other hand, the no sand scenario has shown to be comparable to the zero concentration scenario, only if we manage to minimize the initial release of the contaminant during the decommissioning

process, which has not been accounted for in the present simulation. This transient release could be significant in that it may increase the rate of mass release above that shown in Fig. 2.67.

## **2.6 Summary**

The parametric study has shown the complexity of the system. Groundwater flow and solute transport have shown to be impacted by the contrast in permeability between different zones.

It has been shown that the initial solute concentration in the tailings needs to be accurately modeled in order to correctly predict the downgradient concentration and mass flux. The need for finer mesh especially in the vicinity of the interface boundaries between different zones to correctly simulate the sharp contrast in the initial mass and the properties of the different zones has been demonstrated.

The pervious surround has shown to minimize solute concentration downgradient as well as the mass flux out of the domain by making diffusion the dominant transport mechanism. This has been achieved through the reduction of advection in the tailings by two ways: the first is through lowering the permeability of the tailings; and the second is through lowering the hydraulic gradient across the tailings. The latter has been achieved by increasing the permeability of the pervious surround. The effectiveness of the pervious surround is more

pronounced when there is a large contrast in permeability between the pervious surround and the host rock.

The permeability of the sand layer was shown to impact groundwater flow and solute transport. The main feature of the sand layer permeability is the flushing that occurs in this layer, which was shown to greatly impact the downgradient concentration. The maximum downgradient concentrations and mass flux are directly related to the flushing out of initial mass present in the sand layer due to the selected discretization or due to the initial concentrations within the sand layer at decommissioning. The flushing is more pronounced when the sand layer permeability is higher. As the permeability of the sand layer decreases, the flushing effect in this layer declines resulting in lower downgradient concentrations and mass flux. Moreover, the initial solute concentrations in the sand layer at decommissioning have shown to have a significant impact on the downgradient concentrations and mass flux.

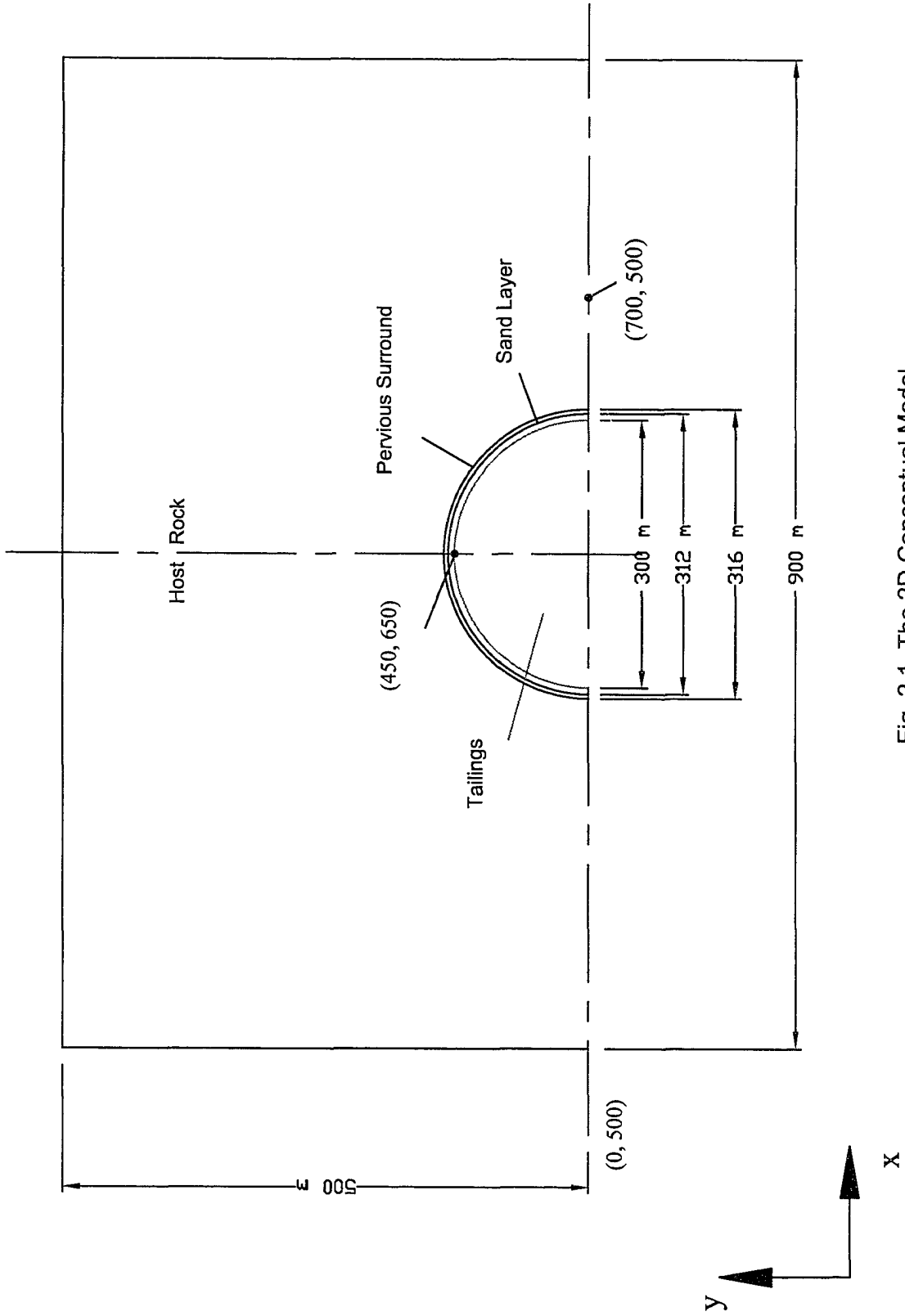


Fig. 2.1 The 2D Conceptual Model.

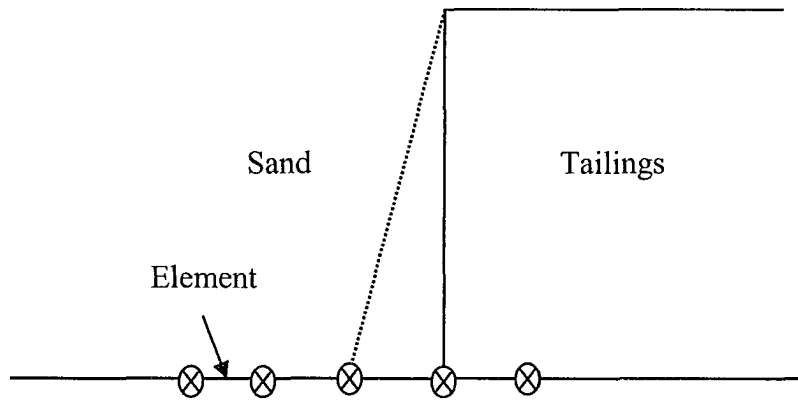


Fig. 2.2 Initial concentration at the sand-tailings interface for one-dimensional element.

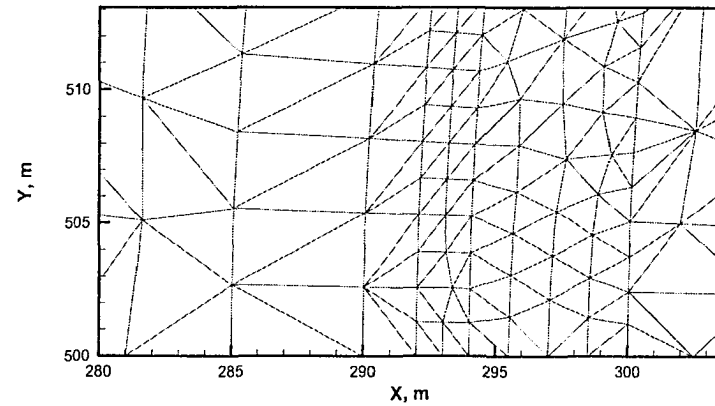


Fig. 2.3 Two blocks in the pervious surround.

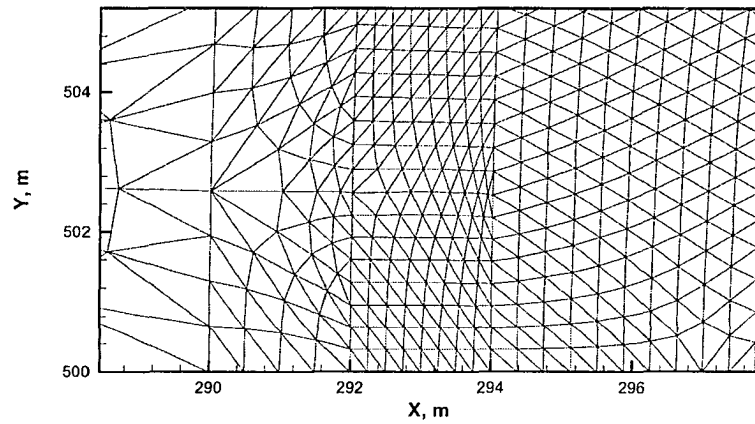


Fig. 2.4 Eight blocks in the pervious surround.

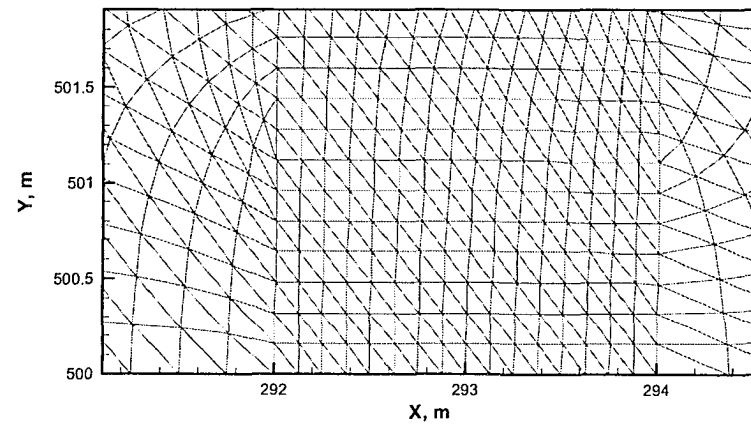


Fig. 2.5 Sixteen block in the pervious surround.

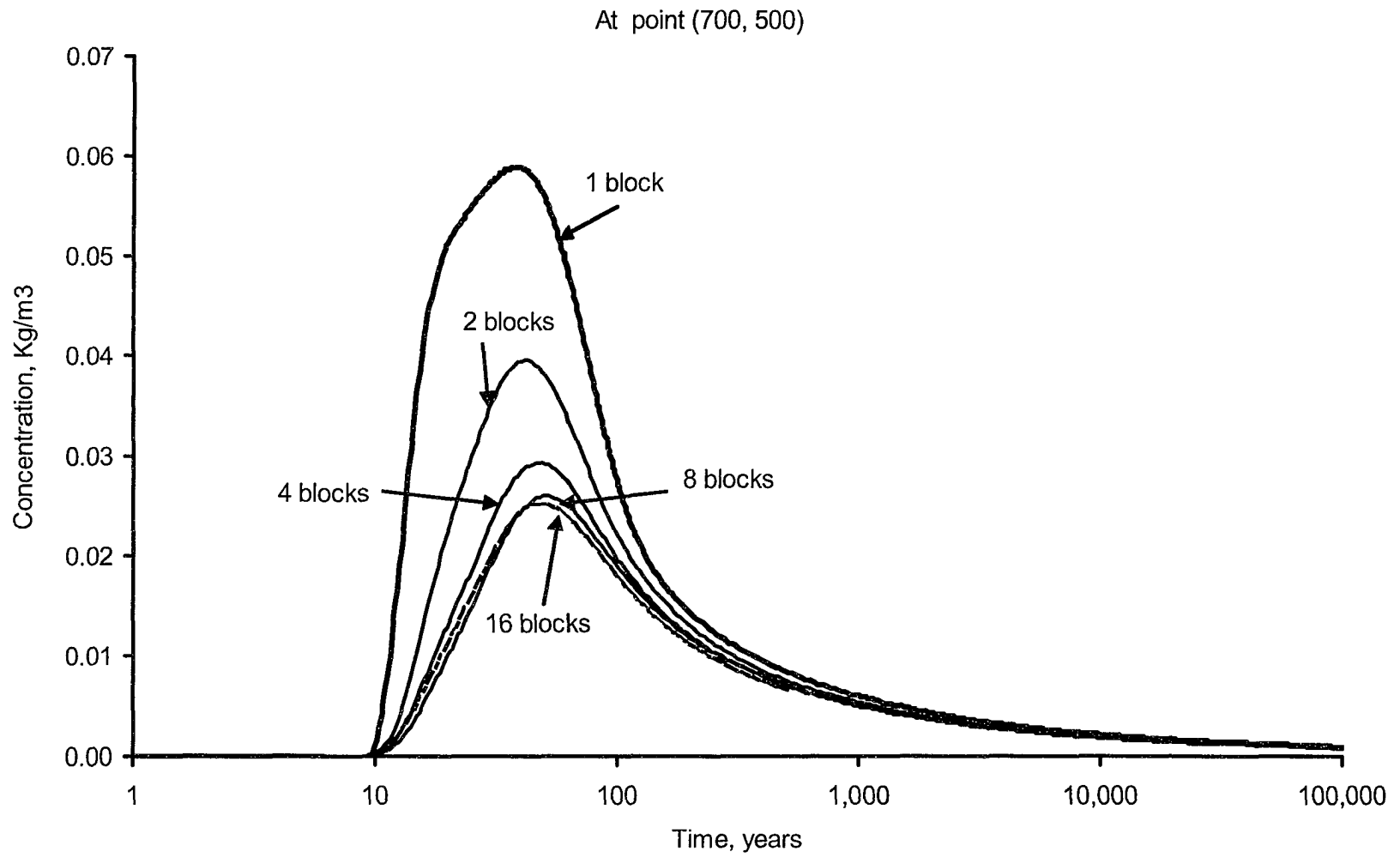


Fig. 2.6 Concentration history at the point (700, 500) for different discretization scenarios

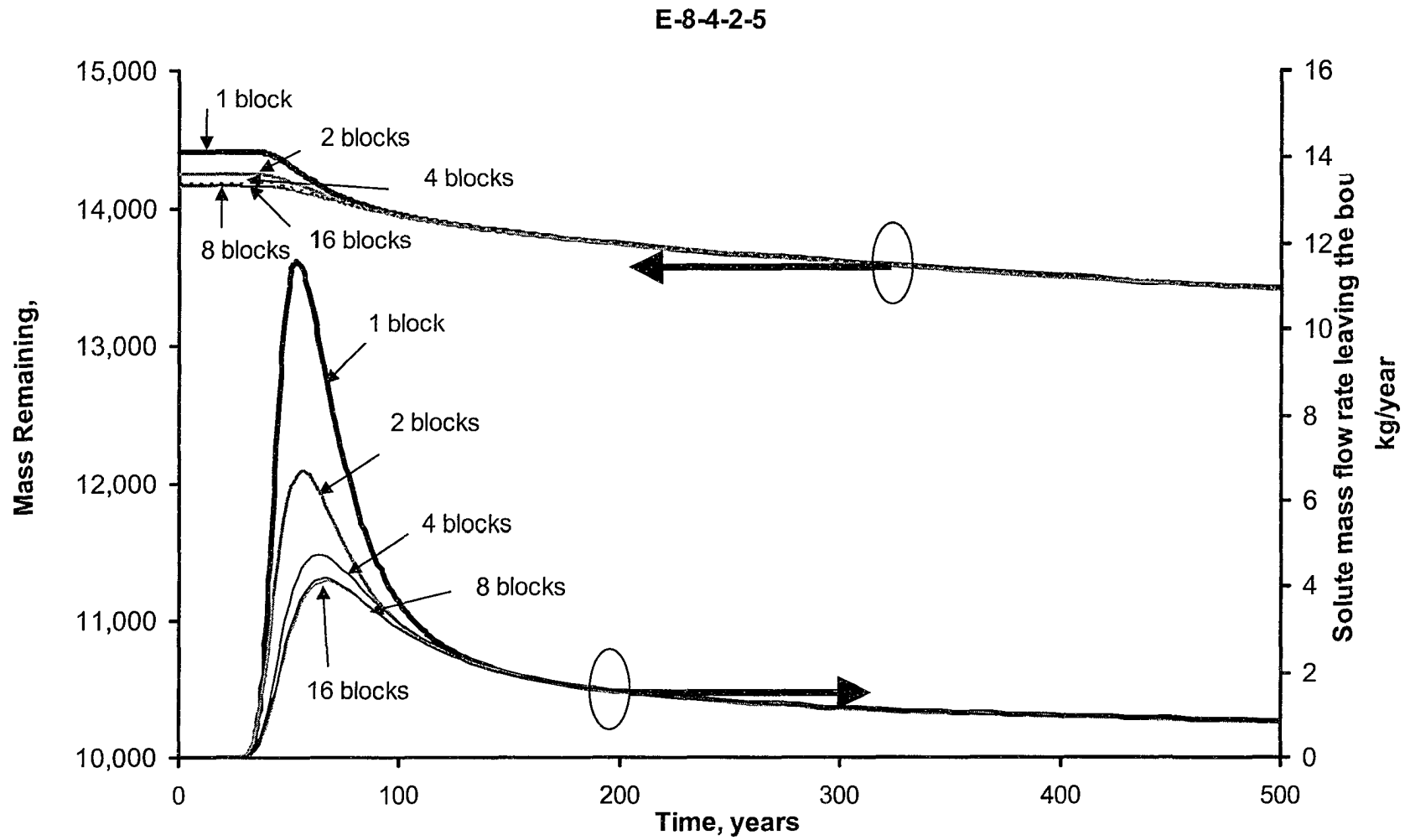


Fig. 2.7 Comparisons of the mass remaining and the rate of solute mass leaving the domain for different discretization scenarios.

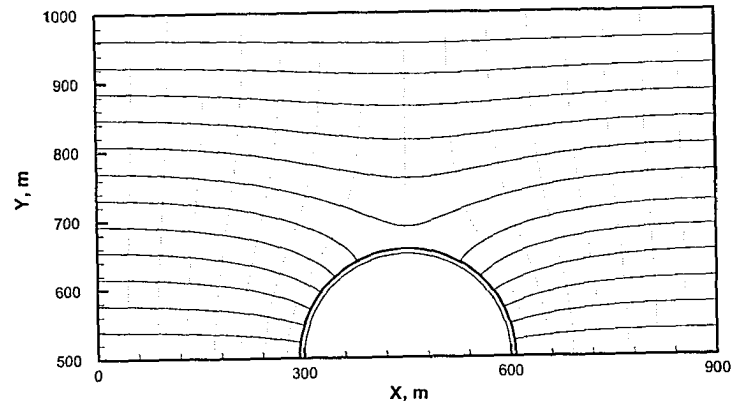


Fig. 2.8 Flow nets for the scenario E-8-4-2-5

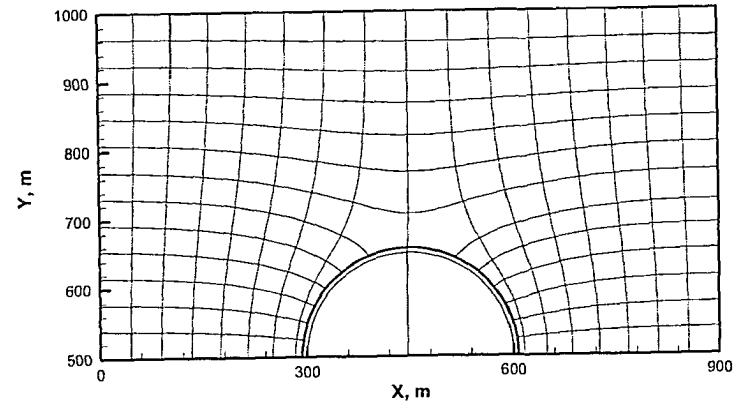


Fig. 2.9 Flow nets for the scenario E-8-4-2.25-5

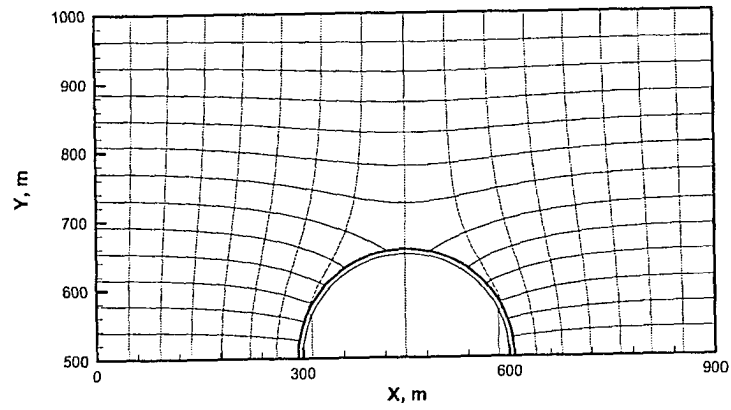


Fig. 2.10 Flow nets for the scenario E-8-4-2.5-5.

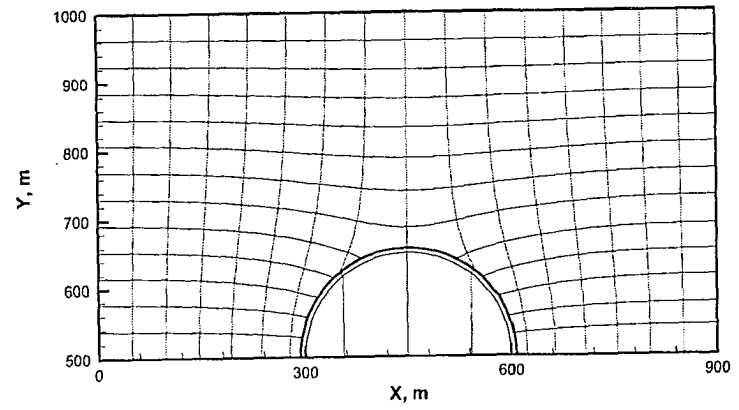


Fig. 2.11 Flow nets for the scenario E-8-4-2.75-5.

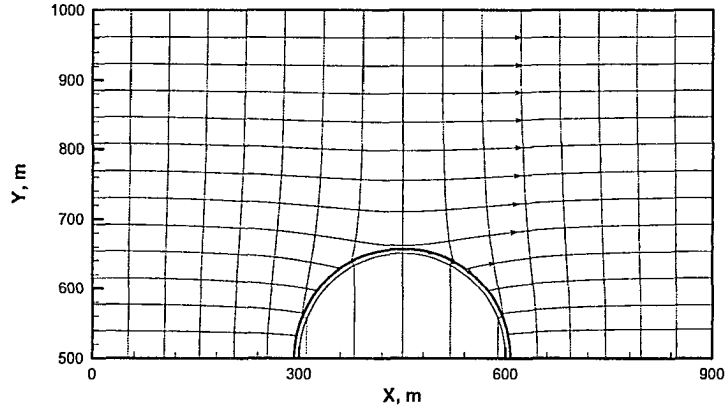


Fig. 2.12 Flow nets for the scenario E-8-4-3-5.

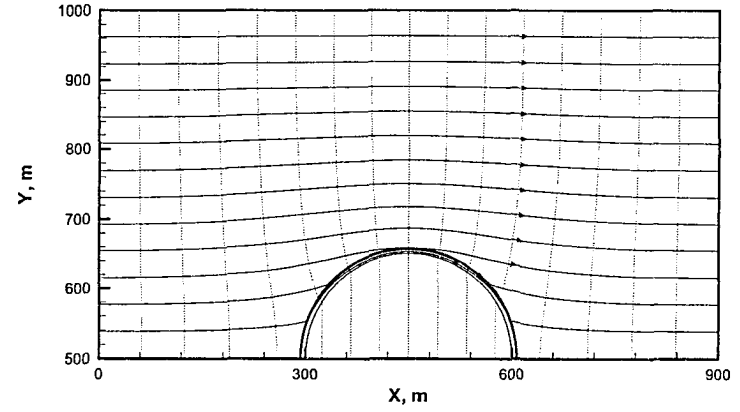


Fig. 2.13 Flow nets for the scenario E-8-4-4-5.

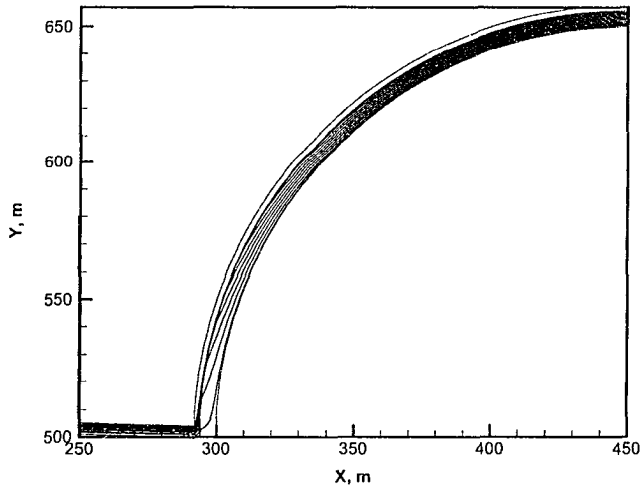


Fig. 2.14 Flow lines through the sand layer for the scenario E-8-4-2-5.

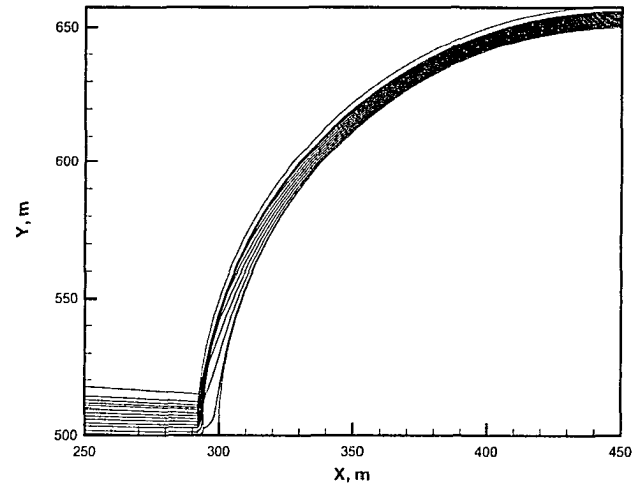


Fig. 2.15 Flow lines through the sand layer for the scenario E-8-4-2.5-5.

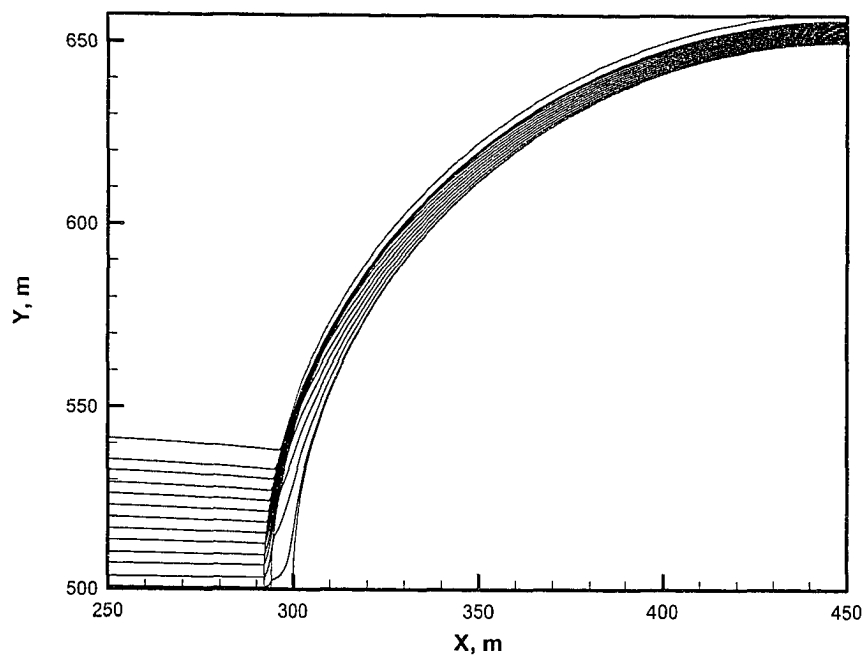


Fig. 2.16 Flow lines through the sand layer for the scenario E-8-4-3-5.

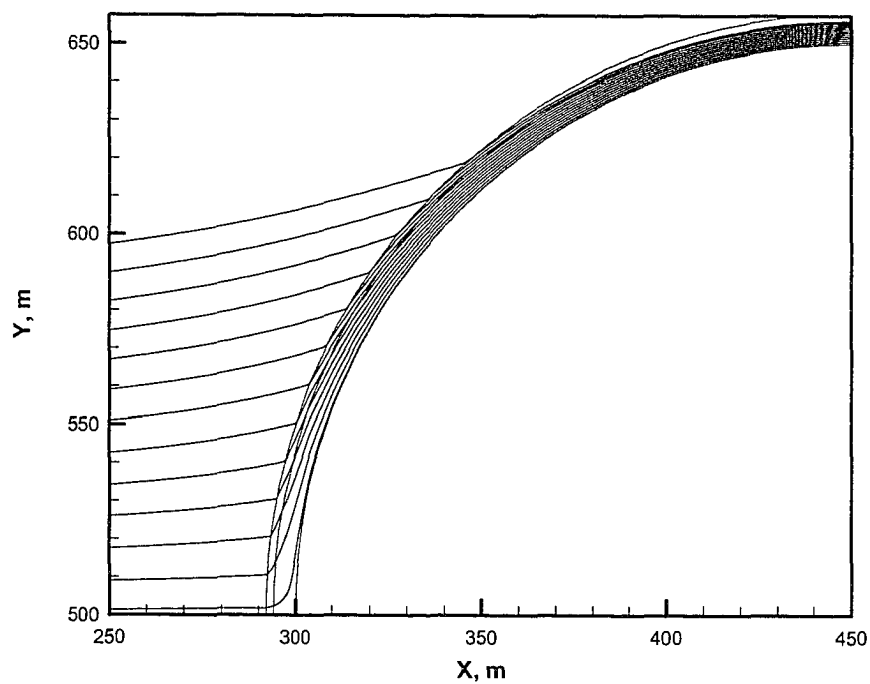


Fig.2.17 Flow lines through the sand layer for the scenario E-8-4-4-5.

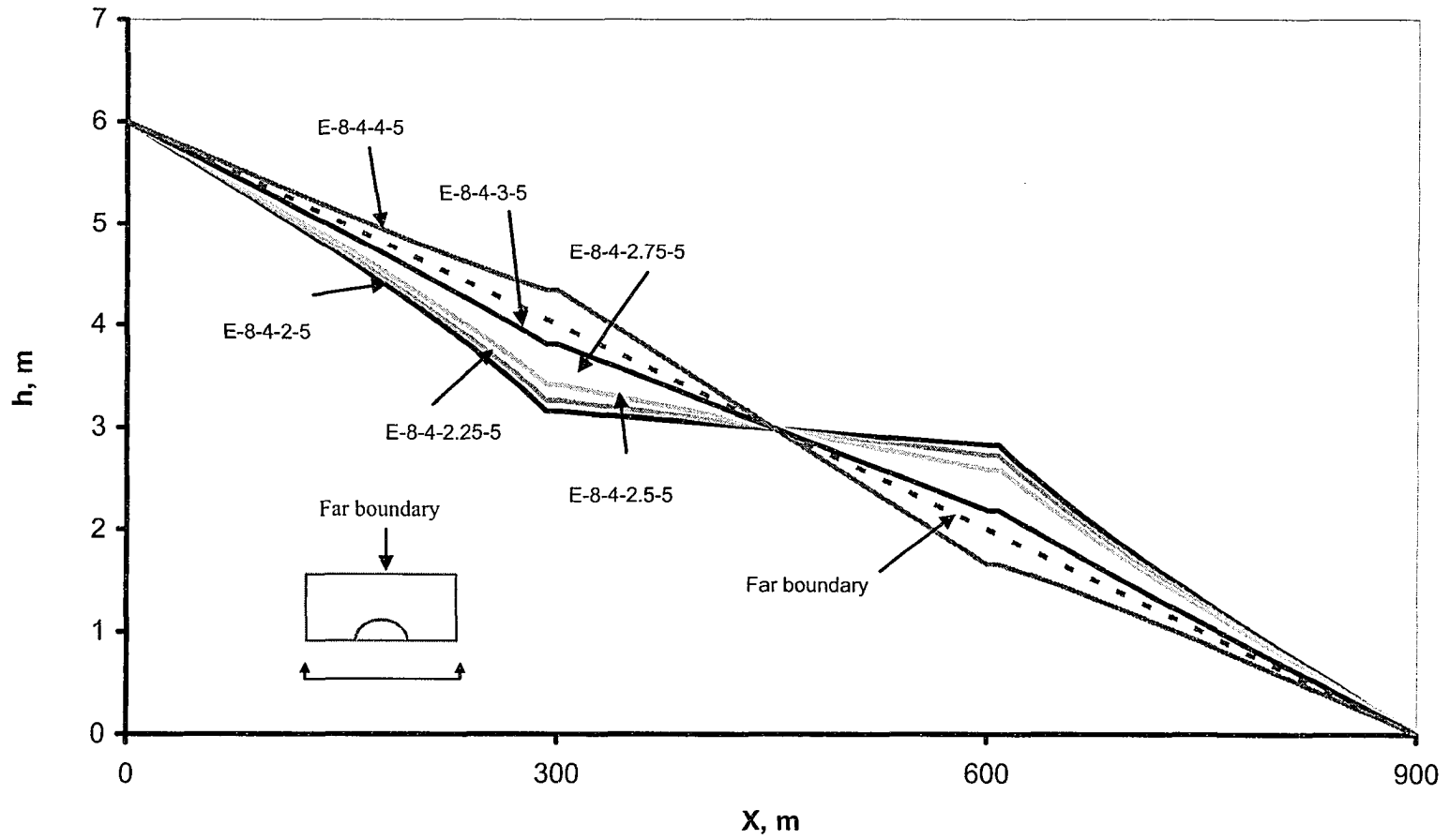


Fig. 2.18 Hydraulic head profiles across the TMF for all the scenarios.

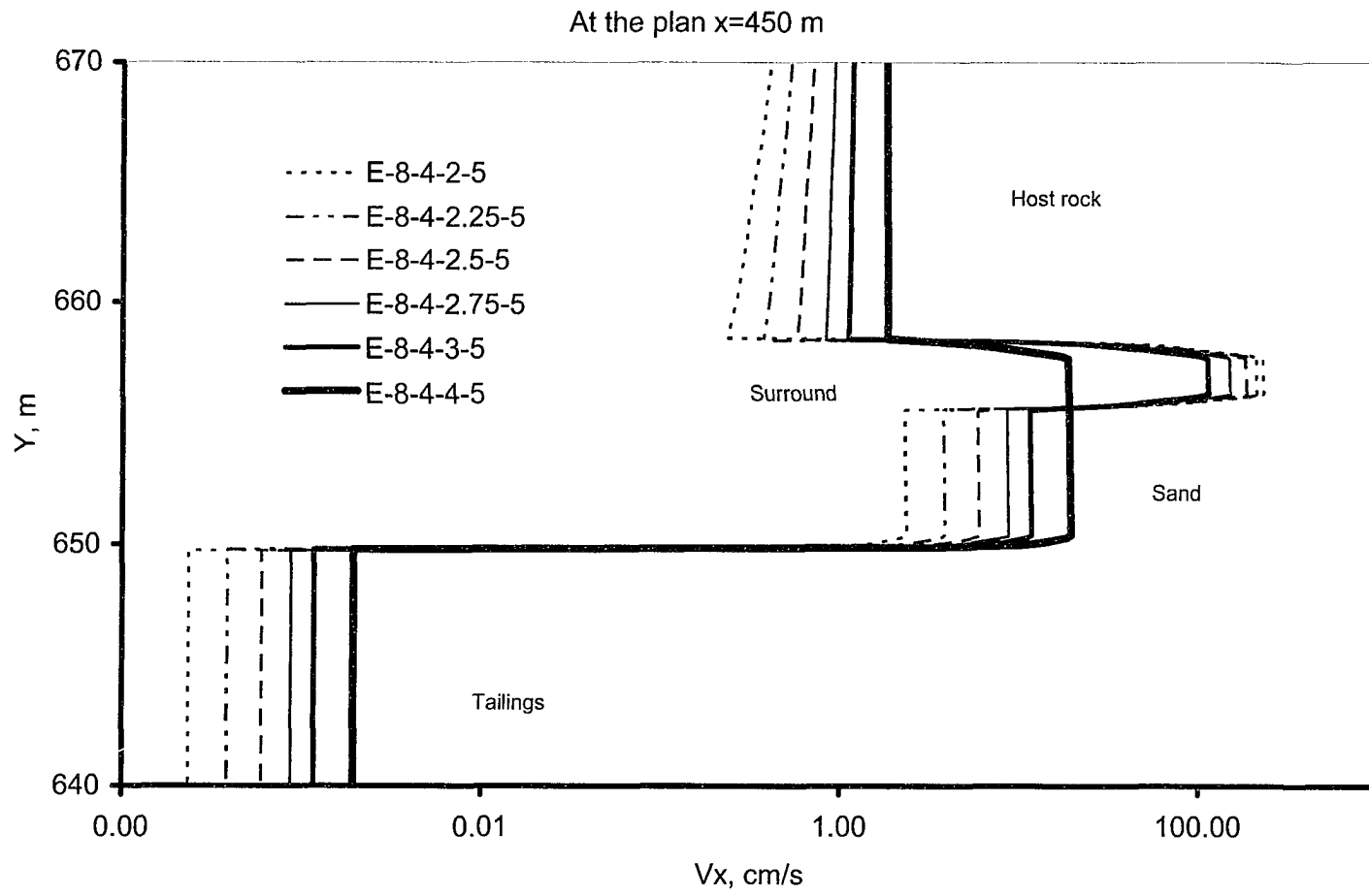


Fig. 2.19 X-component velocity profiles for the different scenarios at the plan x=450, a closer look.

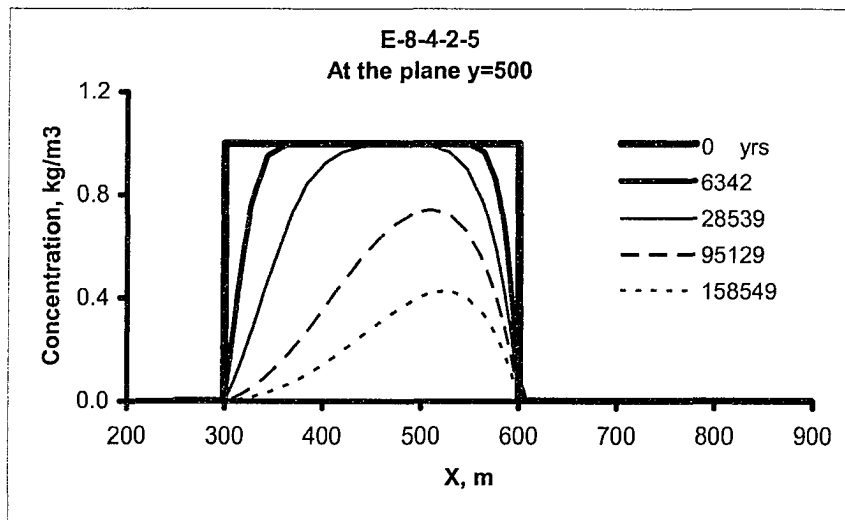


Fig. 2.20 Concentration profiles for the E-8-4-2-5 scenario at the plane  $y=500$ .

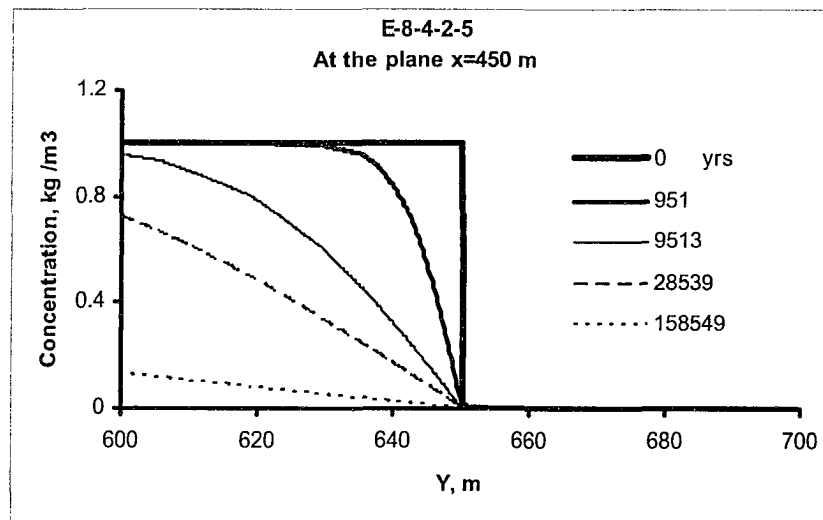


Fig. 2.21 Concentration profiles for the E-8-4-2-5 scenario at the plane  $x=450$ .

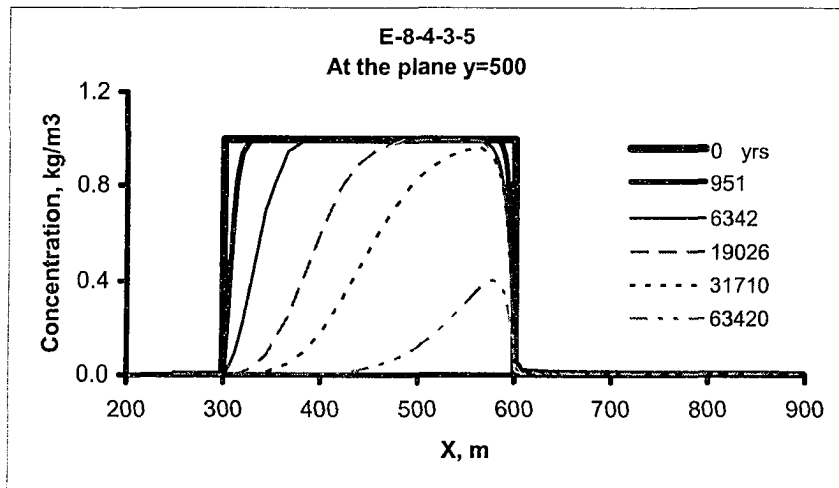


Fig. 2.22 Concentration profiles for the E-8-4-3-5 scenario at the plane  $y=500$ .

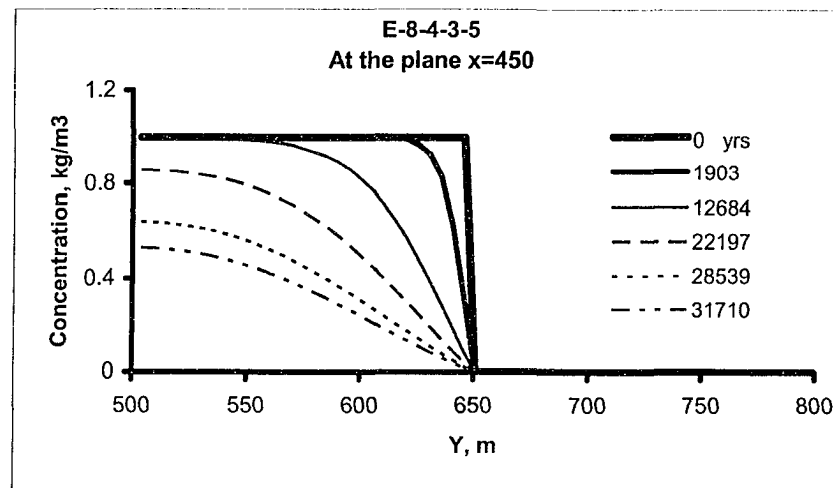


Fig. 2.23 Concentration profiles for the E-8-4-3-5 scenario at the plane  $x=450$ .

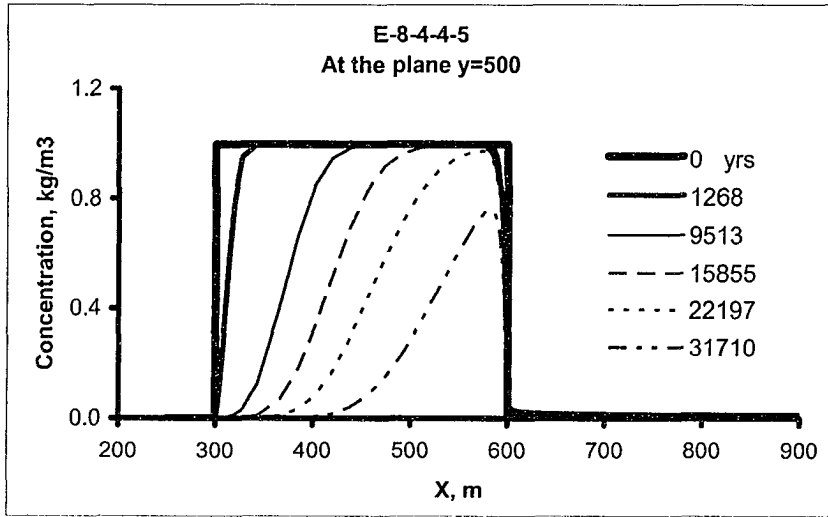


Fig. 2.24 Concentration profiles for the E-8-4-4-5 scenario at the plane  $y=500$ .

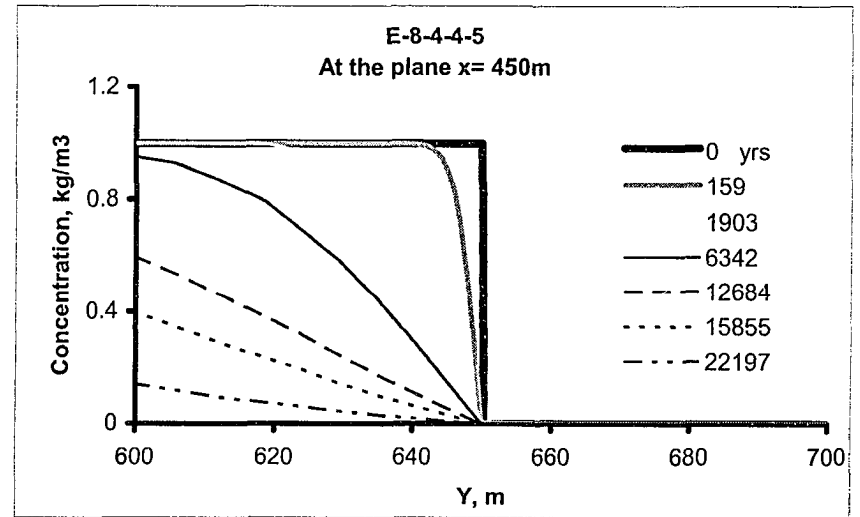


Fig. 2.25 Concentration profiles for the E-8-4-4-5 scenario at the plane  $x=450$ .

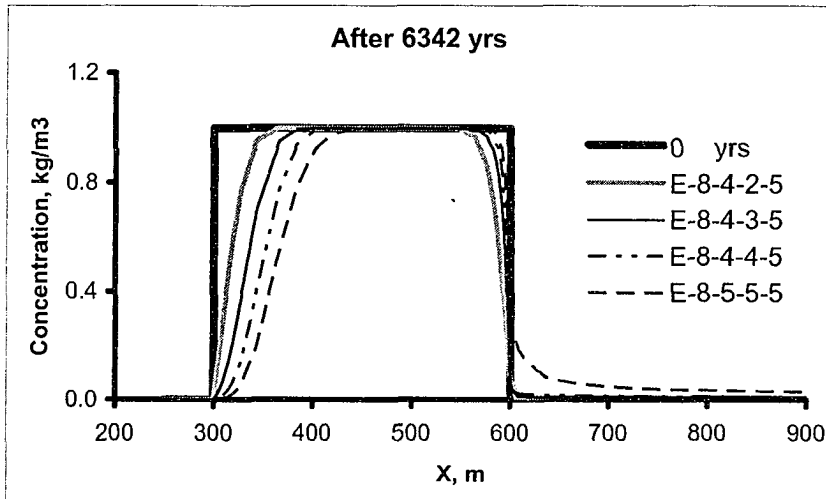


Fig. 2.26 Comparison of concentration profiles for all the scenarios at the plane  $y=500$  after 6342 years.

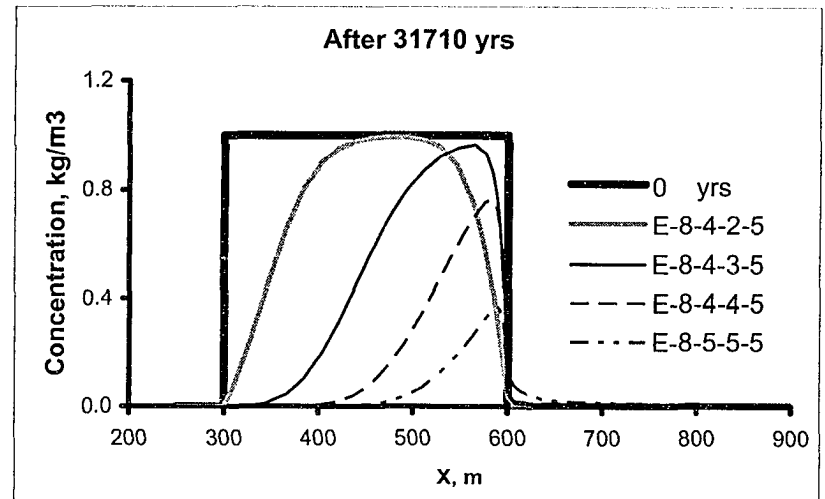


Fig. 2.27 Comparison of concentration profiles for all the scenarios at the plane  $y=500$  after 31710 years.

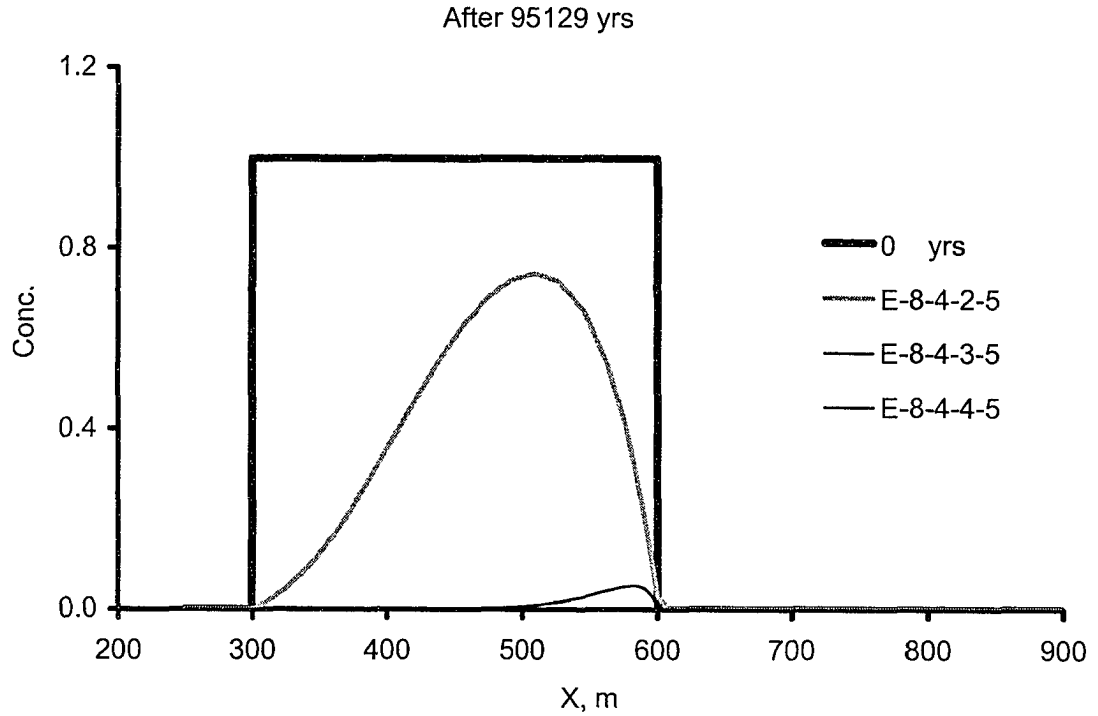


Fig. 2.28 Concentration profiles at the plane  $y=500$  after 95129 years for the different scenarios.

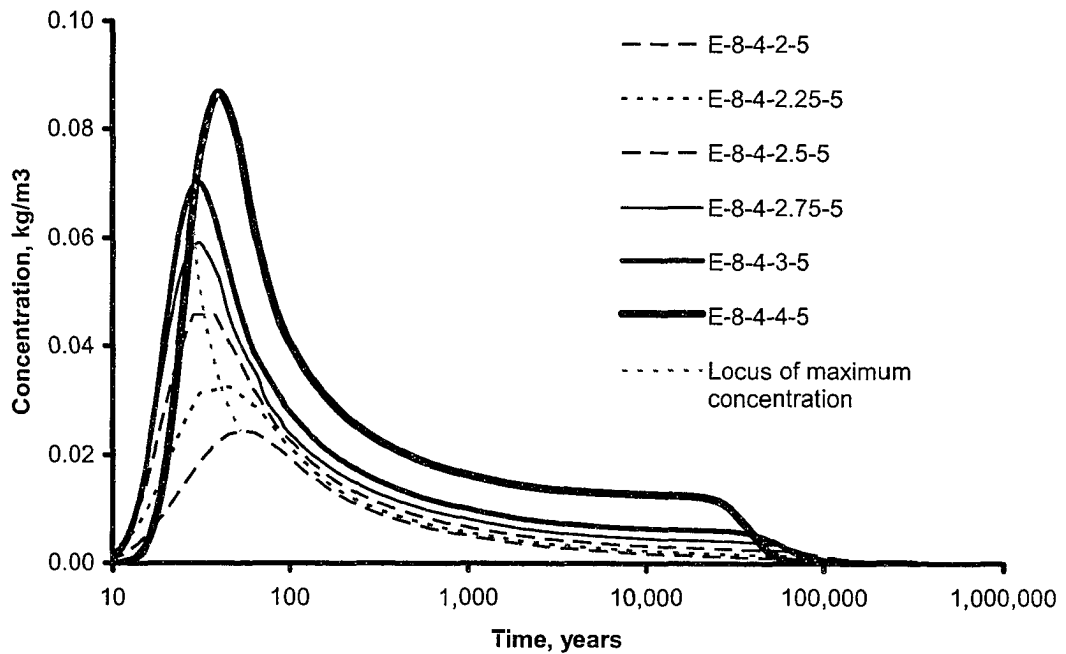


Fig. 2.29 Concentration history at the point  $(700, 500)$  for the different scenarios.

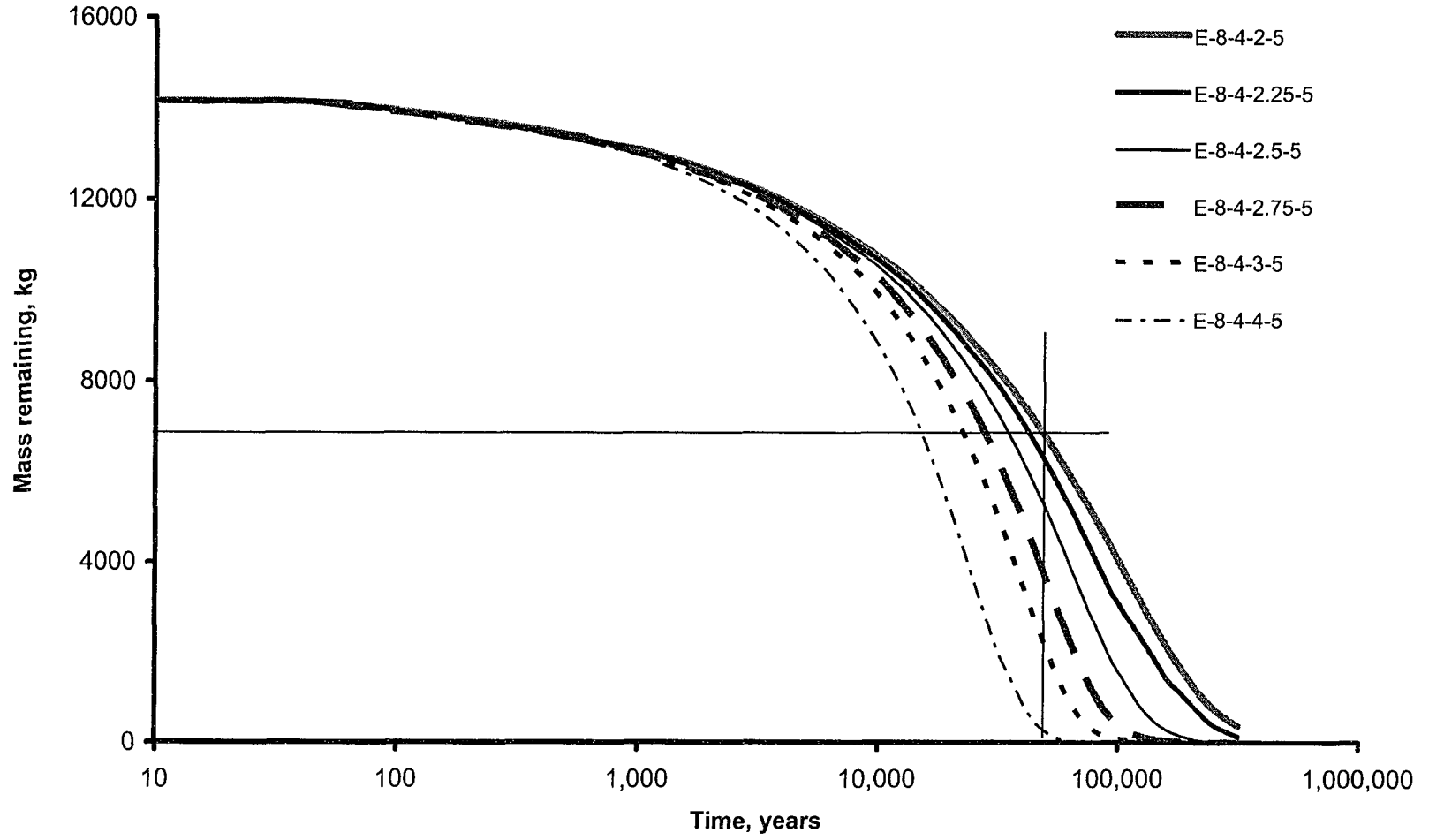


Fig. 2.30 Mass remaining in the domain for the different scenarios.

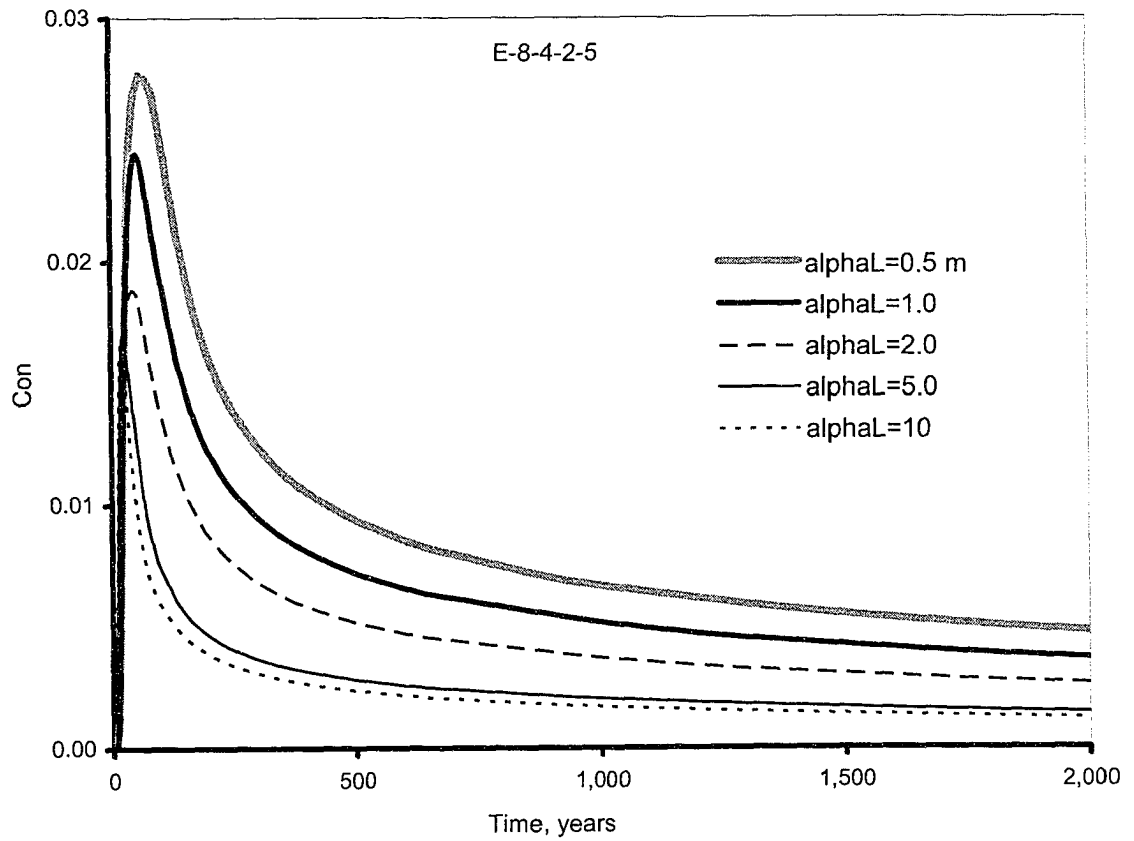


Fig. 2.31 Concentration history at the point (700, 500) for different dispersivity scenarios.

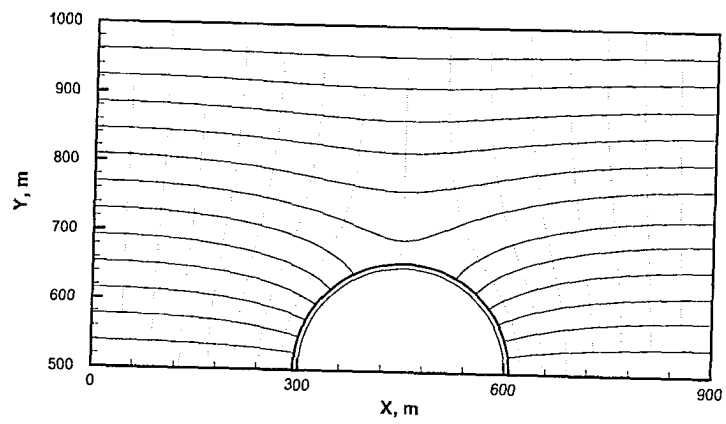


Fig. 2.32 Flow nets for the scenario E-8-4-2-5.

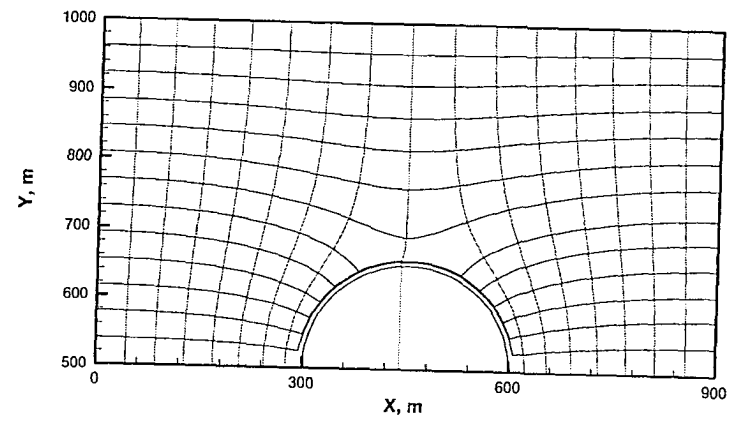


Fig. 2.33 Flow nets for the scenario E-8-5-2-5.

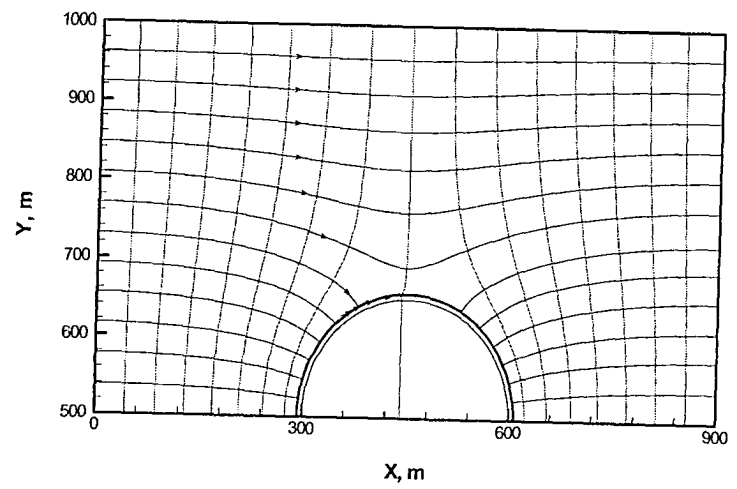


Fig. 2.34 Flow nets for the scenario E-8-6-2-5.

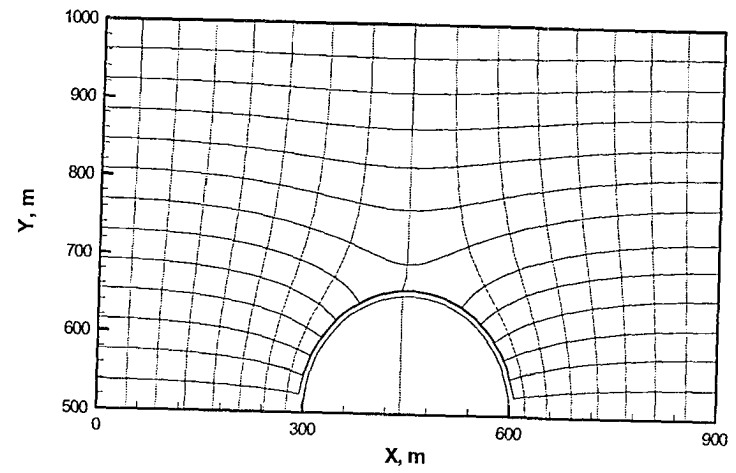


Fig. 2.35 Flow nets for the scenario E-8-7-2-5.

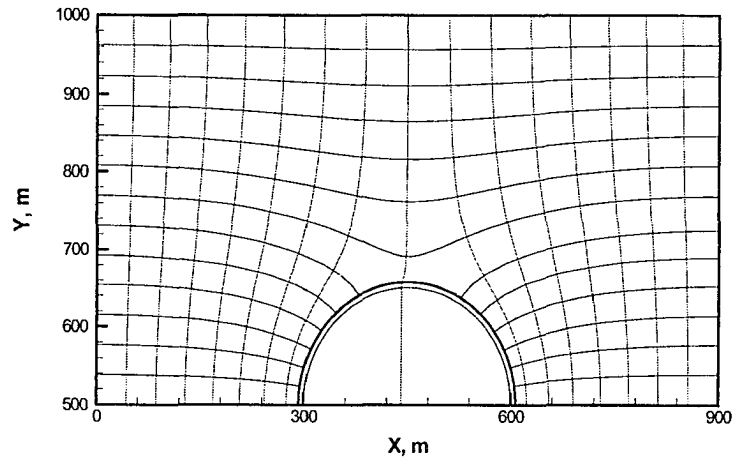


Fig. 2.36 Flow nets for the scenario E-8-8-2-4.

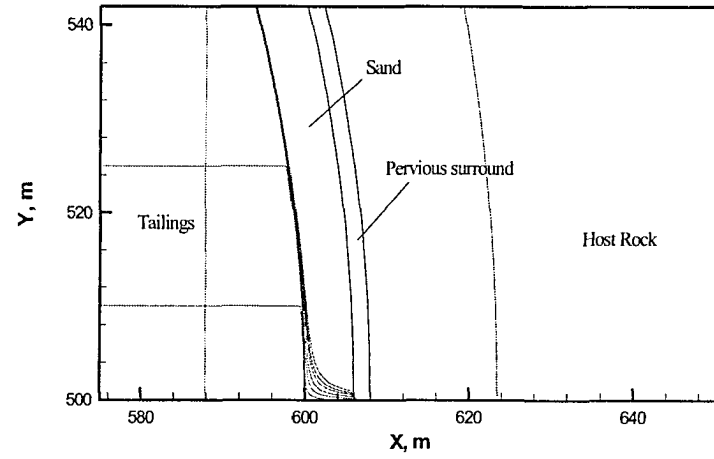


Fig. 2.37 Behaviour of flow lines that cross the tailings as they release to the sand for the scenario E-8-4-2-5, a closer look.

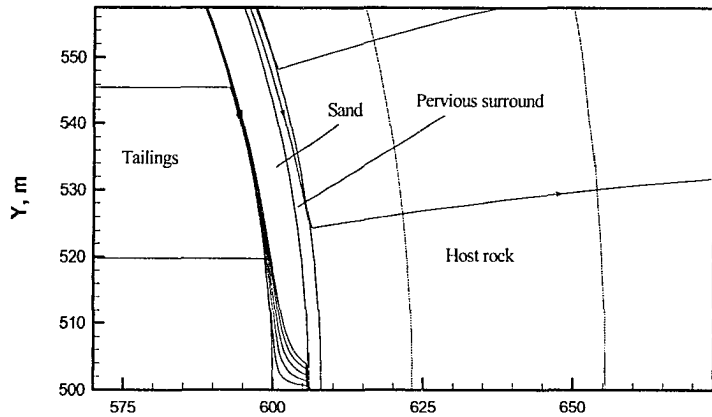


Fig. 2.38 Behaviour of flow lines that cross the tailings as they release to the sand for the scenario E-8-5-2-5, a closer look.

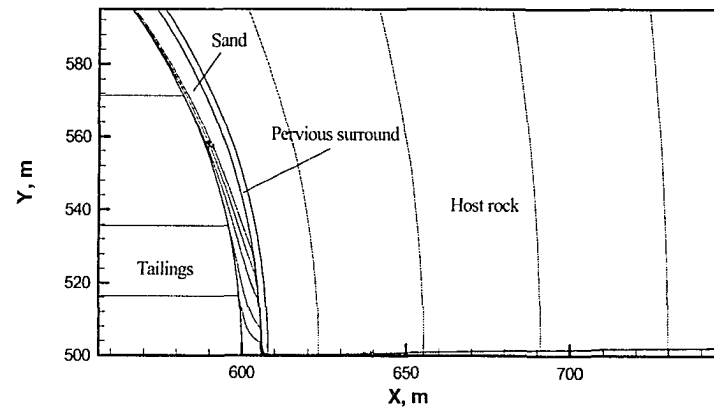


Fig. 2.39 Behaviour of flow lines that cross the tailings as they release to the sand for the scenario E-8-6-2-5, a closer look.

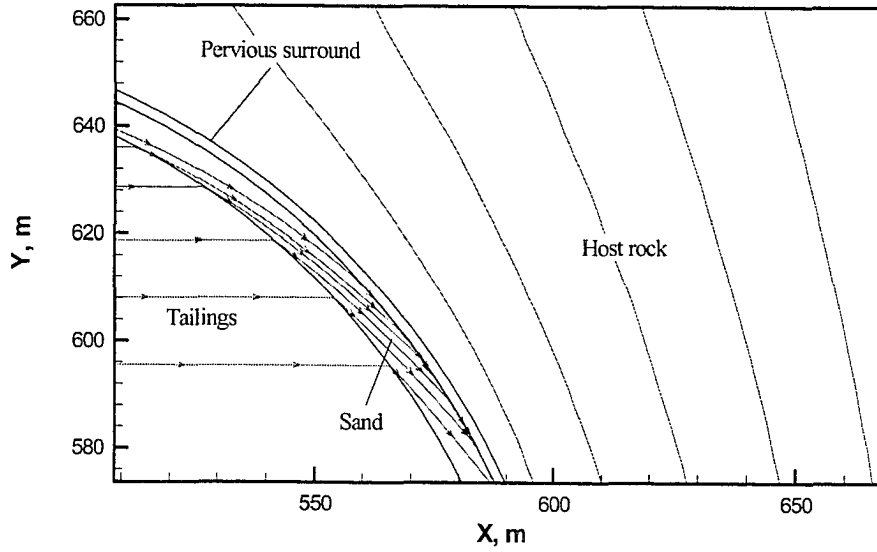


Fig. 2.40 Behaviour of flow lines that cross the tailings as they release to the sand for the scenario E-8-7-2-5, a closer look.

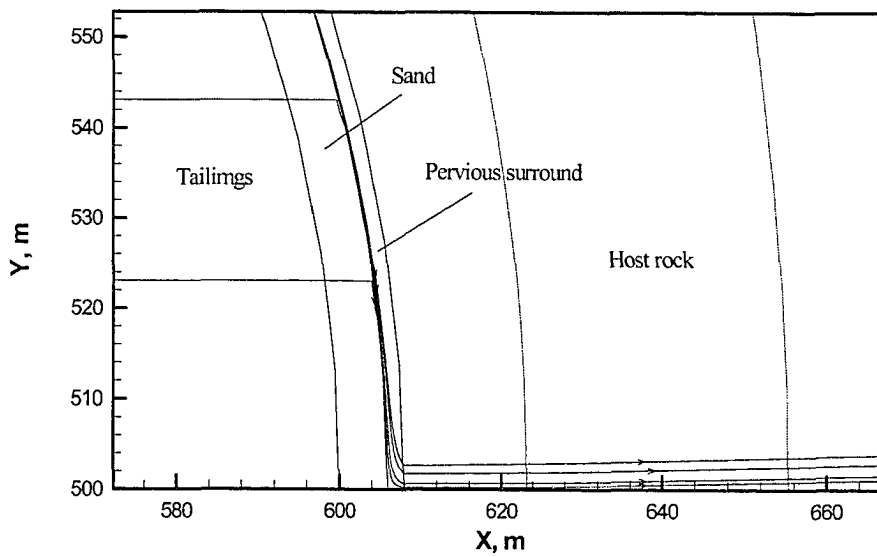


Fig. 2.41 Behaviour of flow lines that cross the tailings as they release to the sand for the scenario E-8-8-2-5, a closer look.

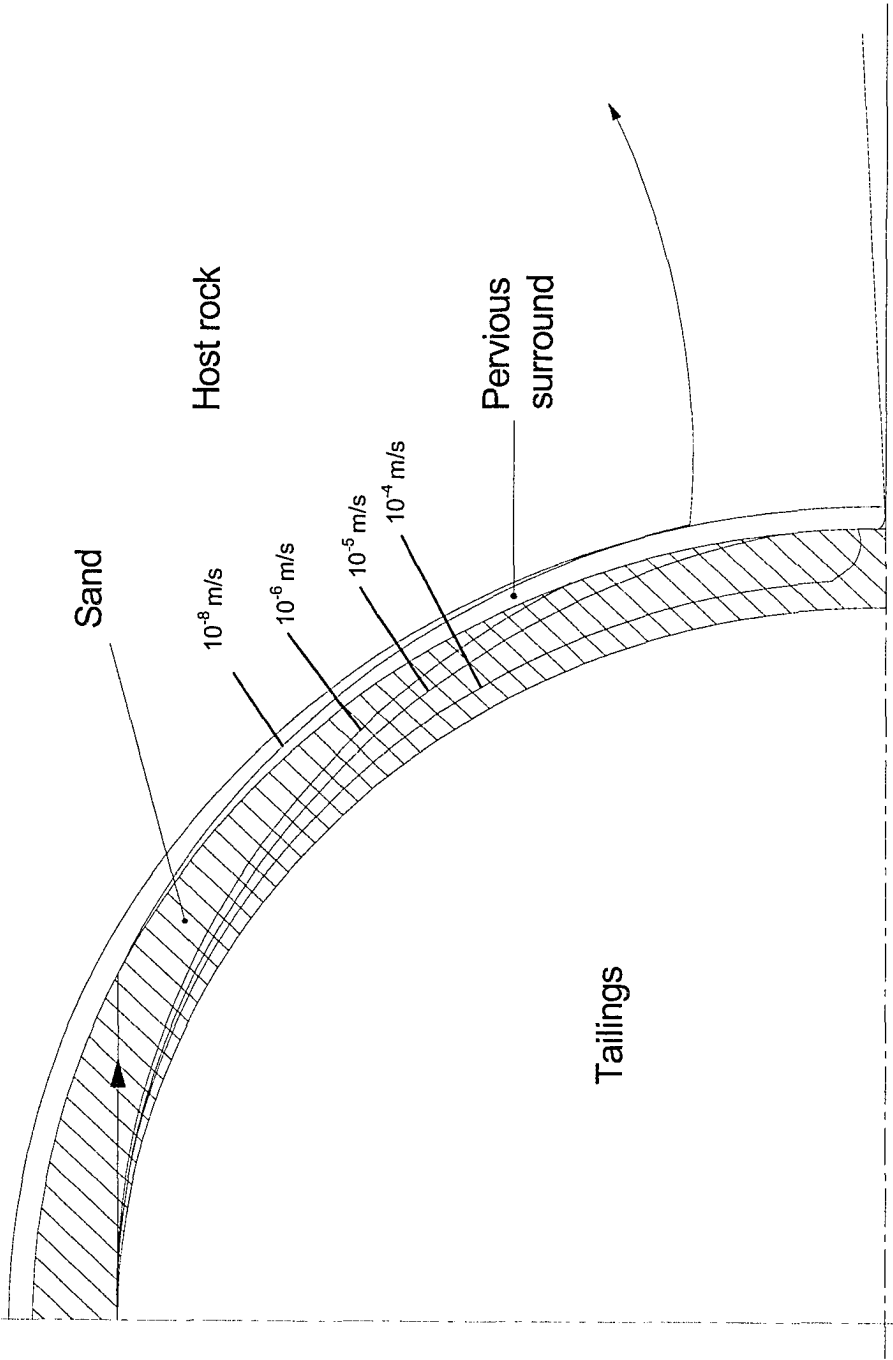


Fig. 2.42 Flow lines at the top of the tailings for different hydraulic conductivity of the sand.

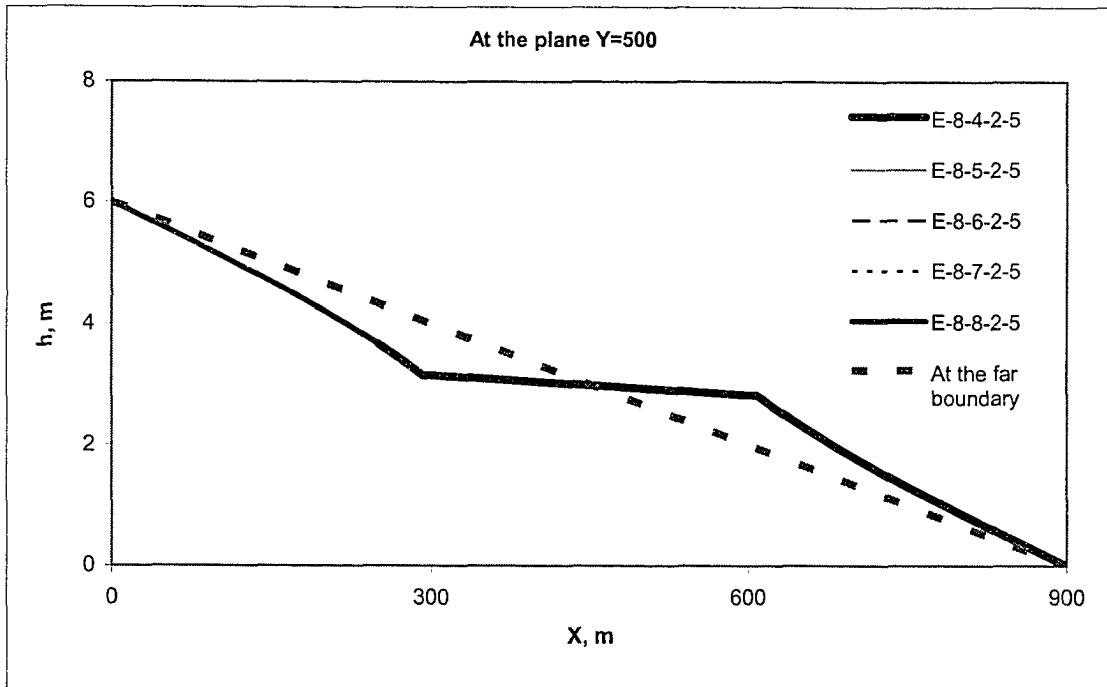


Fig. 2.43 Hydraulic head profiles for the different scenarios at the plane  $y=500$ .

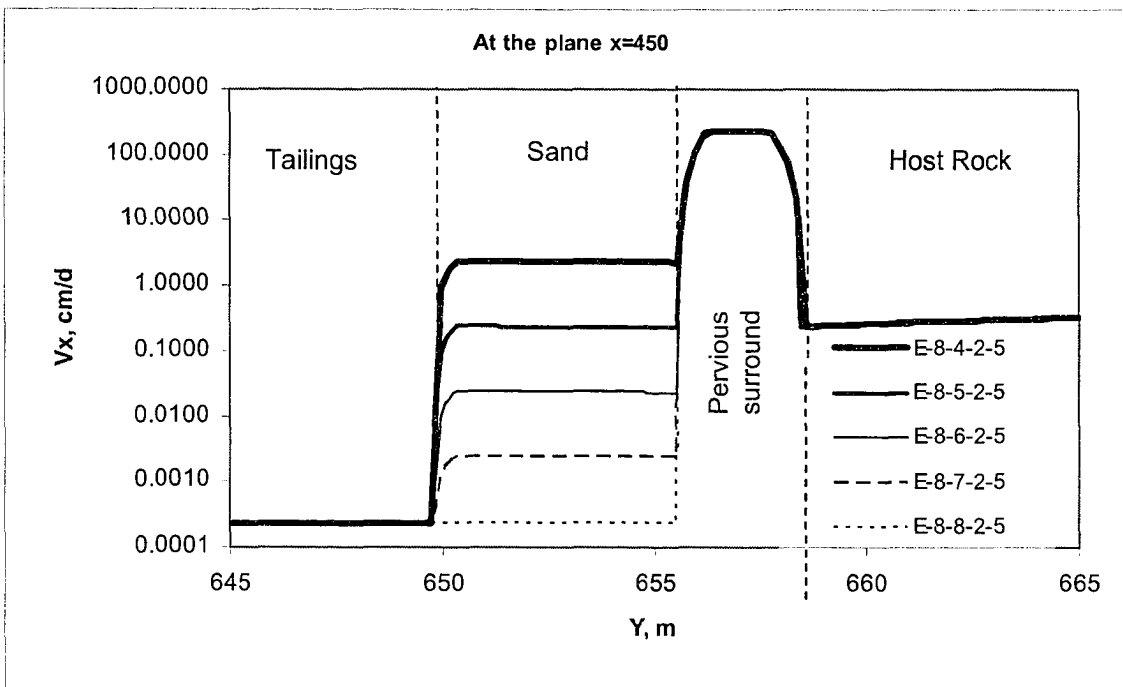


Fig. 2.44 X-component velocity profiles at the plane  $x=450$  for the different hydraulic conductivity of the sand.

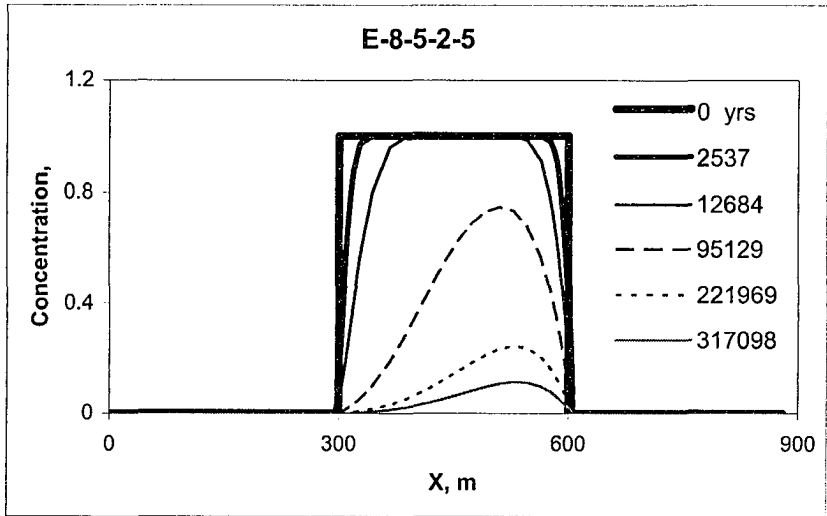


Fig. 2.45 Concentration profiles for the scenario E-8-5-2-5 at the plane y=500.

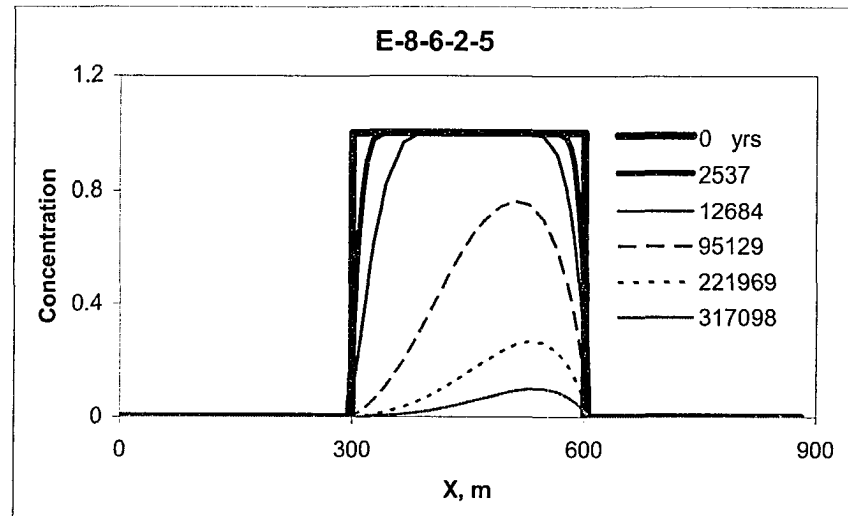


Fig. 2.46 Concentration profiles for the scenario E-8-6-2-5 at the plane y=500.

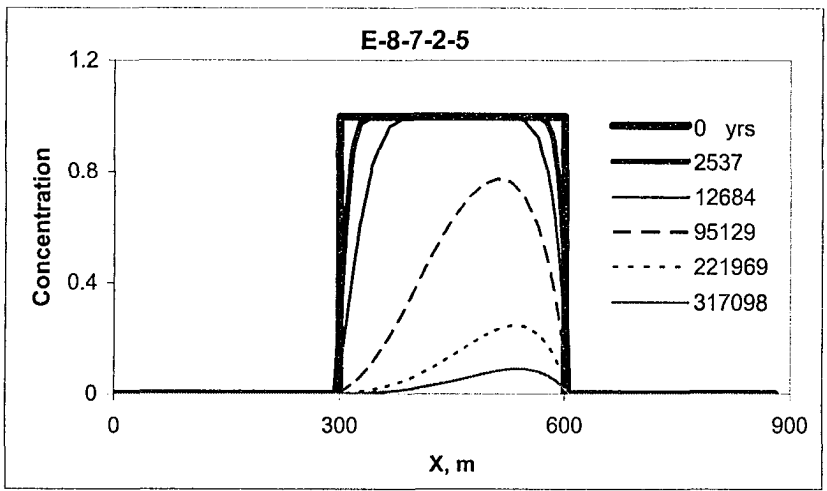


Fig. 2.47 Concentration profiles for the scenario E-8-7-2-5 at the plane y=500.

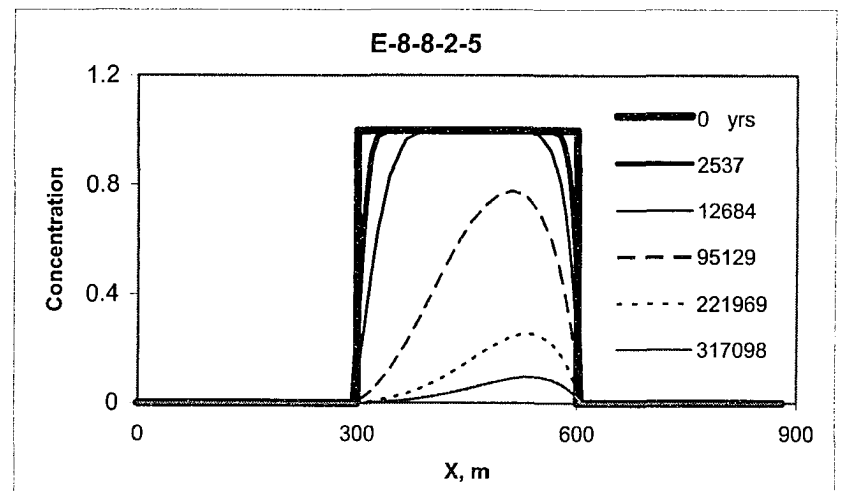


Fig. 2.48 Concentration profiles for the scenario E-8-8-2-5 at the plane y=500.

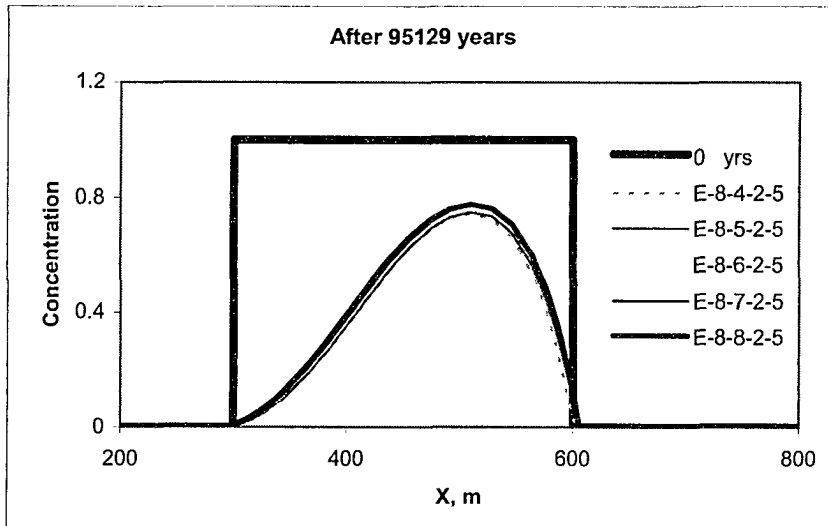


Fig. 2.49 Comparison of concentration profiles for the different scenarios at the plane  $y=500$ .

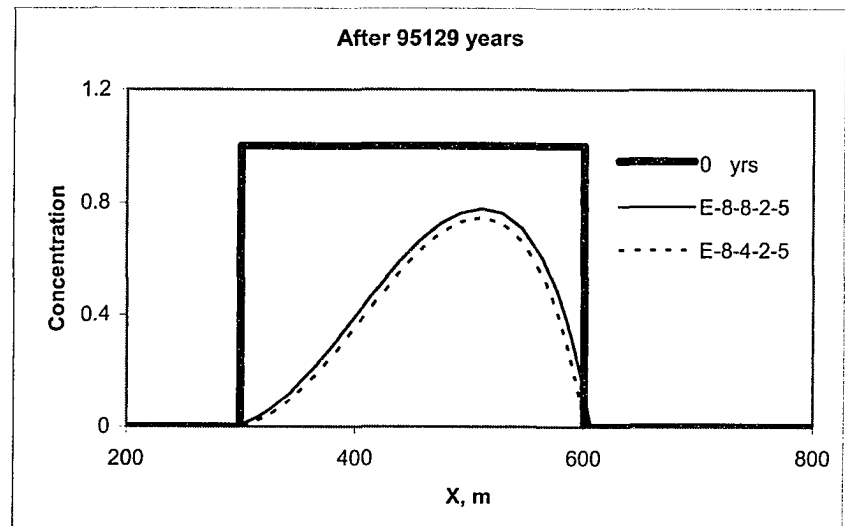


Fig. 2.50 Comparison of concentration profiles for the scenarios E-8-4-2-5 and E-8-8-2-5 at the plane  $y=500$ .

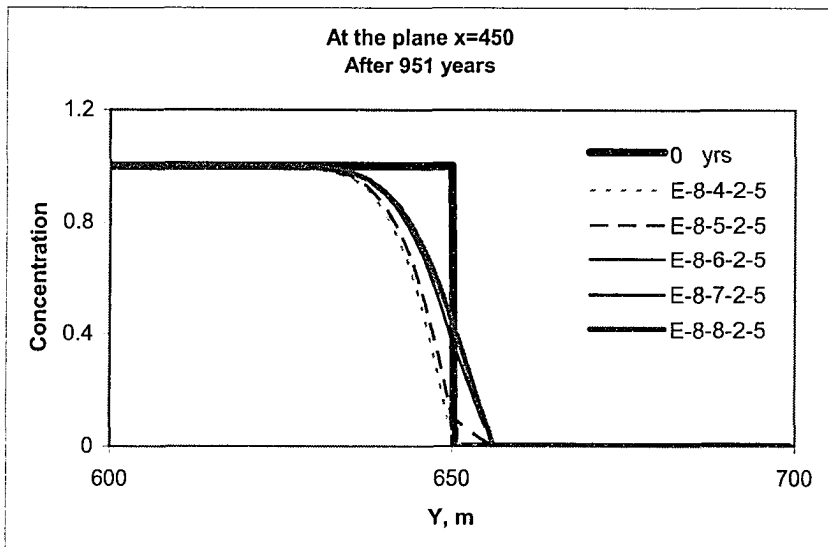


Fig. 2.51 Comparison of concentration profiles for the different scenarios at the plane  $x=450$  after 951 years.

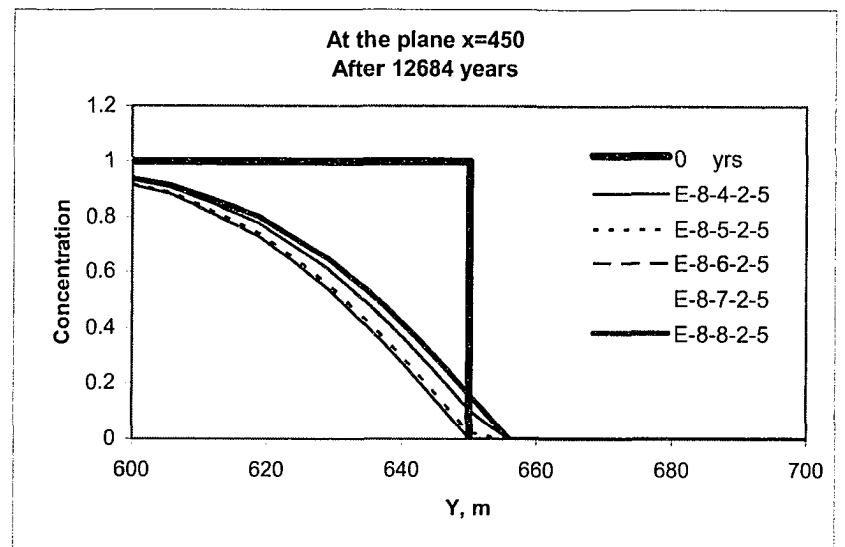


Fig. 2.52 Comparison of concentration profiles for the different scenarios at the plane  $x=450$  after 12684 years.

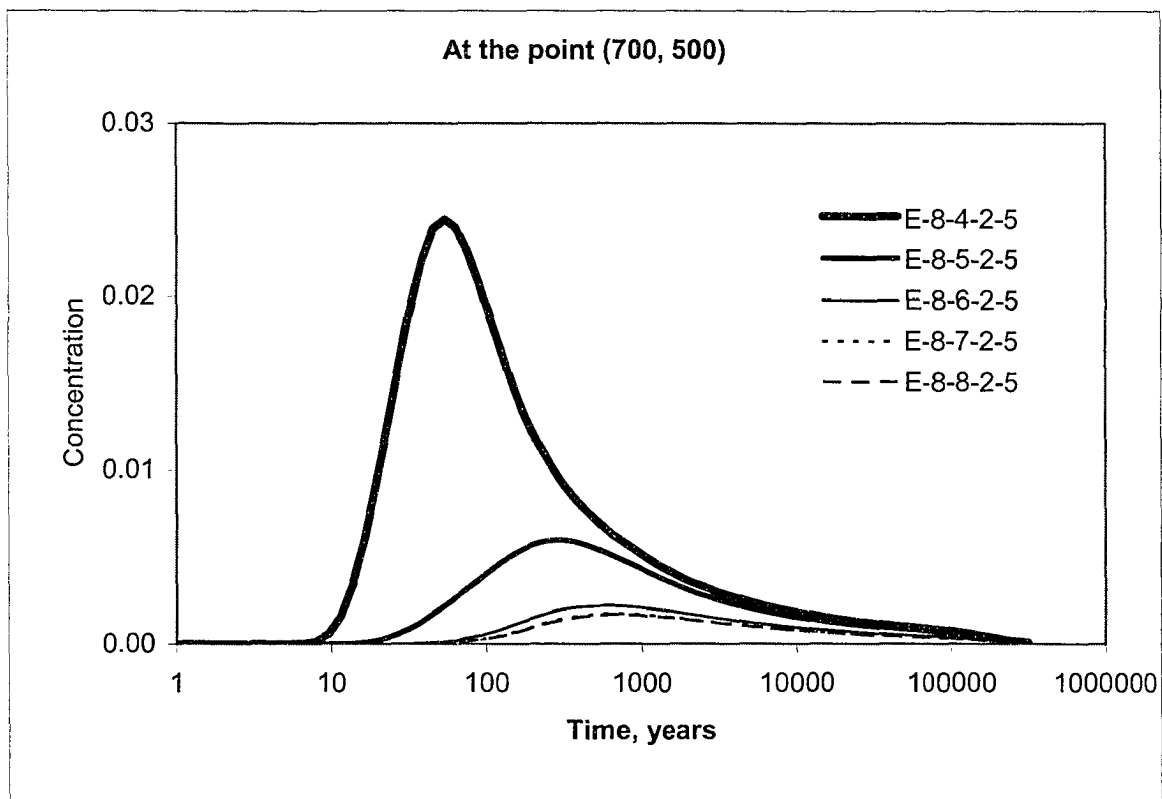


Fig. 2.53 Concentration history for the different scenarios at the point (700, 500).

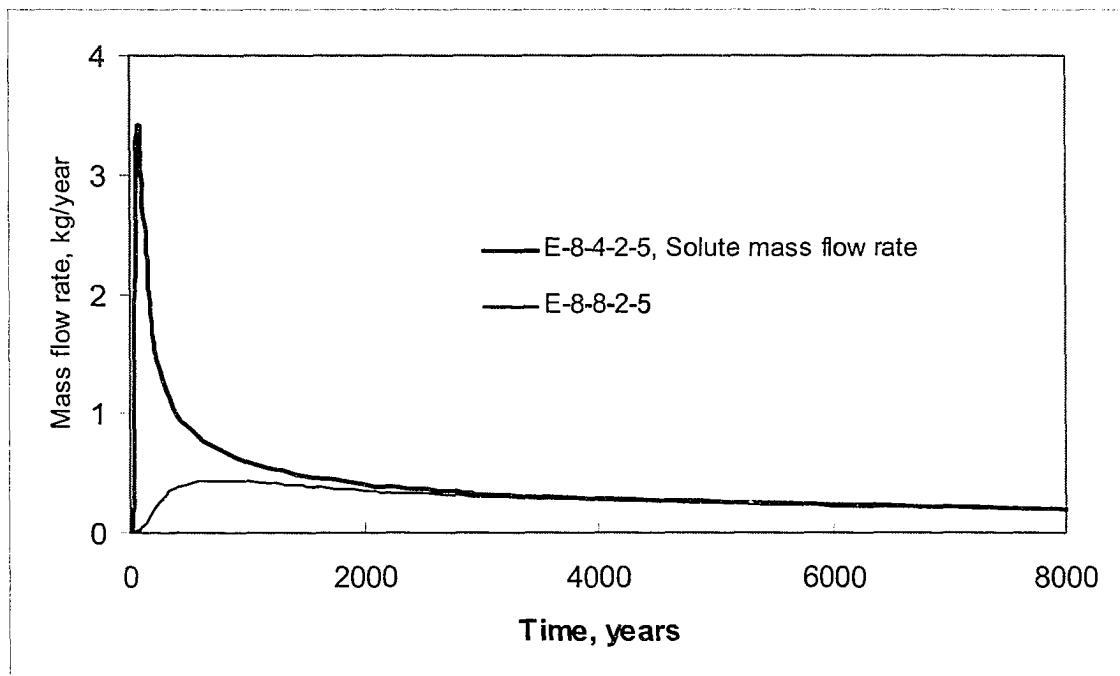


Fig. 2.54 The rate of leaving for the scenarios E-8-4-2-5 and E-8-8-2-5 on a linear scale.

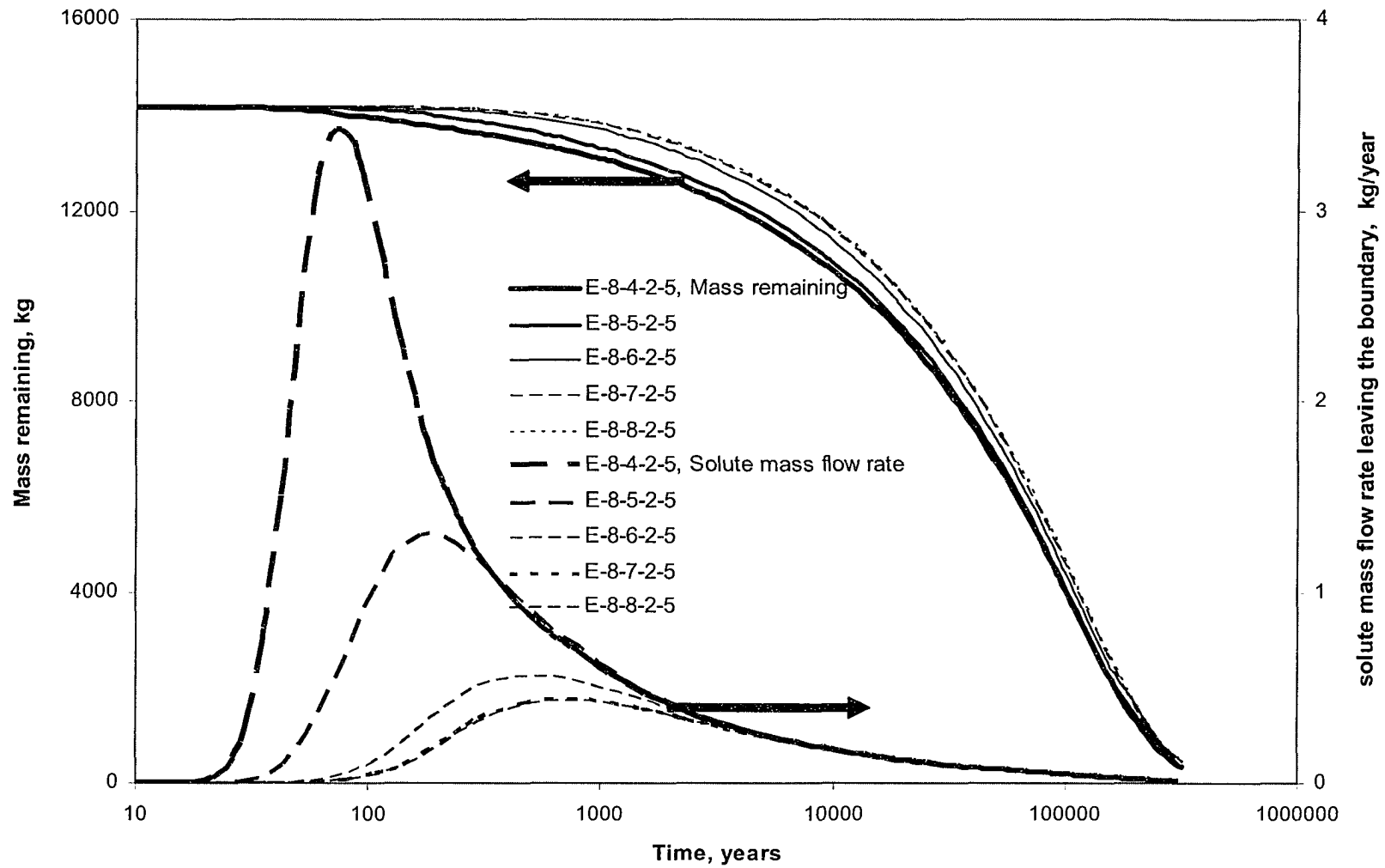


Fig. 2.55 Mass remaining and the solute mass flow rate leaving the boundary for the different scenarios.

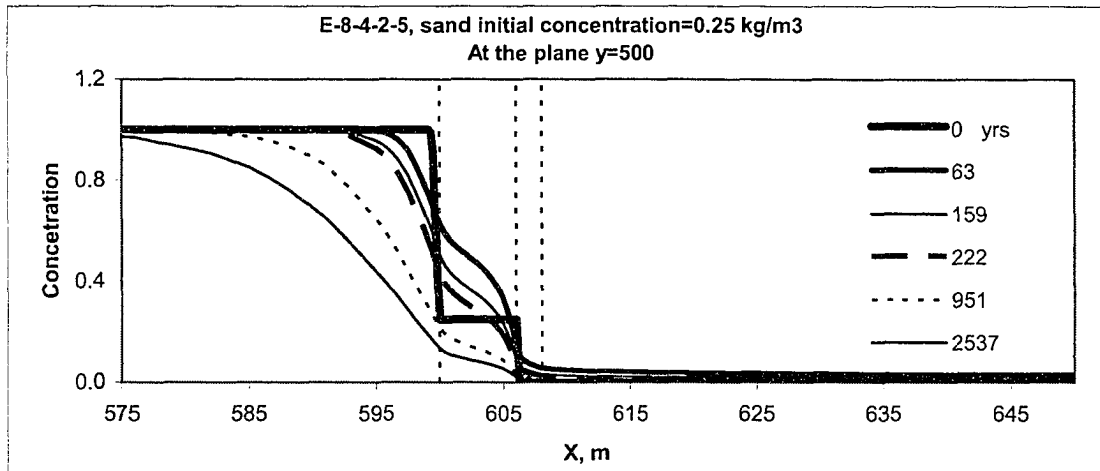


Fig. 2.56 Concentration profiles at the plane y=500 for the scenario E-8-4-2-5 with the sand layer initial concentration 0.25 kg/m<sup>3</sup>.

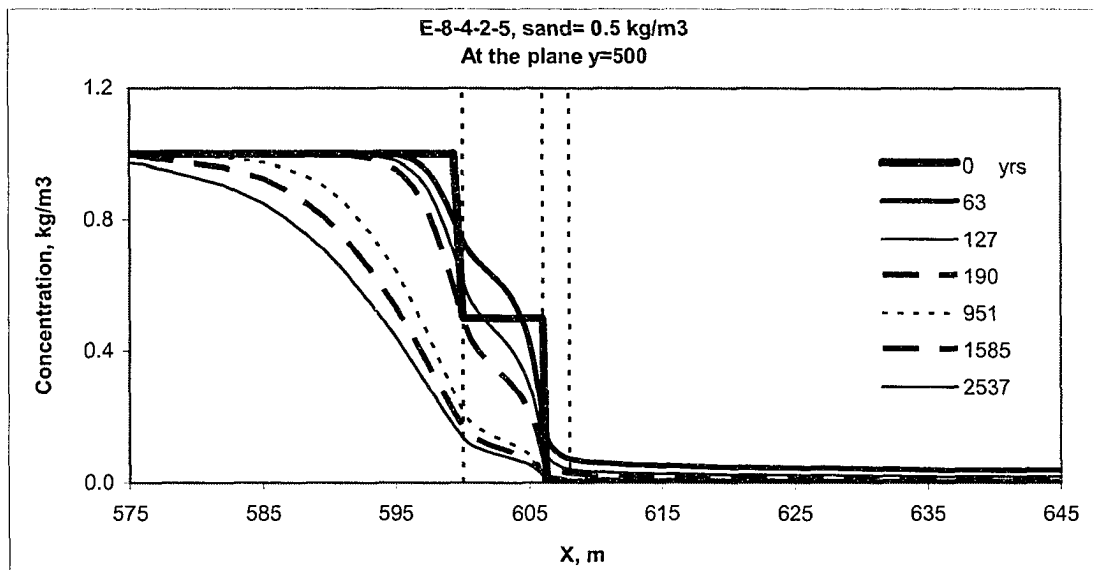


Fig.2.57 Concentration profiles at the plane y=500 for the scenario E-8-4-2-5 with the sand layer initial concentration 0.5 kg/m<sup>3</sup>.

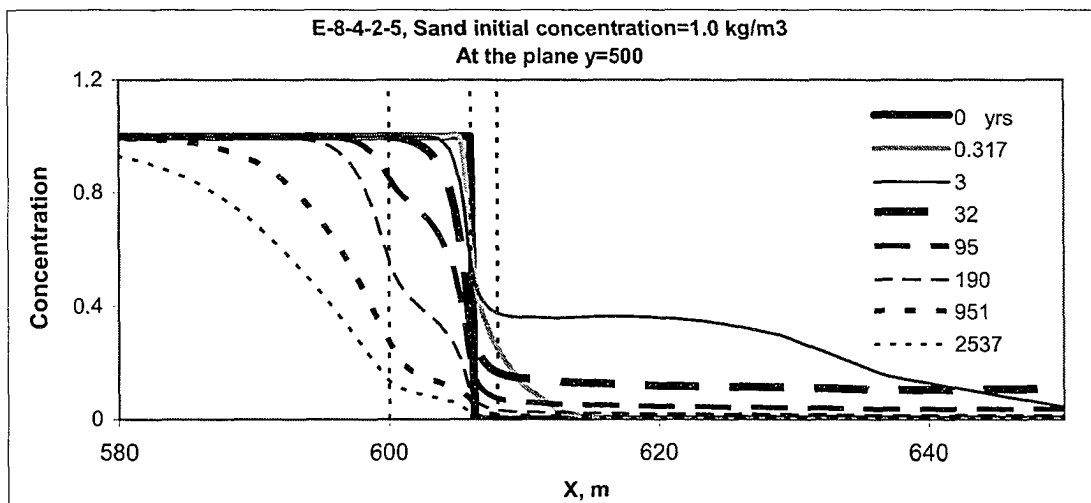


Fig.2.58 Concentration profiles at the plane y=500 for the scenario E-8-4-2-5 with the sand layer initial concentration 1.0 kg/m<sup>3</sup>.

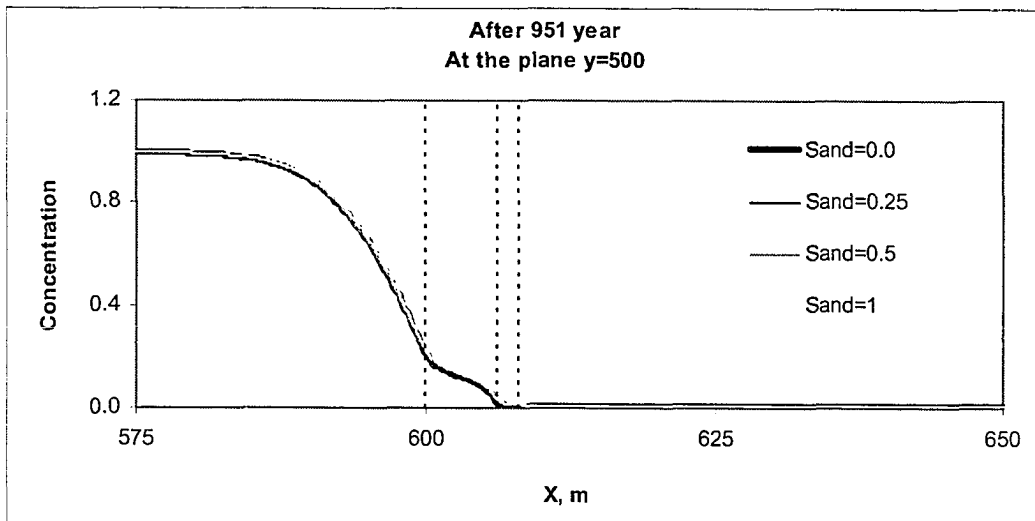


Fig. 2.59 Comparisons of concentration profiles for different sand initial concentration at the plane y=500 after 951 year.

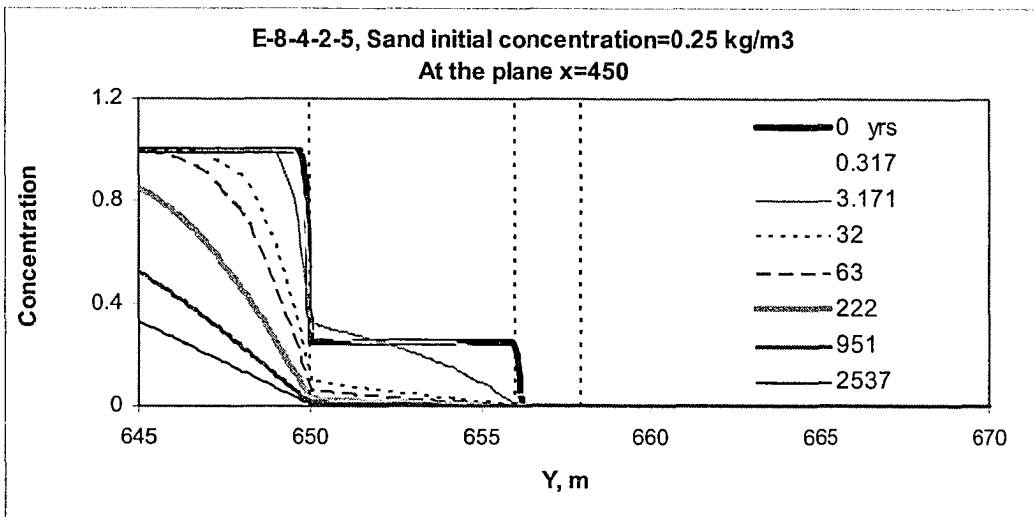


Fig. 2.60 Concentration profiles for the scenario E-8-4-2-5 with the sand initial concentration of 0.25 kg/m<sup>3</sup> at the plane x=450.

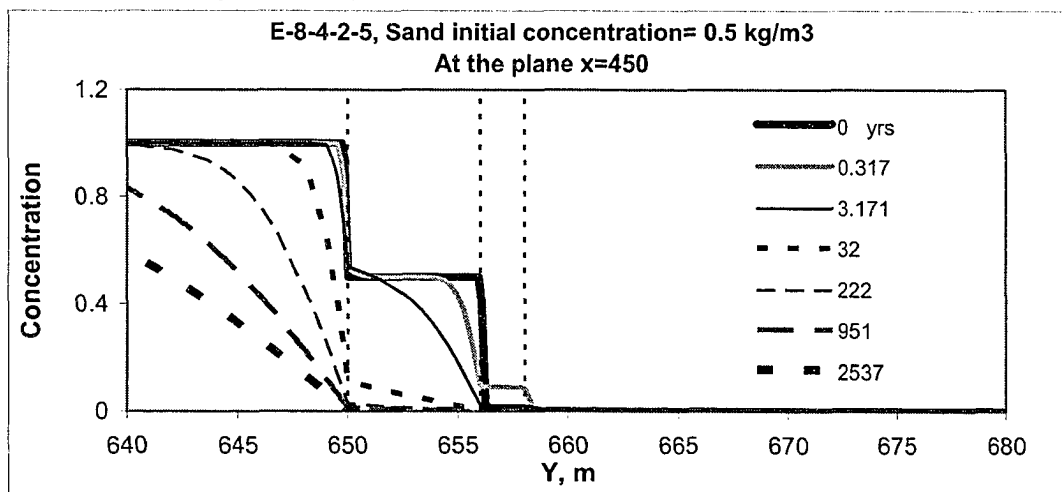


Fig. 2.61 Concentration profiles for the scenario E-8-4-2-5 with the sand initial concentration of 0.5 kg/m<sup>3</sup> at the plane x=450.

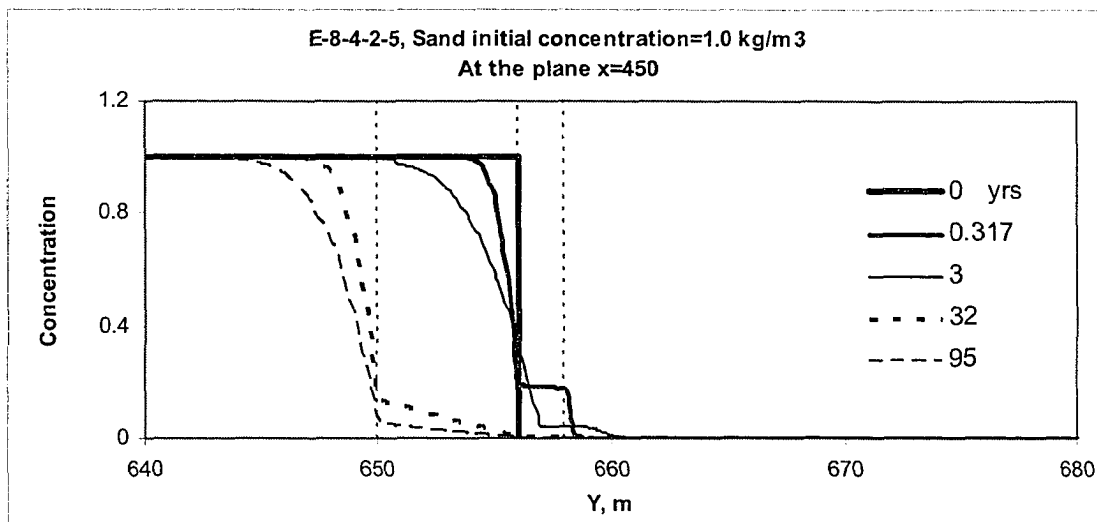


Fig. 2.62 Concentration profiles for the scenario E-8-4-2-5 with the sand initial concentration of 1.0 kg/m<sup>3</sup> at the plane x=450.

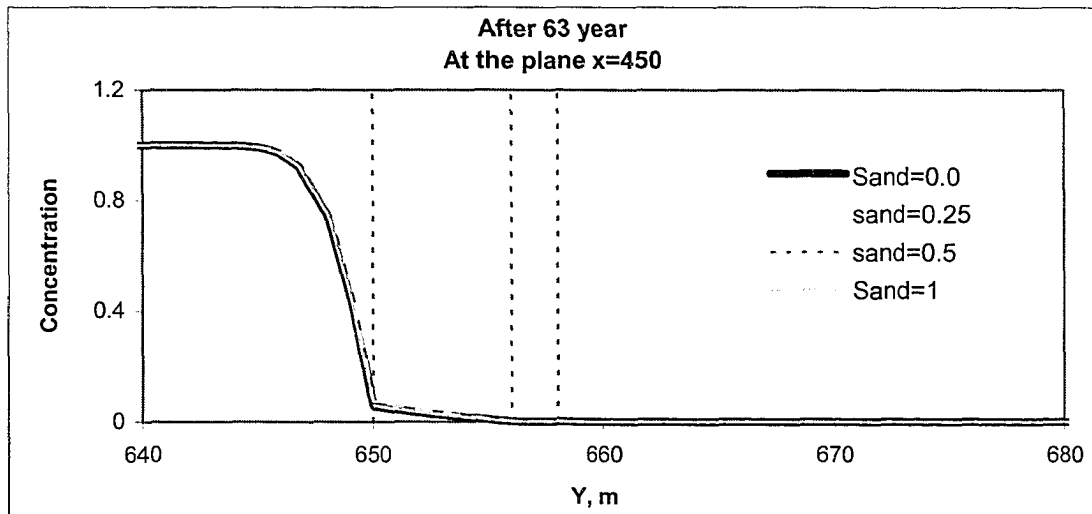


Fig. 2.63 Comparison of concentration profiles for the different scenarios after 63 year at the plane x=450.

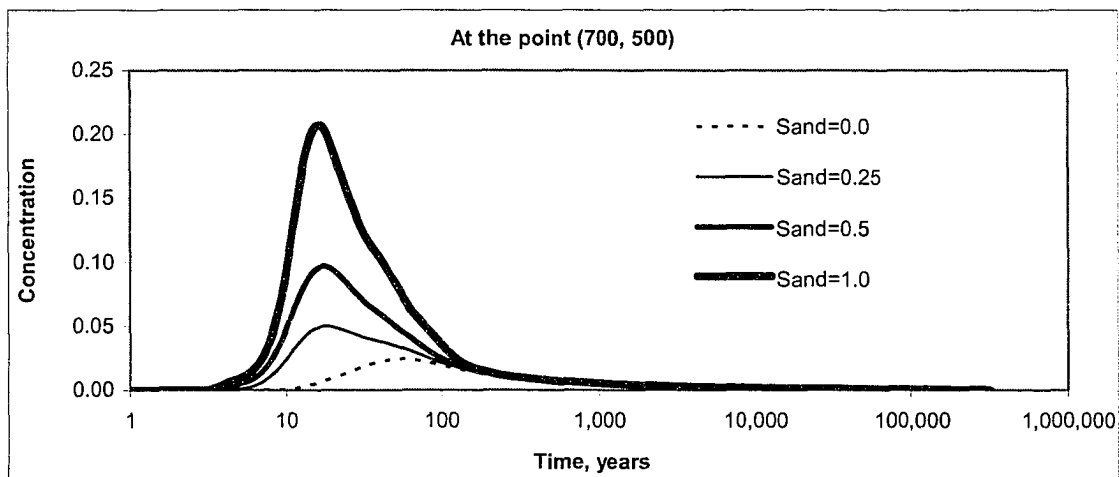


Fig. 2.64 Concentration history for different solute initial concentration in the sand at the point (700, 500).

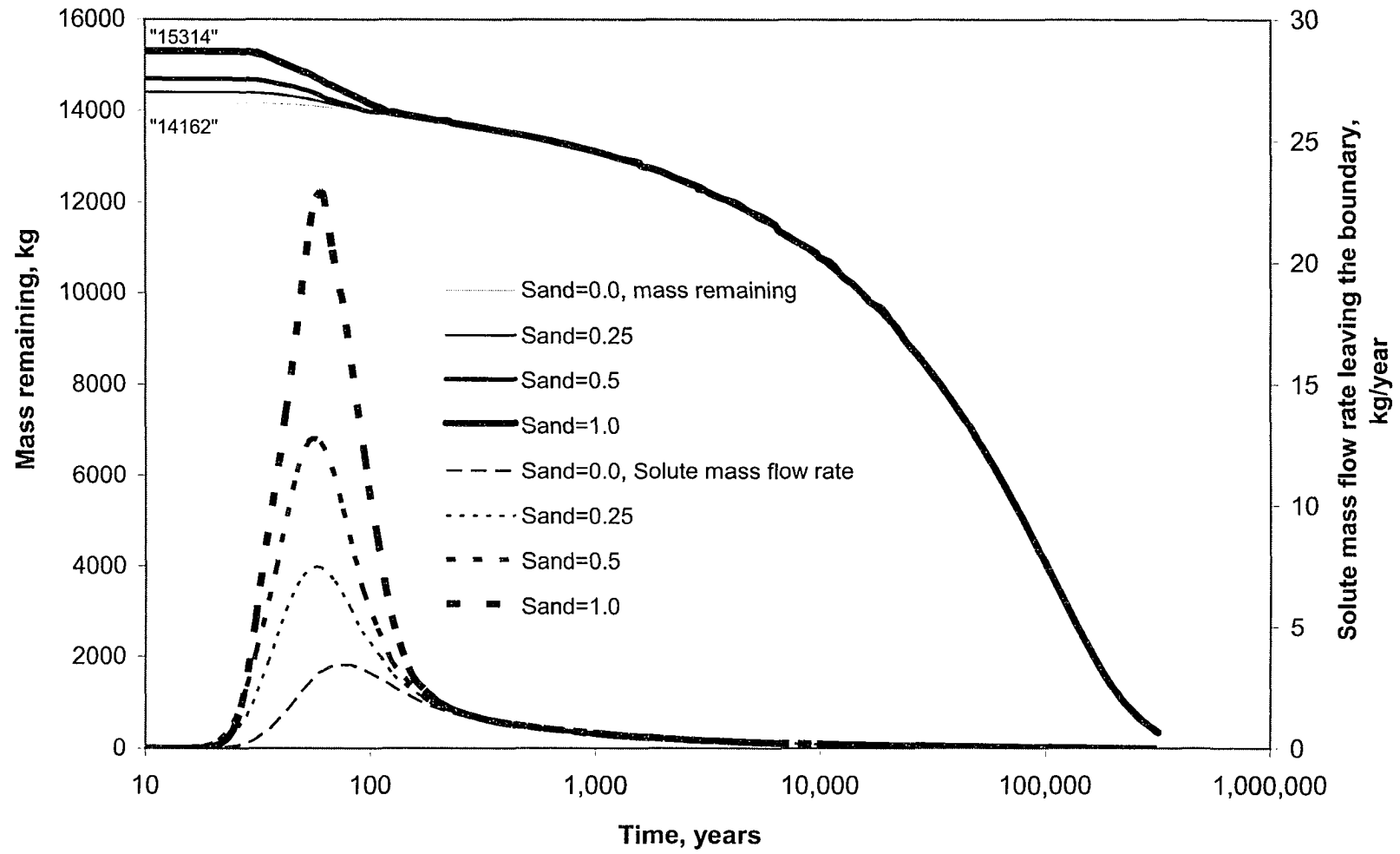


Fig. 2.65 Mass remaining and solute mass flow rate leaving the boundary for the different scenarios.

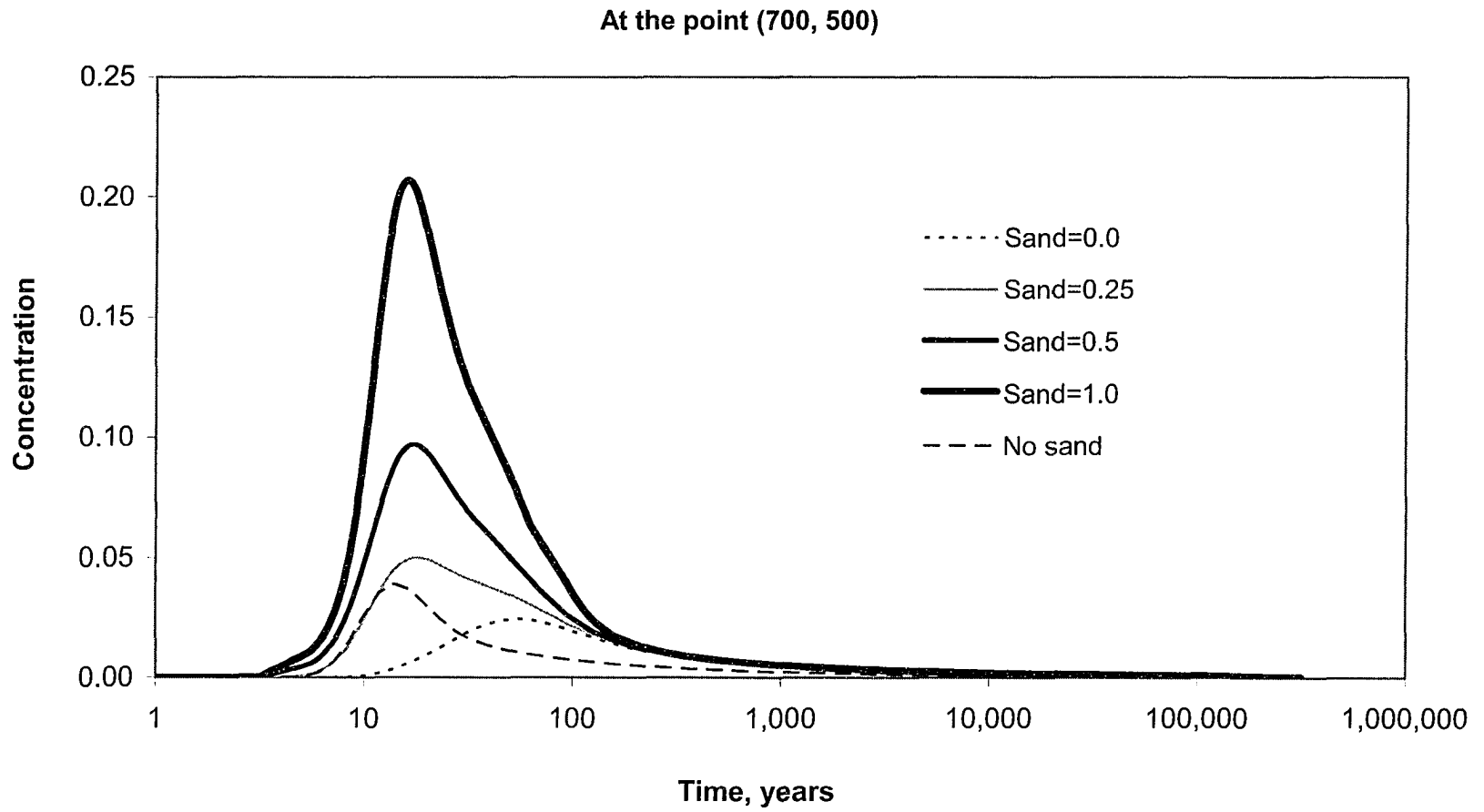


Fig. 2.66 Concentration history for different solute initial concentration in the sand at the point (700, 500).

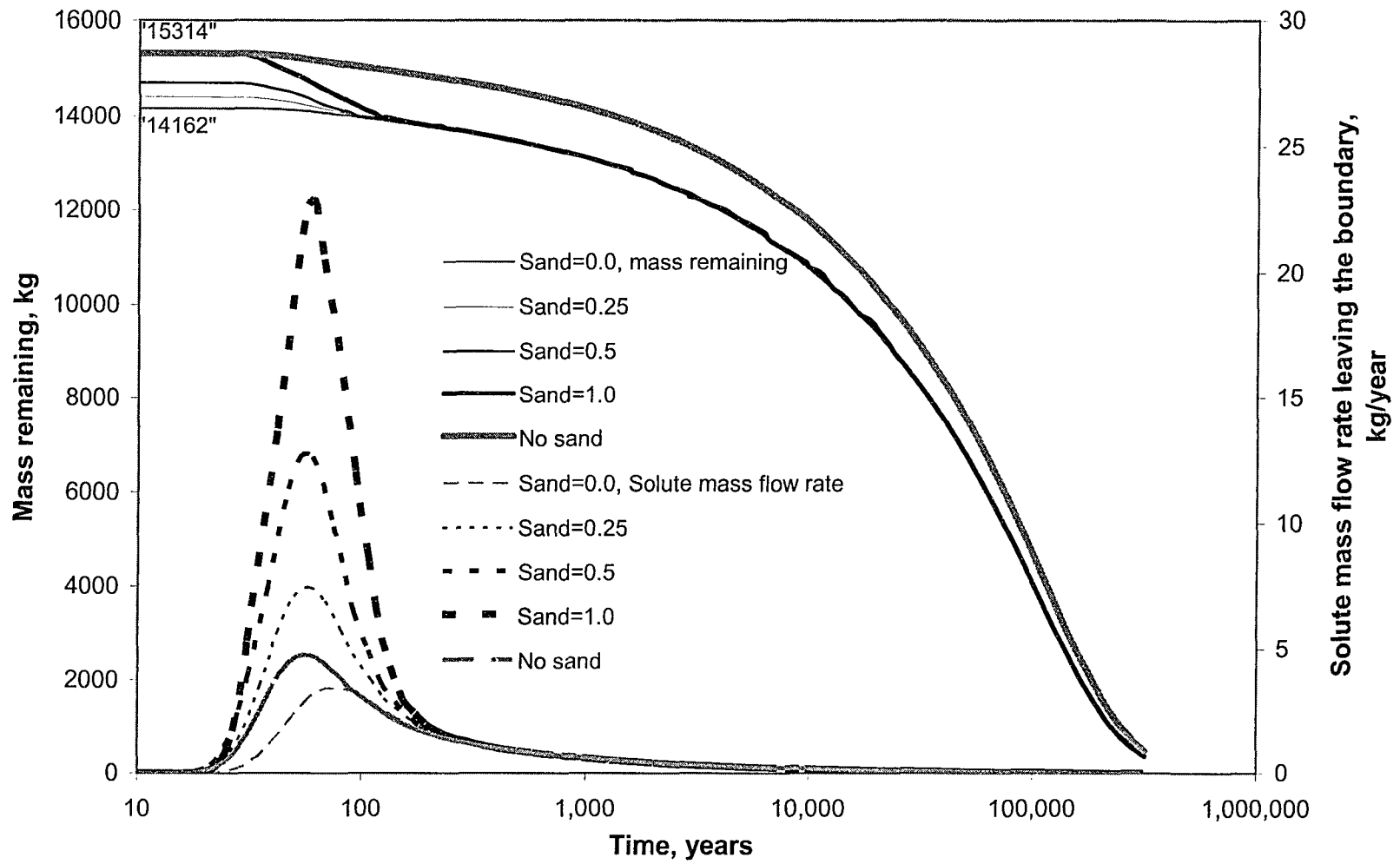


Fig. 2.67 Mass remaining and solute mass flow rate leaving the boundary for the different scenarios.

## CHAPTER 3

### ON THE CONTINUUM HYPOTHESIS

The purpose of this chapter is to provide an overview to the continuum hypothesis; conditions need to be satisfied in order to be able to adopt this approach as well as alternatives to dealing with systems violating these conditions. Length scale constraints are introduced in this chapter. A new constraint (the third constraint) has been identified and derived. Although a version of this constraint was defined in the literature (Carbonell et al. 1984, Bachmat et al. 1986), it is identified here in a new context.

#### **3.1 Microscopic and Macroscopic Point of View.**

Reynolds et al. (1977), in the course of providing a microscopic insight into the concept of the entropy, introduced a nice analogy that could fit the purpose of illustrating the main feature of both the microscopic and the macroscopic views. The example they introduced shows how the insight into the microscopic details of a system could provide a clearer understanding of its macroscopic behavior. The analogy is based on the perception of two observers as they watch the same phenomenon from different proximities. The first one watches a process from a closer proximity while the other describes the same process as he watches it from a great distance.

Assume that the two observers were not told any information about the nature of the process they were asked to describe before hand. The process, as

described by Reynolds et al., is as follows: suppose there is a tray containing a large number of bouncing balls, half red and half white. Initially, let the balls of the same color arranged on one side of the tray and the others arranged on the other side. Our two observers would have different description to this picture. With the distant observers watching a wider view with no details; they may comment that the far object looks white on one side and red on the other. On the other hand, with the closer observers watching narrower view but with great details; they may suggest that the system consists of equal numbers of balls of two different colors arranged equally on both sides. Now let the balls start to jump and thereby trade places; our distant observers might comment, "the process is evolving in time with the red stuff is diffusing through the white". After a while a uniform pinkish color would appear and it would seem that equilibrium was reached and all changes had stopped. From the point of view of our closer observers, they would see continual random motion, with the red and white balls relatively evenly distributed. Occasionally they could see local aggregates of balls of the same color in various spots, but these would disappear quickly and would not be noticed by our distant observer. If the experiment was repeated many times our distant observer would always note the red diffused through the white, and that after a while an equilibrium condition was reached. On the other hand, our closer observer would always note a continuous random change of the balls with, finally, the red and white were relatively evenly distributed. If the balls were changed with smaller or larger ones, our distant observers would notice a change in the process (become slower or faster) and might refer this to a change

in the medium. For our closer observers and by employing theories of classical mechanics, they could, in principal, fully describe the system. Given the balls' initial positions in space and their momenta, they could predict their future positions. However, despite the apparent simplicity of this approach, it can prove exceedingly difficult to solve the problem of the motion of even a small number of balls, in addition to the fact that the initial position and momenta of all the balls may not actually be known a priori. For our distant observers, if they noticed reproducibility in the experiment, they might attempt to construct a mathematical theory that would explain the diffusion, and perhaps even predict its rate. Reynolds et al. commented "even in their ignorance of the motion of individual [balls], they might make a rather good theory". Although the theory may not determine the behavior of the system at the microscopic scale, the results may be satisfactory at the macroscopic level.

As indicated in this example, both observers described the same process differently and justified their opinion by providing a mathematical theory to predict the behavior of the system. A question like, which of them is right, is, in fact, irrelevant. Both of them are right in the sense that they are describing different scale of the same phenomenon. It also indicates that looking at a system from closer proximity (focusing) may reveal a random motion of its constituents while looking at the system from a distance (defocusing), a well defined behavior may be noticed. Describing the behavior of a system by looking at it from a distance provides what is called an upscaled description. An upscaled description of a phenomenon is analogously a reverse process to the focusing process in the

sense that focusing looks for the details while “upscaling or defocusing” integrates the details.

### **3.2 Aspects Related to Macroscopization.**

We all recognize that we as humans have limitations in our sensory organs. We cannot see, for example, but within a certain range of electromagnetic spectra. We cannot distinguish tiny things, nor can we follow things that move at high speed, bounce at high frequency or things that are part of systems composed of a large number of such things that move at random (molecules, particles, etc.). For that reason the natural advancement in science usually begins with our observations to phenomena occurring within the ability of our sensory organs to capture them. Even in the absence of information about the microstructure of the systems under consideration, scientists were able to define laws that govern certain macroscopic behavior of these systems. This indicates many things; perhaps the most important thing may be that, for most physical systems, although the motion of micro parts that constitute the system may look random, these systems behave on the average in a well-defined manner. For example, if we consider a fluid in a container, although the molecules of the fluid may attain a whole range of velocities, they show constant value on the average, which reflect a macroscopic quantity called the temperature. It also indicates that the macroscopic behavior of a system could be explained without the need to know all or perhaps any microscopic details. Thus, in general, one can study phenomena at the macroscopic level without the need

to dig into its microstructure. For this macroscopic description, the influence of microstructure on the macroscopic behavior appears in the macroscopic governing laws as coefficients that are called “material properties” which are usually measurable quantities at macroscopic scale. In addition new expressions that are not needed in studying systems from the microscopic point of view are essentially needed to explain certain macroscopic behavior. The most typical example is perhaps given by the second law of thermodynamics. Despite the reversibility of the microscopic dynamics, macroscopic phenomena are indeed irreversible, and entropy always increases (Toda et al. 1983). Thus, the concept of dissipation, as introduced when studying the physics of viscous fluids, might not be needed when one describes a system at the microscopic level. Moreover, new forces and energies are introduced in the macroscopic descriptions that are not present in the micro world. Pressure, stress, surface tension, enthalpy, Gibbs free energy, etc. are examples of such new terms. One can in general measure these macroscopic forces using macroscopic devices. By macroscopic devices we mean that the size of the measuring prop is much larger than the microstructure of the system.

The second phase in the natural development of science would be to dig into the micro world of the system and try to find the hidden relationships between the macroscopic properties and the microstructure of the system. An example of such a development is apparent in the science of fluid mechanics. As will be discussed later, the first version of the Navier-Stokes equations was introduced in the beginning of the 19<sup>th</sup> century, while it was up until the beginning

of the 20<sup>th</sup> century when scientists showed that the Navier-Stokes equations might be derived through averaging processes using the laws of statistical mechanics.

Likewise, the development of studying flow in porous media has followed the same trend. It was first studied through observation to phenomena occurring within our ability to notice and measure (Darcy's law). Following that, attempts were made to dig into the microstructure of the problem and find the hidden relationships that connect the newly defined material properties and the microstructure of the system, as will be discussed later.

### **3.3. On the Continuum Approach.**

#### **3.3.1 Historical background.**

C. Navier (1785-1836) published his work on the motion of incompressible fluids in 1820. In 1821 he introduced an equation for viscous fluids. G. Stokes (1819-903), published his work on flow of viscous fluids in 1845 where he took into account internal friction in fluids in motion. Since then, the well-known Navier-Stokes equations have become one of the most powerful tools in solving fluid mechanics problems. Scientists and researchers in the field of fluid mechanics at this time believed that they finally had the tools that would enable them to solve any problem in fluid mechanics. In fact this is true in the sense that the Navier-Stokes equations are so general that they could, in principal, be applied to a variety of fluid flow problems. Indeed, there were problems that had

not yet been solved here and there, but that was due to the inadequacy of the mathematical techniques at this time to offer solutions to nonlinear second order partial differential equations. In fact, with the advancement in mathematical techniques today, many fluid flow problems have become amenable to solution. The advent of powerful numerical techniques as well as powerful computers has extended the use of the Navier-Stokes equations far beyond what was expected.

However, there are two problems that the Navier-Stokes equations failed in giving solutions. These are turbulent flows, and flows in porous media. The reasons for that are not due to the inadequacy of the Navier-Stokes equations to solve these problems, but due to our inability to define all the contributing factors that affect the solution. For the case of flow in porous media, the difficulty in using the Navier-Stokes equations stems from the complexity of the boundary configurations and conditions that cannot be defined a priori.

Therefore, the situation for solving problems related to flow in porous media was hopeless up until 1856 when H. Darcy (1803-1858) published the results of his famous experiment describing flow in a sand filter used in the public fountain of the city of Dijon, France. Starting in late 1855, Henry Darcy supervised a succession of experiments with the objective to determine the relation between the volumetric flow rate of water through sand beds and the hydraulic head loss. He concluded his experimentations with his famous law that is considered as the milestone for flow in porous media. The one-dimensional Darcy's law takes the form:

$$u = -\frac{\rho g k}{\mu} \frac{\Delta h}{\Delta L} \quad (3.1)$$

where  $u$  is the Darcy velocity,  $\rho$  is the fluid density,  $g$  is the gravitational acceleration,  $k$  is the permeability,  $\mu$  is the fluid viscosity,  $\Delta h$  is the difference in hydraulic head between measuring ports, and  $\Delta L$  is the distance between the measuring ports. The term  $\rho g k / \mu$  has been named the hydraulic conductivity. This law, though simple, was amazingly able to describe and solve a variety of problems in groundwater, the petroleum industry and in general porous media flows. Darcy's law is invariant with respect to the direction of the flow in the earth's gravity field. Hubbert (1958) stated that "the flow rate remains constant whether the flow is in the direction of gravity or opposed to it or in any other direction in three-dimensional space". Hydrologists, engineers and scientists were pleased that at last they had in hand a simple formula that would enable them to solve problems related to flow in porous media. Hence, they generalized Darcy's law to three-dimensional flow problems. And when they realized the directional properties of permeability, they considered it as a tensor, and Darcy's law took the form:

$$\mathbf{v} = -\mathbf{K} \cdot \nabla h \quad (3.2)$$

where  $\mathbf{v}$  is the velocity vector,  $\mathbf{K}$  is a second order tensor representing the hydraulic conductivity and  $\nabla h$  is the gradient vector of hydraulic head. On the other hand, it has been realized that the relationship between the velocity vector and pressure gradient vector deviates from the linear relationship as the

Reynolds number, based on typical pore or particle diameter, exceeds one (Bear, 1972). This has been attributed to the increased drag due to the increased velocity (Nield, 1992). To extend Darcy's law to account for the contribution of the nonlinear drag, investigators have introduced a quadratic term to Darcy's equation. The modified equation for a homogeneous, isotropic medium takes the form:

$$\nabla p = -\frac{\mu}{k} \mathbf{v} - c_F K^{-\frac{1}{2}} \rho_f |\mathbf{v}| \mathbf{v} \quad (3.3)$$

where  $c_F$  is a dimensionless form-drag constant. This equation is a modification of an equation associated with the names of Dupuit and Forchheimer. The last term is sometimes called the Forchheimer term (Nield et al., 1992).

For situations where the wall effects are important, an additional term was proposed by Brinkman (Nield et al., 1992), which is analogous to the Laplacian term that appears in the Navier-Stokes equation. The equation for a homogeneous, isotropic medium takes the form:

$$\nabla p = -\frac{\mu}{k} \mathbf{v} + \tilde{\mu} \nabla^2 \mathbf{v} \quad (3.4)$$

where the coefficient  $\tilde{\mu}$  is an effective viscosity. Brinkman set  $\mu$  and  $\tilde{\mu}$  equal to each other, but in general that is not true. Experimental checks of Brinkman's theory have been indirect and few in number. Several recent authors suggested adding the Brinkman term to the Forchheimer term in an attempt to get a

generalized equation. However, the validity of this is not completely clear (Nield et. al. 1992).

One important point in the previous discussion is that the attempts to extend Darcy's law to a more general form have been through a heuristic approach by adding ad hoc terms to Darcy's law to account for different situations without a rigorous mathematical proof. Whitaker (1966) stated that "it is surprising to find that no thorough theoretical investigation has been made of an experimental observation that is over one hundred years old. Even in the absence of a reassuring theoretical analysis, investigators have extended the results from a steady, one-dimensional, incompressible flow experiment to include transient, multidimensional, compressible flow in anisotropic, compressible, and elastic porous media". The need for a theoretical investigation of the problem of flow in porous media through which Darcy's law could be proved is thus a must. The question now is: why is it important to derive the governing equations related to transport phenomena in porous media from its first principle? The answer to this question would be:

- to get a better understanding of the different transport phenomena related to flow in porous media,
- to explore different areas that seem to be unsolvable with the current type of equations; examples are flow in heterogeneous porous media, flow of non-Newtonian fluids in porous media, etc.,

- to verify and prove Darcy's law, and to define the length scale restrictions associated with the averaging volume, and
- to justify the addition of the ad hoc terms to the original Darcy's law and define their range of applicability.

Different approaches have been introduced in an attempt to arrive at proper upscaled description of transport phenomena in porous media through rigorous mathematical analysis as well as deep physical insight into the problem. One can perhaps find 4 different approaches in the literature. They are discussed in the following sections.

### **3.3.2 Approaches applied to derive Darcy's law.**

#### **3.3.2.1 The method of geometric modeling.**

As mentioned previously, solving problems related to transport phenomena in porous media by solving the corresponding microscopic transport equations has generally led nowhere. The boundary conditions imposed by the complex internal structure and configurations of the walls of the pores are so complicated that any attempt at solving transport differential equations for these complex boundary conditions is a priori doomed to failure. In addition, the fact that the internal structure of the porous medium is complex does not fully reveal the difficulty arise when dealing with such systems. It may, however, suffice to say that the details of the internal structure are not even known. Initially, researchers tried to simplify the situation in such a way that microscopic transport

equations become solvable. This has been done by simplifying the porous medium as a network of capillary tubes. However, as stated by Scheidegger (1974), “unrealistic oversimplifications are introduced and results obtained are seldom significant”. Scheidegger (1974) has gathered a summary of these models.

### **3.3.2.2 Statistical methods.**

Since Boltzman has introduced his kinetic theory of gases in 1866 and the subsequent development of what is now known as statistical mechanics, many of the macroscopic properties of systems dealt with as a continuum (fluid mechanics, thermodynamics, etc.) have been shown to possibly be derived from the system’s microscopic parameters. Thus, since a porous medium is generally not an ordered structure (i.e. random) it is appealing to consider using statistical methods. Statistical methods is that branch of science in which probabilistic concepts and probabilistic explanation played a fundamental role. In statistical mechanics, for example, the deterministic calculations of the path of each molecule were replaced by considerations of its probable behavior. A number of attempts have been made in this area. For up to date review see Jeulin et al. (2001).

### **3.3.2.3 Method of homogenization**

As has been illustrated in section 3.1, a visual macroscopic view to a system may be established by requiring that the observer be far from the system

of interest to the extent that the fine details of the system can no longer be distinguished. Thus if a typical microscopic parameter of a system (pore or particle diameter in the case of porous medium,  $d$ ) is defined then from our closer proximity to the system we should be able to distinguish individual pores or particles. However, as we get further away from our system, say a distance  $L$ , the details of our pore-particle structure get lost until one may not be able to distinguish pores from particles and the picture of the medium becomes smooth and homogeneous. Thus as the ratio  $d/L$  asymptotically approaches zero, the system can more likely be treated as a continuum.

Likewise, if the functions of interest in the microscopic transport differential equations in a given porous medium are put in the appropriate macroscopic frame work and are parameterized by a parameter (as described earlier), then we could expect to arrive at their macroscopic counterparts as this parameter asymptotically approaches zero. This is the essence of the theory of homogenization. However, this is not as easily done as it is easy said. Several mathematical complexities and limitations are imposed before the microscopic functions may converge to its macroscopic ones. Method of homogenization has been applied in different fields of science and engineering including flow in porous media. The basic idea of homogenization is to consider a whole family of functions  $u^\varepsilon$  where  $\varepsilon > 0$  is a special length scale parameter (the typical size of a pore) (Cioranescu et al. 2000) and investigate whether  $u^\varepsilon$  converges as  $\varepsilon \rightarrow 0$  or not. In other words, one does not work with only one situation for which certain mathematical manipulations are made, but the specific problem in question is

imbedded in a family of problems parameterized by the scale parameter  $\varepsilon > 0$ , and determines the limit

$$u = \lim_{\varepsilon \rightarrow 0} u^\varepsilon \quad (3.5)$$

and considering this limit as the result of the “upscaling” procedure, Fig.3.1, (Hornung 1997).

### **3.3.2.4 Method of local volume averaging.**

This method will be the focus of this work, and hence more details will be given to highlight its philosophy, elements, and limitations.

#### **3.3.2.4.1 History of the development of the method of volume averaging.**

Although it is not easy to exactly find out the origin of this method, as it appeared in several publications as an idea, one can track the early versions of this method in the early work of Hubbert (1956), Anderson and Jackson (1967), Whitaker (1967) and Slattery (1967).

The method is simply to generate an averaging process to a given function by locally integrating the governing partial differential equation describing the function over a given local volume surrounding each point. This will generate a smooth function of averaged values over the whole domain of interest, and therefore define a continuum (provided certain conditions are satisfied as will be discussed later). During the course of the averaging, process length scale restrictions are imposed so that the manipulations of the averaging

processes become easier and tractable. As with one's experience with time averaging in turbulent flow introduced by O. Reynolds (1842-1912), one expects two major problems to happen during averaging over volume. The first is that, when averaging, one loses the details of the microscopic variations of variables. This may be acceptable in light of the fact that, in applications, one is usually not interested in finding the microscopic variations of a phenomenon. Rather it is the averaged values that are of interest, and that is what one can actually measure. The second, and probably the major problem, is that while averaging is meant to work with quantities at macro scale, micro scale parameters appear in the terms given in the averaged equation. The obvious consequence of this is that the obtained averaged equations become unclosed. This in fact, introduces two problems. The first of which is that one needs to develop through experimentation constitutive relationships to account for these microscopic variables. The second is that one needs to develop a closure to the set of the governing partial differential equations.

During early work on the theory, two major problems were encountered that seem of special type. The first is that the averaging process produces an average of the gradient when it is the gradient of the average that is needed. The second one is that one gets the average of the product of two microscopic quantities when it is the product of the average that is of interest.

The first success to the first problem came in 1967 when Whitaker and Slattery were able to describe the average of the gradient in terms of the gradient

of the average and a surface integral term. The second victory also came in 1967 by Whitaker, when he defined microscopic variables as the sum of the average and a spatial variation in a way analogous to what Reynolds did in turbulent flow. Gray in 1975 modified Whitaker's formula and it became the standard way in the method of volume averaging as will be discussed later. Since then, different techniques have been introduced to verify the gradient of the average methodology. For example Gray and Lee in 1977 introduced the use of what they called the phase function, which equals one if the position vector is in the given phase and zero elsewhere, to define the region of the space occupied by fluids (this will define the domain of definition of functions) and then integrated over the whole space. This technique enabled them to exchange the gradient and integral operators. They were able to arrive at a similar representation of Whitaker's formula. However, their approach involved the derivative of the phase function where they defined it as the Dirac-delta function. Cushman criticized this approach in 1982 in the sense that the definition of Dirac-delta function as a point function is mathematically incorrect. He proved Whitaker's formula in the framework of the theory of distributions introduced in 1949 by L. Schwartz (1918-2002). Marle also introduced this technique in 1982. It turned out that the appropriate framework for dealing with flow in heterogeneous media is the theory of distributions.

Moreover, generalizing the local averaging by expressing it as a convolution product was first introduced in 1967 by Matheron, used by Marle in 1981, and then put in the framework of the theory of distributions by Marle in

1982. Quintard and Whitaker in 1994 derived Darcy's law and defined the Brinkman term in the sense of the theory of distributions. On the other hand, refinement of the theory in the sense of Gray was established through a series of papers with Hassanizadeh in 1979.

As a new emerging theory, after the basic principles underlying the theory had been established, researchers began to use it in exploring different areas of interest. Examples are multiphase flow, flow in heterogeneous porous media, heat and mass transfer, dispersion with chemical reactions and more. The first book about spatial averaging in the sense of Gray appeared in 1993, and in the sense of Whitaker in 1999.

### **3.4 Elements of the Theory of Volume Averaging.**

Before introducing the basic ideas and elements of the theory of local volume averaging, it is important that one has a look at the type of equations that are going to be averaged.

#### **3.4.1 Transport partial differential equations.**

For microscopic processes in a multiphase system, the governing equations in each phase are the classical balance laws of continuum mechanics. They may be represented in the general form as, (Hassanizadeh and Gray 1979):

$$\frac{\partial \rho \psi}{\partial t} + \nabla \cdot (\rho \mathbf{v} \psi) - \nabla \cdot \mathbf{l} - \rho f = \rho G \quad (3.6)$$

where $\rho$	mass density;
$\psi$	thermodynamic property;
$\mathbf{l}$	non advective flux vector;
$\mathbf{v}$	velocity vector;
$f$	external supply;
$G$	net rate of production.

The individual balance laws are obtained by substituting appropriate quantities from table 3.1 (Hassanizadeh and Gray 1979).

Table 3.1 Definition of elements used in equation 3.6.

Property	$\psi$	$\mathbf{l}$	$f$	$G$
mass	$1$	$0$	$0$	$0$
species	$c$	$\mathbf{l}$	$0$	$r$
momentum	$\mathbf{v}$	$\mathbf{t}$	$\mathbf{g}$	$0$
energy	$E + (1/2) \mathbf{v} \cdot \mathbf{v}$	$\mathbf{t} \cdot \mathbf{v} + \mathbf{g}$	$\mathbf{g} \cdot \mathbf{v} + h$	$0$

Where $E$	internal energy per unit mass;
$\mathbf{t}$	stress tensor;
$\mathbf{g}$	gravity vector;
$r$	rate of mass production (or decay) as a result of homogeneous reaction;
$h$	external supply of energy per unit mass.

Inspection of these equations shows that they contain a time derivative, gradient and divergence operators as well as point functions. Thus in doing the

averaging, one should find an expression for the average of the variables under the effect of these operators.

### 3.4.2 Averaging processes.

The method of volume averaging is based on the idea that with every point in space there exists an averaging volume. As illustrated in Fig. 3.2 the fluid is designated as the  $\beta$ -phase while the rigid solid is designated as the  $\sigma$ -phase. Average values of any function computed on the basis of this volume are assigned to the centroid of the volume.

If  $\psi_\beta = \psi_\beta(x, y, z)$  is a function defined over the  $\beta$  phase and is varying spatially (this function may be scalar, vector, or tensor) then the phase average of  $\psi_\beta$  over the volume may be given as:

$$\langle \psi_\beta \rangle = \frac{1}{v} \int_{v_\beta} \psi_\beta dv \quad (3.7)$$

where  $\langle \rangle$  indicates average and  $v$  is the averaging volume. Now the averaging volume should be chosen such that the average values do not change if this volume is increased or decreased in a certain range. Whitaker (1967) formulated this condition mathematically as:

$$l_\beta \ll l \ll L \quad (3.8)$$

where  $l$  is the characteristic length of the averaging volume,  $l_p$  is the size of a typical pore or particle diameter, and  $L$  is the length scale over which significant variations of  $\psi$  occur, Fig.(3.2). More discussion on inequality (3.8) will be given later.

Several authors used a weighting function rather than a constant function as defined by equation (3.7). However, Baveye and Sposito in 1984 attached a new significance to the concept of averaging via a weighting function. They made the observation that a weighting function may be associated with an instruments window. The transport equations, when averaged (convolved) with a weighting function, take on meaning only when measurements of physical properties, for use in the transport equations, are taken by an instrument with the corresponding weighting function.

Moreover, a generalization to the averaging technique as introduced by equation (3.7) was suggested and used by Marle (1982), and later by Quintard and Whitaker (1994-a,b,c,d,e). They used the convolution product of a weighting function with the function of interest. Thus for any quantity,  $\psi(\mathbf{x}, t)$  function of space and time, one defines the convolution product  $\psi * m$  (the star, “\*”, indicates a convolution product) with respect to the space variables, as:

$$(\psi * m)(\mathbf{x}, t) = \int_{R^3} \psi(\mathbf{x} - \mathbf{y})m(\mathbf{y})d\mathbf{y} \quad (3.9)$$

This new function  $\psi^*m$  may be considered as the macroscopic quantity associated to  $\psi$ . When  $m$  is equal to  $1/v$ ,  $\psi^*m$  is the ordinary average given by equation (3.7) at the specific location  $\mathbf{x}$ .

Now, let one investigate the average of the gradient of  $\psi$ . This term has to be dealt with carefully, because improper considerations could lead to an erroneous conclusion. Thus,

$$\langle \nabla \psi_\beta \rangle = \frac{1}{v} \int_{v_\beta} \nabla \psi_\beta dv \quad (3.10)$$

Now one obtains an expression for the average of the gradient when it is the gradient of the average that one seeks. It would be expedient if one could interchange the volume integration with the gradient operation. But the limits on this volume integration depend upon position. Hence one cannot interchange between integral and the gradient operators. Whitaker and Slattery have arrived independently at an expression for this term in terms of the gradient of the average in 1967. Whitaker used Leibniz theory of differentiation of functions defined by integral operator, while Slattery used the directional derivative concept and an analogy to the Reynolds transport theory. The equation they presented took the form:

$$\langle \nabla \psi_\beta \rangle = \nabla \langle \psi_\beta \rangle + \frac{1}{v} \int_{A_{\beta\sigma}} \mathbf{n}_{\beta\sigma} \psi_\beta dA \quad (3.11)$$

here  $A_{\beta\sigma}$  represents the interfacial area contained within the averaging volume and  $\mathbf{n}_{\beta\sigma}$  is the outwardly directed unit normal, Fig.(3.2). Different approaches to prove this theory were also introduced subsequently by Gray and Lee (1977), Marle (1982), and Cushman (1982).

It appears that this theory has opened the door for more indepth research to define the appropriate framework to deal with transport phenomena in porous media. The reason for this is related to the nature of the functions defined over the porous media (piecewise continuous functions). These functions experience discontinuities at the interface between the fluid phase and the solid phase. This implies that derivatives in the usual sense are not defined at the interface boundary. Figure 3.3 shows a one-dimensional illustration of what is called the indicator function, which is one if it is in a given phase and zero elsewhere. Thus, when the medium contains multiple phases separated by moving or stationary interfaces, one must consider that all quantities appearing in the transport equations (such as  $\rho$ ,  $c$ ,  $\mathbf{v}$ ,...) are continuous with continuous derivatives in each phase, and have jump discontinuities when one crosses the interfaces. For porous media (liquid-solid system) the value of a given quantity will be indexed  $\beta$  if it is in the liquid phase, and  $\sigma$  if it is in the solid phase. By definition, any quantity indexed by  $\beta$  is equal to zero outside the  $\beta$ -phase. It is apparent that the derivative of these functions could not be defined in the sense of classical mathematics at the surface of discontinuity. It must be taken in the sense of distributions. This will lead to additional terms in the balance equations. They

account for phenomena concentrated on interfaces, and involve the mass excess per unit area, the interfacial concentrations, interfacial stress tensor and energy, and also the chemical reactions occurring on the interfaces.

### **3.5 Proper Averaging Processes and Length Scale Constraints.**

#### **3.5.1 General**

One of the main features of the world we live in is the existence of many length scales ranging from scales measured in light-years to scales measured in microns and less. On studying a phenomenon at a certain length scale one needs to judge the importance of other length scales. For example, if one focuses on the movement of galaxies in the universe, the solar system might not even be mentioned. On focusing on our Galaxy, the whole solar system might be studied as a point mass and our planet is treated as point mass when focusing on our solar system. Even in one's daily life, one enjoys moving between different length scales, from scales of what he/she can see to scales where one uses a magnifying instrument. One can even appreciate length scales that are beyond the magnifying power of current powerful instruments. On the other hand, one sometimes encounters systems composed of a very large number of microscopic units that are very close to each other such that one cannot distinguish between individual microscopic units with his/her own eyes. These systems can be shown to behave macroscopically in a well-defined way (as a continuum), as explained earlier. It is inappropriate and probably impossible to treat such systems by studying the interactions of such a huge number of

microscopic units. Moreover, and in most cases, it is the average behavior that one usually needs to determine. So it is up to the interest of the investigator to decide which scale he/she should use. Each length scale has its own variables and measuring instruments. The momentum (linear and angular) of individual particles is an example of an important parameter related to microscopic description; whereas pressure, temperature, density...etc. are examples of parameters at macroscopic description. There is, however, a link between parameters at the microscopic scale and at the macroscopic scale. For example, temperature is a measure of the speed with which fluid particles move, more precisely it is a measure of their kinetic energy. The higher the temperature, the faster they move. From the kinetic theory of gases, temperature is defined as two-thirds the average kinetic energy of molecules. Moreover, one also needs to build constitutive relationships between macroscopic parameters that describe the response of a given macroscopic system when taken out of equilibrium.

Thus, in general, variables at a certain scale might not have meaning in another scale. On conducting measurements one should be careful in defining the length scale he/she is interested in because this will determine the variables that need to be measured and the suitable measuring instruments to be used. One would expect to have a very tiny probe in investigating systems at the microscopic length scale, and relatively larger probes when investigating phenomena at the macroscopic scale. However, one important requirement related to the size of the measuring probe in relation to the length scale characterizing a phenomenon is that it should be small enough compared with

the region over which significant change in a property occurs and large enough compared with the length scale under which another length scale description might be used. For example, if one is interested in measuring the temperature variations of a fluid in a pipe, the probe should be small enough to capture the variations in the temperature field but not extremely small such that molecular interactions becomes important and in these cases the definition of temperature itself becomes meaningless. At this scale (of order of mean free path of fluid molecules), large variations in the measured temperature occur not due to the physical phenomena itself but due to the violations of the length scale constraints. Figure 3.5 shows hypothesized variations in density as a macroscopic parameter on moving from one scale to another.

### **3.5.2 The choice of an averaging volume.**

The idea behind the method of volume averaging (as indicated previously) is to smooth point functions defined over the fluid phase and to produce functions of averaged quantities defined over a newly defined, fictitious porous medium domain and hence define a continuum. The newly defined, fictitious porous medium is the one over which the newly defined averaged governing laws are valid in addition to the fact that the macroscopic averaged quantities are continuous and may be considered as point functions. But any size of averaging volume (just larger than the size of a typical pore or grain) may do the job. In order, thus, to formulate a useful theory one may need to look at other considerations as well. These have been collected in three criteria. The first of

which is related to the fact that if the averaged quantities (variables) are going to be measured during applications, it is important that the size of the measuring instruments (the averaging volume) do not influence the measured quantities. In other words, the averaged quantities should not change if the averaging volume increased or decreased in a certain range. Secondly, the behavior of the averaged quantities should be explainable in terms of the general averaged conservation laws. In other words, the variations of the averaged quantities over the domain of study should be in such a way that only averaged causes (gradients, forces, etc.) may explain their change. The third criterion, as stated by Hassanizadeh and Gray (1979), that “the primitive concept of a physical quantity, as first introduced into the classical continuum mechanics, must be preserved by proper definition of the macroscopic quantities”.

To illustrate the first point, let us first restrict ourselves to an infinite domain of a statistically homogeneous porous medium. Take for example the phase function defined as

$$\begin{aligned} \gamma_{\beta} &= 1 && \text{in the } \beta\text{-phase within the averaging volume} \\ \gamma_{\beta} &= 0 && \text{elsewhere} \end{aligned}$$

Averaging of this function over the averaging volume should yield the porosity of the  $\beta$ -phase. The relationship between the size of the averaging volume and the porosity is shown in Fig. 3.4. From this figure one can notice the erratic variations in the porosity when the averaging volume is small. These variations get smaller and smaller as the size of the averaging volume increases

and finally an approximately constant value is reached. If the size of averaging volume continues to increase, the porosity will still be approximately constant. Thus, any size of the averaging volume within this region should yield the same value of porosity, and hence would be representative to the given porous medium (Representative Elementary Volume, REV). Representative in the sense that all the averaged properties of that given porous medium in this volume (porosity, permeability, dispersivity...etc.) represent the whole porous medium domain. In other words, if one picked an REV from anywhere in the homogeneous porous medium domain, the averaged properties would be more or less the same. Failure to define an REV would result in failure to define a continuum. Not only does one needs to define an REV but also a range for the REV as well. One reason for that stems from the fact that the size of the REV is generally not known exactly. Hence if a single size for the REV is defined, the measured quantities will be very sensitive if one does not use the appropriate size of the measuring instrument. In addition, since every macroscopic parameter may require certain range of averaging volumes that are in general different from other macroscopic parameters it is important that these ranges overlap such that a common range of averaging volumes may be found that could be used in the averaging techniques.

Local averaging, on the other hand, would not result in single averaged quantities for the whole porous medium domain. To the contrary, it allows for local variations in the averaged quantities, and forms the basis of the second criterion. It describes the acceptable behavior of the averaged quantities in a way

that makes sense. This second criterion may be stated as follows: proper averaging would result in the averaged quantities to vary linearly, (or as close to linear as possible) within the REV. Mathematically, it may be defined as:

$$\langle\langle \psi_\beta \rangle\rangle = \langle \psi_\beta \rangle \quad (3.12)$$

where  $\psi_\beta$  is any conservative quantity,  $\langle \psi_\beta \rangle$  and  $\langle\langle \psi_\beta \rangle\rangle$  is the phase average determined over the actual and the fictitious porous media, respectively. Whitaker (1999), in the course of averaging transport equations indicated that, if the variations of the averaged quantities within the REV deviate significantly from a straight-line relationship, higher order derivatives might be important and this would lead to a mathematically ill-posed problem. However, the above mentioned criterion is not meant to ease mathematical manipulation, rather it is a requirement to obtain a proper presentation of a macroscopic view that makes sense. The easiness of mathematical manipulation upon imposing this criterion is, in fact, a by product.

Failure to define a common REV for the whole domain indicates that the method of volume averaging could not be adapted and a more sophisticated mathematical treatment should be used. Cushman (1983) indicated that it might be difficult to define a single REV for the entire flow domain. He introduced a generalization of the volume averaging concept by averaging over varying size REV, as long as one can find a smoothly varying REV. In this case, the system may be called statistically locally homogeneous.

### **3.6 On the Length Scale Constraints in Porous Media.**

One of the crucial characteristics of porous media is the existence of several length scales. These length scales arise for different reasons and from different sources. However, one might be able to distinguish two main types of length scales associated with the averaging processes and they are:

1. Length scales due to the structure of the porous medium (sometimes they are known as geometrical length scales). For example, length scales inherent to particles diameters, pores diameters, and length scales associated with regional heterogeneity, e.g., extent to where boundaries between porous medium domain and other media (water bodies, atmosphere, etc.).
2. Length scale constraints arise during volume averaging of the governing partial differential equations for the sake of making the averaged equations amenable to mathematical treatment.

There is a fundamental difference between both kinds of constraints. While the first one represents a real constraint that is strictly related to the structure of the porous medium, the second one represents only a restriction due to our inability to consider higher order terms that arise from Taylor series expansion as will be discussed later. It turned out, however, that the length scale constraints generated during the course of the averaging processes of transport equations are automatically satisfied once the geometric length scale constraints are satisfied, as will be discussed later.

### **3.6.1 Length scale constraints due to the heterogeneity of porous media.**

Whitaker (1967) indicated that if  $l_\beta$  represents a typical pore diameter (p.s. there is no exact definition of  $l_\beta$ , i.e.,  $l_{\beta 10}$ ,  $l_{\beta 50}$  or  $l_{\beta 90}$ , it only reflect an order of magnitude)  $l_\sigma$  represents a typical particle diameter (assuming that  $l_\beta$  and  $l_\sigma$  are of the same order of magnitude),  $L$  represents a characteristic length of the domain (thickness, width or extent), Fig. 3.2, then the length scale of the averaging volume,  $l$ , should satisfy the following length scale constraints:

I.  $l \gg l_\beta$

This length scale constraints ensures that the erratic changes in the averaged quantities due to pore scale heterogeneity have been damped away as shown in Fig. 3.4.

II.  $l \ll L$

This length scale constraint ensures that the studied porous medium domain is large enough compared with the averaging volume such that the boundary regions are of little effect. Take the measurements of the permeability in the laboratory as an example. Permeability of a given porous medium is measured in the lab using a permeameter, either fixed head or falling head. If the diameter of the permeameter is not large enough such that condition [II] is satisfied, every time one changes the diameter of the permeameter, different value of the permeability will be measured due to the boundary effects, which increase as the diameter decreases.

These two length scale inequalities constitute the main length scale constraints that should be satisfied in order for an REV to be defined. Another requirement is yet to be declared at this stage:

### 3.6.2 A new requirement.

As indicated previously, the second criterion (section 3.5.2) requires that the variation of averaged quantities within the averaging volume be linear (or as close to linear as possible). This criterion stems from the requirement that sampling an averaging volume in both the real and the newly defined, fictitious porous medium, where the averaged quantities apply should be the same. For instance consider any conservative quantity,  $\psi_\beta$ , which may be a scalar (e.g., mass per unit volume, energy per unit mass, etc.), or a vector (e.g., linear momentum per unit mass). The total amount of  $\psi_\beta$  in a given volume (REV in this case) of a given porous medium may be evaluated as:

$$\psi_{total} = \int_{rev} \rho_\beta(\mathbf{r}, t) \psi_\beta(\mathbf{r}, t) \gamma_\beta(\mathbf{r}, t) dv \quad (3.13)$$

where  $\psi_\beta$  is a function representing a conservative quantity over the  $\beta$ -phase per unit mass,  $\gamma_\beta$  is the phase function defined earlier, and  $\mathbf{r}$  represents the position vector spanning the REV. The time,  $t$ , in the argument of the indicator function,  $\gamma_\beta$  represents the scenario of moving interfaces (e.g., immiscible multiphase system). In our case, however, the time may be omitted due to the

fact that for our solid-fluid systems, the interface boundaries are assumed fixed in space. Refer to Fig. 3.5 for a geometrical illustration.

The total amount of  $\psi_\beta$  should be equal to that evaluated over the same volume in the fictitious porous medium, that is:

$$\psi_{total} = \int_{rev} \langle \rho_\beta \rangle^\beta(\mathbf{r}, t) \langle \psi_\beta \rangle^\beta(\mathbf{r}, t) \varepsilon_\beta(\mathbf{r}) dv \quad (3.14)$$

where  $\langle \rho_\beta \rangle^\beta$  is the intrinsic phase average density which would equal the point density for incompressible fluids,  $\langle \psi_\beta \rangle^\beta$  is the intrinsic mass average function (per unit mass of the fluid filling the pores of the REV), and  $\varepsilon_\beta$  is the porosity function over the REV.

There is yet another requirement in that sampling the same volume (REV) in both the actual porous medium and the fictitious one should yield the same conservative quantity. Collectively one may write the above two equation together with this requirement as:

$$\int_{REV} \rho_\beta(\mathbf{r}, t) \psi_\beta(\mathbf{r}, t) \gamma_\beta(\mathbf{r}) dv = \int_{REV} \langle \rho_\beta \rangle^\beta(\mathbf{r}, t) \langle \psi_\beta \rangle^\beta(\mathbf{r}, t) \varepsilon_\beta(\mathbf{r}) dv =$$

$$\langle \rho_\beta \rangle^\beta(\mathbf{x}, t) \langle \psi_\beta \rangle^\beta(\mathbf{x}, t) \varepsilon_\beta(\mathbf{x})(REV) \quad (3.15)$$

where  $\langle \psi_\beta \rangle^\beta(\mathbf{x}, t)$  and  $\varepsilon_\beta(\mathbf{x})$  are the intrinsic-mass average and the porosity at the centroid of the REV. For the case of constant density, incompressible fluids we have  $\rho_\beta(\mathbf{r}, t) = \langle \rho_\beta \rangle^\beta(\mathbf{r}, t) = \langle \rho_\beta \rangle^\beta(\mathbf{x}, t) = \text{const.}$  and hence we can cancel

them out. Equation (3.15) then implies that the product  $\langle \psi_\beta \rangle^\beta(\mathbf{r}, t) \varepsilon_\beta(\mathbf{r})$  changes linearly over the REV. There are at least three possibilities for the product  $\langle \psi_\beta \rangle^\beta(\mathbf{r}, t) \varepsilon_\beta(\mathbf{r})$  to change linearly within the REV:

1. both  $\langle \psi_\beta \rangle^\beta$  and  $\varepsilon_\beta$  remain constant within the REV.
2.  $\langle \psi_\beta \rangle^\beta$  changes linearly and  $\varepsilon_\beta$  remains constant.
3.  $\langle \psi_\beta \rangle^\beta$  remains constant and  $\varepsilon_\beta$  changes linearly.

The requirement that averaged conservative quantities vary linearly within the REV, is rather restrictive. One can still live with acceptable relaxation to this requirement by allowing the conservative quantities to vary as close to linear as possible.

In most applications, averaged conservative quantities are likely to change within the REV, (e.g. solute concentration). In this case, and to have a proper macroscopic presentation, porosity needs to be almost constant within the REV. To be less restrictive, porosity should not change significantly within the REV. One may define this condition as: If  $\ell_\varepsilon$  represents the length scale over which significant variation in porosity occur within the REV, and  $\ell_\psi$  represents that length scale over which significant deviation from the straight line variation of the intrinsic phase average of the conservative quantity  $\langle \psi_\beta \rangle^\beta$  may occur, then

$$\text{III} \quad l \ll \min(\ell_\varepsilon, \ell_\psi)$$

As will be seen in the next section Whitaker and his coworkers introduced this constraint in another context. Bachmat et al. (1986) suggested that all the

macroscopic properties change linearly within the averaging volume which may not be quite the case as suggested by the previous analysis.

### 3.6.3 Length scale constraints arising during averaging processes.

Confining ourselves to flow in porous media and presenting the work of Whitaker and his co-workers when they applied the method of volume averaging to Stokes flow over the porous medium domain shown in Fig. 3.2, flow is defined by the following boundary value problem.

$$\nabla \cdot \mathbf{v}_\beta = 0, \quad \text{in the } \beta \text{ phase} \quad (3.16)$$

$$0 = \nabla p_\beta + \rho_\beta \mathbf{g} + \mu_\beta \nabla^2 \mathbf{v}_\beta, \quad \text{in the } \beta \text{ phase} \quad (3.17)$$

$$\text{B.C. 1 } \mathbf{v}_\beta = 0, \quad \text{at } A_{\beta\sigma}, \quad (3.18)$$

$$\text{B.C. 2 } \mathbf{v}_\beta = f(\mathbf{r}, t) \quad \text{at } A_{\beta e} \quad (3.19)$$

Where  $\mathbf{v}_\beta$  is the velocity vector in the  $\beta$ -phase,  $p_\beta$  is the pressure in the  $\beta$ -phase,  $\mathbf{g}$  is the gravity vector,  $\mu_\beta$  is the viscosity of the  $\beta$ -phase, and  $\rho_\beta$  is the density of the  $\beta$ -phase. Here  $A_{\beta\sigma}$  represents the area of the  $\beta - \sigma$  interface contained in the macroscopic region while  $A_{\beta e}$  represents the area of the  $\beta$ -phase entrances and exits associated with the macroscopic system.

Consider Fig. 3.2 and let  $\psi_\beta$  be any quantity, scalar, vector, or tensor defined over the  $\beta$ -phase. Averaging this quantity over an REV will yield the superficial phase average defined by:

$$\langle \psi_\beta \rangle = \frac{1}{V} \int_{V_\beta} \psi_\beta dV \quad (3.20)$$

Another formula may also be used to define what was previously called the intrinsic phase average defined by:

$$\langle \psi_\beta \rangle^\beta = \frac{1}{V_\beta} \int_{V_\beta} \psi_\beta dV \quad (3.21)$$

here  $V_\beta$  represents the volume of the  $\beta$ -phase contained within the averaging volume. There is, however, a relationship between (3.20) and (3.21) given by:

$$\langle \psi_\beta \rangle = \varepsilon_\beta \langle \psi_\beta \rangle^\beta \quad (3.22)$$

where  $\varepsilon_\beta$  is the porosity of the  $\beta$ -phase. Moreover, the average of the gradient can be formulated in terms of the gradient of the average using:

$$\langle \nabla \psi_\beta \rangle = \nabla \langle \psi_\beta \rangle + \frac{1}{V} \int_{A_{\beta\sigma}} \mathbf{n}_{\beta\sigma} \psi_\beta dA \quad (3.23)$$

Here  $A_{\beta\sigma}$  represents the interfacial area contained within the averaging volume and  $\mathbf{n}_{\beta\sigma}$  is the outwardly directed unit normal vector for the  $\beta$ -phase. Now the averaging of the gradient produced, in addition to the required quantity, the gradient of the average, an unwanted quantity that incorporates point function.

To deal with the point function in the integral defined in equation (3.23), Gray (1975) proposed decomposing the point value into the intrinsic phase average and a spatial deviation, such that:

$$\psi_\beta = \langle \psi_\beta \rangle^\beta + \tilde{\psi}_\beta \quad (3.24)$$

Thus substituting into (3.23) yields:

$$\langle \nabla \psi_\beta \rangle = \nabla \langle \psi_\beta \rangle + \frac{1}{v} \int_{A_{\beta\sigma}} \mathbf{n}_{\beta\sigma} \langle \psi_\beta \rangle^\beta dA + \frac{1}{v} \int_{A_{\beta\sigma}} \mathbf{n}_{\beta\sigma} \tilde{\psi}_\beta dA \quad (3.25)$$

The second term in the right hand side of eqn (3.25) represents a non-local term since the dependent variable  $\langle \psi_\beta \rangle^\beta$  is evaluated at points other than the centroid of the averaging volume. Non-local problems have been studied by Koch and Brady (1987), Cushman and Ginn (1993), Quintard and Whitaker (1993 a,b), and many others. Whitaker (1999) indicated that the analysis of non-local phenomena is extremely complex; thus there is a great deal of motivation for avoiding a non-local problem whenever possible. He also indicated that one could extract a local theory provided certain length scale constraints are satisfied. Thus by taking Taylor series expansion of  $\langle \psi_\beta \rangle^\beta$  around the centroid, one gets:

$$\langle \psi_\beta \rangle^\beta \Big|_r = \langle \psi_\beta \rangle^\beta + \mathbf{r} \cdot \nabla \langle \psi_\beta \rangle^\beta + \frac{1}{2} \mathbf{r} \mathbf{r} : \nabla \nabla \langle \psi_\beta \rangle^\beta + \dots \quad (3.26)$$

Since the function  $\langle \psi_\beta \rangle^\beta$  and its gradients are evaluated at the centroid, they are constants with respect to the integration process and hence can be removed from the integrals, thus:

$$\begin{aligned} \frac{1}{v} \int_{A_{\beta\sigma}} \mathbf{n}_{\beta\sigma} \langle \psi_\beta \rangle^\beta dA &= \left\{ \frac{1}{v} \int_{A_{\beta\sigma}} \mathbf{n}_{\beta\sigma} dA \right\} \langle \psi_\beta \rangle^\beta + \left\{ \frac{1}{v} \int_{A_{\beta\sigma}} \mathbf{n}_{\beta\sigma} \mathbf{y}_\beta dA \right\} \cdot \nabla \langle \psi_\beta \rangle^\beta + \\ &+ \left\{ \frac{1}{v} \int_{A_{\beta\sigma}} \mathbf{n}_{\beta\sigma} \frac{1}{2} \mathbf{y}_\beta \mathbf{y}_\beta dA \right\} : \nabla \nabla \langle \psi_\beta \rangle^\beta + \dots \end{aligned} \quad (3.27)$$

where  $\mathbf{y}_\beta$  is the position vector with respect to the centroid, Fig. 3.7. The terms in brackets represent a series of geometrical integrals that are related to the

structure of the porous medium. Quintard and Whitaker (1994-a,b,c,d,e) have evaluated these integrals and put them in the following forms:

$$\frac{1}{v} \int_{A_{\beta\sigma}} \mathbf{n}_{\beta\sigma} dA = -\nabla \langle 1 \rangle \quad (3.28)$$

$$\frac{1}{v} \int_{A_{\beta\sigma}} \mathbf{n}_{\beta\sigma} \mathbf{y}_{\beta} dA = -\nabla \langle \mathbf{y}_{\beta} \rangle \quad (3.29)$$

$$\frac{1}{v} \int_{A_{\beta\sigma}} \mathbf{n}_{\beta\sigma} \mathbf{y}_{\beta} \mathbf{y}_{\beta} dA = -\nabla \langle \mathbf{y}_{\beta} \mathbf{y}_{\beta} \rangle \quad (3.30)$$

Where they indicated that  $\langle 1 \rangle$ ,  $\langle \mathbf{y}_{\beta} \rangle$ ,  $\langle \mathbf{y}_{\beta} \mathbf{y}_{\beta} \rangle$ , etc., should be thought of as the zeroeth, first, second, etc., superficial spatial moments of the  $\beta$ -phase contained in the averaging volume. Noting that:

$$\langle 1 \rangle = \frac{1}{v} \int_{v_{\beta}} 1 dv = \varepsilon_{\beta} \quad (3.31)$$

hence

$$\frac{1}{v} \int_{A_{\beta\sigma}} \mathbf{n}_{\beta\sigma} dA = -\nabla \langle 1 \rangle = -\nabla \varepsilon_{\beta} \quad (3.32)$$

and equation (3.27) becomes

$$\frac{1}{v} \int_{A_{\beta\sigma}} \mathbf{n}_{\beta\sigma} \langle \psi_{\beta} \rangle^{\beta} dA = -\nabla \varepsilon_{\beta} \langle \psi_{\beta} \rangle^{\beta} - \nabla \langle \mathbf{y}_{\beta} \rangle \cdot \nabla \langle \psi_{\beta} \rangle^{\beta} - \nabla \langle \mathbf{y}_{\beta} \mathbf{y}_{\beta} \rangle : \nabla \nabla \langle \psi_{\beta} \rangle^{\beta} \dots \quad (3.33)$$

Introducing this term into equation (3.21) yields

$$\begin{aligned} \langle \nabla \psi_{\beta} \rangle = & \nabla \langle \psi_{\beta} \rangle - \nabla \varepsilon_{\beta} \langle \psi_{\beta} \rangle^{\beta} - \nabla \langle \mathbf{y}_{\beta} \rangle \cdot \nabla \langle \psi_{\beta} \rangle^{\beta} - \nabla \langle \mathbf{y}_{\beta} \mathbf{y}_{\beta} \rangle : \nabla \nabla \langle \psi_{\beta} \rangle^{\beta} \dots + \\ & + \frac{1}{v} \int_{A_{\beta\sigma}} \mathbf{n}_{\beta\sigma} \tilde{\psi}_{\beta} dA \end{aligned} \quad (3.34)$$

Now, if the  $\beta$ -phase is uniformly distributed around the centroid of the averaging volume one might assume  $|\langle \mathbf{y}_\beta \rangle| \ll 1$  and thus  $[\nabla \langle \mathbf{y}_\beta \rangle] \ll \mathbf{I}$  where  $\mathbf{I}$  is the 2<sup>nd</sup> order unit tensor. Note that this condition might not be satisfied in the vicinity of the interface boundary between a porous medium and other systems. Whitaker also indicated that

$$\langle \mathbf{y}_\beta \mathbf{y}_\beta \rangle = \mathbf{o}(\varepsilon_\beta r_o^2) \quad (3.35)$$

which leads to

$$\nabla \langle \mathbf{y}_\beta \mathbf{y}_\beta \rangle = \mathbf{o}(\Delta \varepsilon_\beta r_o^2 / L_\varepsilon) \quad (3.36)$$

where  $L_\varepsilon$  is the length scale associated with the porosity and  $r_o$  is the radius of the REV. It is the length scale over which significant changes in the porosity occur. In an infinite homogeneous porous medium this length scale extends to infinity, in a finite homogeneous medium it extends to coincide with the characteristic length scale of the domain,  $L$ , while for heterogeneous medium with slowly varying heterogeneity it coincides with  $\ell_\varepsilon$ . Hence,

$$\nabla \langle \mathbf{y}_\beta \mathbf{y}_\beta \rangle = \nabla \nabla \langle \psi_\beta \rangle^\beta = \mathbf{o} \left( \left[ \frac{r_o^2}{L_\varepsilon L_\psi} \right] \Delta \varepsilon \nabla \langle \psi_\beta \rangle^\beta \right) \quad (3.37)$$

where  $L_\psi$  is the length scale associated with  $\psi$ . It represents the length scale over which significant change in  $\psi$  occurs. Thus to neglect the last term in equation (3.33), the following length scale constraints should be satisfied

$$r_o^2 \ll L_\varepsilon L_\psi \quad (3.38)$$

Now based on what  $\psi$  defines, one might be able to define similar constraints for pressure, velocity, etc. It is apparent that inequality (3.38) would automatically be

satisfied once inequality III is satisfied. Thus in conclusion, for flow in porous media, the geometrical length scale constraints represent the most important kind of constraints that must be satisfied. Other kinds of constraints arising from averaging processes are generally automatically satisfied as long as the geometrical length scale constraints are satisfied. In general, one might be able to define the following categories:

1. Homogeneous infinite porous media

For homogeneous infinite porous media, satisfaction of the geometrical length scale inequalities I and III is sufficient for one to define a continuum. Inequality II is automatically satisfied for this system. It is to be noted however, that the length scale associated with the porosity is infinitely large, thus it is the length scales associated with the conservative quantities that need to be checked based on inequality III. In this system Darcy's law is sufficient to handle flow problems provided the Reynolds number constraint is met.

2. Homogeneous finite porous media

For this system one may consider two cases. The first of which represents the case when the extent of the domain is so large such that inequality II is satisfied. For this system, apart from the boundary region, one can still consider Darcy's law. Again the length scale associated with the porosity would be as large as the extent of the domain. Hence, length scales associated with conservative quantities need to be checked. Bear and Bachmat (1986) suggested extending the macroscopic properties to the

boundary regions, even though they are violating inequality III there. They further suggested that the errors due to this may be neglected.

The second represents the case when the extent of the domain is small such that inequality II is not met. In this case, the boundary region for which one cannot even define an REV and where the length scale constraints are violated may have significant influence on the behavior of such systems. Using Darcy's law and the macroscopic governing laws in these regions may lead to significant errors. Even the method of volume averaging faces difficulties in these regions. Some success has been demonstrated when evaluating the boundary between a homogeneous fluid and a porous medium. Oacha-Tapia and Whitaker (1995-a,b) introduced a momentum jump condition at such an interface to be able to extend the averaged equation to the boundary region, as will be discussed later. Hassanzadeh and Gray (1989-a,b) provided an interesting approach to deal with the boundary regions by treating them as a two-dimensional interface region surrounded by two three-dimensional regions. However, these approaches introduce constitutive equations that are problem dependent and need to be determined experimentally.

3. Heterogeneous infinite porous medium with smooth, slowly varying properties.

In these systems, the length scale constraints defined by inequality III represent the key constraint. In such systems the length scales associated

with the porosity and each of the conservative quantities must be examined such that criterion III is satisfied.

4. Heterogeneous infinite porous medium with sharp varying properties.

If the heterogeneity prevails such that length scale constraint III is violated and an REV could not be defined, then neither Darcy's law nor the volume averaging method can treat such systems. In this case, the solution may be to evaluate the problem at an even larger scale and define another continuum, Figs. 3.6 and 3.7. When the heterogeneity is local, especially in layered systems where one or more layers are thin such that inequality (II) is not satisfied, one can treat these layers as two-dimensional layers separating two continua as described by Hassanzadeh and Gray (1989 a,b).

### **3.8 Problems associated with the Interface Boundary.**

It has to be mentioned that although averaging techniques may have helped in smoothing functions that suffer from analyticity problems in the domain of study, they can, however, lead to unrealistic situations if no careful investigation of the length scale constraints is carried out. As an example, in situations where there exist two or more zones in the domain of study of very different structure (e.g., a porous medium adjacent to a fluid body, a solid wall or another very different porous medium), averaging over the whole domain will not only smooth the functions of interest in the different zones but also will smooth the interface boundaries. In other words, the averaging processes will not

maintain the interface boundaries as sharp but rather smoothly varying properties will result that do not really exist. Figure (3.8) illustrates a multi scale layered system where the boundary regions show nonlinear variations in the averaged quantities as the averaging volume moves from one layer to the other. From this figure and recalling inequality III, one may conclude that in the neighborhood of the interface boundary between one porous medium and another porous medium, a fluid body or a solid boundary, the averaging processes could not be performed.

Thus, in general, the continuum approach could not be adapted at the interface boundary (with a thickness equal to the radius of the averaging volume from both sides). Moreover local variations in porous medium characteristics in the vicinity of the interface boundary due to, for example, the presence of a confining surface or the penetration of smaller size grains of a given porous layer into the pores of an adjacent layer of different porosity have also been observed. That is to say, the structure of the porous medium in the neighborhood of interface boundaries may not be the same as that in the main body. Several studies on the effects of confining layers on local porosity have confirmed its fluctuations in the vicinity of a confining wall up to approximately 10 particle radii (Smith et al. 1970). In beds of uniform spheres, Benenati and Brosilow (1962) showed that the fluctuations extend to around five particle radii. This would lead to many effects like channeling, by-pass phenomena, etc. Moreover, the properties of the porous media will depend on factors that are not unique characteristics of the structure of the porous media. For example, in addition to

the structure of the porous medium, the permeability will depend on factors like the shape of the wall, the length scale associated with the confining surface compared with the average grain size, the packing characteristics, etc. Figure 3.9 shows a schematic of the fluctuation in local porosity in the vicinity of a confining wall. Different techniques were found in the literature to deal with the boundary based on the two mediums encompassing the interface as will be discussed in the next sections.

### **3.8.1 The interface between a porous medium and a fluid body.**

#### **3.8.1.1 The Beavers and Joseph boundary condition.**

For the cases where there is an incompressible fluid flowing in the presence of porous bodies, one generally assumes that outside the porous regions the fluid obeys the Navier-Stokes equations. On the other hand, Darcy's law can be applied to flow within the porous domain. However, to make the problem determinate, one must make assumptions regarding the nature of the boundary conditions at the interface between porous region and clear fluid. One obvious condition is the continuity of mass flow and hence continuity of normal velocity. A second assumption would be continuity of the normal component of stress. However, these conditions are not sufficient and a third is required. At first it was argued that for materials with a small permeability, the surface of a porous body could be regarded as a solid surface containing many tiny holes (an analogy to surface roughness in solid surfaces), and therefore the no slip condition may be applied. This no-slip condition cannot be correct for bodies of

large permeability where obviously slip must occur at the surface. Therefore, a more sophisticated boundary condition was required which captured the essential behavior of the fluid flow at any fluid/porous interface.

Beavers and Joseph (1967), considered the rectilinear flow of a viscous fluid through a two-dimensional parallel channel formed by an impermeable upper wall and a permeable lower region Fig. 3.10. They postulated that the fluid slip velocity at the permeable interface must differ across a boundary layer from the mean velocity in the porous region. This boundary layer can greatly alter the nature of the tangential motion near the interface. Assuming that the fluid slip velocity,  $u_f$ , is proportional to the shear rate at  $z=0$ , they derived an ad hoc boundary condition at the interface,

$$\frac{du_f}{dz} = \frac{\alpha}{\sqrt{K}}(u_f - u_m), \quad (3.39)$$

where  $K$  is the permeability of the porous region. Quantities  $u_f$  and  $\frac{du_f}{dz}$  are evaluated at  $z = 0^+$ , while  $u_m$  is evaluated at some small distance from the plane  $z=0$ .

The dimensionless quantity  $\alpha$  is independent of the viscosity of the fluid or the height of the clear fluid channel. Instead it depends only on the material parameters, which characterize the structure of the permeable material. Beavers and Joseph carried out a number of experiments in order to quantify  $\alpha$  for a variety of materials of varying average pore size. For example, they examined three foametal blocks having average pore sizes 0.41, 0.86 and 1.14 mm, and

found that  $\alpha$  had the values 0.78, 1.45 and 4.0, respectively. Taylor (1971) and Richardson (1971) examined the Beavers and Joseph boundary condition by considering a comparable model for a porous region. In particular, their experiment results and theory confirmed Beavers and Joseph's model, provided the channel height is much larger than pore width.

### **3.8.1.2 Volume averaging techniques as applied to momentum transfer at the boundary between a porous medium and a homogeneous fluid.**

Ochoa-Tapia and Whitaker (1995-a,b) and (1998-b) by not imposing the length scale constraints introduced previously to simplify transport equations were able to use volume averaging techniques to develop generalized averaging transport equations that are valid everywhere in the region (whether in the porous medium, in the fluid body or at the interface). Referring to Figs 3.10,11, they started from Stokes' equations and realized the mismatch of boundary conditions at the boundaries  $y=h$  and  $y=-H$  in the sense that at  $y=h$  the point velocity is zero while at  $y=-H$  the averaged normal velocity is zero. The mismatch between point and volume averaged quantities at the interface between a porous medium and a homogeneous fluid has been noted also by various authors (Somerton et al., 1982; Haber et al. 1983; Nield et al. 1992; Prat, 1989, 1990, 1992). Their basic theme was based on the idea that volume averaged quantities should be continuous at boundaries that involve a porous medium. By averaging equations (3.16) and (3.17) over an REV (refer to Fig. 3.5) they were able to arrive at the following set of equations for the whole domain:

$$\nabla \cdot \langle \mathbf{v}_\beta \rangle = 0 \quad (3.40)$$

for continuity and

$$0 = -\nabla \langle p_\beta \rangle^\beta + \rho_\beta \mathbf{g} + \varepsilon_\beta^{-1} \mu_\beta \nabla^2 \langle \mathbf{v}_\beta \rangle - \mu_\beta \varepsilon_\beta^{-1} (\nabla \varepsilon_\beta) \cdot [\nabla (\varepsilon_\beta^{-1} \langle \mathbf{v}_\beta \rangle)] - \mu_\beta \boldsymbol{\Phi}_\beta \quad (3.41)$$

for momentum which represents the volume averaged Stokes' equations. The vector  $\boldsymbol{\Phi}_\beta$  in equation (3.40) is defined by

$$\mu_\beta \boldsymbol{\Phi}_\beta = -\frac{1}{V_\beta} \int \mathbf{n}_{\beta\sigma} \cdot [-(p_\beta|_{\mathbf{x}+\mathbf{y}_\beta} - \langle p_\beta \rangle^\beta|_{\mathbf{x}}) + \mu_\beta (\nabla \mathbf{v}_\beta|_{\mathbf{x}+\mathbf{y}_\beta} - \nabla \langle \mathbf{v}_\beta \rangle^\beta|_{\mathbf{x}})] dA \quad (3.42)$$

Solution of these two equations to produce velocity and pressure fields would require a closed form of equation (3.41). Ochoa-Tapia and Whitaker (1995-a,b) indicated that this could be avoided if an acceptable jump condition can be constructed.

In homogeneous porous medium,  $\boldsymbol{\Phi}_\beta$  can have a special simple form provided that certain length scale constraints are satisfied, namely:

$$\frac{r_o^2}{L_\varepsilon L_{p1}} \ll 1, \quad \frac{r_o^2}{L_\varepsilon L_{v2}} \ll 1, \quad \text{and} \quad l_\beta \ll r_o$$

where  $r_o$  is the radius of the averaging volume,  $L_\varepsilon$ ,  $L_{p1}$ ,  $L_{v2}$  and  $l_\beta$  are length scales associated with an order of magnitude analysis to the following terms:

$\nabla \varepsilon_\beta$ ,  $\nabla \nabla \langle p_\beta \rangle^\beta$ ,  $\nabla \nabla \nabla \langle \mathbf{v}_\beta \rangle^\beta$ , respectively. Quintard and Whitaker (1993-a)

proved that  $\boldsymbol{\Phi}_\beta$  in this case might be given by  $\boldsymbol{\Phi}_\beta = \mathbf{K}_{\beta\omega}^{-1} \cdot \langle \mathbf{v}_\beta \rangle$  in the

homogeneous  $\omega$ -region, where  $\mathbf{k}_{\beta\omega}$  is the usual Darcy's law permeability tensor, and thus,

$$\langle \mathbf{v}_\beta \rangle = -\frac{\mathbf{k}_{\beta\omega}}{\mu_\beta} \cdot (\nabla \langle p_\beta \rangle_\omega^\beta - \rho_\beta \mathbf{g} - \varepsilon_\beta^{-1} \mu_\beta \nabla^2 \langle \mathbf{v}_\beta \rangle_\omega) \quad (3.43)$$

This is Darcy's law with the first Brinkman correction. In conclusion, one might indicate that far from the interface boundary the following averaged equations may be used:

$$\nabla \cdot \langle \mathbf{v}_\beta \rangle_\omega = 0 \quad \text{in the } \omega\text{-region} \quad (3.44)$$

$$0 = -\nabla \langle p_\beta \rangle_\omega^\beta - \rho_\beta \mathbf{g} - \varepsilon_\beta^{-1} \mu_\beta \nabla^2 \langle \mathbf{v}_\beta \rangle_\omega - \mu_\beta \mathbf{k}_{\beta\omega}^{-1} \langle \mathbf{v}_\beta \rangle \quad \text{in the } \omega\text{-region} \quad (3.45)$$

$$\nabla \cdot \langle \mathbf{v}_\beta \rangle_\eta = 0 \quad \text{in the } \eta\text{-region} \quad (3.46)$$

$$0 = -\nabla \langle p_\beta \rangle_\eta^\beta - \rho_\beta \mathbf{g} - \mu_\beta \nabla^2 \langle \mathbf{v}_\beta \rangle_\omega \quad \text{in the } \eta\text{-region} \quad (3.47)$$

In the absence of the length scale constraints given previously, one should use equations (3.41-42); keeping in mind that they are not closed since the vector  $\boldsymbol{\phi}_\beta$  depends on point functions as well as averaged quantities. Ochoa-Tapia and Whitaker (1995-a,b) indicated that equations (3.44-47) could still be used in the boundary region keeping in mind that quantities such as  $\langle \mathbf{v}_\beta \rangle_\omega$  and  $\langle p_\beta \rangle_\eta^\beta$  may not accurately predict the local volume averaged velocity and pressure. The errors generated by the use of equations (3.44-47) inside the boundary region might be corrected by means of the jump conditions, which ensure that equations (3.37-38) are satisfied on average. Thus by integrating equations (3.41-42) over a large volume surrounding the interface boundary, Fig.

(3.11), they were able to link equations (3.40-43) through the following boundary conditions defined at the interface surface, which are:

$$\langle v_{\beta} \rangle_{\omega} = \langle v_{\beta} \rangle_{\eta} \quad (3.48)$$

$$\begin{aligned} \mathbf{n}_{\omega\eta} \cdot [ -I(\langle p_{\beta} \rangle_{\omega}^{\beta} - \langle p_{\beta} \rangle_{\eta}^{\beta}) + \mu_{\beta} (\varepsilon_{\beta\omega}^{-1} \nabla \langle \mathbf{v}_{\beta} \rangle_{\omega} - \nabla \langle \mathbf{v}_{\beta} \rangle_{\eta}) ] = \\ -\mu_{\beta} \delta \mathbf{D} \cdot [ \mathbf{K}_{\beta\omega}^{-1} \cdot \langle \mathbf{v}_{\beta} \rangle_{\omega} ] + \mu_{\beta} \delta^{-1} \mathbf{A} \cdot (\varepsilon_{\beta\omega} - 1)^2 (\varepsilon_{\beta\omega}^{-3} \langle \mathbf{v}_{\beta} \rangle_{\omega} + \langle \mathbf{v}_{\beta} \rangle_{\eta}) \end{aligned} \quad (3.49)$$

where  $\mathbf{D}$  and  $\mathbf{A}$  are dimensionless adjustable tensors coefficient on the order of unity, and  $\delta$  is the thickness of the boundary region.

The idea was that if one used equations (3.44-47) the velocity profile will be given by the dashed line shown in Fig. 3.12-a. This means, in terms of the continuity equation, that an excess flux should be defined to represent the difference between the actual velocity and the calculated ones. Ochoa-Tapia and Whitaker (1995-a,b) represented this excess mass flux and the excess stresses (arising from momentum equations) at the interface surface as a momentum jump condition, Fig. 3.12-b.

### 3.8.2 The interface between a porous medium and a solid surface.

The influence of confining walls on local porosity has long been recognized. For irregular particles such as Berl saddles and fractured media, the void fraction decreases regularly from one at the wall to the bulk average value at about one particle radius from the wall, Roblee et al. (1958). For regular particles the results differ with individual shape. Spheres and cylinders exhibit a sinusoidal distribution of porosity ranging from one to a minimum value at one particle

radius from the wall. The amplitude of the cycling decreases with distance into the bed, and the bulk value is reached about five particle diameters into the bed, as indicated previously in Fig. 3.9. The main feature of these porosity fluctuations is the channeling and bypass of fluids near the walls because it represents a comparatively low resistance region.

These phenomena have been recognized especially on studying flow in packed beds. However, most of the studies in this area were for one-dimensional systems. The main idea was to divide the flow cross-sectional area into regions of different porosities and applying the Ergun equation to each area (Ergun 1952). This has resulted in volumetric flow rates near the wall that are more than that at the core, and that the predicted velocity field is discontinuous. Moreover these approaches involve empirical judgments in the division of the bed cross section. In addition, the extensions are very application specific and are not directly applicable to generalized nonuniform systems. Many authors suggested that the wall effect may be important for column to particle diameter ratios in the range of 8:1 to 50:1. If this ratio is less than 50 to 1, the wall effect on the hydraulic radius (the characteristic length dimension in the Reynolds number) is significant (Mehta and Hawley 1969).

Hoagland et al. (1981) have applied the method of volume averaging to Navier-Stokes equations. For non-uniform systems, they indicated that expressions for the average of the product of spatial deviations of the velocity,  $\langle \tilde{v}\tilde{v} \rangle$ , the deviation of the surface forces exerted by the flowing fluid on

the solid matrix, the average of the position vector relative to the centroid of the averaging volume,  $\langle \mathbf{y}_\beta \rangle$ , and the average of the product of the position vector,  $\langle \mathbf{y}_\beta \mathbf{y}_\beta \rangle$ , must be evaluated. The strong dependence of these quantities on particle geometry and local porosity make a detailed knowledge of the porous media a prerequisite and this will complicate the analysis. By ignoring the inertia, the averaged equations are simplified considerably. They considered the one-dimensional flow in packed bed as an example of systems of known variation in porosity and used the Karman-Kozney relation in an attempt to close the obtained averaged equations.

### **3.8.3 The interface between a porous medium and another porous medium.**

This kind of interface is the focus of this research; hence it will be discussed in more detail. This situation is usually encountered in aquifers where the porous medium contains different layers of different properties or through a man-made engineering design (e.g. in landfill, tailings management facilities, etc.). The main feature of this system is the existence of layers of either a low permeability porous medium (clay liners in landfills, clay lenses in aquifers, etc.) or a high permeability porous medium (pervious surround in tailings management facility, fractures filled with crushed materials in aquifers, etc.). These layers, though sometimes thin, play a crucial role in groundwater flow and solute transport in these systems. Thus, proper considerations in dealing with this system stems from the fact that improper assumption could lead to significant errors.

In the neighborhood of the interface boundary inequality III may not be satisfied. That is the variations in both the porosity as well as the averaged conservative quantities within the averaging volume deviate significantly from the required linear relationship, Fig. 3.9. It is not correct to assign to these boundary regions macroscopic properties measured in systems where all length scale constraints are satisfied.

Two approaches have been found in the literature to address this problem. In the first, Bachmat and Bear (1986) suggested extending the properties of this dividing layer, measured in large systems, to the neighborhood of the interface boundary. While this approach may be adapted with negligible error in systems where the thickness of this layer is large enough such that condition II is satisfied, it might presumably lead to errors when this layer is thin such that condition II is violated. The second approach was introduced by Hassanizadeh and Gray (1989-a,b). They defined two kinds of interfaces; the first one is the interface between two porous media where averaging processes fail to work, which they called a simple interface, and the second one is concerned with intermediate layers between two porous medium that are either of a very low permeability (clay lenses) or a very high permeability (fractures filled with crushed materials), which they called a nonsimple interface, Fig. 3.13. In the second one, while the flow may be considered as three-dimensional in the region, it may be considered two-dimensional in the intermediate region. Thus the regular interface boundary condition, given by:

$$\left[ \langle \rho \rangle_\alpha \bar{\psi}^\alpha (\bar{\mathbf{v}}^\alpha - \mathbf{w}) - \mathbf{i}^\alpha \right] \cdot \mathbf{n} = 0 \quad (3.50)$$

where the bracket represents the jump and indicates the difference across the interface,  $\langle \rho \rangle_\alpha$  is the phase average density for phase  $\alpha$ ,  $\bar{\psi}^\alpha$  and  $\bar{\mathbf{v}}^\alpha$  are the mass averaged  $\psi$  and velocity of phase  $\alpha$ ,  $\mathbf{w}$  is the velocity of the surface of discontinuity,  $\mathbf{i}^\alpha$  is the macroscopic nonadvective flux of the  $\alpha$  phase, and  $\mathbf{n}$  is the unit normal to the interface, may not be adapted. Even the more general form given by:

$$\left[ \langle \rho \rangle_\alpha \bar{\psi}^\alpha (\bar{\mathbf{v}}^\alpha - \mathbf{w}) - \mathbf{i}^\alpha \right] \cdot \mathbf{n} = f_b^\alpha \quad (3.51)$$

where  $f_b^\alpha$  account for the contribution of the interface to thermodynamic properties of the  $\alpha$  phase (may be considered as a source/sink at the boundary), may be inadequate. The derivation of jump conditions for a general interface does not completely characterize the flow and transport. Constitutive postulates similar to those needed to completely define a multiphase body are needed to fully describe interface behavior. The postulates supplement the jump conditions. Although the general jump conditions are universal, the constitutive postulates vary depending on the system under study. Thus within the framework adopted by Gray (1982), for transforming three-dimensional point equations to two-dimensional averaged equations, equation (3.6) may be averaged by considering an REV which is essentially constant in time and space. This REV is depicted in Fig. 3.14. Note that in the direction (approximately) normal to the interface, the length scale of the REV is greater than  $b$  while in the lateral direction; the length scale is smaller than or the same as  $b$ . The volume of the REV is denoted as  $\delta V_b$ .

and its cross section by  $\delta S$ . The area of intersections of  $A_1$  and  $A_2$  in  $\delta V_b$  are denoted as  $\delta A_1$  and  $\delta A_2$ , respectively. Additionally, the portion of the boundary surface of  $\delta V_b$  which is in the intermediate zone, not including  $\delta A_1$  and  $\delta A_2$ , is indicated as  $\delta A$ . The interfacial area of the  $\alpha$  phase with another phase  $\beta$  within the REV and within the intermediate zone is  $\delta A_{\alpha\beta}^b$ . Finally, a distribution function

$\gamma_{\alpha}^b(\mathbf{x}, t)$  is defined such that:

$$\gamma_{\alpha}^b(\mathbf{x}, t) = 1 \quad \text{for } \mathbf{x} \text{ in the } \alpha \text{ phase within the interface zone}$$

$$\gamma_{\alpha}^b(\mathbf{x}, t) = 0 \quad \text{otherwise,}$$

Thus, the averaged equation took the form:

$$\begin{aligned} & \frac{\partial}{\partial t} (b \langle \rho \rangle_{\alpha}^b \bar{\psi}^{b\alpha}) + \nabla' \cdot (b \langle \rho \rangle_{\alpha}^b \bar{\mathbf{v}}^{b\alpha} \bar{\psi}^{b\alpha} - \\ & - \nabla' \cdot (b \bar{\mathbf{i}}^{b\alpha} \bar{f}^{b\alpha}) - b \langle \rho \rangle_{\alpha}^b \bar{f}^{b\alpha} - b \langle \rho \rangle_{\alpha}^b \bar{G}^{b\alpha} - \\ & - \sum_{\beta \neq \alpha} \frac{1}{\delta S} \int_{\delta A_{\alpha\beta}^b} [\rho \psi(\mathbf{w} - \mathbf{v}) + \mathbf{i}] \cdot \mathbf{n}^{\alpha\beta} da = \\ & = \frac{1}{\delta S} \int_{\delta A_1} \gamma_{\alpha}^b [\rho \psi(\mathbf{w} - \mathbf{v}) - \mathbf{i}] \cdot \mathbf{n} da + \frac{1}{\delta S} \int_{\delta A_2} \gamma_{\alpha}^b [\rho \psi(\mathbf{w} - \mathbf{v}) - \mathbf{i}] \cdot \mathbf{n} da \end{aligned} \quad (3.52)$$

where  $\mathbf{w}$  is the velocity of the area of integration, the prime denotes a two-dimensional spatial vector,  $\mathbf{n}$ , the outward normal vector, on  $\delta A_1$  and  $\delta A_2$  points out of the domains I and II respectively,  $\bar{f}^{b\alpha}$  is the mass average of  $f$  of the  $\alpha$  phase of the interface, and  $\nabla'$  refers to the gradient operator in two dimensions (in the directions tangential to the interface). Furthermore,

$$\langle \rho \rangle_a^b = \frac{1}{b \delta S} \int \rho \gamma_a^b dv \quad (3.53)$$

$$\bar{\psi}^{b\alpha} = \frac{1}{b \langle \rho \rangle_a^b \delta S} \int \rho \psi \gamma_a^b dv \quad (3.54)$$

$$\mathbf{i}'^{b\alpha} = \frac{1}{b \delta S} \int (\mathbf{i}' - \rho \tilde{\psi}^{b\alpha} \tilde{\mathbf{v}}^{b\alpha}) \gamma_a^b dv \quad (3.55)$$

$$\tilde{\psi}^{b\alpha} = \psi - \bar{\psi}^{b\alpha} \quad (3.56)$$

Also,  $\bar{\mathbf{v}}'^{b\alpha}$ ,  $\bar{f}^{b\alpha}$  and  $\bar{G}^{b\alpha}$  are defined analogously to  $\bar{\psi}^{b\alpha}$ . All microscopic quantities are functions of time and three spatial dimensions, whereas the averaged quantities depend on time and only the two spatial dimensions tangent to the interface. Equation (3.52) serves as the link between the two domains. The terms to the right of equation (3.52) may be defined as source terms and they should be formulated in terms of properties of domain I and II at the boundaries of the interface zone. For the case of a permeable fracture within a porous medium Hassanizadeh and Gray (1989-a,b) were able to develop the following equations:

- **Mass**

$$\frac{\partial(b \varepsilon^b s^{b\alpha} \rho^{b\alpha})}{\partial t} + \nabla' \cdot (b \varepsilon^b s^{b\alpha} \rho^{b\alpha} \mathbf{v}'^{b\alpha}) = [\rho^\alpha \mathbf{u}^\alpha] \cdot \mathbf{N} \quad (3.57)$$

where  $s^{b\alpha}$  is the saturation of phase  $\alpha$  in the interface, and  $\mathbf{u}^\alpha$  is Darcy velocity of phase  $\alpha$ . This equation relates the storage and flux of mass of the fluid in the plane of the fracture to the mass entering (leaving) the fracture from (into) the main domains. Additional relations for  $\rho^{b\alpha}$ ,  $s^{b\alpha}$  and  $\mathbf{v}'^{b\alpha}$  must be provided by

constitutive equations of state and by momentum balance. The fracture orientation, thickness, and porosity are assumed to be known functions of position and time.

- **Momentum**

$$\begin{aligned}
 & b\varepsilon^b s^{b\alpha} \rho^{b\alpha} \frac{\partial(\mathbf{v}^{b\alpha})}{\partial t} + b\varepsilon^b s^{b\alpha} \rho^{b\alpha} \mathbf{v}^{b\alpha} \cdot \nabla'(\mathbf{v}^{b\alpha}) - \nabla' \cdot (b\mathbf{t}^{b\alpha}) - \\
 & - b\varepsilon^b s^{b\alpha} \rho^{b\alpha} \mathbf{g} - \sum_{\beta \neq \alpha} \frac{1}{\delta S_{\delta A_{\alpha\beta^b}}} \int \mathbf{t} \cdot \mathbf{n}^{\alpha\beta} da = [\rho^\alpha (\mathbf{v}^\alpha - \mathbf{v}^{b\alpha}) \mathbf{u}^\alpha - \mathbf{t}^\alpha] \cdot \mathbf{N}
 \end{aligned} \tag{3.58}$$

Hassanizadeh and Gray (1989-a,b) showed that the last term in the left hand side of equation (3.58) might be written as:

$$\begin{aligned}
 \sum_{\beta \neq \alpha} \frac{1}{\delta S_{\delta A_{\alpha\beta^b}}} \int \mathbf{t} \cdot \mathbf{n}^{\alpha\beta} da = & p^{b\alpha} \nabla'(b\varepsilon^b s^{b\alpha}) - [p^\alpha \varepsilon^\alpha] \mathbf{N} + \varepsilon^b s^{b\alpha} [p^\alpha] \mathbf{N} - \\
 & - b\mathbf{R}^{n\alpha} \cdot \mathbf{u}'^{b\alpha} - bR_N^\alpha [\chi^\alpha \mathbf{u}^\alpha \cdot \mathbf{N}] \mathbf{N}
 \end{aligned} \tag{3.59}$$

where  $p$  is the thermodynamic pressure,  $\mathbf{R}^{n\alpha}$  is the medium resistance to the flow within the fracture,  $R_N^\alpha$  accounts for the resistance to the flow from domain I and II across the fracture,  $\mathbf{u}'^{b\alpha}$  is the two dimensional Darcy velocity vector tangent to the fracture,  $\chi_1^\alpha$  and  $\chi_2^\alpha$  apportion the resistance to the flow entering the fracture from domain I and II, respectively. Also, they approximated the fluid stress tensor as:

$$\mathbf{t}'^{b\alpha} = -\varepsilon^b s^{b\alpha} p^{b\alpha} \mathbf{I}'' \tag{3.60}$$

$$\mathbf{t}^\alpha = -\varepsilon^b s^\alpha p^\alpha \mathbf{I} \tag{3.61}$$

where  $\mathbf{I}''$  is the unit tensor in two dimensions and  $\mathbf{I}$  is the unit tensor in three dimensions. These assumptions are based on the fact that porous media flow is

macroscopically inviscid. Thus using these equations, Hassanizadeh and Gray were able to introduce the following equation:

$$\begin{aligned}
& b\varepsilon^b s^{b\alpha} \rho^{b\alpha} \frac{\partial(\mathbf{v}^{b\alpha})}{\partial t} + b\varepsilon^b s^{b\alpha} \rho^{b\alpha} \mathbf{v}'^{b\alpha} \cdot \nabla'(\mathbf{v}^{b\alpha}) - \nabla' \cdot (b\varepsilon^b s^{b\alpha} p^{b\alpha}) - \\
& - b\varepsilon^b s^{b\alpha} \rho^{b\alpha} \mathbf{g} - p^{b\alpha} \nabla'(b\varepsilon^b s^{b\alpha}) + p^{b\alpha} \nabla'(b\varepsilon^b s^{b\alpha}) + [\varepsilon s^\alpha p^\alpha] \mathbf{N} - \varepsilon^b s^{b\alpha} [p^\alpha] \mathbf{N} + \\
& + b\mathbf{R}^{n\alpha} \cdot \mathbf{u}'^{b\alpha} - bR_N^\alpha [\chi^\alpha \mathbf{u}^\alpha \cdot \mathbf{N}] \mathbf{N} = [\rho^\alpha (\mathbf{v}^\alpha - \mathbf{v}^{b\alpha}) \mathbf{u}^\alpha - \varepsilon s^\alpha p^\alpha] \cdot \mathbf{N}
\end{aligned} \quad (3.62)$$

When the flow in the porous medium is slow such that the inertia term is negligible, equation (3.62) reduces to:

$$\begin{aligned}
& b\varepsilon^b s^{b\alpha} (\nabla'(p^{b\alpha} - \rho^{b\alpha} \mathbf{g}) - [\varepsilon s^\alpha p^\alpha] \mathbf{N} - \varepsilon^b s^{b\alpha} [p^\alpha] \mathbf{N} + \\
& + b\mathbf{R}^{n\alpha} \cdot \mathbf{u}'^{b\alpha} + bR_N^\alpha [\chi^\alpha \mathbf{u}^\alpha \cdot \mathbf{N}] \mathbf{N} = 0
\end{aligned} \quad (3.63)$$

This equation has components in directions normal and tangential to the interface zone. The tangential components of this equation, after rearrangement, yield an equivalent form of Darcy's law within the fracture that is:

$$\mathbf{u}'^{b\alpha} = -\varepsilon^b s^{b\alpha} (\mathbf{R}^{n\alpha})^{-1} \cdot (\nabla' p^{b\alpha} - \rho^{b\alpha} \mathbf{g}') \quad (3.64)$$

The mass and momentum equations for the fractures can be solved only in conjunction with the equations of mass and momentum of the two main domains.

Additional equations, which link the interface zone process to  $\mathbf{u}_1^\alpha \cdot \mathbf{N}_1$  and  $\mathbf{u}_2^\alpha \cdot \mathbf{N}_2$  can be obtained from the normal component of equation (3.63), that is:

$$-b\varepsilon^b s^{b\alpha} \rho^{b\alpha} \mathbf{g} \cdot \mathbf{N}_1 - \varepsilon^b s^{b\alpha} (p_1^\alpha - p_2^\alpha) + bR_N^\alpha (\chi_1^\alpha \mathbf{u}_1^\alpha \cdot \mathbf{N}_1 - \chi_2^\alpha \mathbf{u}_2^\alpha \cdot \mathbf{N}_2) = 0 \quad (3.65)$$

which may be rearranged to the form:

$$\begin{aligned} & \{bR_N^\alpha \chi_1^\alpha \mathbf{u}_1^\alpha \cdot \mathbf{N}_1 + \varepsilon^b s^{b\alpha} [(p^{b\alpha} - p_1^\alpha) - \chi_1^\alpha b \rho^{b\alpha} \mathbf{g} \cdot \mathbf{N}_1]\} - \\ & - \{bR_N^\alpha \chi_2^\alpha \mathbf{u}_2^\alpha \cdot \mathbf{N}_2 + \varepsilon^b s^{b\alpha} [(p^{b\alpha} - p_2^\alpha) - \chi_2^\alpha b \rho^{b\alpha} \mathbf{g} \cdot \mathbf{N}_2]\} = 0 \end{aligned} \quad (3.66)$$

This equation describes the transfer of momentum in the normal direction between the main domains and the fracture. It may be split into two parts, one accounting for momentum transfer between domain I and the fracture and another accounting for transfer between domain II and the fracture. Thus from equation (3.66) it follows that

$$\mathbf{u}_1^\alpha \cdot \mathbf{N}_1 = \frac{-\varepsilon^b s^{b\alpha}}{R_N^\alpha} \left[ \frac{p^{b\alpha} - p_1^\alpha}{b \chi_1^\alpha} - \rho^{b\alpha} \mathbf{g} \cdot \mathbf{N}_1 \right] \quad (3.67)$$

$$\mathbf{u}_2^\alpha \cdot \mathbf{N}_2 = \frac{-\varepsilon^b s^{b\alpha}}{R_N^\alpha} \left[ \frac{p^{b\alpha} - p_2^\alpha}{b \chi_2^\alpha} - \rho^{b\alpha} \mathbf{g} \cdot \mathbf{N}_2 \right] \quad (3.68)$$

Hassanizadeh and Gray (1989-a,b) also indicated that the constitutive parameter  $\chi_1^\alpha (=1-\chi_2^\alpha)$  might be specified based on the system under consideration. For example, when the interface zone is permeable but the flow normal to the zone is negligible such that the pressure is hydrostatic,  $\chi_1^\alpha = 0.5$ ; when the main domain I is impermeable to the  $\alpha$  phase,  $\chi_1^\alpha = 0.0$  and  $p_1^\alpha = p^{b\alpha}$ , when  $R_N^\alpha$  is infinite such that the interface zone is impermeable, equations (3.67) and (3.68) reduce to  $\mathbf{u}_1^\alpha \cdot \mathbf{N}_1 = \mathbf{u}_2^\alpha \cdot \mathbf{N}_2 = 0$ ; and when the main domains I and II have the same properties (porosity, permeability, temperature, density),  $\chi_1^\alpha = \chi_2^\alpha = 0.5$ . Other cases may be modeled by appropriate selection of a value of  $\chi_1^\alpha$  between 0.0 and 1.0.

- **Mass balance for species**

The balance of mass for a species existing in the  $\alpha$  phase reads:

$$\begin{aligned} \frac{\partial(b\varepsilon^b s^{b\alpha} \rho^{b\alpha} \omega^{b\alpha})}{\partial t} + \nabla' \cdot (b\varepsilon^b s^{b\alpha} \rho^{b\alpha} \omega^{b\alpha} \mathbf{v}'^{b\alpha}) - \nabla' \cdot \mathbf{j}'^{b\alpha} = b\varepsilon^b s^{b\alpha} \rho^{b\alpha} r^{b\alpha} + \\ + \sum_{\beta \neq \alpha} \frac{1}{\delta S_{\delta A_{\alpha\beta}^b}} \int \mathbf{j} \cdot \mathbf{n}^{\alpha\beta} da + \quad (3.69) \\ + [\rho^\alpha \omega^\alpha \mathbf{u}^\alpha - \mathbf{j}^\alpha] \cdot \mathbf{N} \end{aligned}$$

where  $\omega$  refers to the mass fraction for the species and  $\mathbf{j}$  refers to the dispersion flux vector. The first term on the right side accounts for homogeneous reactions and/or decay, and the second term denote the heterogeneous mass exchange of the species between the  $\alpha$  phase and all other phases as a result of adsorption and interface diffusion process. Constitutive equations have to be provided for

$\mathbf{j}'^{b\alpha}$  and  $\sum_{\beta \neq \alpha} \frac{1}{\delta S_{\delta A_{\alpha\beta}^b}} \int \mathbf{j} \cdot \mathbf{n}^{\alpha\beta} da$ . In particular, they proposed a Fickian type relation for

$$\mathbf{j}'^{b\alpha} \text{ as: } \quad \mathbf{j}'^{b\alpha} = \rho^{b\alpha} \mathbf{D}^{nb\alpha} \cdot \nabla' \omega^{b\alpha} \quad (3.70)$$

where  $\mathbf{D}^{nb\alpha}$  is the dispersion tensor for the fracture zone. Moreover, constitutive relations for  $\mathbf{j}_1^\alpha \cdot \mathbf{N}_1$  and  $\mathbf{j}_2^\alpha \cdot \mathbf{N}_2$  must be proposed in terms of  $(\omega_1^\alpha, \omega^{b\alpha})$ , and  $(\omega_2^\alpha, \omega^{b\alpha})$  respectively. They proposed the formulas:

$$\mathbf{j}_1^\alpha \cdot \mathbf{N}_1 = (\omega^{b\alpha} - \omega_1^\alpha) / (\chi_1^{\omega\alpha} R_N^{\omega\alpha}) \quad (3.71)$$

$$\mathbf{j}_1^\alpha \cdot \mathbf{N}_1 = (\omega^{b\alpha} - \omega_2^\alpha) / (\chi_2^{\omega\alpha} R_N^{\omega\alpha}) \quad (3.72)$$

where they referred  $R_N^{\omega\alpha}$  as a mass transfer resistance coefficient and it is to be determined empirically depending on the system under study, and  $\chi_1^{\omega\alpha}$ ,  $\chi_2^{\omega\alpha}$  are weighting parameters that sum to 1.0 and are related to the resistance to the nonadvective fluxes. Equations (3.57) through (3.63) together with the transport

equation for domain I and II comprise a set of equations to be solved for  $\omega^{b\alpha}$  and the mass fraction in I and II.

### 3.9 Conclusions

From the previous study it is apparent that volume averaging method is a powerful tool that provides a standard framework that might be used for dealing with nonhomogeneous systems.

Three main length scale constraints were defined to justify the applicability of the continuum approach. The third one was introduced in this work through a rigorous physical insight into the problem. This approach is different from that introduced in the literature (Whitaker and his coworkers, and Bear and his coworkers) and provides more understanding. That is in the one hand this length scale constraints appeared in the work of Whitaker and his coworkers during an order of magnitude analysis to terms arising when performing Taylor expansion during the course of averaging. In order to neglect higher order terms, they introduced some length scale constraints. On the other hand Bear and his coworkers suggested that all the macroscopic properties and variables change linearly within the averaging volume. In this work, this length scale constraints appear naturally as a result of applying predefined postulates that have been set to ensure proper upscaling processes.

Difficulty in dealing with the interface boundary between different regions has inspired researchers and theoreticians to come up with different ideas to deal

with the processes at the interface. One, probably, may be able to distinguish the two main approaches as follows: The first approach was formulated by Whitaker and his group through the development of a momentum jump defined at the interface boundary between a porous medium and a liquid region. In this approach, the averaged equations developed for the main domains were extended to the boundary regions and the error was corrected by adjusting the boundary condition through a momentum jump relationship. Information about the thickness of the boundary region is needed. This is difficult to determine, especially for nonuniform systems. Moreover, more experimental work is needed to verify this approach. On the other hand, equations describing other transport phenomena like energy, species, and entropy should also be developed.

The second approach is that proposed by Gray and his group. The main feature of this approach is to deal with the boundary region as a two-dimensional region separating two three-dimensional regions. The developed two-dimensional equation of transport in this region is linked with that in the two three-dimensional regions through parameters that are system dependent. The advantages of this approach in dealing with the interface region are obvious once the required constitutive parameters can be evaluated. However, these terms can prove to be extremely difficult to measure. For example, how can one measure the medium resistance to flow within the fracture  $\mathbf{R}^{\alpha}$ . This resistance should be a function of the thickness of the intermediate layer, the type of the porous material surrounding the fracture as well as the type of particles, distribution, mingling, etc. at the interface boundary. Moreover, the resistance to

flow from domain I and II across the fracture,  $R_N^\alpha$ , is also difficult to correctly measure as it depends on the interface conditions, degree of compaction, etc., which might not be easily mimicked even in a laboratory experiment. Also, what values of the weighting functions might one assume? In terms of the species mass balance equation, the term  $R_N^{\omega\alpha}$ , defined as the mass transfer resistance coefficient, would face the same difficulties as discussed for the measurements of the resistance to flow across the fracture. Most probably, it will end up for all these parameters to work as fitting parameters to match the real flow field as well as species plume. However, the importance of such derivations stems from highlighting, from a theoretical basis, what are the significant contributing factors in the problem of interest rather than adding ad hoc terms without justifications as it was used to be in the past. Finally, it should be mentioned that when the boundary region between two different porous media is small compared with the length scale characterizing the thickness of these two regions, Bear indicated that the errors arising from extending the governing averaged equations may be neglected.

### **3.10 Length Scale Constraints as Applied to the Pervious Surround**

#### **Concept.**

The pervious surround in Rabbit Lake TMF, approximately 1 m wide, is filled with crushed rocks mainly from the excavation activity. A wide range of rock grain sizes is introduced ranging from as small as on the order of millimeters to as large as on the order of several centimeters. Thus an REV may be required to be as large as the whole thickness of the domain or may not be defined at all.

Furthermore, the second length scale constraint is violated since the width of the domain is comparable with the length scale characterizing the REV (if one exists). Also, the region where the third length scale constraint is violated (the interface region) may span the whole thickness of the pervious surround layer. Thus in general, all length scale constraints defined for one to be able to apply the continuum approach are violated. Perhaps the approach proposed by Hassanizadeh and Gray (1989-a,b) may be appropriate for this system. However, given the difficulty in determining the coefficients introduced through this approach that were defined to link the three-dimensional encompassing regions with the two-dimensional averaged region, an easy and applicable approach may be needed as will be discussed in the next chapter.

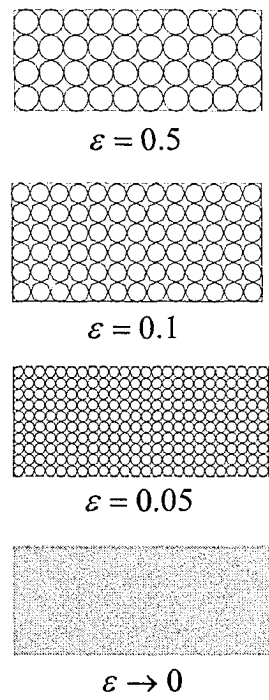


Fig.3.1 Homogenization limit

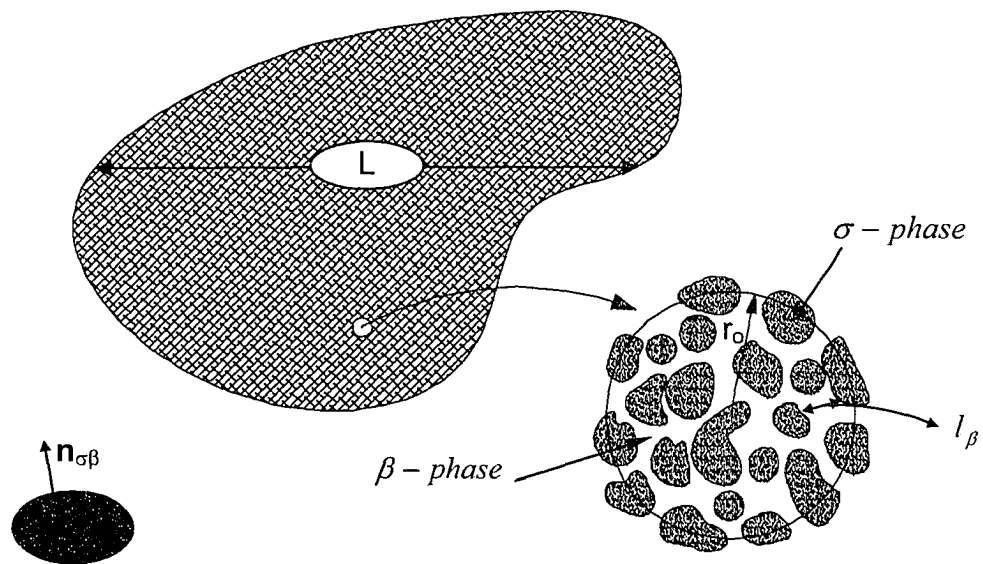


Fig.3.2 Representative region of a porous medium domain.

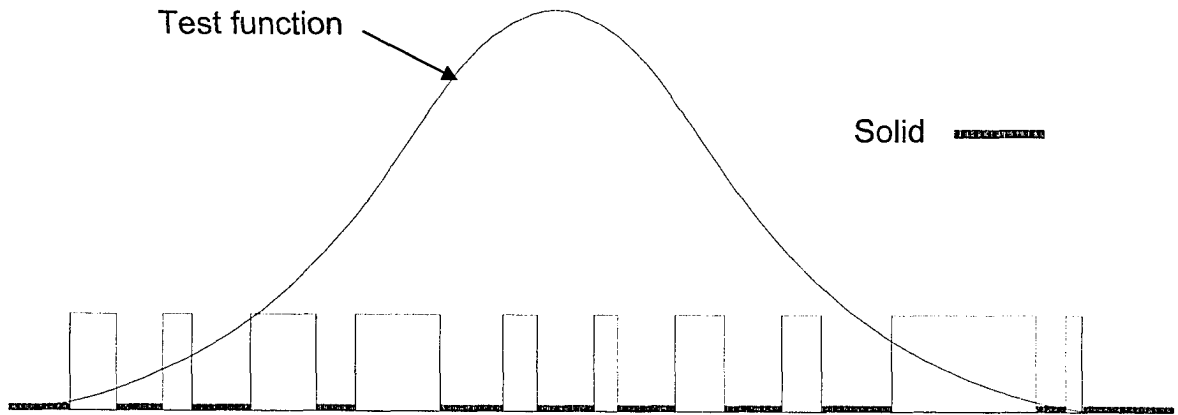


Fig.3.3 One-dimensional presentation of piece wise continuous function (indicator function).

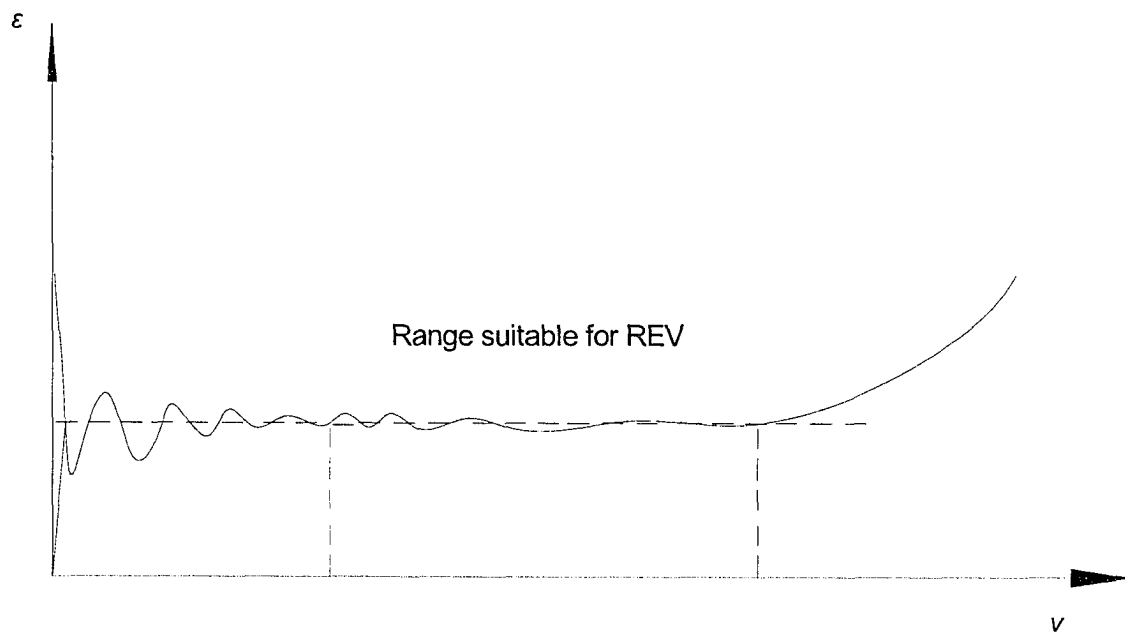


Fig. 3.4 Selecting an REV

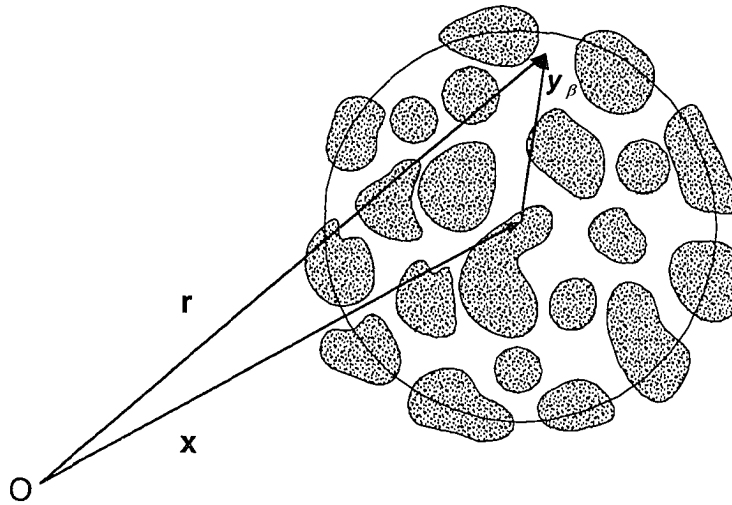


Fig. 3.5 Fluid-solid system

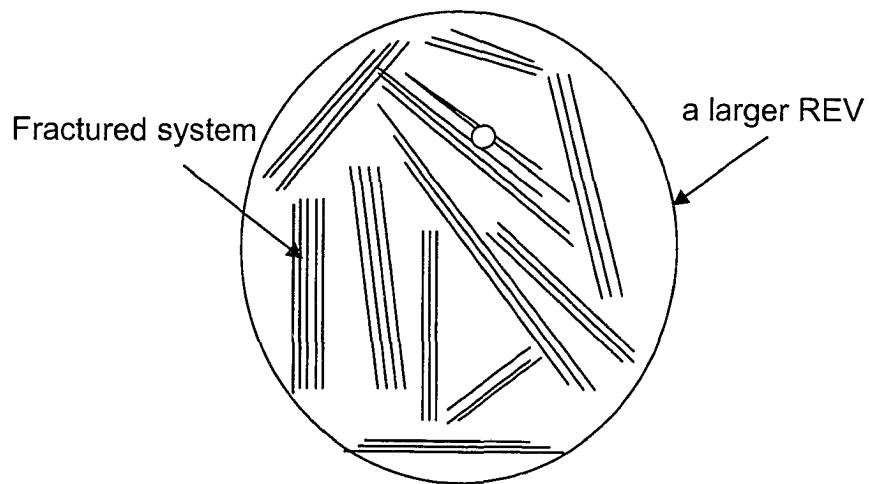


Fig. 3.6 Larger scale description

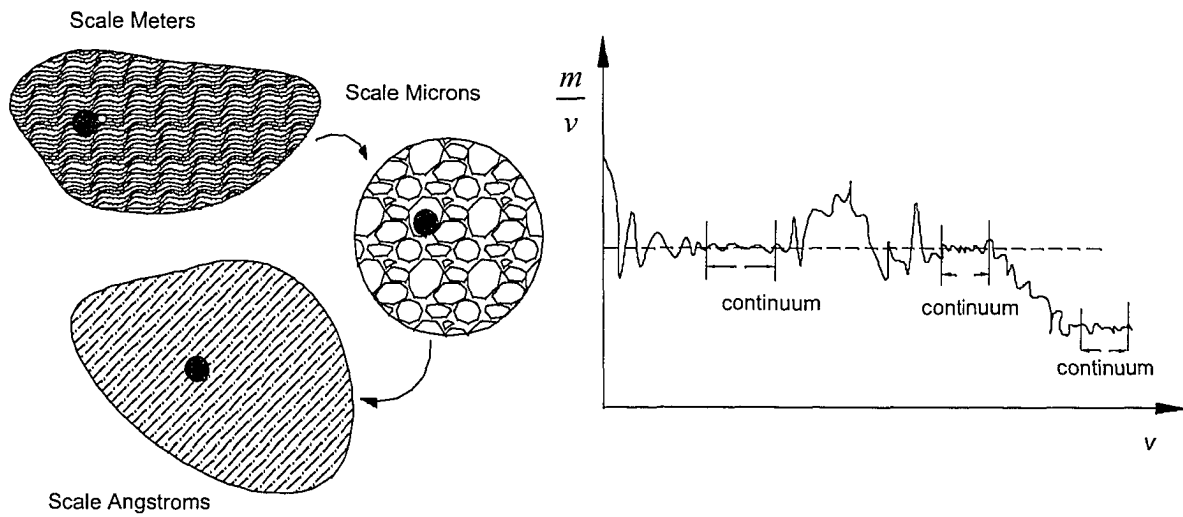


Fig. 3.7 Schematic of material viewed on different scales of observation (from Cushman)

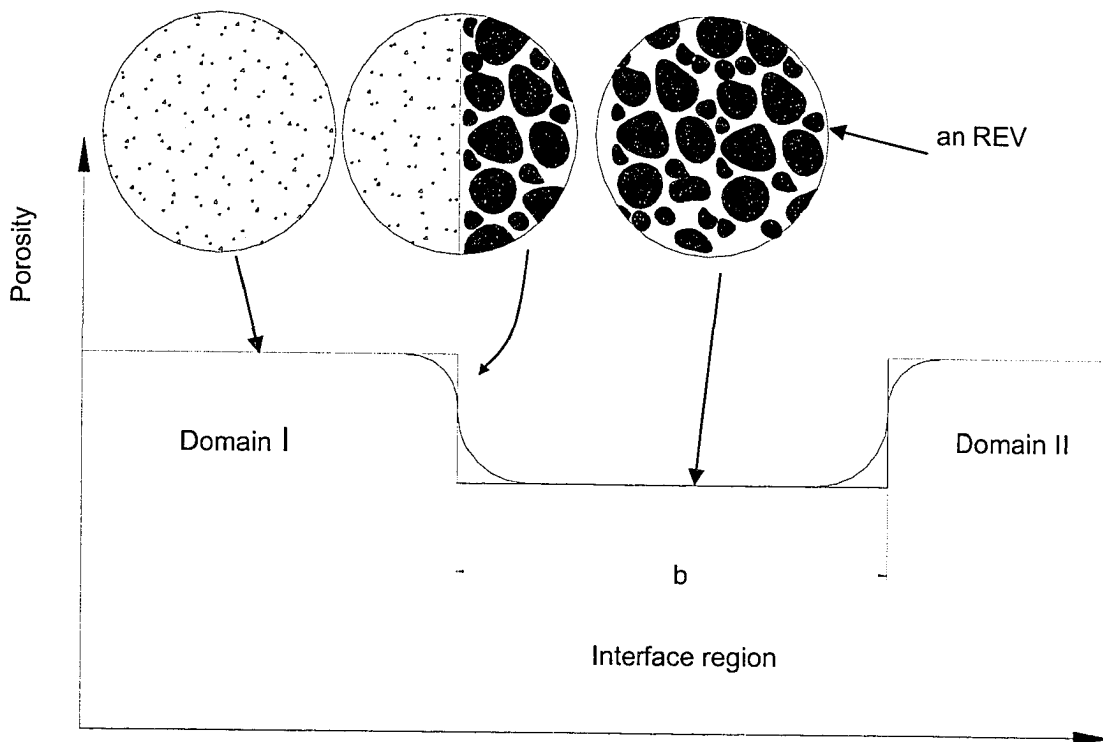


Fig. 3.8 Porosity variations at the interface region due to averaging process.

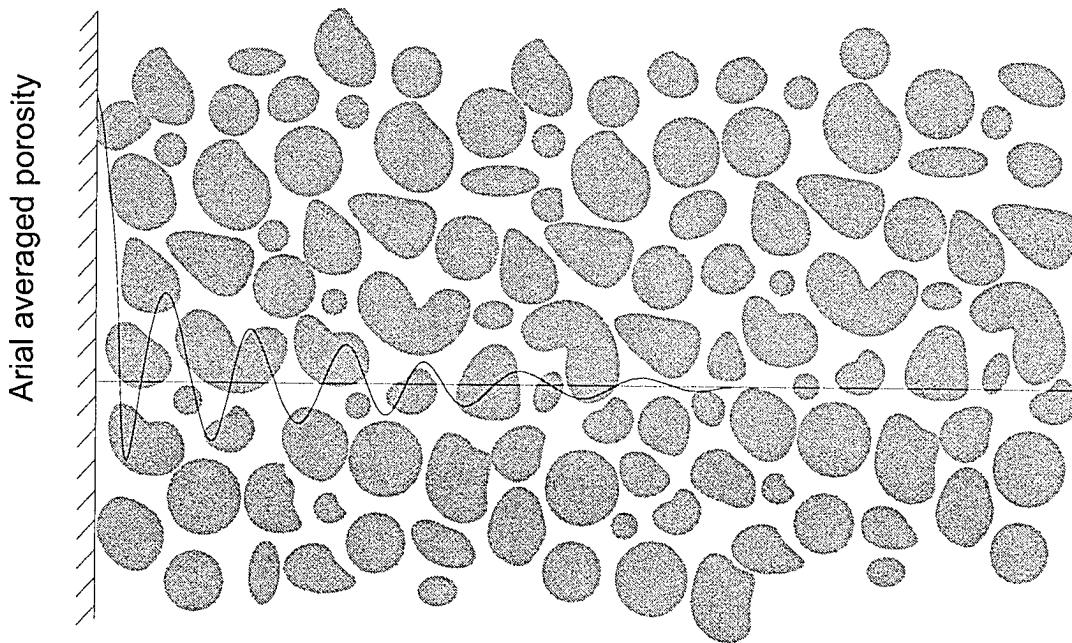


Fig. 3.9 Fluctuations in local porosity in the vicinity of a confining wall.

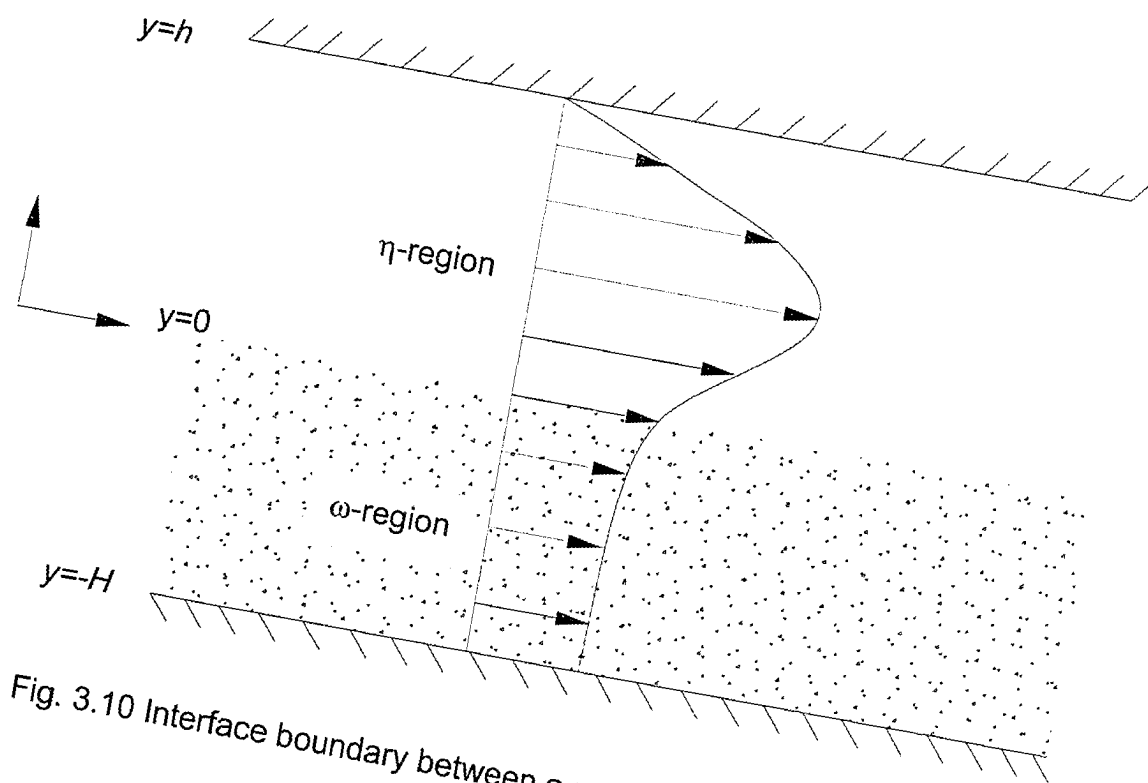


Fig. 3.10 Interface boundary between a porous layer and a liquid body

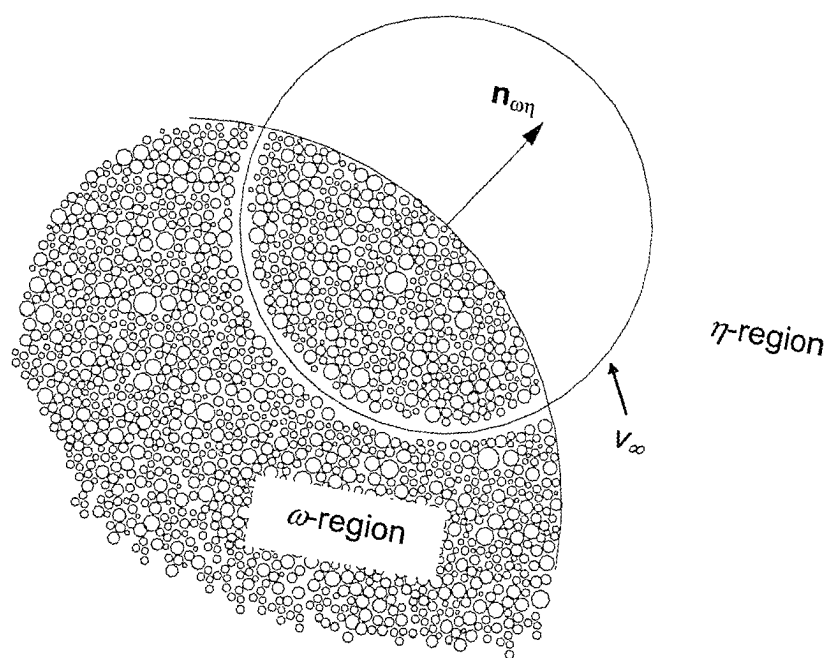


Fig. 3.11 Averaging volume at the interface boundary.

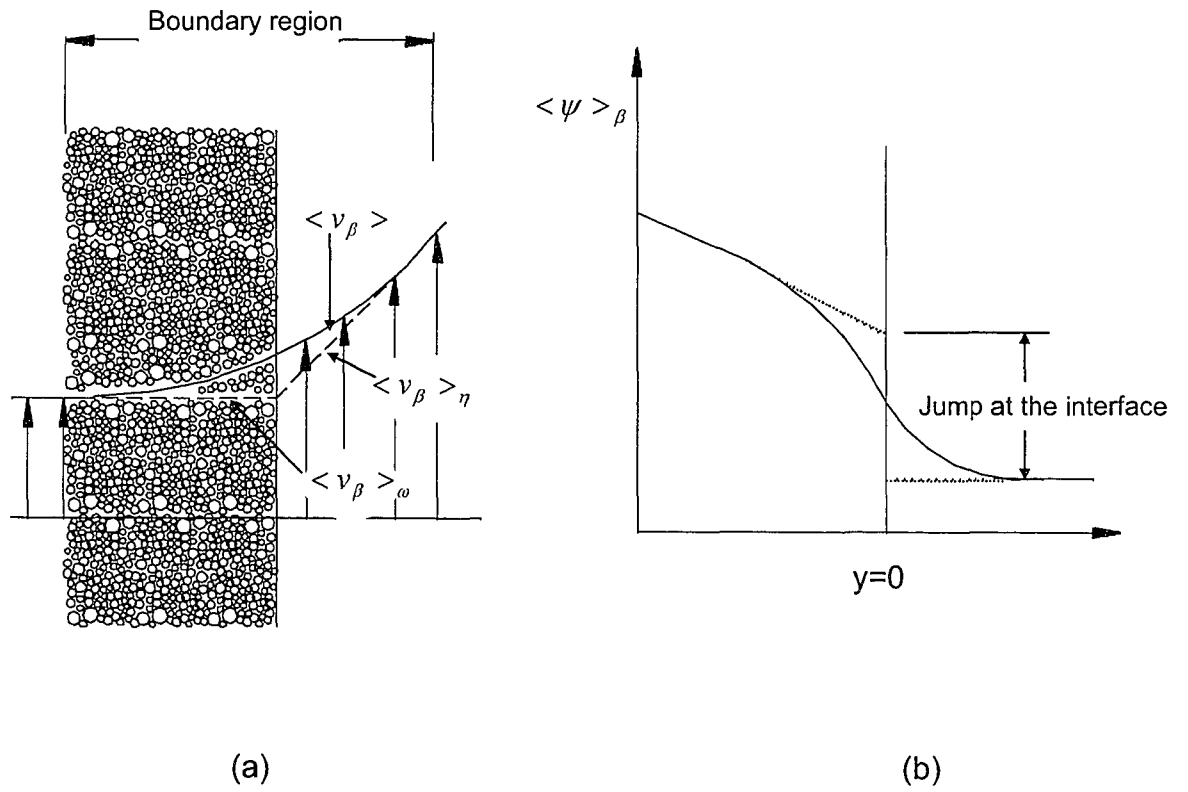


Fig. 3.12 Jump condition at the interface between porous medium and homogeneous fluid.

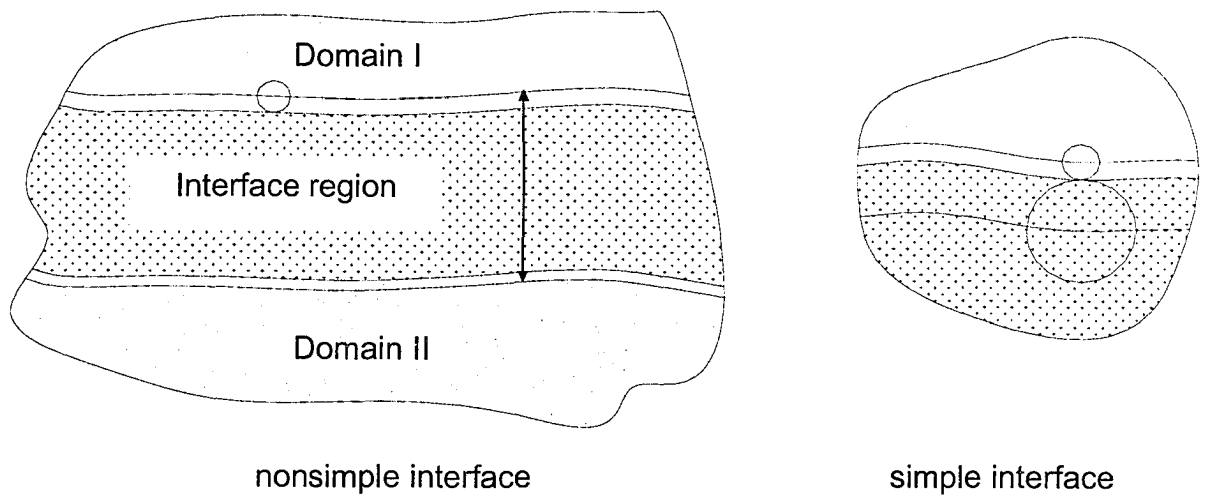


Fig. 3.13 Simple and nonsimple interfaces

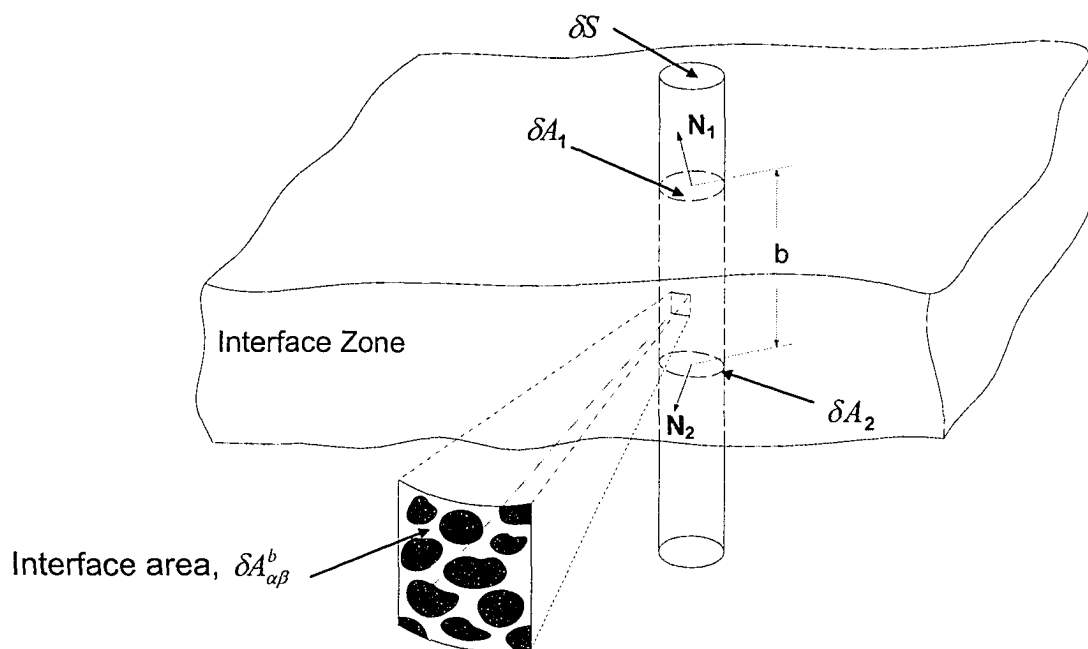


Fig. 3.14 Averaging volume for a nonsimple interface.

## CHAPTER 4

### METHODOLOGY

#### 4.1 General.

To study any phenomenon, it is important to define the most significant factors and isolate them from those whose effects are only minor. Lebedev (1958) stated that “any phenomenon occurring in nature is bound with an infinite set of other phenomena. In choosing any such phenomenon as a subject of study, it may be found that among these connections there are essential ones, which determine the basic features of the phenomena under study; but there are also nonessential ones, which affect only some secondary features. In studying the phenomenon it is necessary to find out and take into account all the essential connections and simultaneously to disregard nonessential details caused by subsidiary connections. Thus, not every phenomenon in all its complexity is subject to analysis, only a simplified model of it, whose behavior coincides basically with the behavior of the subject of study in all but minor and nonessential details. The study of the model constructed leads to the setting up of some laws. Only the abstract model of the phenomenon follows these laws. However, if the schematization of the latter has been carried out properly, the laws also describe the basic features of the phenomenon studied. Thus the

criterion of correctness of a model adopted in some theory is the agreement between theoretical results and practical, experimental data".

#### **4.2 Methodology.**

As indicated in the previous chapter, the continuum hypothesis may not be adapted in the pervious surround in TMF. All length scale constraints are violated in this region and hence groundwater flow as well as solute transport equations may not be valid in this system. Moreover, because no field data are available that might shed light on the behavior of the system under these circumstances, experimental work may indeed be needed. The experimental work that has been done before by West et al. (2003) was not aiming at addressing this issue, rather it was aiming to explore the effectiveness of the pervious surround in diverting groundwater flow around the tailings and hence reducing the rate of solute release out of the tailings, which in fact would occur whether or not the continuum hypothesis is adapted. The difficulty would arise in conducting numerical simulations since the usual macroscopic equations may not be valid in this region. In addition, they considered a three-dimensional conceptualization of a TMF with all its geometrical and experimental complexities which increase the sources of uncertainties. The pervious surround in the 3-D equivalent porous medium (EPM) experiments, which they considered, was 2 cm wide and filled with 3 mm to 6 mm filter gravel, which definitely violates the REV length scale constraints. In conducting the numerical modeling, West et al. (2000) had to adjust different parameters to match the experiments with the simulations

through calibration exercises. For example, they had to adjust the hydraulic conductivity of the EPM host rock to match the overall flow rate through the model. They also adjusted the porosity of the EPM host rock to match the plume front. Longitudinal and transverse dispersivities of the EPM host rock were also chosen approximately 20 times those suggested by the tracer testing. West et al. used the hydraulic conductivity of the pervious layer as measured in the permeameter and didn't measure the dispersivities of the pervious filter gravel. It is believed that part of these discrepancies that had forced them to adjust drastically some of the measured parameters were due to the violation to the continuum approach in the pervious layer in addition to other sources of uncertainties introduced due to the complexities in their 3-D experimental setup. It would not be straightforward to quantify the contribution of violating the continuum approach on the discrepancy between experiments and simulations in their system due to the presence of other sources of uncertainties. On the other hand, to our knowledge, no experimental work has been done to address the significance of violating the continuum hypothesis on our ability to model such systems. Thus it is important that an experimental set up be constructed for the sole purpose of quantifying the effect of violating the continuum hypothesis on simulation prediction and to give answers to questions such as those introduced at the beginning of chapter 2. That is, if a system is violating the continuum hypothesis, could one still be able to simulate the system regardless of this violation and get acceptable results?

The idea is as follows; given the fact that we are unable to use the groundwater flow and solute transport equations in the pervious region, simulating this system with the usual measured macroscopic porous media parameters will, in general, lead to a mismatch between measurements and simulations. The discrepancy is expected to show in both groundwater flow and in solute transport. Would this mismatch be significant or insignificant suggests the kind of experimentations that need to be designed to explore this situation. The main idea is to construct a system that complies with all length scale constraints needed for one to be able to apply the continuum approach. Simulating such a system (flow and solute transport) with the measured macroscopic parameters is expected to show reasonable agreement with experimental results. The system would then be allowed to violate some of the length scale constraints in one of its zones and measurements for flow and solute transport will be taken in such cases. Simulating this system with the same measured macroscopic porous medium parameters would indicate whether there were discrepancies between simulations and measurements or not and how significant these discrepancies would be.

The experimental set up constructed to test this concept was composed of a porous medium of two zones, where a layer of gravel was encompassed in sand in a relatively large box. Gravel of approximately 0.8 cm mean grain diameter was used. Thus approximately 50 times the mean grain size may be a reasonable extent for a domain to be dealt with as a continuum, although a larger domain would be better. Bear (2002) suggested 100 times the mean grain size.

First, the macroscopic properties of sand and gravel (hydraulic conductivity, and dispersivity) were measured using two experimental boxes (2.3 x 1.46 m), as will be detailed in next chapter. The boxes were large enough to ensure the applicability of the continuum hypothesis for both media. A base scenario was then constructed in which a gravel zone (0.5 x 0.5 x 0.6 m) was inserted into the box and was surrounded with sand. This also ensures the validity of the continuum hypothesis for the sand-gravel system.

Now if a solute is injected in the sand upgradient of the gravel layer and samples were collected in the sand downgradient of the gravel (Fig. 4.1), these measurements should fit reasonably well with the results of simulating the system assuming the measured macroscopic porous media parameters. In subsequent experiments, the thickness of the gravel layer was allowed to get smaller and smaller to the extent where the length scale constraints began to be violated. For each experimental set up, flow and solute transport were modeled numerically using the previously measured macroscopic properties. Comparisons were then made between measurements and simulations to explore the impact of the violation of the continuum hypothesis and to shed light on the behavior of the system under these circumstances.

The benefit of this approach, in addition to exploring the behavior of similar systems as suggested by the experimental work, is that it may guide us when conducting simulations by suggesting increasing (or decreasing) the macroscopic porous medium properties (permeability and dispersivity) of this

region in order to correctly simulate the system. Although uncertainties in porous media properties are, in general, unavoidable, even if the greatest amount of care is taken to generate a homogeneous medium in the laboratory, it may be suggested that the errors associated with violating the continuum approach be added to other sources of error uncertainty and that these errors are taken care of during an overall calibration exercise of the model. While this may occur as a post process by following the evolution of the plume and readjusting the model's parameters, it may not be the case during the design and construction processes where no data are available. In this case, the proponents of such systems as well as regulatory agencies have to rely only on simulations to test the system and to check whether or not the rate of release of contaminants would result in acceptable limits. Thus, an accurate estimation is needed by eliminating as many sources of uncertainty as possible. In addition, studying system behavior under these circumstances is important on its own. In conclusion, the experimental set up used for this research was specifically designed to be as simple as possible to minimize the complexity and potential sources of error and to address the questions posed herein related to the violation of the length scale constraints.

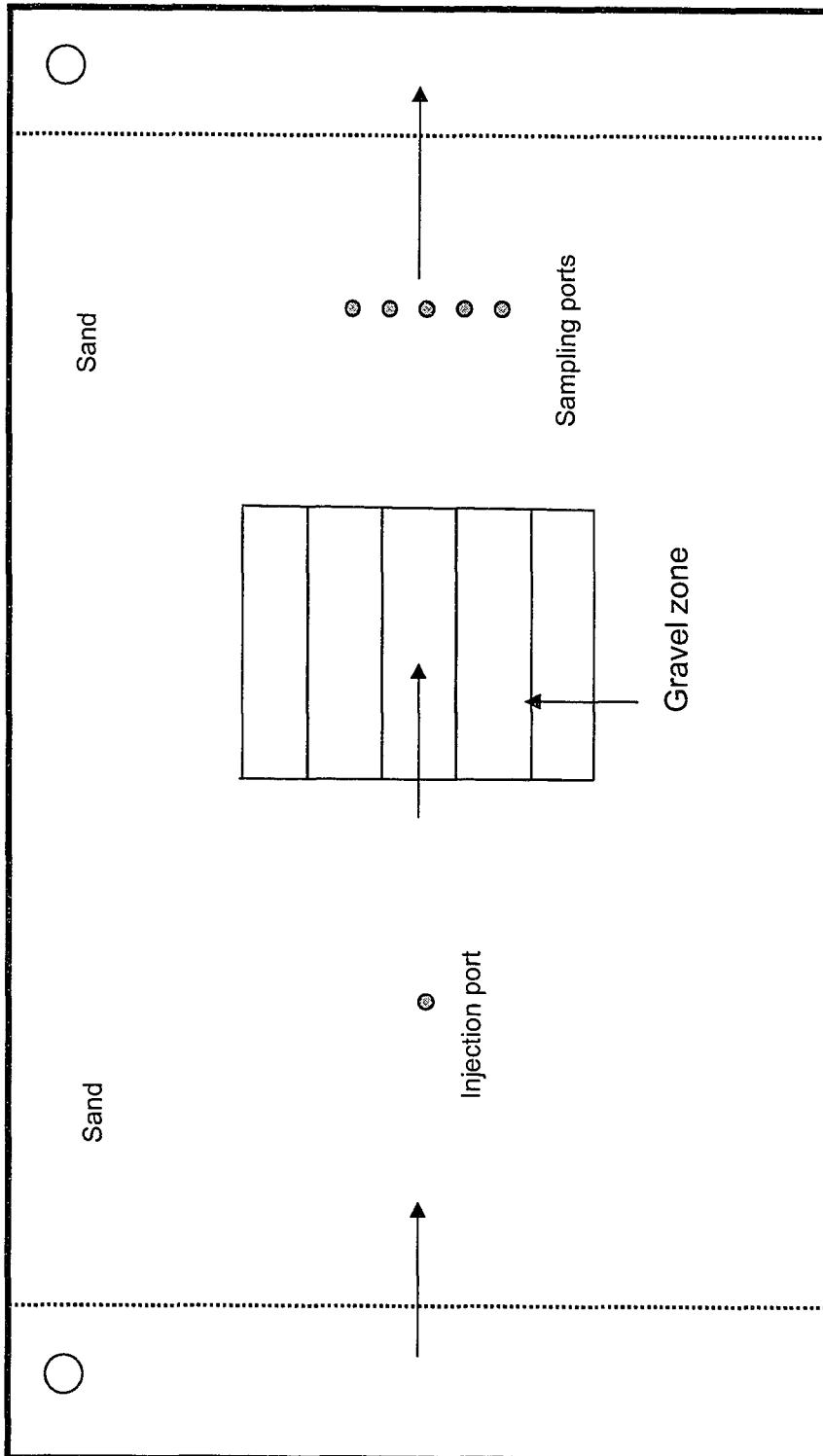


Fig. 4.1 Schematic of the proposed experimental set up.

## CHAPTER 5

### EXPERIMENTAL WORK

#### 5.1 Macroscopic Porous Media Properties Measurements.

As has been indicated in the previous chapter, the experimental setups involve two zones; one of sand and the other of gravel. The macroscopic porous media properties of importance for simulation include porosity, hydraulic conductivity and dispersivities of both zones. To correctly determine these properties, it is important that the continuum hypothesis be satisfied. The following sections describe the experimental setups and results, as well as comparing results with the analytical solutions of the solute transport equation.

#### 5.2 Containers and Constant-Head Reservoirs.

The experimental work was implemented in two containers. One was for properties measurements of gravel and the other was for the sand gravel system. The containers were constructed during the work of West et al. (2003). Figure 5.1 shows a schematic of the boxes. They were constructed of 10 mm thick steel plates welded together to form an open-topped box. The outside dimensions of these boxes were 2.7 x 1.66 x 1.0 m. These dimensions allowed for a 2.3 x 1.46 x 0.9 m physical model, with a 0.2 m wide reservoir at each end.

One 50 mm diameter hole was drilled through the steel wall into the reservoir portion at each end of the containers. A bulkhead fitting was installed in

each hole, and an adjustable overflow was attached to the fitting. The two reservoirs were separated from the host rock portion of the EPM model with a 10 mm thick perforated steel plate lined with permeable geotextile material.

### **5.3 Material Testing and Emplacement.**

#### **5.3.1 Sand.**

Screened, washed mortar sand from a local sand pit was chosen as the sand medium. Sieve analysis indicated it to be uniform medium sand with a mean grain size of approximately 0.3 mm (West 2000). Sieve analysis results are included in Appendix A.

The sand was packed moist, in 10 cm lifts. The procedure for each lift was to dump the total volume of sand in the lift into the model. The sand was then spread evenly through the box and compacted using a hand tamper. Before a new lift, the sand was raked to a depth of approximately 3 cm, and the new lift was spread evenly and watered to homogenize the structure. The watered lift was shoveled with the previous layer to approximately 10 cm to prevent bedding. The sand was then compacted with a 20 cm x 20 cm five kilogram plate tamper lifted and dropped from approximately 30 cm height. The sand filled 64 cm of the height of the box. Following the emplacement of the mortar sand, hydraulic and tracer testing was carried out.

## I Sand porosity

The in-situ porosity of the mortar sand was determined using the same technique as West (2000). By excavating a small hole in the sand, the dry weight of the sand excavated from this hole was determined by oven drying and weighing. The volume of the hole was determined by lining it with plastic wrap, and filling it to the top with water. The quantity of water used to fill the hole was measured to determine the hole volume. The porosity of the sand was then calculated using the following equation:

$$\varepsilon = 1 - \frac{\rho_d}{\rho_s} \quad (5.1)$$

where  $\varepsilon$  is the porosity,  $\rho_d$  is the dry mass density, and  $\rho_s$  is the particle mass density. The dry mass density was found by dividing the oven-dried mass of the soil by the volume of the hole. The particle mass density was assumed to be 2.65 g/cm<sup>3</sup> (Freeze et al. 1979). The porosity of the sand was found to be approximately 0.38. Data are included in Appendix A.

## II Sand hydraulic conductivity

Hydraulic testing was also carried out in the box. The purpose of the hydraulic testing was to determine the average in-situ hydraulic conductivity of the host material. Data are included in Appendix B. The testing was carried out by using the model, Fig.5.2, as a type of large permeameter, with a specified head drop and a measured flow rate. The difference between the model

apparatus and a true permeameter, however, is that the upper surface of the sand in the model apparatus was exposed to the atmosphere. This upper boundary condition, leads in general to a zone of tension-saturated sand above the water table. The consequence of the tension-saturated zone was that the effective cross-sectional area of the test was not known, and could only be estimated by application of unsaturated flow theory. The effects of the tension-saturated region would be significant in cases when the water table is much lower than the level of the sand. However, given the fact that in all the experiments considered, the hydraulic head differences across the test set up were kept approximately  $5 \pm 1$  cm and water level in the upgradient reservoir was kept approximately 1 cm below the level of the sand, it is believed that the effects of the unsaturated zone were insignificant in these scenarios and hence its effects were neglected. This assumption was experimentally demonstrated by lowering the water table and performing an instantaneous point source tracer test. It has been found that when water table was significantly lower than sand level, the plume's peak reached the sampling point significantly slower than those suggested by the analytical solution based on cross-sectional area assuming a height equal to the water level in the upgradient reservoir as shown in Fig. 5.3. In this figure, when water level in the upgradient reservoir was lowered to a height of 47 cm (approximately 16 cm below sand level) the analytical solution based on this height reached the point of measurement (50 cm downstream) faster than measurements. The analytical solution matched measurements when the height was adjusted in calculations to 61 cm which

indicated that the effective height in this case should be 61 cm rather than 47 cm. When water level of the upgradient reservoir was raised to the previously mentioned level (approximately 1 cm below sand level) the plume's peak reached the sampling port in approximately the expected time as suggested by the analytical solution assuming again cross sectional area based on the upgradient reservoir water level, as will be shown later. This confirmation was important in order to avoid adding more factors into the model and hence reduced more sources of uncertainty.

The head drop across the experimental set up was measured through inverted tube manometers inserted into both reservoirs. The distance between the measuring ports was 2.3 m. The hydraulic conductivity was estimated to approximately be  $9 \times 10^{-5}$  m/s. Moreover, the hydraulic conductivity of the sand was also measured in a constant head permeameter during the work of West (2000). It was found to be approximately  $7.0 \times 10^{-5}$  m/s for densely-compacted sand.

### **III Sand dispersivity**

A tracer test was conducted in the fully saturated model. A set of experiments were conducted using an instantaneous point source as well as instantaneous line source.

In the instantaneous point source experiments, Fig. 5.4, three point sources at three different levels (within 10 cm) and 38 cm apart were installed. A

one milliliter, 10,000 ppb, uranine dye ( $D_0 = 4.5 \times 10^{-10} \text{ m}^2/\text{s}$ , Skagius and Neretnieks 1986) sample was injected in each of the three injecting ports and data were collected in ports at distances 50, 60, 80, 90 and 100 cm from the injection points as shown in Fig. 5.4. Uranine dye is sensitive to light; however, in the experiments the dye was not at all subjected to any source of light. Moreover, it is also conservative with no potential for adsorption with the material used in the experiments, which was confirmed in a patch experiment. Samples were collected through a set of sampling ports which consisted of plastic tubing 1 mm O.D. At each downstream sampling location a set of 3 sampling ports 2.5 cm apart were inserted to locate the center of the plume. Samples were taken by first purging the plastic tubing of one pore volume and then approximately 0.5 ml were taken and analyzed for fluorescence. TD-700 was used for fluorescence measurements which were then converted to concentration units in ppb. The device was regularly calibrated to measure a maximum of 600 ppb.

The advantage of this set up was that it gives, in addition to its main purpose which was to determine the value of dispersivities, information about the homogeneity of compaction by comparing travel time in each of the three solute paths. The data are included in Appendix B. The results were analyzed by fitting the collected concentration vs. time data to that produced from an analytical solution of the 3D advection-dispersion equation with an instantaneous point source in homogeneous porous media (Baetsle 1969).

$$C(x, y, z, t) = \frac{M / \varepsilon}{8(\pi t)^{3/2} (D_x D_y D_z)^{1/2}} \exp \left\{ -\frac{(x - vt)^2}{4D_x t} - \frac{y^2}{4D_y t} - \frac{z^2}{4D_z t} \right\} \quad (5.2)$$

where  $M$  is the mass injected,  $\varepsilon$  is the porosity,  $D_x$ ,  $D_y$ , and  $D_z$  are the coefficients of hydrodynamic dispersion; and  $v$  is the seepage velocity.

The value of dispersivity that was found to best fit the data was approximately 0.8 mm (longitudinal) and 0.09 mm (transverse) with a ratio of 0.11. Figure 5.5 shows the measured and calculated concentrations versus time for all the downgradient sample points. From this figure it may be noticed that at some points the analytical solution matched those of the experiments when the distance from the injection points to measuring ports were adjusted. For example, the point at a distance of 60 cm from the injection point fits with the analytical solution assuming the distance to be 61.5 cm. Although this is insignificant, it may be attributed to the fact that this particular point may have moved a bit during the compaction process. This may also have occurred to the last point; however, the difference is a bit larger, which may be attributed to the fact that the permeability in this particular path may be slightly higher. Moreover, the concentration at this particular point was relatively lower than those suggested by the analytical solution, which may also be attributed to mispositioning of the sampling point probably during compaction processes.

Another setup was constructed to confirm the previously estimated values of sand dispersivity. An instantaneous point source was inserted in the sand at

the centerline of the box and data were collected at 50 and 75 cm from the source. The results were analyzed by fitting the collected concentration vs. time data to that produced from the analytical solution. The value of dispersivity that was found to best fit the data was 0.725 mm (longitudinal) and 0.09 mm (transverse) with a ratio of 0.125 which are fairly close to those estimated previously. Fig. 5.6 shows the measured and calculated concentrations versus time at these two points. Data are contained in Appendix A.

Moreover, instantaneous line source experiments were also conducted. A 1.4 cm diameter stainless steel mesh wrapped with geotextile material was used as a well. A copper tube closed from one end by a rubber diaphragm was filled with uranine dye solution. The tube was carefully inserted into the well and stayed there for approximately half an hour until the flow system established steady state. Then, the rubber diaphragm was ruptured using a steel wire and the copper tube was withdrawn slowly. Data were collected 117 cm away from the line source at two different elevations 10 cm apart. At each elevation, a set of 5 sampling ports approximately 5 cm apart from each other were constructed. Data were compared with the 2D analytical solution (Wilson et al. 1978).

$$C(x, y, t) = \frac{M' / \varepsilon}{4\pi t (D_x D_y)^{1/2}} \exp \left\{ -\frac{[(x - x_0) - vt]^2}{4D_x t} - \frac{(y - y_0)^2}{4D_y t} \right\} \quad (5.3)$$

where  $M'$  is the mass injected per unit length,  $\varepsilon$  is the porosity,  $D_x$ , and  $D_y$  are the coefficients of hydrodynamic dispersion; and  $v$  is the seepage velocity.

Figures 5.7, 5.8 and 5.9 show the measured data at the upper, “0” level, and the lower level, “-1” level, respectively, as well as the analytical fit. The measured data at the lower level (Fig. 5.9) suggested the sampling points to be shifted to the left (a few millimeters) but the arrival time was very close which gives confidence in the homogeneity of the sand and the compaction processes. Determining the best fit for the data suggested 0.7 mm longitudinal and 0.196 mm transverse dispersivities with a ratio of 0.28 for the “0” level measurements and 0.75 longitudinal and 0.22 transverse dispersivities with a ratio of 0.29 for the “-1” level measurements which are fairly close. In comparison with point source estimation of dispersivities, one may notice a large discrepancy in the ratio of transverse to longitudinal dispersivity (the ratio for the line source experiments was approximately 2.5 as high compared with the point source estimation). The reason for this discrepancy may be attributed to the fact that the analytical solution assumes a point or a line source when in reality appreciable volume was injected (i.e., we did not have a true point source or line source but an initial concentration within a finite or definite volume). To correctly estimate the value of dispersivity, the two-dimensional system was modeled numerically, Fig.5.10. The best numerical techniques to model this system with these very low dispersion coefficients are the method of characteristics (MOC) and the third-order Total Variation Dimensioning Methods (TVD). Other methods (upstream finite difference/element methods) were prone to high numerical dispersion unless an extremely fine mesh was used which would certainly require excessive computing power. More discussion on this issue is given in the next chapter. For

this system, half of the domain was discretized into 1 mm squares and the solute was assigned to a set of cells to represent the initial mass. This simulation was also important as it gives confidence in the discretization scheme and the numerical engine, which will be used throughout the rest of the numerical work as will be discussed later. The simulation also revealed that the ratio of transverse to longitudinal dispersivity based on this simulation was found to be approximately one-third that suggested by the analytical solutions, with 0.65 mm longitudinal, 0.052 mm transverse, and 0.08 for the ratio. This may be attributed (as discussed earlier) to the fact that, it is not correct to assume a point or a line source as required by the analytical solution when an appreciable volume was injected. Hence, the dispersivity estimated from the numerical simulation of line source experiments was used for the remainder of the study.

### **5.3.2 Gravel.**

Gravel of 0.8 cm mean grain size was packed in 10 cm lifts the same way as the sand but no watering was introduced. The gravel filled 56 cm of the height of the box for the hydraulic and tracer tests. Appendix A contains sieve analysis of the gravel.

#### **I- Gravel porosity.**

The porosity of the gravel was determined by measuring the volume of water required to fully saturate a 20 L container packed with washed, dry gravel.

The porosity was found to be approximately 0.38. Data are contained in Appendix A.

## **II- Gravel hydraulic conductivity.**

The hydraulic conductivity of the gravel was measured in the box in exactly the same way as the sand. Measuring the hydraulic conductivity of the gravel was a challenge in the sense that the porous material used to simulate the pervious layer is expected to have a very high hydraulic conductivity and hence the resulting pressure drop, if one uses a permeameter, is expected to be very small and difficult to measure. Moreover, since the size of the pervious material is relatively large, it requires a larger diameter permeameter to satisfy the length scale constraints and to neglect the boundary effects. To account for these effects the experimental box was used to measure the hydraulic conductivity of the gravel. The experimental box is wide enough such that the boundary effect may be neglected and is long enough such that the pressure drop may be measurable. Figure 5.11 shows the results of the hydraulic conductivity measurements of the gravel. Best fit of the experimental data suggests the hydraulic conductivity to be approximately 0.28 m/s.

Moreover, the Idelchik method (Idelchik 2001) was used to verify measurements. The Idelchik method determines the pressure drop across the bed given Darcy's velocity and is based on the following relations:

$$\text{Re} = \frac{0.45V_{wp} d\rho}{\mu(1-n)\sqrt{n}} \quad (5.4)$$

$$\Delta P = \frac{1.53L}{n^{4.2}d} \left\{ \frac{30}{\text{Re}} + \frac{3}{\text{Re}^{0.7}} + 0.3 \right\} \frac{\rho V_{up}^2}{2} \quad (5.5)$$

where  $V_{up}$  is the upstream Darcy's velocity (m/s),  $\rho$  is the fluid density (kg/m<sup>3</sup>),  $\mu$  is the dynamic viscosity (Pa.s),  $\Delta P$  is the pressure drop (Pa),  $n$  is the porosity, and  $d$  is the mean grain diameter (m). Although Idelchik's relations were developed for beds containing spherical particles, one may use it as a guide for beds containing nonspherical particles. Idelchik's relations would enable one to check the measured pressure drop. The hydraulic conductivity was estimated, using this method to range from 0.305 to 0.492 m/s which is slightly higher than that estimated from the experimental values which may be attributed to the fact that gravel grains were not perfectly spherical.

### III Gravel dispersivity.

A set of tracer tests were conducted to estimate longitudinal and transverse dispersivities. Two different kinds of tracer tests were used; instantaneous point source and continuous point source. In the instantaneous point source experiments, 1 ml of 9,000 ppb uranine dye solution was injected at the center of the gravel box and samples were collected at two downstream locations at distances 0.75 and 1.25 m from the source. To locate the center of the plume a set of sampling points were set at spacings <5 cm apart. Samples were collected through stainless steel tubing 3 mm OD through 60 ml syringes. A volume of approximately 30 ml were drawn in each sampling event and is analyzed for florescence. This volume is believed to be representative based on

the fact that it represents a volume of 79 ml of gravel, i.e., a cube of length approximately 5 cm. Data were graphed and fitted with the analytical solution by adjusting the value of dispersivities to match the experimental data, Figs 5.12 and 5.13. The average values of dispersivity for the experiments were 1.25 cm for longitudinal dispersivity and 0.05 for the ratio of longitudinal to transverse dispersivities. Appendix A contains the measured data.

A set of continuous point source tests were also conducted to confirm the values of transverse dispersivities assumed from the fitting of the instantaneous point source experimentations. A 20 L Marriot bottle was constructed approximately 100 cm above the gravel surface to feed a constant flow of dye regardless of the head drop in the bottle, Fig. 5.14. The bottle was connected to a flow restriction section, which was a small plastic tube, 10 cm long, filled with sand, Fig. 5.15. The purpose of this small tube section was to restrict the flow rates such that they were close to the local seepage velocity at the injection point in order to allow no radial flow of the dye and to facilitate the use of the analytical solution. The flow restriction section is connected to a valve at the injection point to help the initiation of the experiments as well as to prevent air from entering into the tubes during installation. The valve had an extension to the surface (approximately 32 cm) to allow for opening and closing from the top of the gravel. A set of sampling points were installed 1m downgradient from the injection points. The sampling points span an area of 35 x 35 cm in a 5 cm grid. The experiments were allowed to run for a long time (order of days) and data were collected repeatedly at the downgradient sampling points. The dye flow rates

were adjusted by changing the level of Marriot bottle with respect to the gravel. Data were shown to be largely stable with time. Sometimes variations in flow were noticed due, probably, to this very low flow rate of dye. Data were compared with the analytical solution (Wexler 1992) using the values of dispersivity as determined from the instantaneous point source experiments.

$$C(x, y, z, t) = \frac{C_o Q \exp\left[\frac{V(x - X_c)}{2D_x}\right]}{8\varepsilon\gamma\pi\sqrt{D_y D_z}} \cdot \left\{ \exp\left[\frac{\gamma\beta}{2D_x}\right] \operatorname{erfc}\left[\frac{\gamma + \beta t}{2\sqrt{D_x t}}\right] + \exp\left[\frac{-\gamma\beta}{2D_x}\right] \operatorname{erfc}\left[\frac{\gamma - \beta t}{2\sqrt{D_x t}}\right] \right\} \quad (5.6)$$

Where

$$\gamma = \left[ (x - X_c)^2 + \frac{D_x(y - Y_c)^2}{D_y} + \frac{D_x(z - Z_c)^2}{D_z} \right]^{1/2} \quad (5.7)$$

and

$$\beta = [V^2 + 4D_x\lambda]^{1/2} \quad (5.8)$$

Where

V= velocity in x-direction

Q= dye injection rate

$X_c, Y_c, Z_c$  = coordinates of point source, and

$D_x, D_y,$  and  $D_z$  are the dispersion coefficient in the x, y and z directions, respectively.

There were good agreements between the measured and the analytical solution using the dispersivities estimated from the instantaneous source experiments, Figs 5.16 and 5.17. Appendix B contains the collected data.

#### 5.4 Sand-Gravel System.

The experimental set up was designed to be as simple as possible such that parameters other than those of the pervious region were kept almost the same during the course of the different experimental set up. Figure 5.18 shows a three-dimensional schematic of the set up. Six cases were studied for the sand-gravel system. The transverse thicknesses of the gravel layer in these systems were chosen to be 5, 10, 15, 20, 30, and 50 cm. In each case a painted steel (5x5 cm, 12 gauge) wire mesh enclosure was constructed with length 50 cm, height 70 cm and the desired thickness. The wire mesh enclosures were wrapped with geotextile material to prevent the migration of fines into the gravel and hence deteriorate its role and at the same time to not constitute restriction to the flow. The wire mesh enclosure was inserted in the empty experimental box almost 1 m downgradient the upgradient reservoir. A stainless steel wire mesh tube with inner diameter of 1.4 cm and wrapped with geotextile, was used as an injection well. The stainless steel tube was wrapped with geotextile to prevent sand from filling the tube. A copper tube slightly less in diameter was initially inserted into the stainless steel tube mesh during installation to hold the tube during compaction. In the six experimental setups, the well was installed approximately 30 cm upgradient of the gravel box in exactly the centerline of the box. Sand and gravel layers were compacted as described earlier in determining the soil properties.

Earlier, it was decided that an instantaneous point source be used upgradient of the gravel but difficulties in catching the plume downgradient of the gravel as well as the large memory requirements to model this system had led us to consider the 2D case instead.

#### **5.4.1 Instrumentation.**

Each of the six cases studied for the sand-gravel systems were equipped with manometers to measure the hydraulic head distributions and sampling ports to measure the concentration. Moreover, the water flow rates through each system as well as the concentration in the downgradient reservoir were also measured to allow for mass balance calculations. A submerged pump was immersed into the downgradient reservoir to circulate the water and homogenize the solute content within the reservoir. Details of measuring instrument locations and specifications are given in the following section.

##### **I- Manometers.**

A set of manometers was inserted into the experiments to monitor hydraulic head variations. Figure 5.19 show the location of the manometers. The first one was installed in the upgradient reservoir and the second one was inserted about 30 cm from the reservoir. The readings of these two manometers were used to estimate the average hydraulic conductivity of the sand since at this distance the flow lines were not impacted by the downgradient gravel. Another three manometers were inserted in the sand. The first of them was upgradient

the sand and the other two were measuring the head across the gravel. One more manometer was also inserted in the downgradient reservoir.

## **II- Concentration Sample Ports.**

Dye concentrations 30 cm on average downgradient of the gravel, were measured at three levels 10 cm apart. A set of seven ports were used at each level spanning a width of 40 cm. The ports were attached to a stainless steel grid to maintain equal spacing and to ease assembly and disassembly. A set of ports were also installed around the gravel.

### **5.4.2 Water supply and flow rate measurements.**

Tap water was used for the water supply. It was piped into a 200 L reservoir with an over flow. Water in the reservoir was then gravity fed into the upgradient reservoir of the model. The flow rate into the model was adjusted such that sufficient water was available to satisfy the flow rate dictated by the difference in head across the model, as well as to ensure that the reservoir was constantly overflowing. The flow rate through the model was determined by measuring the volume of water that overflowed the downgradient reservoir during a known period of time.

### **5.4.3 Experiment operation.**

After constructing each experimental setup, water was allowed to rise slowly in the upgradient reservoir. It took approximately 8 hours to fill the

experimental system to the desired level. The water was allowed to flow for about one day to wash the sand from any dye residuals from previous experiments. The copper tube used to sustain the well mesh during compaction is then withdrawn and the system is left to reestablish steady state. The copper tube is closed at one end by a rubber diaphragm and is filled with a dye. The tube is then carefully and slowly reinserted into the well and is left for approximately one hour. A steel rod is then used to cut the rubber diaphragm and the copper tube was lifted slowly and a stop watch is pressed indicating the start of the experiment. In some cases samples were collected ahead and across the gravel to follow the plume. The main concentration measurements were taken at the sample ports that were approximately 30 cm downgradient of the gravel. Measurements were recorded at approximately 21 sample ports of one hour intervals until the plume passed. Certain experiments were repeated two or three times and sometimes more to establish confidence in the reproducibility of the results.

Once the transport part was finished, manometers were inserted in the desired location and the system is left for few hours then head measurements were recorded. Flow measurements were taken many times during the course of the experiment.

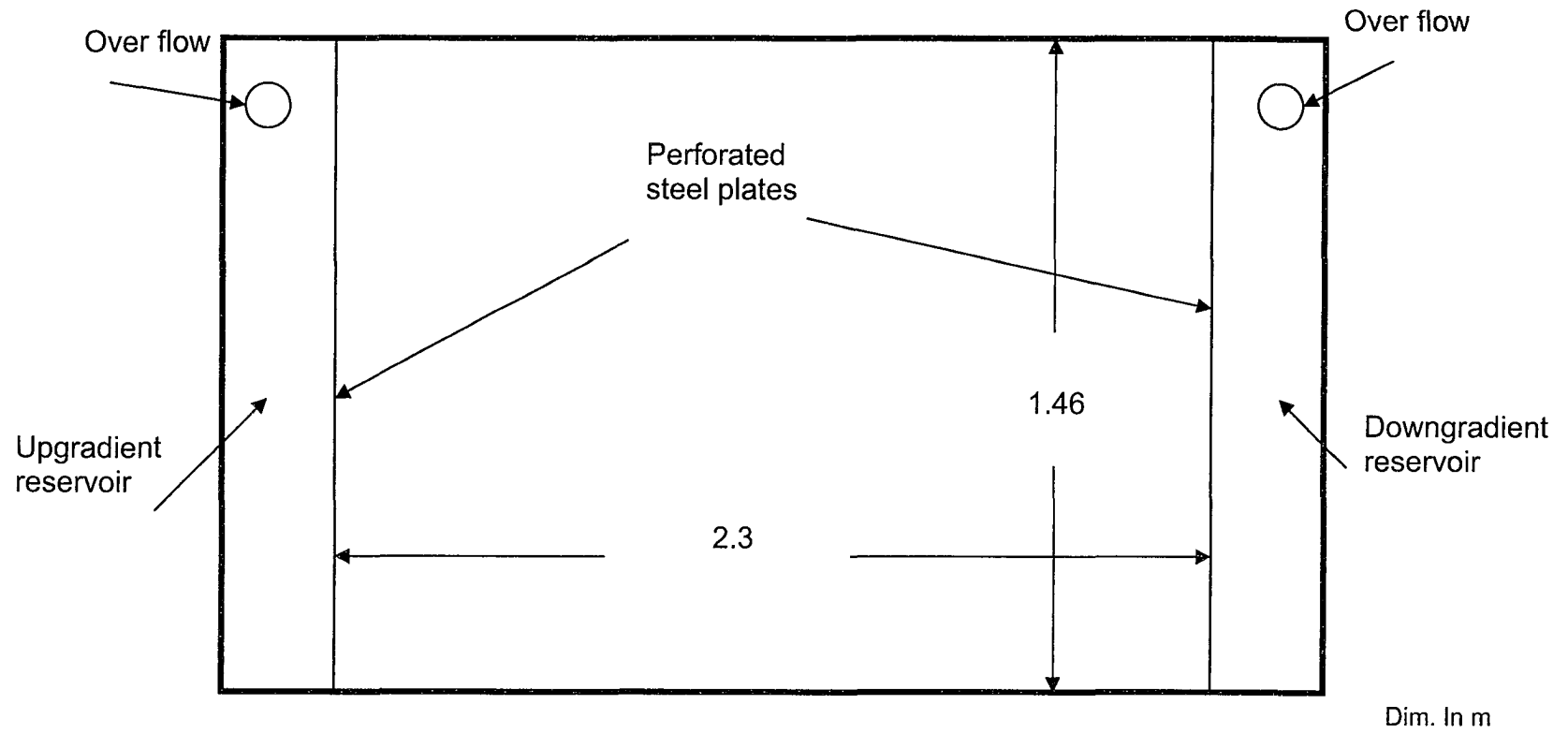


Fig. 5.1 Schematic of the steel boxes.

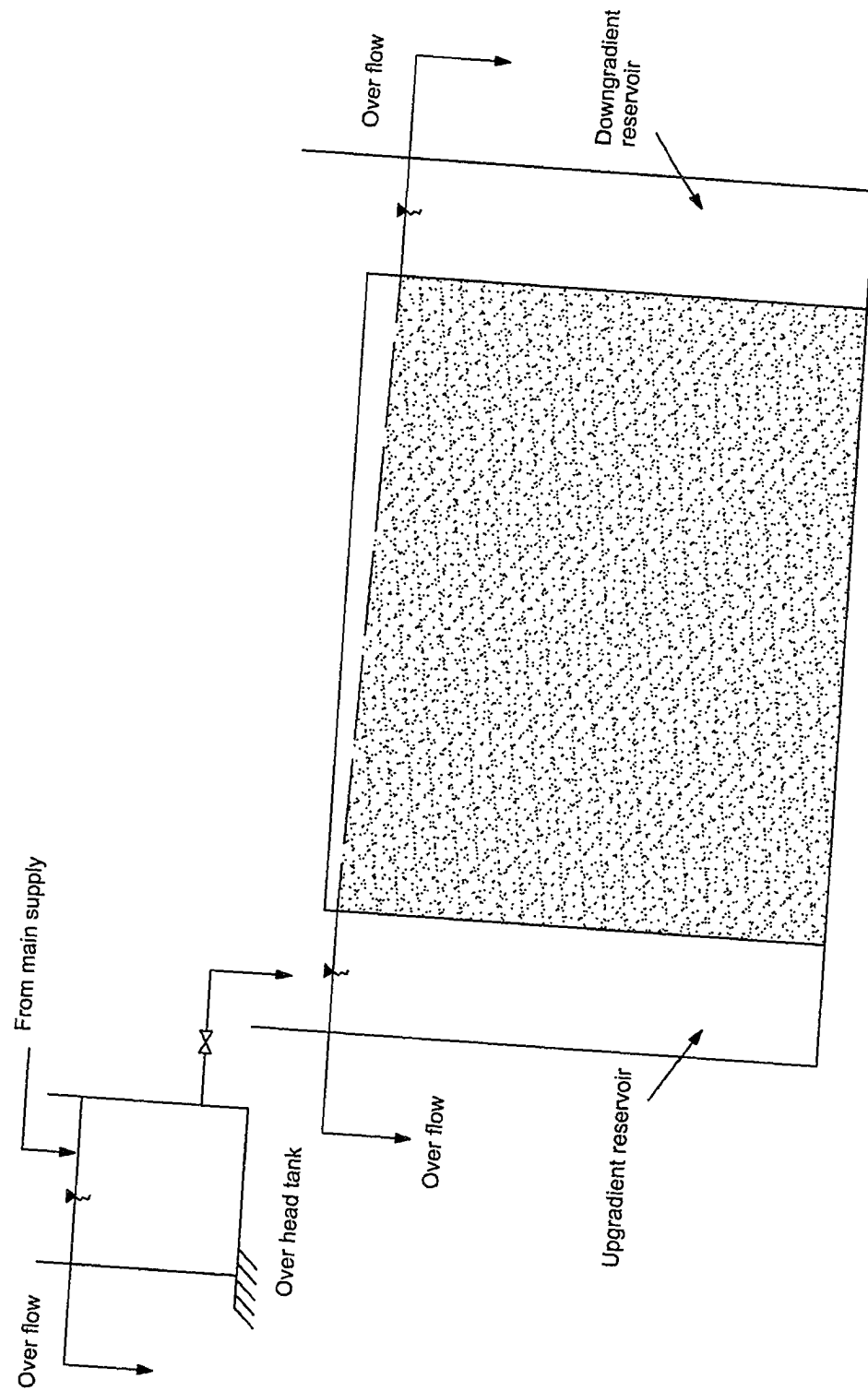


Fig. 5.2 Schematic of sand experiment.

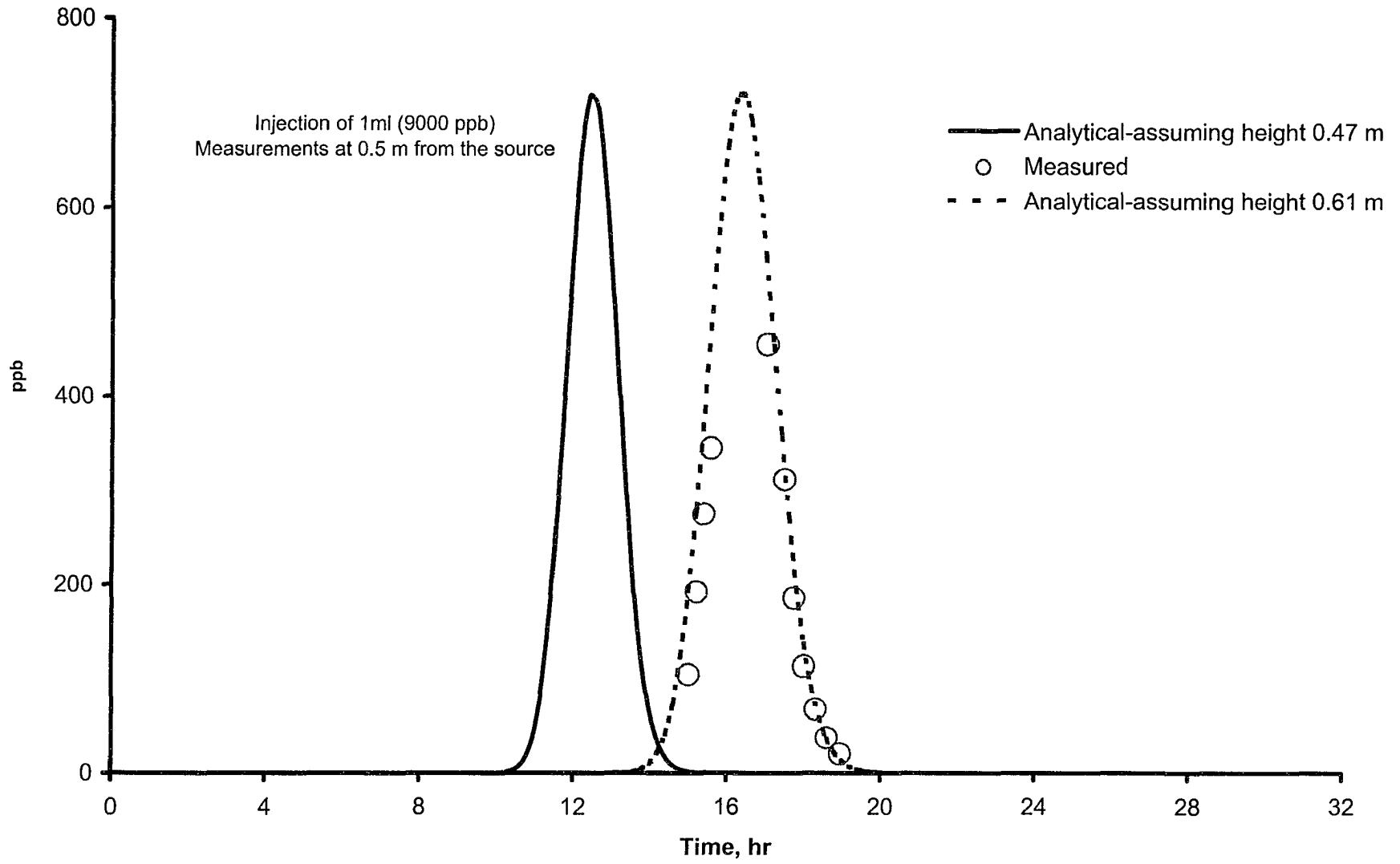


Fig. 5.3 Effect of lowering upgradient reservoir water level on plume arrival time.

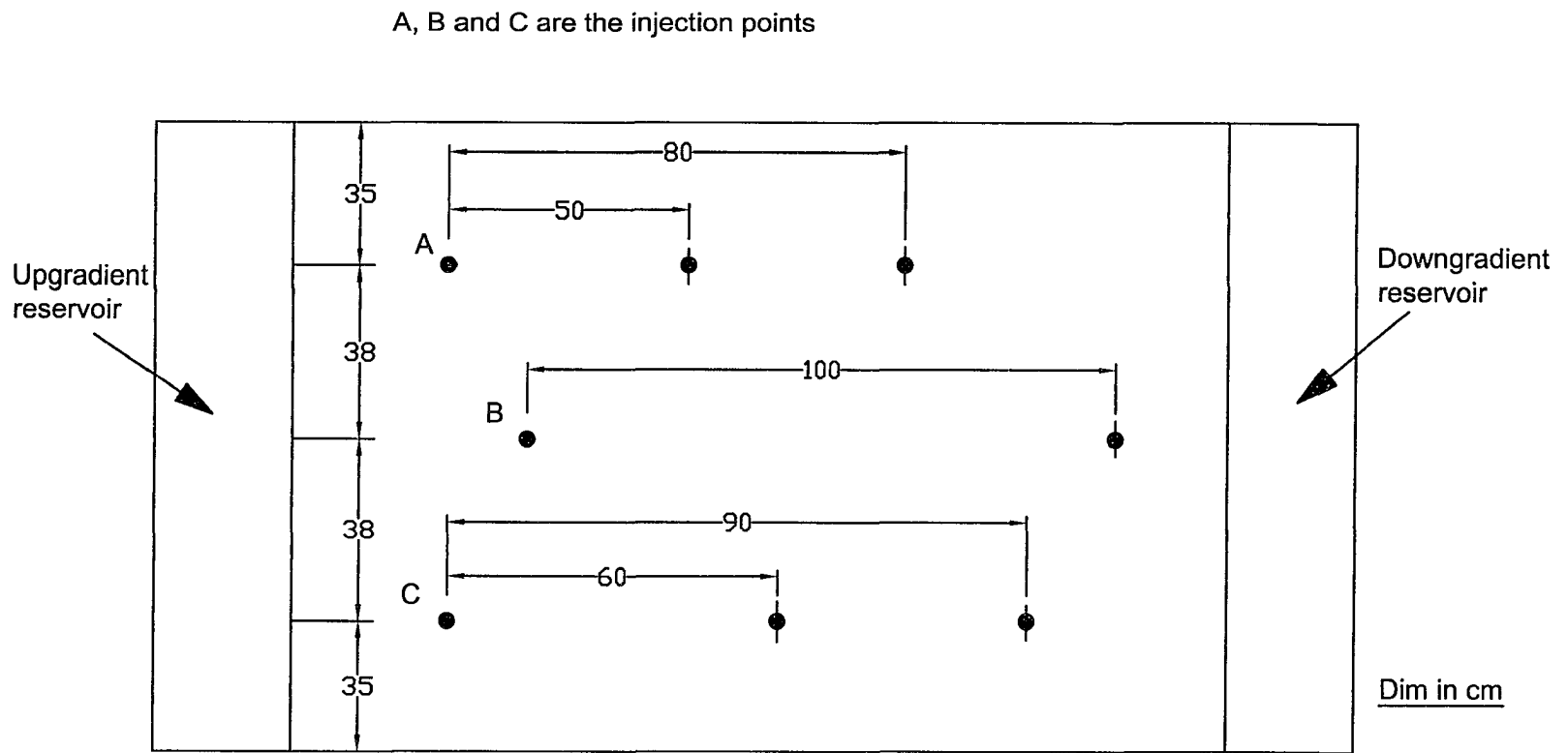


Fig 5.4 Injection and measuring ports in the instantaneous point source experiment in sand.

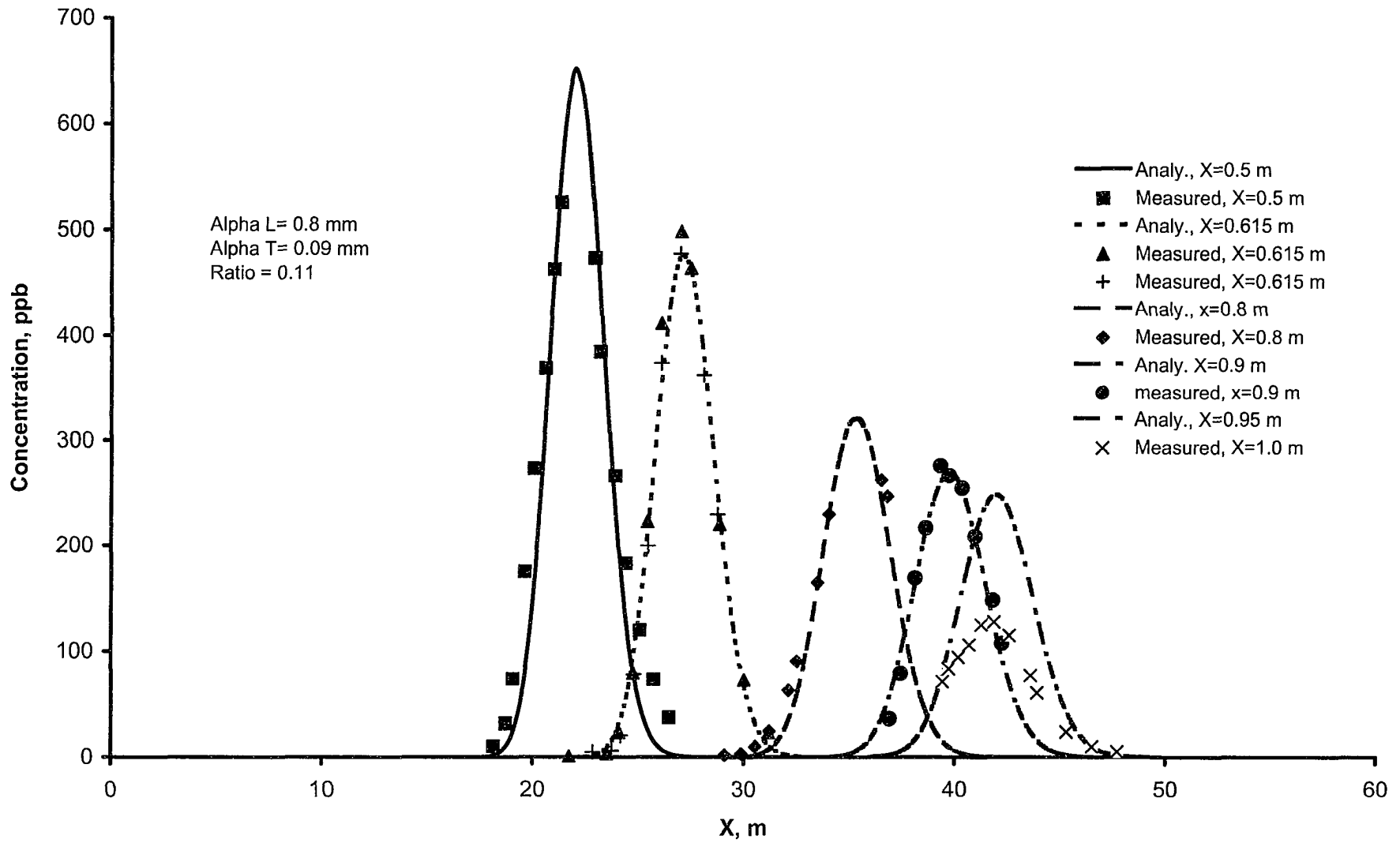


Fig. 5.5 Instantaneous point source experiments in sand, set up #1.

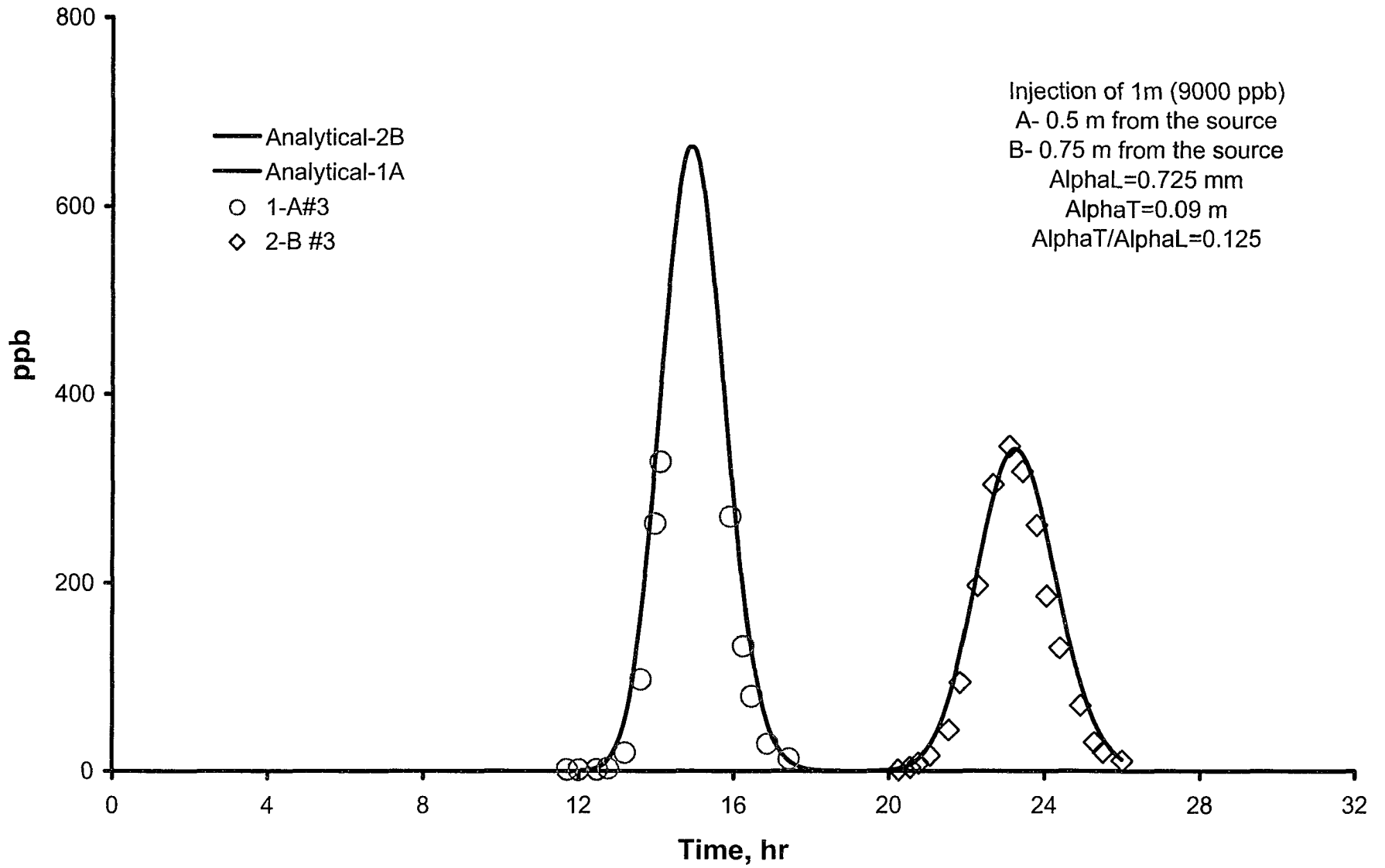


Fig. 5.6 Instantaneous point source experiments in sand, set up #2.

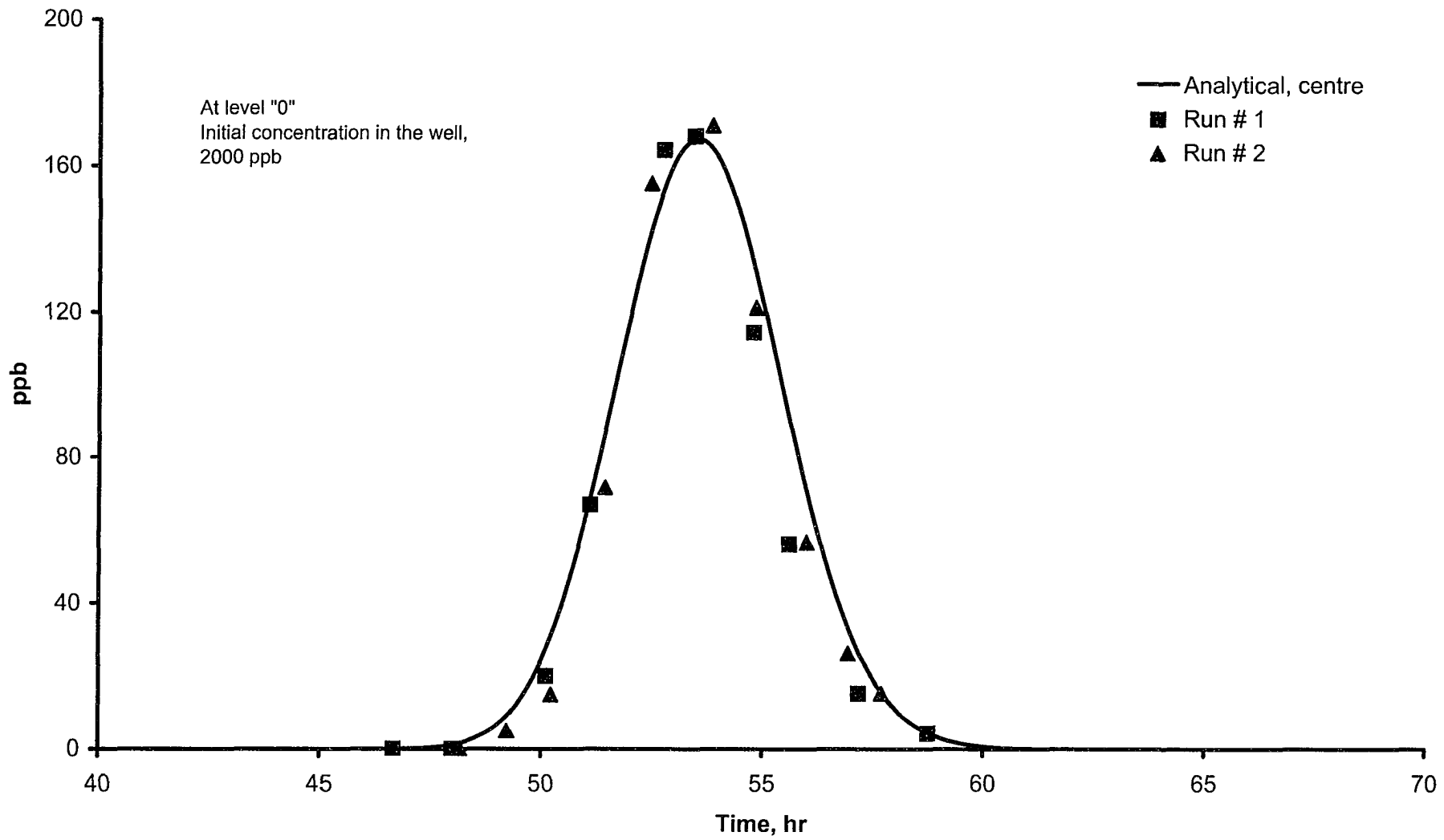


Fig. 5.7 Concentration measurements at level "0", 117 cm downstream from the well, point B.

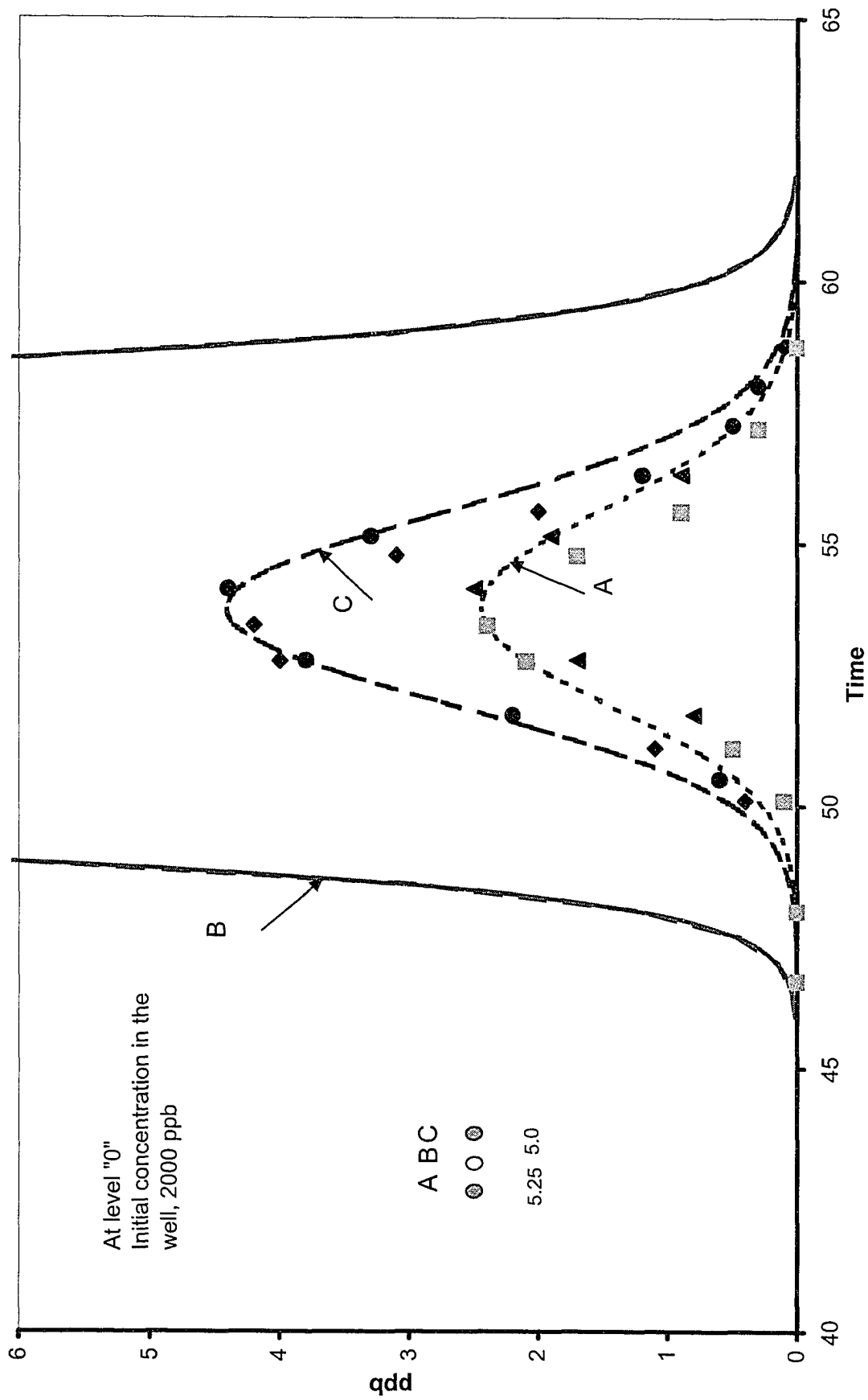


Fig. 5.8 Concentration measurements at level "0", 117 cm downstream from the well, points A,B,C. 190

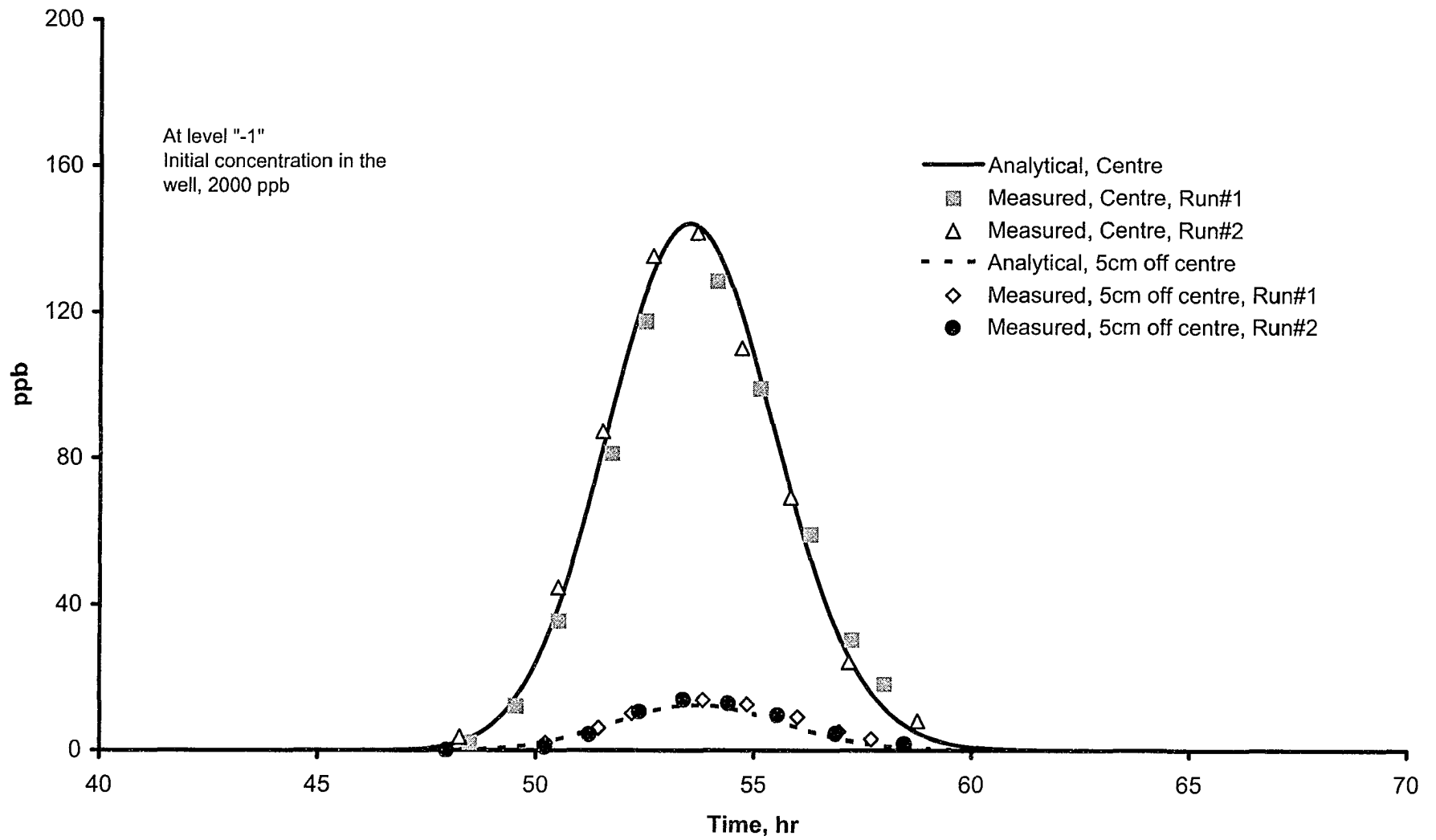


Fig. 5.9 Concentration measurements at level "-1", 117 cm downstream from the well.

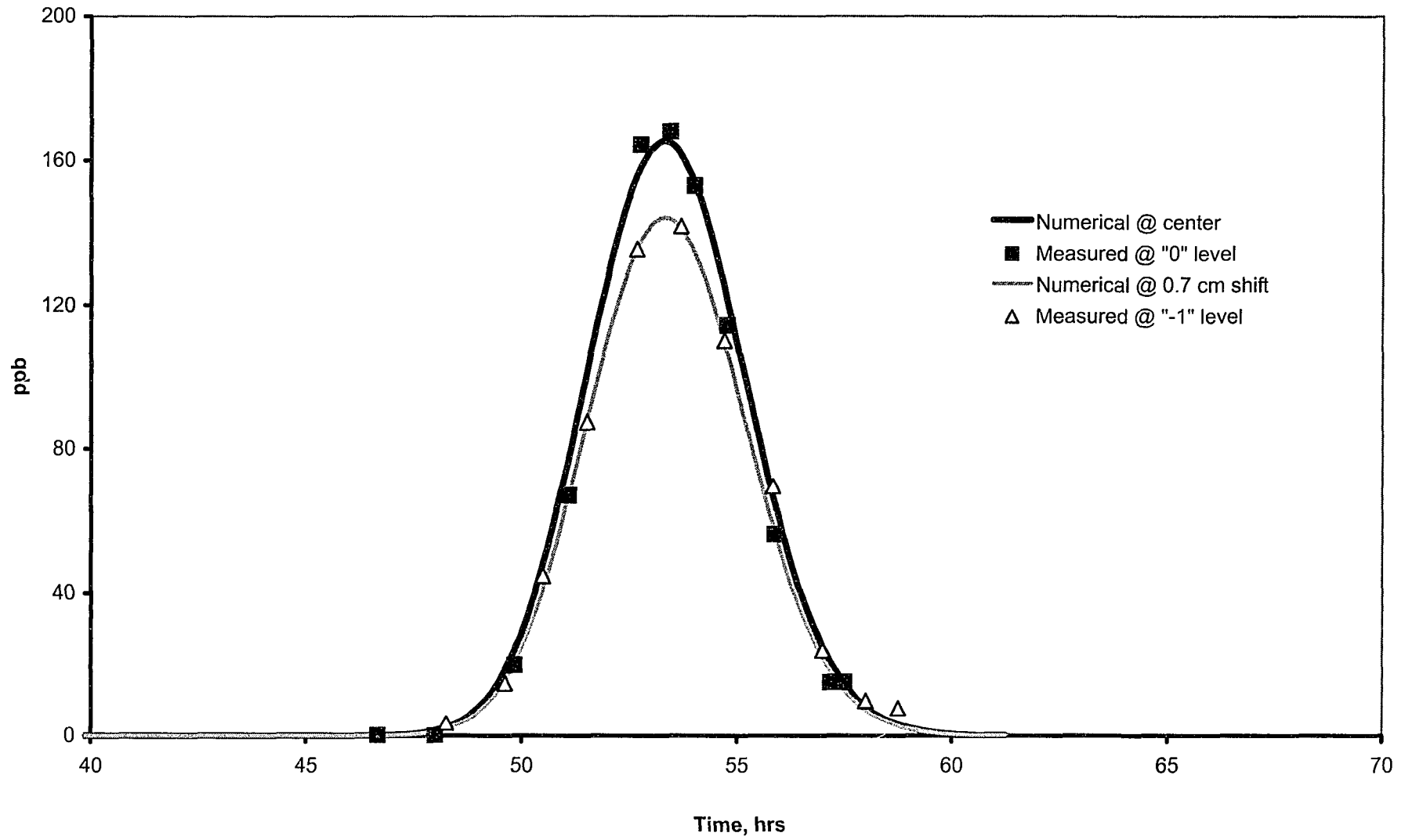


Fig. 5.10 Comparison of measured and numerically calculated line source experiments.

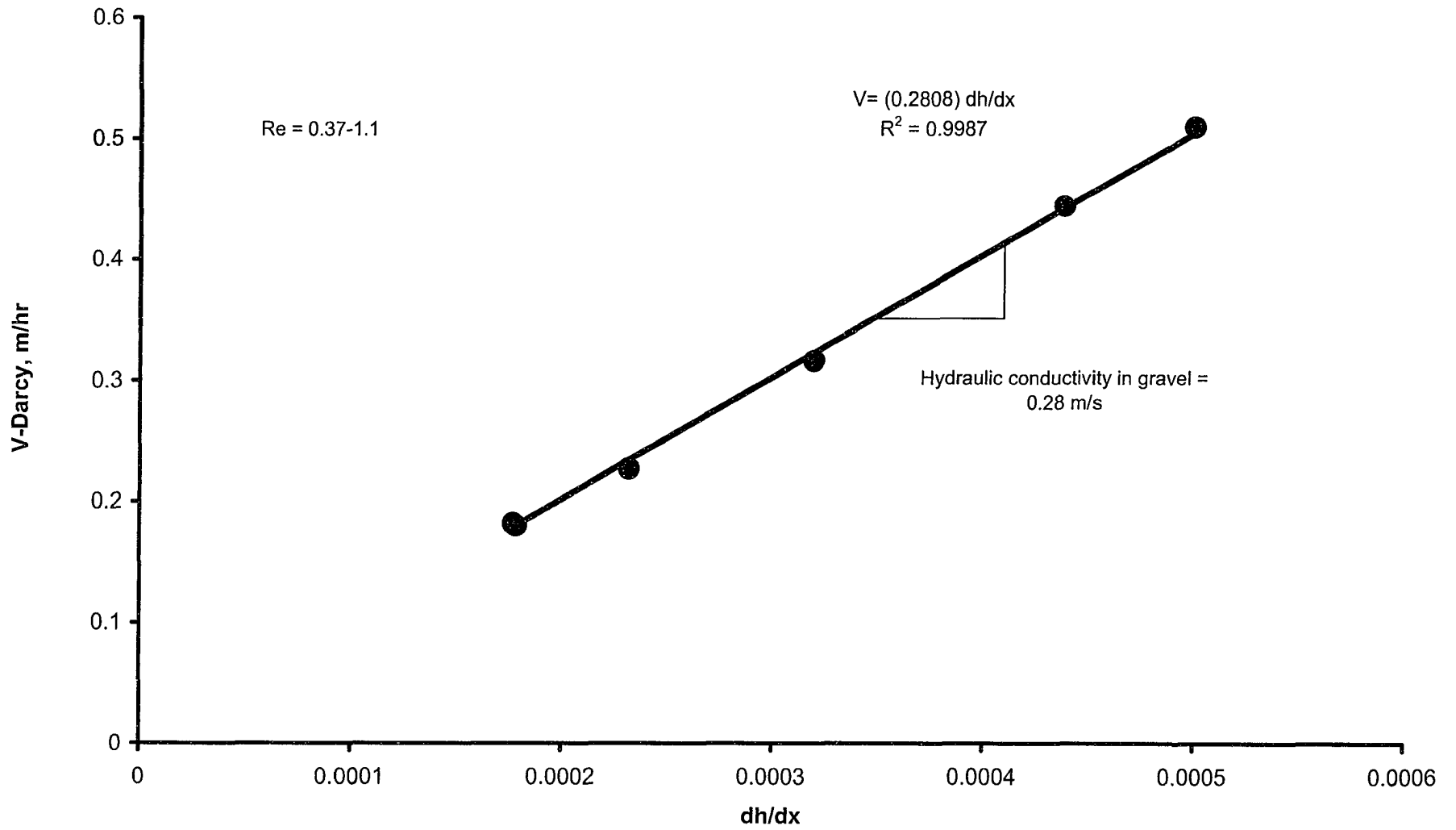


Fig. 5.11 Hydraulic conductivity estimation for the gravel.

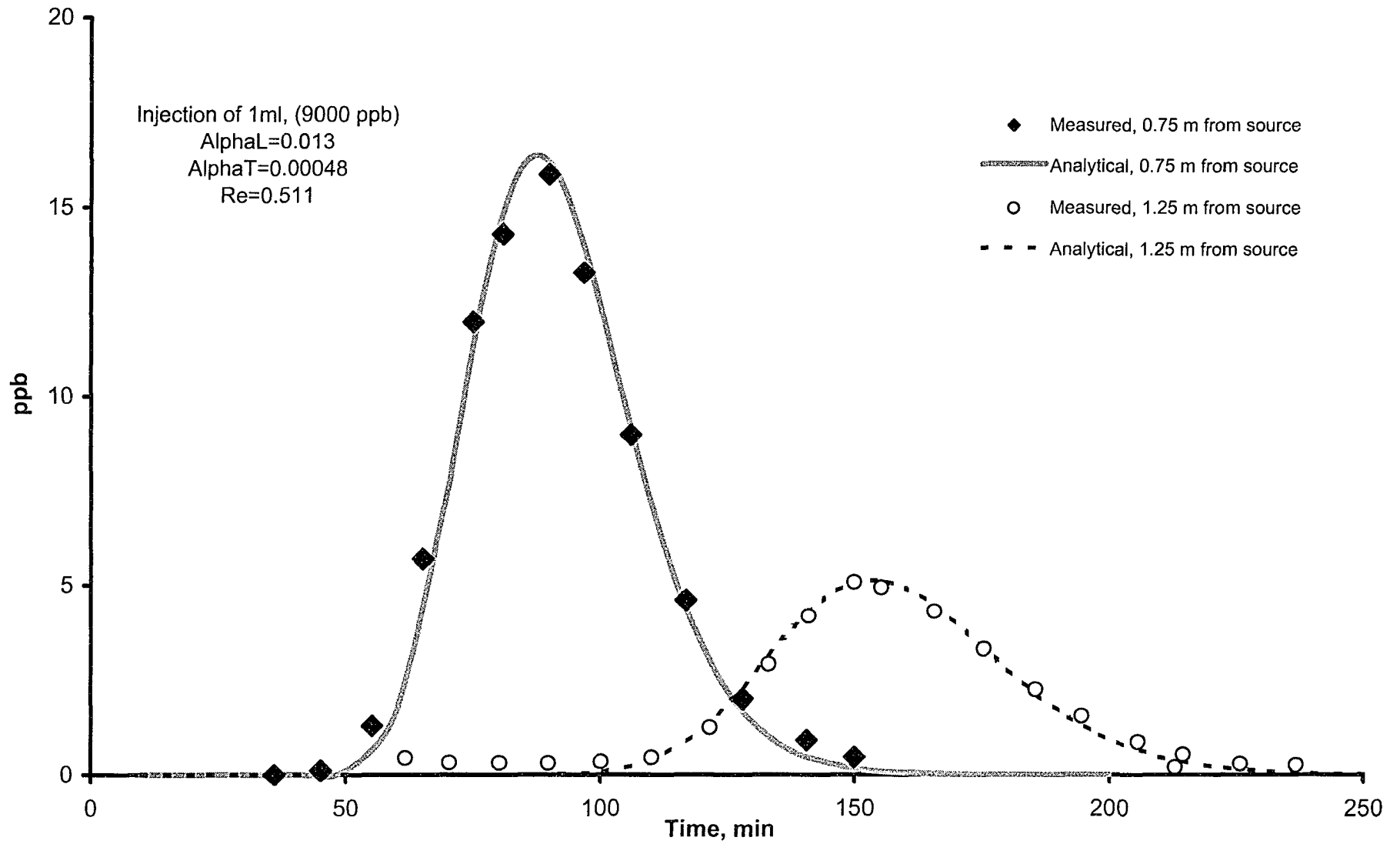


Fig. 5.12 Tracer test in gravel, #1.

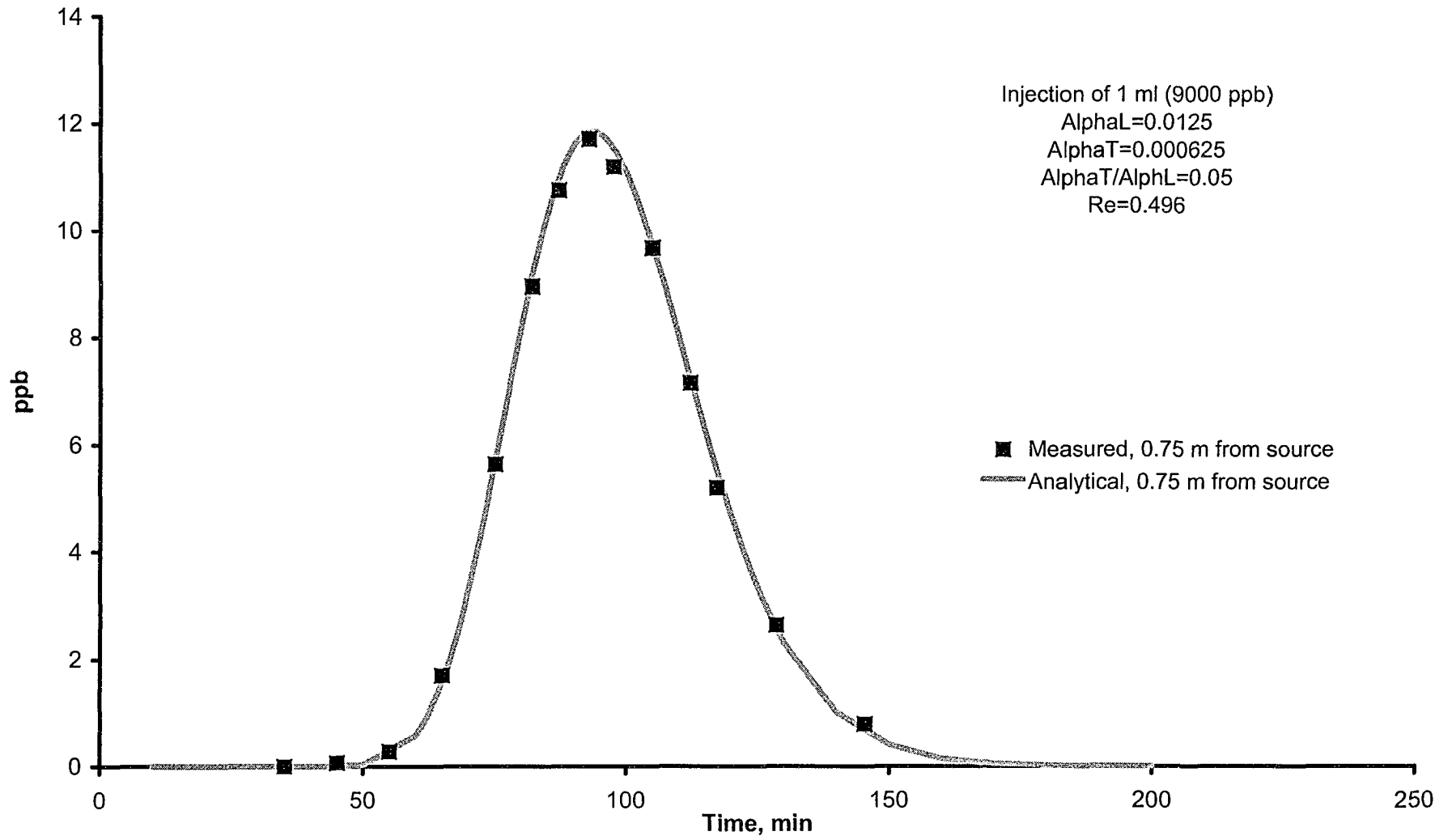


Fig. 5.13 Tracer test in gravel, #2.

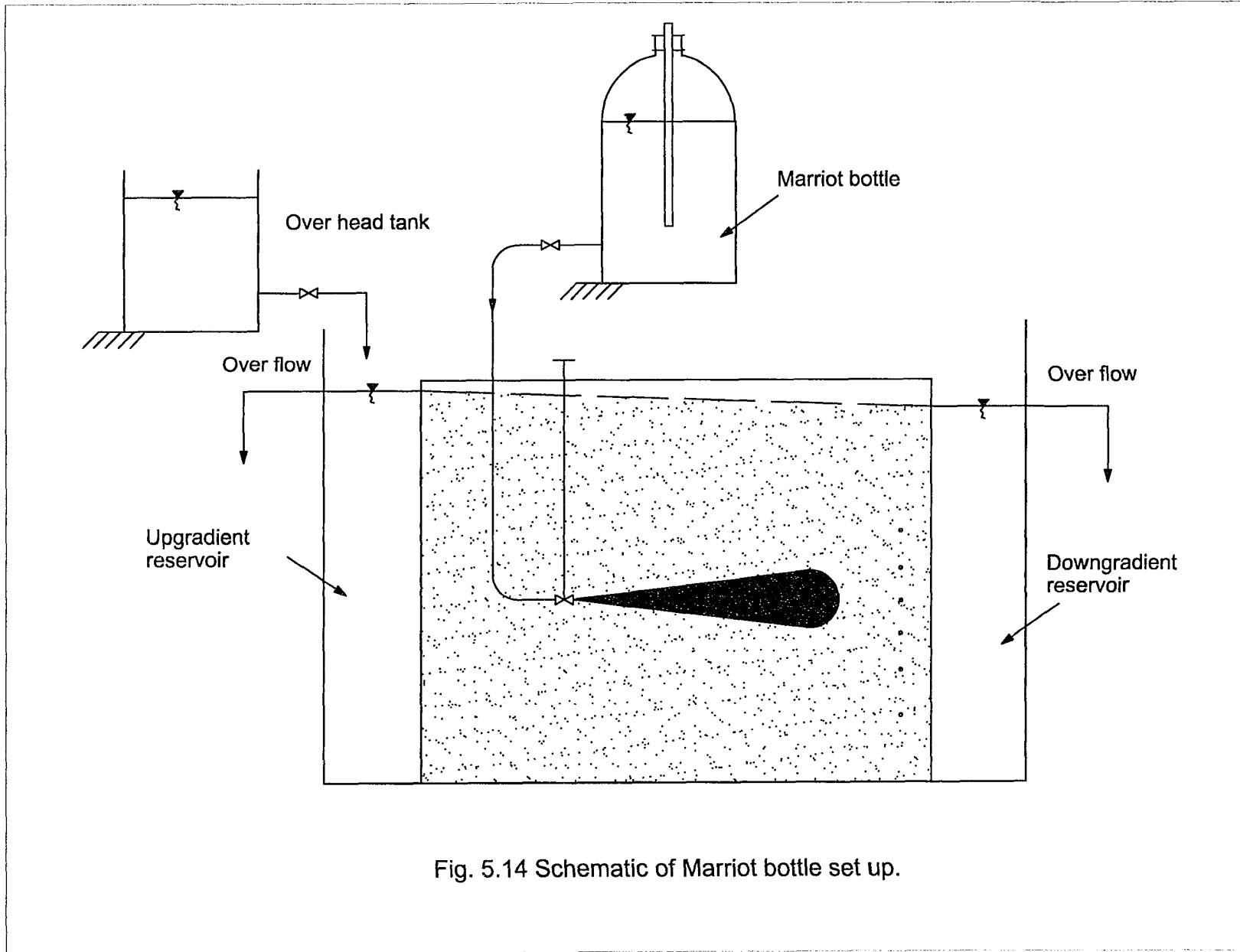


Fig. 5.14 Schematic of Marriot bottle set up.

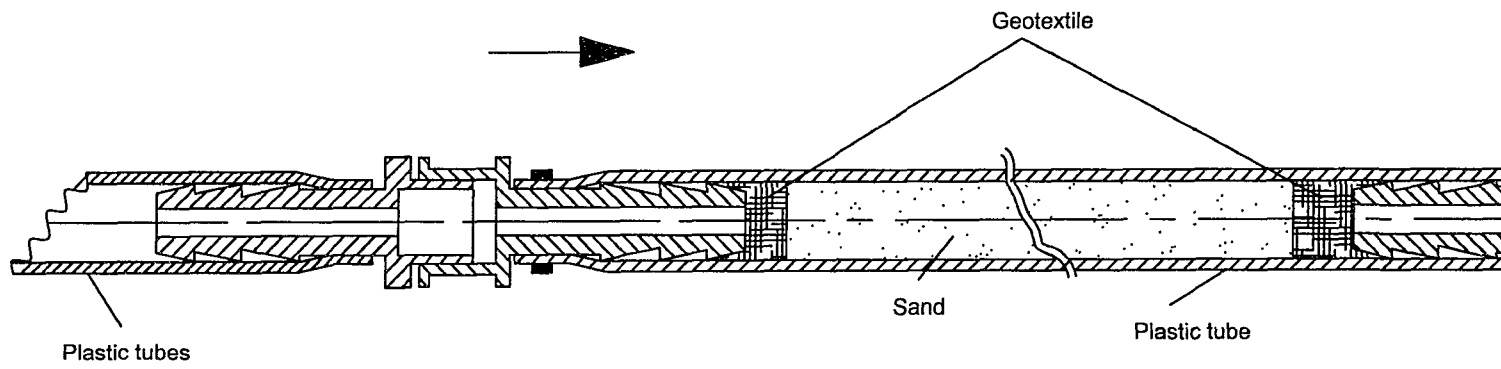


Fig. 5.15, Dye flow restriction for the continuous point source experiment

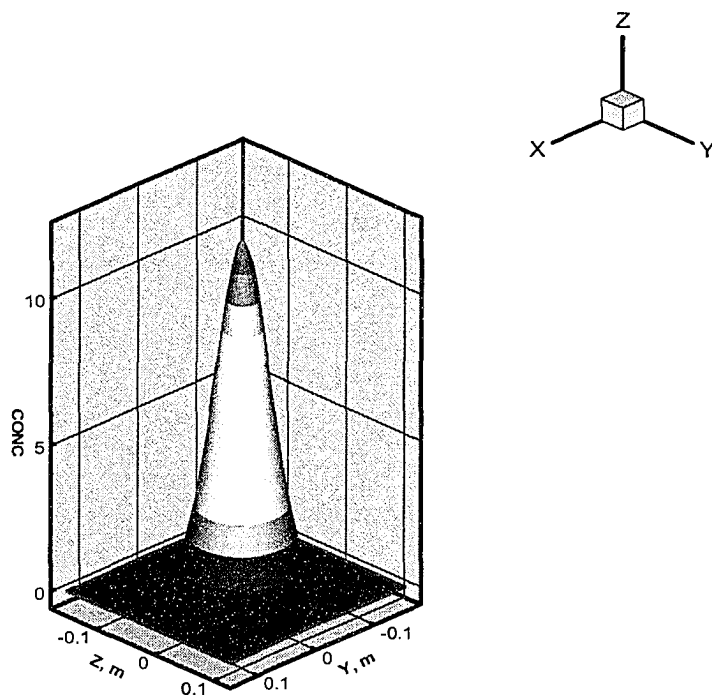


Fig. 5.16 Continuous point source analytical solution.

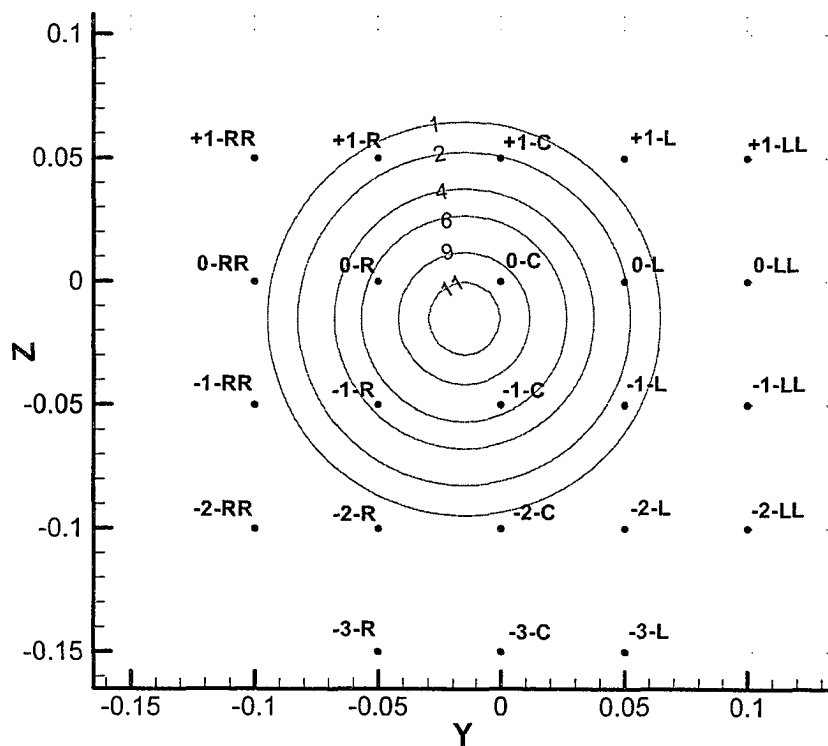


Fig. 5.17 Concentration contours at the measuring ports.

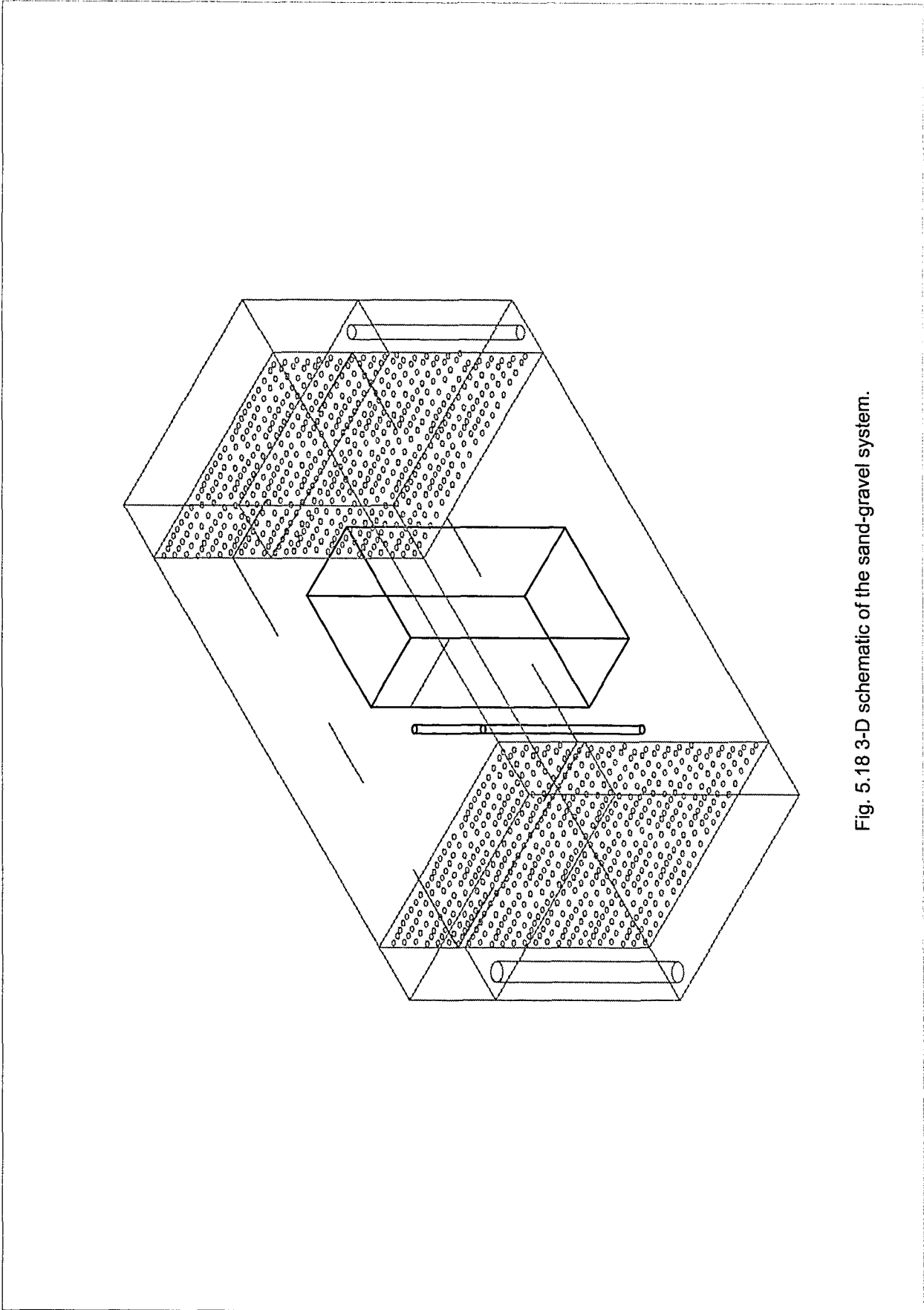


Fig. 5.18 3-D schematic of the sand-gravel system.

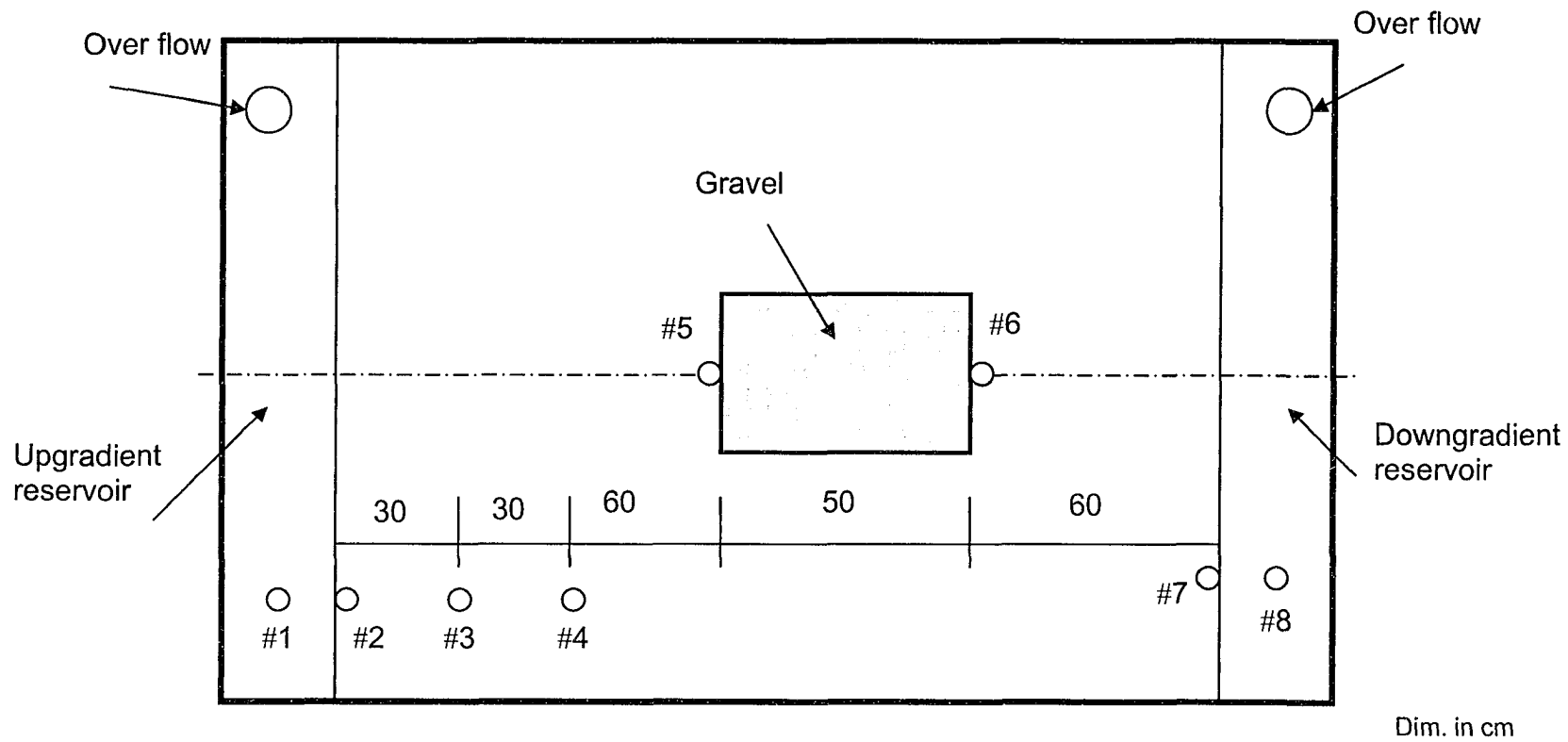


Fig. 5.19 Location of the manometers.

## CHAPTER 6

### NUMERICAL INVESTIGATIONS OF THE EXPERIMENTAL WORK

#### 6.1 General.

As indicated in the previous chapter, the only way to assess the significance of violating the continuum hypothesis on our ability to describe such systems would be through experimentation in which the only source of possible deviation between experimentation and simulation may be attributed to this violation and not to other unaccounted factors. Hence, it was quite important to eliminate, as much as possible, all other sources of uncertainty. Potential sources of uncertainty in this system include the presence of local heterogeneity during experimental setup. All efforts have been made to minimize this and other sources as indicated previously. In brief, experiment wise, it is believed that the setups maintain such criteria. Unfortunately, other sources of errors may also be introduced, but this time not because of uncertainties in the experimental setup; rather they are due to the numerical formulation used to model this system. Simulating the instantaneous line source in the sand experiment, as described in chapter 5, has shown great discrepancy when using upstream weighting finite element or finite difference compared with MOC and TVD. Additional dispersion was introduced when modeling the system using upstream weighting finite difference or finite element schemes. These discrepancies, as will be described later, represent a characteristic to these methods when solving hyperbolic or nearly hyperbolic partial differential equations. In fact, this

highlighted the importance of taking care in choosing the proper numerical technique. It does not make sense to spend much effort to eliminate as much as possible any source of errors in the experimental setup when the numerical technique itself introduces significant errors due to inherent characteristics of the numerical formulation when solving the partial differential equations used in this work. The next section describes the main source of errors when using finite element or finite difference techniques in solving solute transport equations for this system. It is believed that these introductory sections may be important to highlight some of the limitations of certain numerical techniques when dealing with problems associated with this work.

## 6.2 Numerical Difficulties.

Partial differential equations (PDEs) may be classified as linear and nonlinear. However, it is also important for the purpose of providing computational solutions to know that there are other classes of PDEs as well. This classification is related to the physics from which the PDEs arise and it entails the appropriate numerical method that may be adapted to each class.

Consider the following second-order PDE of two independent variables:

$$a \frac{\partial^2 f(x, y)}{\partial x^2} + b \frac{\partial^2 f(x, y)}{\partial x \partial y} + c \frac{\partial^2 f(x, y)}{\partial y^2} + d \frac{\partial f(x, y)}{\partial x} + e \frac{\partial f(x, y)}{\partial y} = F(x, y) \quad (6.1)$$

It may be classified on the basis of the quantity  $(b^2 - 4ac)$ , into three types based upon the conic sections of the same name to:

$b^2 - 4ac > 0$           hyperbolic

$b^2 - 4ac = 0$           parabolic

$b^2 - 4ac < 0$           elliptic

Examples of hyperbolic, parabolic, and elliptic equations are the wave equation, the diffusion equation, and Laplace's equation, respectively. The appropriate numerical solution for each of these equation types may be quite different. Elliptic equations produce stationary and energy-minimizing solutions, parabolic equations produce a smooth-spreading flow of an initial disturbance, and hyperbolic equations produce a propagating disturbance.

Transport of incompressible, passive solutes in homogeneous porous media is described by a second-order, linear partial differential equation of parabolic nature of the form:

$$\frac{\partial c}{\partial t} + \mathbf{v} \cdot \nabla c = D \nabla^2 c \quad (6.2)$$

where  $c$  is solute concentration,  $\mathbf{v}$  is the seepage velocity vector, and  $D$  is the dispersion coefficient.

This equation describes two mechanisms involved in the movement of solute in a homogeneous porous medium domain. The advection mechanism, described by the term involving the dot product of the velocity vector and the concentration gradient vector, and the dispersion mechanism described by the

term involving dispersion coefficient and the Laplacian of concentration. When dispersion is very small the movement of solute becomes largely due to advection and the above equation may be reduced to

$$\frac{\partial c}{\partial t} + \mathbf{v} \cdot \nabla c = 0 \quad (6.3)$$

which is now of hyperbolic nature. There are special difficulties associated with solving this class of equations that are not seen elsewhere and must be dealt with carefully in developing numerical methods. A brief description on the characteristics of hyperbolic PDE's is given in the next section.

### 6.2.1 Hyperbolic first-order equations.

For the sake of describing some of the analytic prospective associated with this class of equations; consider the relatively more general case of first order quasi-linear equations which may be written as:

$$a(x, y, U) \frac{\partial U}{\partial x} + b(x, y, U) \frac{\partial U}{\partial y} = c \quad (6.4)$$

where a, b and c are in general functions of  $x$ ,  $y$ , and  $U$  but not of  $\partial U / \partial x$  and  $\partial U / \partial y$ , i.e. the first-order derivatives occur only to the first degree although the equation need not be linear in  $U$ . Such an equation is said to be quasi-linear, Smith (1985). For this equation, there is a certain direction in the domain of definition of the function through which the above mentioned equation may be reduced to an ordinary differential equation at each point in the domain. This

direction is defined by the equation  $ady - bdx = 0$  and the solution is given by  $cdx - adU = 0$ . These equations may further be written in the form

$$\frac{dx}{a} = \frac{dy}{b} = \frac{dU}{c} \quad (6.5)$$

When  $c = 0$ ,  $U$  is constant along the characteristic and hence the solution may be described, for the case when  $a=1$ , as

$$U(x, y) = U_0(x - by) \quad (6.6)$$

From which one can conclude that, whereas (6.4) appears to make sense only if  $U$  is differentiable, (6.6) requires no differentiability of  $U_0$ .

### 6.2.2 Propagation of discontinuities in first order equations.

Consider the equation

$$\frac{\partial U}{\partial x} + \frac{\partial U}{\partial y} = 0, \quad y \geq 0, \quad -\infty < x < \infty,$$

where  $U$  is known at points  $P(x_p, 0)$  on the  $x$ -axis, Fig. 6.1. The characteristic direction is given by  $dx = dy$  and along the characteristics,  $dU = 0$ . Hence the characteristic through  $P$  is the line  $y = x - x_p$ .

Smith (1985) stated that "when the initial values are discontinuous at a particular point, then the solution is discontinuous along the characteristic curve. Moreover, the effect of this initial discontinuity does not diminish as we move

away. This will also occur if there are discontinuities in the initial derivatives, that is the solution is continuous along the characteristic but the initial discontinuities in the partial derivatives are propagated undiminished along the characteristic. With parabolic and elliptic differential equations the effect of an initial discontinuity is quite different as it tends to be localized and to diminish fairly rapidly with distance from the point of discontinuity”.

### **6.3 Discontinuities and Numerical Methods.**

As has been discussed earlier, discontinuity in the initial data of a first-order hyperbolic PDE is propagated across the solution domain along the characteristics from the point of discontinuity. This situation is expected to cause troubles to numerical techniques due to the fact that a consistent numerical formalization to such kind of equations means that the numerical solution converges to the analytical one as the size of the mesh approaches zero. We should not expect this to happen when there is discontinuity due to the fact that the derivative is not even defined where discontinuities exist and hence the partial differential equation itself may not be defined at such points. Applying finite difference or finite element to this problem has shown the discontinuity to be smeared as time propagates. To illustrate this point, we shall focus on finite difference methods.

#### **6.3.1 Discontinuities and finite difference methods.**

For the sake of illustration let us consider the one-dimensional advection problem described by:

$$\frac{\partial c}{\partial t} + v \frac{\partial c}{\partial x} = 0 \quad (6.7)$$

If the velocity,  $v$ , is independent of the concentration,  $c$ , this equation is a linear, first-order partial differential equation for which a wide variety of methods can be devised by using finite difference approximations. A few possibilities are listed in Table 6.1, along with their stencils.

Table 6.1 Possible difference presentation of the first order hyperbolic PDE (LeVeque 1992).

Name	Difference Equations	Stencil
Backward Euler	$c_j^{n+1} = c_j^n - \frac{\Delta t}{2\Delta x} v(c_{j+1}^{n+1} - c_{j-1}^{n+1})$	
Upstream weighting	$c_j^{n+1} = c_j^n - \frac{\Delta t}{\Delta x} v(c_j^n - c_{j-1}^n)$	
Forward weighting	$c_j^{n+1} = c_j^n - \frac{\Delta t}{\Delta x} v(c_{j+1}^n - c_j^n)$	
Lax-Friedrichs	$c_j^{n+1} = \frac{1}{2}(c_{j-1}^n + c_{j+1}^n) - \frac{\Delta t}{2\Delta x} v(c_{j+1}^n - c_{j-1}^n)$	
Lax-Wendroff	$c_j^{n+1} = c_j^n - \frac{\Delta t}{2\Delta x} v(c_{j+1}^n - c_{j-1}^n) + \frac{\Delta t^2}{2\Delta x^2} v^2 (c_{j+1}^n - 2c_j^n + c_{j-1}^n)$	

First of all, one should not expect that any of the above mentioned schemes would ever absolutely converge to the actual analytical solution in

cases when an initial discontinuity in the function or its first derivative exists. This is because the differential equation itself is not even defined at the point of discontinuity and hence other methods need to be devised. It is hoped, however, that a closer behavior be obtained by refining the mesh in space and time. Some of the above mentioned methods show erroneous behavior even in case of smooth initial data. For example, the forward in time forward in space scheme results in no convergent solution at all. For the other methods, a major problem exists related to the consistency between the original differential equation and the difference scheme approximating it. That is, for a difference scheme to be consistent, it should result in the original differential equation as the grid size diminishes. A useful technique to test the consistency of a given finite difference scheme is through the modified equation. Next section illustrates briefly this technique.

#### **6.4 Modified Equations and Consistency.**

Warming and Hyett (1974) introduced the concept of the modified equations during their investigation of the various finite difference schemes proposed to solve the same type of equations. They were trying to give an answer to questions like: are they all the same? Their idea was to model the difference equation by a differential equation. This might be confusing in the sense that the difference equation was originally derived by approximating a PDE, and so we can view the original PDE as a model for the difference equation, but there are other differential equations that are better models. In

other words, there are other PDEs that the numerical method solves more accurately than the original PDE. LeVeque (1992) stated that “it may seem strange to approximate the difference equation by a PDE. The difference equation was introduced in the first place because it is easier to solve than the PDE. This is true if one wants to generate numerical approximations, but on the other hand it is often easier to predict the qualitative behavior of a PDE than of a system of difference equations. At the moment it is the qualitative behavior of the numerical methods that one wishes to understand”. Good descriptions of the theory and the use of modified equations can be found in Warming and Hyett (1974) or Hedstrom (1975). Their method in the derivation of the modified equations is closely related to the calculation of the local truncation error for a given method. Consider Lax-Friedrichs, for example, the truncation error was found to be,  $o(\Delta t)$ . However, if  $c(x, t)$  was taken to be the solution of the PDE,

$$\frac{\partial c}{\partial t} + v \frac{\partial c}{\partial x} + \left( \frac{\Delta t}{2} \frac{\partial^2 c}{\partial t^2} - \frac{\Delta x^2}{2\Delta t} \frac{\partial^2 c}{\partial x^2} \right) = 0 \quad (6.8)$$

then the truncation error based on Lax-Friedrichs would be  $o(\Delta t^2)$ . Thus it may be concluded that the Lax-Friedrichs method produces a second-order accurate approximation to the solution of equation (6.8). This equation is called a modified equation for the Lax-Friedrichs method (LeVeque, 1992).

If  $\frac{\partial^2 c}{\partial t^2}$  is expressed in terms of x-derivatives, one obtains an equation that

is easier to analyze. It turns out that (6.8) may be written as

$$\frac{\partial c}{\partial t} + v \frac{\partial c}{\partial x} = \frac{\Delta x^2}{2\Delta t} \left( 1 - \frac{\Delta t^2}{\Delta x^2} v^2 \right) \frac{\partial^2 c}{\partial x^2} \quad (6.9)$$

This equation is conditionally consistent in the sense that  $\Delta t$  should be in the order of  $(\Delta x^{2-r})$  (i.e.  $\Delta t = o(\Delta x^{2-r})$ ) where  $0 < r < 2$  for equation 6.9 to converge to equation 6.7 (Chattot 2002).

The modified equation for the upstream method can be derived similarly and is found to be

$$\frac{\partial c}{\partial t} + v \frac{\partial c}{\partial x} = \frac{\Delta x}{2} v \left( 1 - \frac{\Delta t}{\Delta x} v \right) \frac{\partial^2 c}{\partial x^2} \quad (6.10)$$

which is unconditionally consistent (Chattot 2002). This implies that equation 6.10 converge to the solution of equation 6.10 as  $\Delta x, \Delta t \rightarrow 0$  independently.

For a finite  $\Delta x$  and  $\Delta t$ , equations (6.9) and (6.10) represent advection-dispersion type of equations which are different than the original equation, (6.7). The artificial dispersion coefficient for the Lax-Friedrichs modified equation may be written as:

$$D = \frac{\Delta x^2}{2\Delta t} \left( 1 - \frac{\Delta t^2}{\Delta x^2} v^2 \right) \quad (6.11)$$

whereas for the upstream weighting may be written as:

$$D = \frac{\Delta x}{2} v \left( 1 - \frac{\Delta t}{\Delta x} v \right) \quad (6.12)$$

This discussion indicates that the finite difference scheme approximates not equation (6.7); rather it approximates an equation of the form

$$\frac{\partial c}{\partial t} + v \frac{\partial c}{\partial x} = D \frac{\partial^2 c}{\partial x^2} \quad (6.13)$$

In other words, the numerical scheme introduces dispersion into the physical phenomena that do not, in fact, exist in real situations. It may also be noted that for a given  $\Delta t / \Delta x$ , say one, we have  $D_{up} / D_{Lax} = v / (1 + v)$ , so one can expect upstream weighting to be less dispersive than Lax-Friedrichs. To minimize numerical dispersion in upstream weighting, one needs to make  $\Delta x$  and consequently  $\Delta t$  very small provided that stability is maintained.

### 6.5 Stability.

The numerical scheme must satisfy other conditions besides consistency before one can conclude that it is convergent. The important property that is required is stability. The concept of stability requires the definition of what is called the “norm” and the basic idea is to study the behavior of this norm as time evolves. A difference scheme is stable when its norm is bounded in some sense. Stability analysis may impose certain restrictions on the grid size (in space and time) before it may be concluded that the scheme is stable. Different kinds of norms may be defined. They, generally, are not all equivalent in the sense that a

scheme may be stable in one norm while unstable in the other. To introduce this concept, Strikwerda (1989) stated that, a finite difference scheme  $L_{\Delta t, \Delta x} u_m^n = 0$  (where  $L_{\Delta t, \Delta x}$  stands for the difference operator associated with the differential operator,  $L = \partial / \partial t + v \partial / \partial x$ ) is stable if there exist  $J$  and positive numbers  $\Delta x_0, \Delta t_0$  such that for any time  $t$ , there is a constant  $A_t$  such that

$$\Delta x \sum_{m=-\infty}^{\infty} |u_m^n|^2 \leq A_t \Delta x \sum_{j=0}^J \sum_{m=-\infty}^{\infty} |u_m^j|^2 \quad (6.14)$$

for  $0 < n\Delta t < t$ ,  $0 < \Delta x \leq \Delta x_0$  and  $0 < \Delta t \leq \Delta t_0$ .

It is to be noted that an expression of the form  $\|w\|_{\Delta x} = \left( \Delta x \sum_{m=-\infty}^{\infty} |w_m|^2 \right)^{1/2}$  for any grid function,  $w$ , is called the  $L^2$  norm. With this notation the inequality (6.14) can be written as

$$\|u^n\|_{\Delta x} \leq \left( A_t \Delta x \sum_{j=0}^J \|u^j\|_{\Delta x}^2 \right)^{1/2} \quad (6.15)$$

which is equivalent to

$$\|u^n\|_{\Delta x} \leq A_t^* \Delta x \sum_{j=0}^J \|u^j\|_{\Delta x} \quad (6.16)$$

for some constant  $A_t^*$ . Inequalities (6.15) and (6.16) express the idea that the norm of the solution at any time  $t$  is limited in the amount of growth that can occur. The growth is at most a constant multiple of the sum of the norms of the

solution on the first  $J+1$  steps. To demonstrate whether or not the estimate given by equation (6.14) holds for a particular scheme can be quite formidable unless one uses methods from Fourier analysis.

### 6.6 The CFL Condition.

Courant, Friedrichs, and Lewy (1967) used finite difference methods as an analytic tool for proving the existence of solutions of certain PDEs. In the course of proving convergence of this sequence, they recognized that the domain of dependence of the finite difference method should include the domain of dependence of the PDE in the limit as  $\Delta t, \Delta x \rightarrow 0$ . As illustrated in Fig. 6.2, this condition implies that point  $R$  should always be between  $Q$  and  $T$  as  $\Delta t$  and  $\Delta x$  become smaller and smaller. As a general principle, for hyperbolic PDEs, Courant number is best selected close to the stability limit (i.e., close to one) to keep the dispersion small (Strikwerda 1989).

In conclusion, since the measured dispersivities in sand were very small, it is expected that numerical dispersion would be a major problem when using finite difference or finite element schemes. If these methods were to be used a very fine mesh would be needed which would create memory problems. Figure 6.3 shows comparison between upstream finite difference, MOC, and TVD methods (accompanied with MT3DMS package) based on a 1 mm square mesh. It is clear from this figure that upstream finite difference produces larger dispersion as compared with MOC and TVD methods, which showed identical results. MOC, on the other hand, uses the Lagrangian description when modeling the advection

term and the Eulerian description when modeling the dispersion term. So it is presumably free from numerical dispersion. Hence, it has showed reasonable agreement with measurements even with the 1 mm square mesh. The third order Total Variation Dimensioning Methods, TVD, (in MT3DMS) supplemented with a universal flux limiting procedure to minimize oscillations, which may occur if sharp concentration fronts are involved, was also used. This method evolved in an attempt to overcome problems related to obtaining convergence analysis by requiring that the total variation of the solution be nonincreasing with time.

### **6.7 Experimental Results and Numerical Simulations.**

As has been discussed in chapter 4, six sand-gravel setups were constructed to test the significance of violating the continuum hypothesis. A base scenario, where the continuum hypothesis is believed to be satisfied, was first performed and simulated. This scenario represents the set up when the gravel layer spans a transverse width of 50 cm. The other experiments were then followed by changing the transverse width of the gravel layer. Data for solute transport were compared with those calculated using MT3DMS. Two main difficulties appeared during comparisons, the first was that the plume in some setups appeared to be shifted to the right or left of the center line due to some unavioded experimental imperfections and/or due to inherent characteristics of the experiment as will be explained in the following sections. The plume was readjusted to the center when it was appropriate to do so or otherwise left with an explanation of its behavior. The second was that the solute sometimes reached

the measuring points with some slight difference in arrival time than expected. For example, it may reach points further to the right or left slightly faster than at the center, which is probably due to slight inhomogeneity in the hydraulic conductivity field, a matter that is common in the study of porous media phenomena. Adjustment of the arrival time was also made when it was appropriate. The experiments were duplicated to build confidence in the data. In each duplicate the setup was built from scratch. Data of the multiple runs are contained in Appendix B. The following section describes a typical experiment and its corresponding numerical simulation for each scenario.

#### **6.7.1 The base scenario (gravel width 50 cm).**

In this scenario the gravel zone spanned a width of 50 cm. Dye was injected approximately 30 cm upgradient of the gravel in the centerline of the box and samples were collected 30 cm downgradient of the gravel zone. Hydraulic heads were measured using manometers located at eight points as described in chapter 5. The measurements are collected in Appendix B. This scenario was modeled using Visual Modflow for flow and both MOC and TVD for solute transport, which show similar results. Half of the domain was modeled because of the existence of a plane of symmetry. A uniform grid 1 x 1 mm was constructed. The region of the domain in which no solute transport was taking place was deactivated, Fig. 6.4, to minimize memory usage and accelerate the solution. The model allocated approximately 1.4 GB of the total memory and the 25 hour simulation was completed in approximately 20 hours.

### **6.7.1.1 Hydraulic heads.**

The sand average hydraulic conductivity was calculated based on measurements of the total flow rate and the hydraulic gradient measured by the first two manometers that were 30 cm apart and located closest to the upgradient reservoir. At this location, equipotential lines are not impacted by the gravel system as will be shown subsequently. The average hydraulic conductivity was found to be approximately  $9 \times 10^{-5}$  m/s, which was the same value estimated during the experiments to determine the sand properties. The hydraulic conductivity of the gravel used in the model was that measured in the gravel box, (0.28 m/s). Figure 6.5 shows the hydraulic head distribution calculated by the model. The experimental data are superimposed on the graph and show good agreement. One may notice that the existence of the gravel zone has deflected equipotential lines such that flow will preferentially move through the gravel zone. Moreover, the equipotential lines within the first 30 cm of the upgradient reservoir are perpendicular to the primary flow direction which validates the assumption of using the head drop in this region to estimate the sand average hydraulic conductivity. Figure 6.6 depicts the simulated flow lines for this system. It shows that approximately 70% of the upgradient flow is drawn towards the gravel zone.

### **6.7.1.2 Solute transport.**

This scenario was modeled using both MOC and TVD methods. Both methods show comparable results. The values of dispersivities used for both gravel and sand were those values measured in the large boxes. Figures 6.7-9

show the simulated concentrations contours at different times. Figure 6.10 represents the simulated concentrations with time at the experimental observation points located 30 cm downgradient of the gravel zone. Figure 6.11 represents the measured concentrations with time at the measuring ports superimposed with that simulated at the center of the plume. Generally, good agreement is observed. Figure 6.12 shows comparisons at the lateral cross section (30 cm downgradient the gravel zone) after 27.9 hours. This figure reveals that the plume was shifted approximately 3 cm to the left. Figure 6.13 shows the profile after adjusting the plume to the center. Figures 6.14-17 show comparisons of measured and calculated concentrations at different times. Good agreement is observed. This in fact, builds confidence in the assumption of validity of the continuum hypothesis for the 50 cm scenario.

### **6.7.2 The 30 cm scenario.**

In this scenario the gravel zone was 30 cm in width centered in the sand box, approximately 120 cm from the upgradient reservoir. The dye was injected, as in the previous set up; approximately 30 cm ahead of the gravel and samples were collected 30 cm downgradient. The system was modeled using both MOC and TVD methods with the same grid used in the previous scenario.

#### **6.7.2.1 Hydraulic heads.**

The sand average hydraulic conductivity estimated using the measured head drop in the first 30 cm of the box and the measured overall flow rate was

found to be  $9.5 \times 10^{-5}$  m/s. The macroscopic hydraulic conductivity of the gravel measured in the box (0.28 m/s) was used for simulation. Figure 6.18 shows the distribution of equipotential lines superimposed with the measuring points. Good agreement was generally obtained. One also may notice that the gravel zone has diverted equipotential lines to allow for the flow to move towards the path of less resistance. Figure 6.19 depicts the simulated flow lines for this system. It also shows that approximately 60% of the flow is drawn into the gravel zone.

#### **6.7.2.2 Solute transport.**

For this scenario extra sampling points were inserted to capture the plume for a total of 11 ports at each level. The location of the sampling ports is shown in Fig. 6.20. Figures 6.20-22 show the simulated concentration contours after 15, 20 and 30 hours, respectively. Figure 6.21 indicates that the simulated plume widens as it exits of the gravel zone. This may be attributed to the fact that flow lines diverge at the exit of the gravel zone. Figure 6.23 shows the simulated concentration profiles at different times, 30 cm downgradient the gravel zone. On comparing measured and simulated concentration profiles at this section, Figs. 6.24-28, large differences may be noticed to the degree that makes comparisons irrelevant. The simulated plume is centered at the centerline (Fig. 6.23), and the measured plume is not at all centered. Note, the measured concentrations are connected based on our interpretation as to the most likely distribution of the dye and are named fitted on the figures. The observation that the plume is off centre may be explained by the suspected channeling of the flow at the sand-gravel

interface where the resistance to flow may be lower. A set of measurements were also taken at the entrance, mid and exit of the gravel to confirm channeling. Data are collected in Appendix B. Moreover, one may also notice that the plume was moving faster in one branch (the right hand side) than the other one which indicated that the resistance in this particular path was relatively less than in the other one. On the other hand, while simulation may indicate that the largest concentration would be at the centerline, in reality, if one measured only at centerline, lower than expected concentrations may result and one might falsely attribute this to higher dispersion coefficient in the gravel.

This experiment reveals the fact that channeling is an important factor for such systems at this scale, as will be supported in the experimental data for the following setups. At this scale when the system begins to violate the second length scale constraint, the effect of the boundary on the behavior of the system is pronounced. No match was observed between measured and simulated concentrations at the downgradient measuring points. However, had we measured the concentrations further downgradient, we may have generated a better match as a greater travel time may have allowed greater averaging (dispersion) to occur across the width of the plume. In other words, the mismatch between measurements and simulation for this system may be pronounced because the measurements were taken within close proximity of the zone where the second length scale constraint may be violated. Furthermore, had the characteristic length of the gravel zone in the direction of the flow been longer, a better match may have resulted as greater dispersion may have occurred

outward from the zone of channeling causing the solute to mix across the gravel zone.

It may also be noted that the measured maximum concentration was comparable to the calculated one. In natural systems, on the other hand, it is unlikely to find such an abrupt change in properties as there is a natural tendency for gradation at the interface and this channeling may not exist or is at least minimized. In this case no significant error is expected to be found in simulating this system assuming the macroscopic measured parameters. This conclusion is based on the fact that, even with the existence of channeling, experiments have shown no significant difference upon comparing the peak downgradient concentrations. For man made systems, careful considerations need to be taken to assess whether or not channeling may be a significant factor. Figure 6.29 illustrates the simulated concentration history at the measuring ports.

### **6.7.3 The 20 cm scenario.**

In this scenario, a 20 cm in wide gravel zone was inserted in sand as previously described. The system was modeled using Visual Modflow for flow and both MOC and TVD methods for transport with the same grid used in the previous scenarios.

#### **6.7.3.1 Hydraulic heads.**

The estimated hydraulic conductivity of the sand using the measured head drop in the first 30 cm of the box was found to be  $1.0 \times 10^{-4}$  m/s. The hydraulic

conductivity of the gravel used in the model was initially set to the value that was measured in the gravel box (0.28 m/s); however, the calculated and measured plume travel time did not match. Hence the hydraulic conductivity of the gravel was adjusted in a series of runs until a good match was achieved. The value of gravel hydraulic conductivity that best approximated the travel time was 0.24 m/s. The adjusted hydraulic conductivity is approximately 86% of the value measured in the large box experiment. This is an insignificant change in the sense that it may be of the order of the uncertainty in the measured sand average hydraulic conductivity or in the estimated specified head boundary conditions. Figure 6.30 shows equipotential lines distribution superimposed with the measuring points. Good agreement was generally obtained. One also may notice that the gravel zone has diverted equipotential lines to allow for the flow to move towards the path of less resistance. Figure 6.31 depicts the simulated flow lines for this system. It shows that approximately 46% of the flow is drawn into the gravel zone.

#### **6.7.3.2 Solute transport.**

Figures 6.32-35 show the simulated plume's concentration contour lines after 12, 15, 20 and 25 hours, respectively. Figure 6.33 shows that the plume widens as it exits the gravel zone. This may be attributed to the fact that flow lines diverge beginning of the second half of the gravel zone. Again, on comparing measured and calculated concentration profiles at the downgradient section where the measuring ports exist, Figs. 6.36-39, large differences may be

noticed. That is while the calculated plume is centered at the centerline, the measured plume is not at all centered. To the contrary, the highest concentration was measured away from the center towards the right side. This may be explained, again, as due to channeling of the flow at the sand-gravel interface where the resistance is lower. Moreover, in this scenario, the whole plume appears to be shifted towards the right hand side, which may indicate that the initial source (initial condition) was slightly shifted towards the right hand side.

Once again, this experiment reveals the fact that channeling is an important factor for such systems at this scale. It may also be noted that the measured maximum concentration was slightly higher than that simulated. Had channeling not occurred, one may get a reasonable match between simulated and measured data even with the use of the measured macroscopic gravel properties. Again for man made systems, careful considerations need to be taken to assess whether or not channeling may be significant factor. Figure 6.40 shows the calculated concentration history at the center together with the measurements at the measuring ports. It is apparent from the figure that the highest concentration was shifted. It also shows that the travel time was in agreement with measurements.

#### **6.7.4 The 15 cm scenario.**

In this scenario, a 15 cm wide gravel zone was inserted in sand as previously described. The system was modeled using Visual Modflow for flow

and both MOC and TVD methods for transport with the same grid as used in the previous scenarios.

#### **6.7.4.1 Hydraulic heads.**

The estimated hydraulic conductivity of the sand using the measured head drop in the first 30 cm of the box was found to be  $1.0 \times 10^{-4}$  m/s. To match the travel time, the macroscopic hydraulic conductivity of the gravel needed to be adjusted to 0.22 m/s which is approximately 79 % of the value measured in the large box experiment (0.28 m/s). Again this is assumed to be an insignificant change in the sense that it may be of the order of the uncertainty in the estimated sand average hydraulic conductivity or in the measured specified head boundary conditions. Figure 6.41 shows the distribution of equipotential lines superimposed with the measuring points. Good agreement was generally obtained. Figure 6.42 depicts the simulated flow lines for this system and indicates that approximately 43% of the flow is drawn into the gravel zone.

#### **6.7.4.2 Solute transport.**

Figures 6.43-46 show the simulated concentration contours after 12, 15, 20 and 25 hours, respectively. Figure 6.43 shows that the plume widens as it exits the gravel zone. The plume in this scenario is shown to fill the whole thickness of the gravel layer at the exit. On comparing measured and simulated concentration profiles at the section where measuring ports exist (Figs. 6.47-49), the differences are not as large as compared with the previous two scenarios.

The difference for this scenario is largely attributed to the plume shift towards the left side due probably to imperfections in adjusting the initial source (slight misalignment of the well at exactly the center). Channeling is still a contributing factor, however, if this shift does not exist, the plume may equally be channeled to both sides.

Hence, this experiment reveals the fact that, channeling is an important factor for such systems at this scale. It may also be noted that the measured maximum concentration was slightly higher than that calculated. Figure 6.50 shows the calculated concentration history at the center together with the measurements at the measuring ports. It is apparent from the figure that the highest concentration was shifted. It also shows that the travel time was in conformity with measurements.

As indicated previously, one may anticipate the existence of a downgradient region in which the violation to the continuum hypothesis results in mismatch between measured and simulated data. However, further downgradient of this region a better match may be achieved as a greater time beyond the gravel layer will result in additional smoothing to the point where channeling effect is no longer evident. On the other hand, if the length of the gravel layer in the direction of the flow was longer, a better match may also have been achieved since additional dispersion within the gravel section would have to mix solute across the gravel section and reduced the impact of the channeling of the plume as it exits the gravel zone.

### **6.7.5 The 10 cm scenario.**

In this scenario, a 10 cm wide gravel zone was inserted in the sand as described earlier. The system was modeled using Visual Modflow for flow and the TVD method for transport with the same grid as discussed before in the previous scenarios. MOC demonstrated some convergence difficulties when modeling this scenario.

#### **6.7.5.1 Hydraulic heads.**

The estimated hydraulic conductivity of the sand was found to be  $1.0 \times 10^{-4}$  m/s. To match the travel time, the macroscopic hydraulic conductivity of the gravel needed to be adjusted to 0.22 m/s which is approximately 79 % of that measured in the box (0.28 m/s). Again this is assumed to be an insignificant change in the sense that it may be of the order of the uncertainty in the estimated sand average hydraulic conductivity or in the measured specified head boundary conditions. Figure 6.51 shows equipotential lines distribution superimposed with the measuring points. Good agreement was obtained. Figure 6.52 depicts the simulated flow lines for this system and illustrate that approximately 41% of the flow is drawn into the gravel zone.

#### **6.7.5.2 Solute transport.**

Figures 6.53-56 show the simulated plume's concentration contours after 12, 15, 20 and 25 hours, respectively. Figure 6.53 shows that the plume widens as it exits the gravel zone. Again, the plume in this scenario is shown to fill the

whole thickness of the gravel layer, however; this appears to occur earlier in the gravel layer for this scenario in comparison to the previous one (Fig. 6.43). For this scenario, the simulated plume exits from the sides of the gravel layer. The seepage velocities in the sand adjacent to the gravel layer are decreasing and hence the portion of the plume that exits the side of the gravel layer tends to lag the center of the plume, enhancing the “U-shape” of the plume in plan view (Figs. 6.55 and 6.56) and creates the two symmetric lagging tails to the left and right of the centerline. This will cause the plume to be two sided as it further moves downstream. On comparing measured and simulated concentration profiles at the section where measuring ports exist (Figs. 6.57-60), the difference between the measured and simulated values are not as large as those indicated previously. The differences for this scenario, as for the previous one, may largely be attributed to the plume shift towards the right side due again to imperfections in placing the initial source. Had this shift been eliminated, the plume may have been symmetric and a better match may have been achieved. Although channeling is expected to exist, the small thickness of the gravel layer may have caused the plume to mix across its width.

In situations where channeling may be eliminated, one may obtain similar profiles as that calculated even with the use of the measured macroscopic gravel properties when the length scale constraints are violated. Figure 6.61 shows the simulated concentration history with time at the measuring ports. Figure 6.62 shows the simulated concentration history at the center together with the measurements at the measuring ports. It may be noticed that the experimental

data indicated a larger longitudinal dispersion than that calculated. It is apparent from the figure that the highest concentration was shifted. It also shows that the travel time was in agreement with measurements.

As indicated previously, there may exist a downgradient zone closer to the exit of the gravel layer where the effect of violating the continuum hypothesis is more pronounced. If the measurement points are beyond this zone, a better match may be obtained. This will be discussed in greater detail in the summary of the main findings at the end of this chapter.

#### **6.7.6 The 5 cm scenario.**

In this scenario the gravel zone spanned a width of 5 cm. It was modeled using Visual Modflow for flow and TVD for solute transport. MOC shows convergence difficulties when modeling this scenario.

##### **6.7.6.1 Hydraulic heads.**

The sand average hydraulic conductivity was found to be  $9 \times 10^{-5}$  m/s based on the hydraulic gradient measured by the first two manometers located 30 cm apart. The hydraulic conductivity of the gravel was adjusted 0.2 m/s (approximately 72% of that measured in the gravel box) to meet the measured travel times. Figure 6.63 shows the hydraulic head distribution calculated by the model. The experimental data are superimposed on the graph and show good agreement. Figure 6.64 depicts the simulated flow lines for this system. It shows that approximately 38% of the flow is drawn into the gravel zone.

### **6.7.6.2 Solute transport.**

Figures 6.65-69 show the simulated concentration contours at different times. It is apparent that the plume spans the whole width of the gravel zone well in advance of exiting the gravel layer. Hence one would expect a better match with experimental data since channeling and complete mixing across this gravel zone should result in similar results downgradient of the gravel. Figure 6.70 shows comparison between the measured and simulated concentration history at the centerline. A reasonable match may be noticed, although a slightly larger longitudinal dispersion is suggested by the measured data. Figures 6.71-75 provide comparisons of measured and simulated data at different times and good agreement was observed. This good agreement is most probably due to the fact that the thickness of the gravel zone was small enough such that even with the existence of channeling, dispersion was able to bring solute to the center of the gravel layer. Based on the previous discussion, in this scenario, the measuring ports may be well beyond the hypothetical region where the violation to the continuum approach is more pronounced.

### **6.8 Summary of the Main Findings of the Experimental Work.**

As has been stated in chapter 3, from the mathematical point of view, violation to the continuum hypothesis in a region/s of a given porous medium domain will render the system unsolvable with the macroscopic equations adapted based on the assumption of the validation of the continuum approach. Unfortunately, no theoretical technique is available to solve this system other

than that adopted by Hassanizaheh and Gray as discussed earlier in chapter 3. However, their complex formulation introduced several new parameters which are difficult to determine or assess. The complexity of their approach and the difficulty in establishing the required parameters renders this approach uneconomical to almost impossible for implementation at a field scale problem. The basic question that was raised at this stage was; what if one simulates the system assuming the applicability of the continuum hypothesis in these regions and using the macroscopically determined porous medium properties? Will simulation of the system based on that assumption render a reasonable match or significant differences? This experimental work was unique to provide some of the answers to such questions and illuminate aspects related to this issue.

The main finding of this study confirms the already expected idea that using the macroscopically determined properties to model a system that violates the continuum hypothesis may result in a mismatch between simulation results and measurements. However, one may supplement the above mentioned statement with the following observations based on the results of this experimental work:

- When all length scale constraints were satisfied within the gravel layer (the 50 cm scenario) reasonable match between measurements and simulations were obtained. Although the third length scale constraint may not be satisfied in the vicinity of the interface boundaries between

the gravel and the surrounding sand for this system, it does not seem to have significantly affected the established match.

- For the experimental scenarios between 50 cm and 5 cm, the match between the simulated and experimental data varied and was a function of different processes (channeling, slight misalignment of source, slight heterogeneity, etc.) and a function of sampling location. However, the author is not confident in drawing a general rule or conclusion based on the 50 cm scenario that the second length scale constraint is met such that  $L \geq 60d$ . In other words, for different materials and interface conditions, this relationship may be different.
- It has been established through this study that when the thickness of the gravel layer was small (5 cm) such that all length scale constraints were violated, good match between experiments and simulations was achieved. This has been attributed to the fact that in both the simulations and experiments, the solute was mixed across the entire thickness of the gravel layer, though the mixing processes may be different in the two cases. This has also been attributed to the fact that the comparison of the measured and simulated concentrations was conducted at a distance of 30 cm from the downgradient edge of the gravel; a distance 6 times the width of the gravel layer. The numerical simulation showed that the flow is progressing in the gravel domain (at the centerline) and the dispersion was able to spread the plume across the thickness of the gravel layer. In the experimentation, on the other

hand, the flow may have been generally directed along the interface boundaries and dispersion may have occurred towards the center. However, at a measurement plane 30 cm downgradient of the 5 cm gravel layer, the experimental and simulated data indicate similar results. From this measurement location, the detailed processes of channeling vs. dispersion are lost as the dye migrates 30 cm to the measurement location.

- From the flow point of view and for this particular system, channeling appeared to be a significant process. That is flow is likely going to move along the interface boundaries rather than through the center of the gravel domain as predicted by the numerical model. This may result in the plume, which is transported with the flow, to also move in the vicinity of these interface boundaries and hence any measurements of the plume concentrations immediately downgradient of this region will not match a numerical simulation. To remedy this shortcoming and to correctly predict the position of the plume, one may need to assign a higher permeability envelop in this interface region to simulate channeling and to better reflect reality.
- Unfortunately, the condition of the interface is case dependent (depends on many factors like the type of the interface, the degree of compaction, the grain sizes and distributions, etc.). Hence, again no definitive statement can be made to accurately quantify the second

length scale constraint in terms of grain size. Likewise, this problem is further complicated by the measurement location (or scale).

- In natural systems where there is more gradation of properties at the interface boundaries, channeling may be minimized and the plume may move in the main domain as simulated. However, it is to say at this point that the conditions at the interface boundary need to be assessed on a case-by-case basis. This is in fact a consequence of violating the continuum hypothesis; that is the system becomes case dependent and no general conclusion may be deduced.
- Despite this fact, the hydraulic conductivity of the gravel layer as defined in this experimental work did not require significant adjustment in order to match plume arrival time.
- Moreover, and most importantly, the downgradient peak concentrations did not show large discrepancy as compared with simulation even with the existence of channeling (or the violation to the length scale constraints).
- Generally for this particular system, one may conclude that there exist transition thicknesses when the system begins to violate the continuum hypothesis. In these cases channeling is significant and large discrepancies between measurements and simulations are expected. However, as the layer thickness was further reduced (5 cm) the experimental and simulated data were in good agreement. The reason for that, as described earlier, may be attributed to the fact that in both

cases the plume filled the entire thickness of the gravel layer (although, due to two different mechanisms) and hence any downgradient measurements resulted in a good match with the numerical simulation.

Moreover, the peak downgradient concentration, even with the channeling, did not show large differences as compared with the simulation data.

- Based on the experimental work conducted in this study, one may state that there may exist a hypothetical region downgradient of the gravel zone where the impact of the violation to the continuum approach are pronounced. In this region, a poor match is expected between measurements and simulation based on the macroscopic properties of porous media in this region. Outside from this region the impacts of this violation may not be as great and a better match may be expected. The size of the region may depend on the ratio of the length of the gravel layer along the flow to the width of the gravel layer perpendicular to flow. The smaller this ratio, the larger this region may need to be and the larger this ratio, the smaller this region may need to be.

### **6.9 Implications on the TMF in Northern Saskatchewan.**

As has been indicated in the first chapter, some of the TMFs in northern Saskatchewan use the concept of the pervious surround. In chapter 3 it has been realized that there is a definite violation of the length scale constraints in the

pervious surround region of TMFs such that the continuum hypothesis may not be adapted.

The implications of violating the length scale constraints drawn from this experimental work can be discussed in the context of channeling, in the context of the sampling or observation point, and in the context of the lost detail at the microscale.

At the sand/surround interface and at the surround/rock interface, one might argue that channeling may occur. One might argue that the channeling at the sand/surround interface may be reduced due to the intermingling of soils at this interface. In any case, if one is to apply the continuum approach across these three media within the vicinity of the previous surround, the length scale constraints are violated. The second and third length scale constraints address the channeling issue. In the case of the second length scale constraint, if channeling does occur, its impacts are negligible if the domain of interest is significantly large in comparison to the width over which the channeling or interface effects occur. This is not the case for the pervious surround. In the case of the third length scale constraint, channeling will not ensure a gradual or linear change in properties across this interface and hence the third length scale constraint is violated.

As suggested earlier, one may attempt to include the impact of channeling by adding a high permeability zone at this interface, however, it is difficult to estimate the flow and transport parameters needed to represent the interface and

the applicability of the continuum approach across this interface is not valid. If one ignores the channeling and applies the continuum approach, the result may be the adjustment of the macroscopic porous media parameters to indirectly account for the impact of the channeling. How to adjust the parameters is not clear and hence a parametric study or sensitivity analysis, as conducted in chapter 2, becomes an important exercise to address this uncertainty. In the end, one should likely consider the worst case or conservative scenario when assigning properties and simulating such systems.

The observation point is also important. If one is calibrating a numerical model based on samples collected from within the pervious surround, this may not be an appropriate approach since the continuum approach is violated in this region. However, if one is calibrating a numerical model based on samples collected at a sufficient distance downgradient of the TMF, the detailed processes occurring in the vicinity of the surround become averaged and accounted for in the adjusted or estimated macroscopic properties (e.g. dispersion). Hence, if one is interested in the loading to a downgradient lake, the calibrated model should be effective in estimating this provided the correct parameters are adjusted in the calibration. Hence, from a compliance approach, if one is evaluating the impacts at a location significantly downgradient of the TMF, one could use the continuum approach and consider the worst case or conservative scenario. However, the details related to processes occurring in the immediate vicinity of the pervious surround may be lost and not accurately simulated.

This relates to the last point raised earlier, the lost detail at the microscale. If one is evaluating the downgradient concentrations and mass flux of a conservative substance, it is assumed that the source term is reasonably well understood and the parameter adjustments made during model calibration account for transport processes occurring in the vicinity of the surround. Note that for the conservative tracer considered in this study, the processes are limited to advection, dispersion and diffusion to address the mixing in this area. If one is considering a more complex scenario with a reactive species and a variable or uncertain source term that may be impacted by mixing etc., the details are lost. If one is looking at the mixing of the tailings porewater with the natural groundwater drawn into the pervious surround (i.e., possibility of complex redox conditions with nonlinear rates of reactions), this detail is important as it may impact the mobility and transport processes for certain contaminants (e.g., arsenic). In this case, model calibration through the adjustment of a greater number of parameters to match data collected at a downgradient receptor, generates greater concerns related to one's confidence in their model predictions and the impacts of violating the continuum approach. Attempting to simulate the processes occurring in the vicinity of the pervious surround and comparing these with measured values from samples collected in this region would be inappropriate given the violation to the continuum approach and the concepts upon which the length scale constraints are formulated.

It is also important to note that important to note that in dealing with the more complex field scenario, there may be a large degree of uncertainty in the

soil parameters, variability in the layer thicknesses, and several heterogeneities that can not be quantified. Hence, the errors associated with violating the length scale constraints when modeling this system may only represent a small fraction of the errors or uncertainties related to the overall problem. This reinforces the recommendation that a worse case or conservative scenario be considered when evaluating such a system.

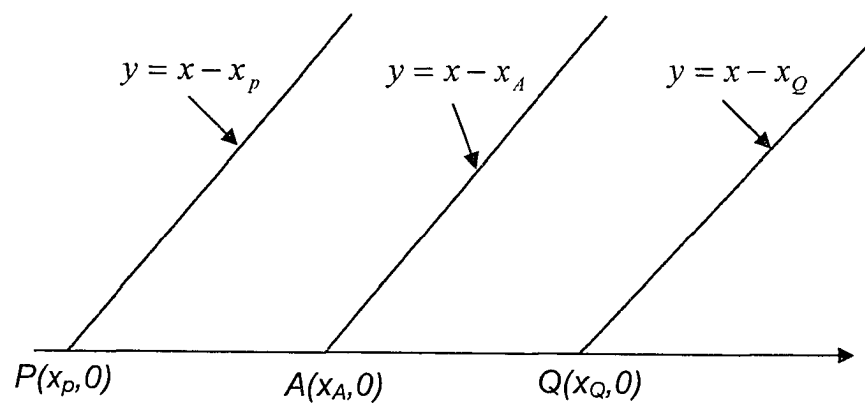


Fig. 6.1 Propagation of discontinuity along characteristics.

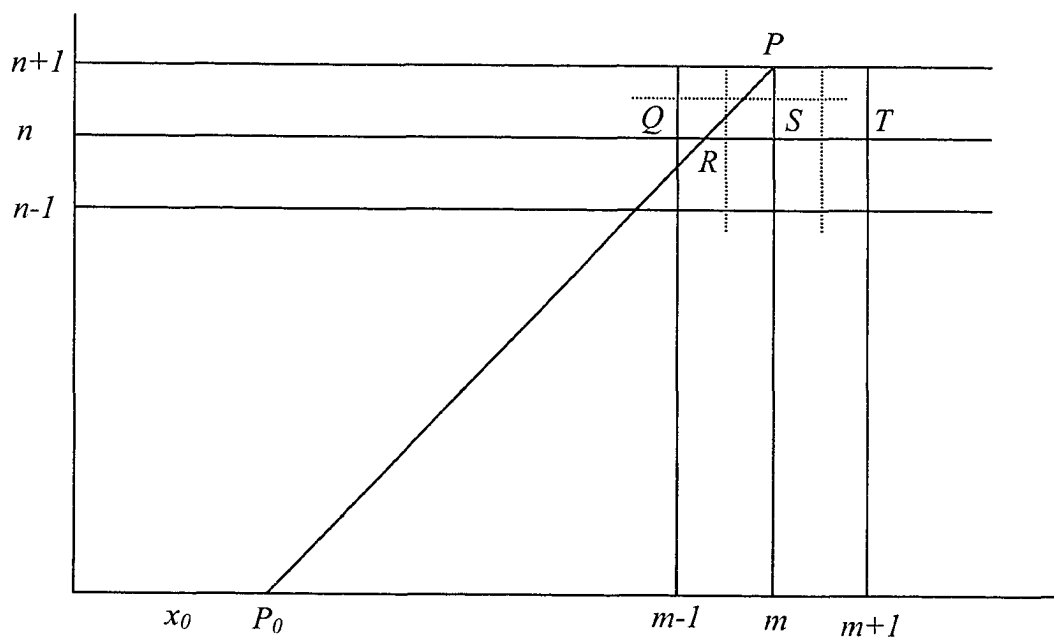


Fig. 6.2 Illustration of CFL criterion.

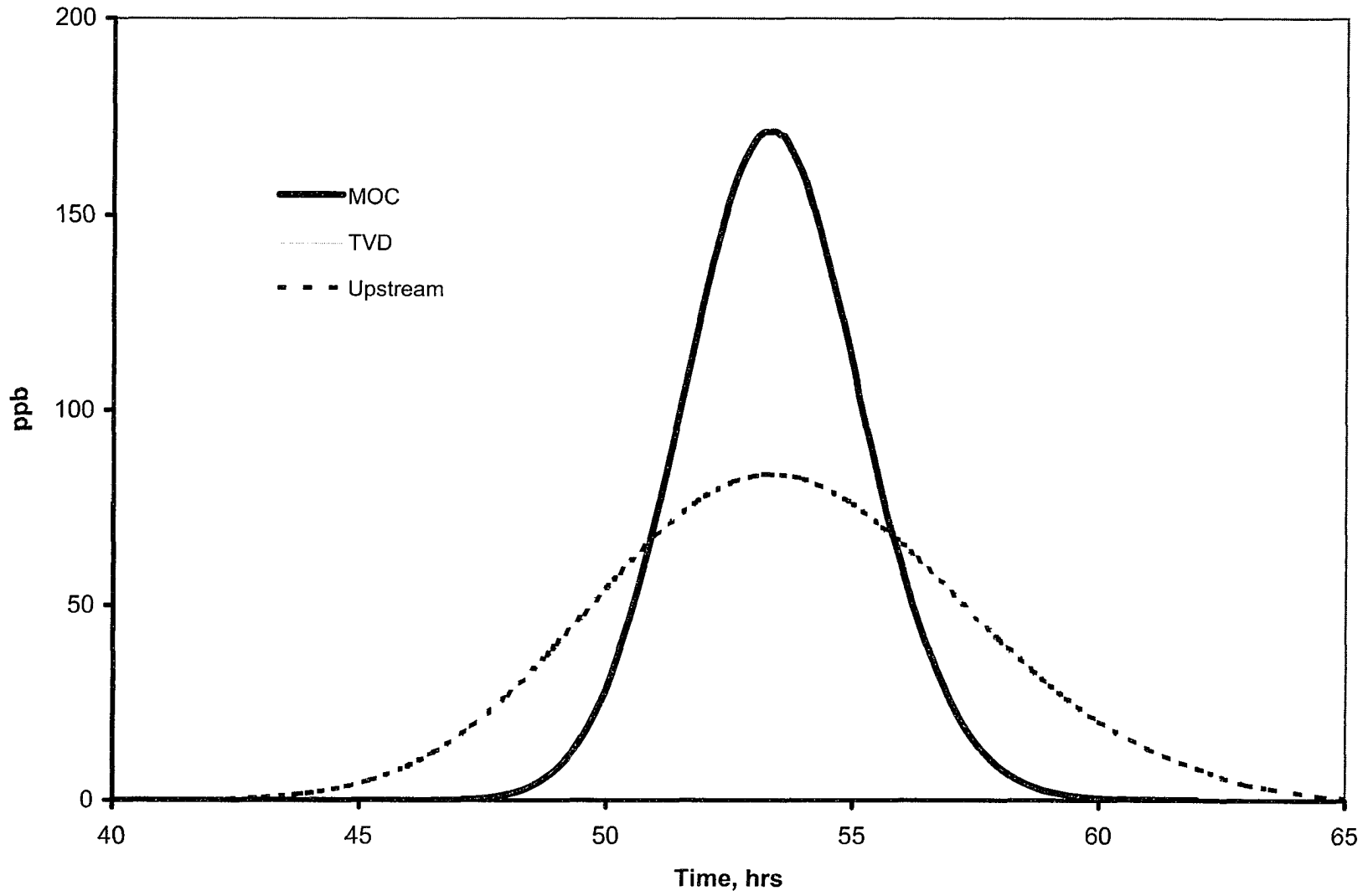


Fig. 6.3 Comparison of simulated concentration history downgradient using different numerical techniques.

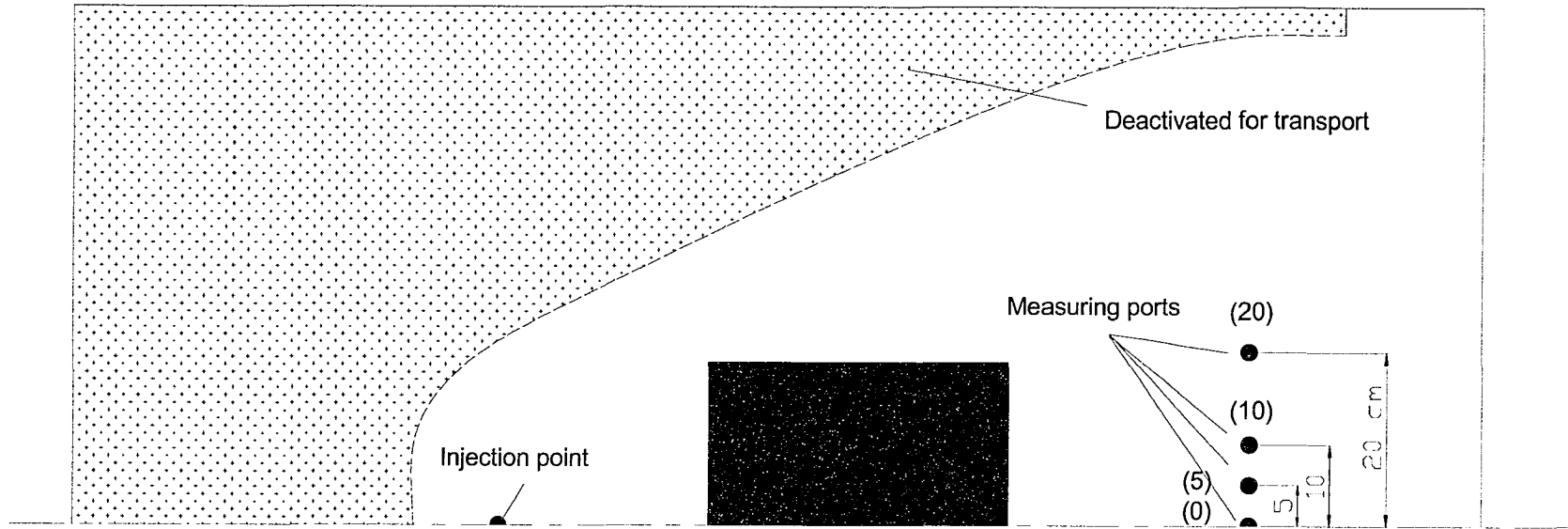


Fig. 6.4 Deactivated region for solute transport for numerical runs.

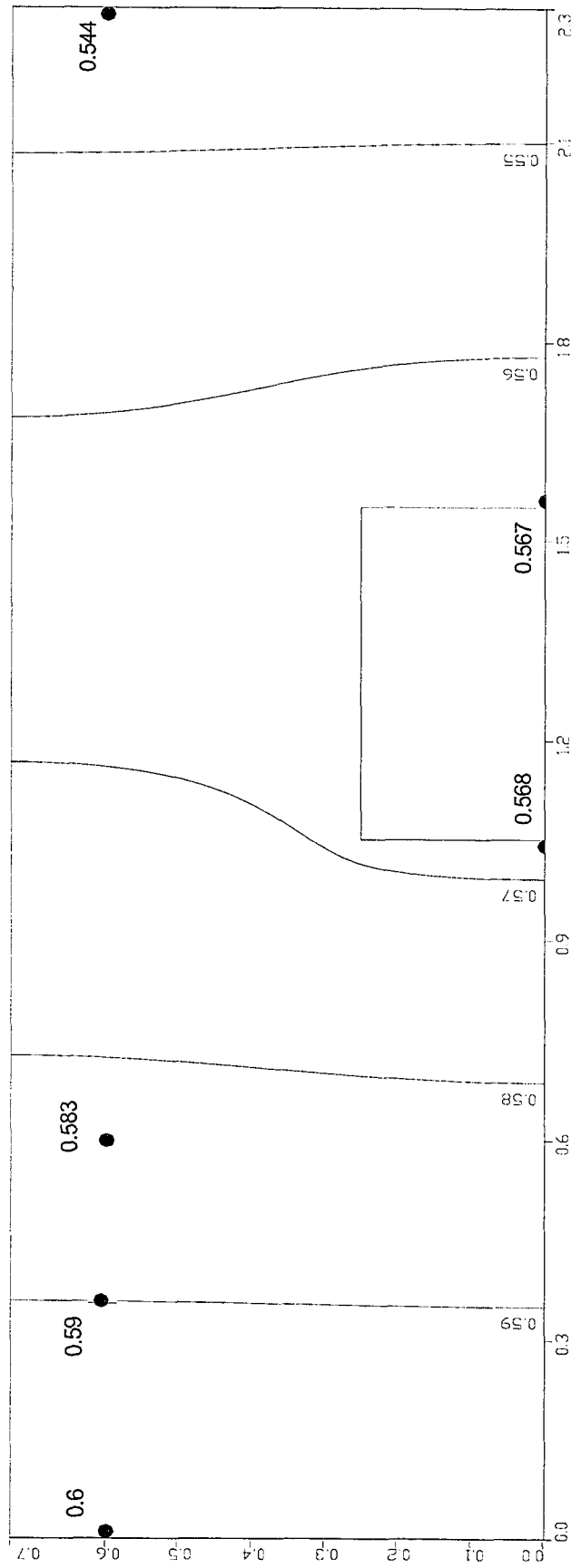


Fig. 6.5 Hydraulic heads distribution for the 50 cm sand-gravel system.

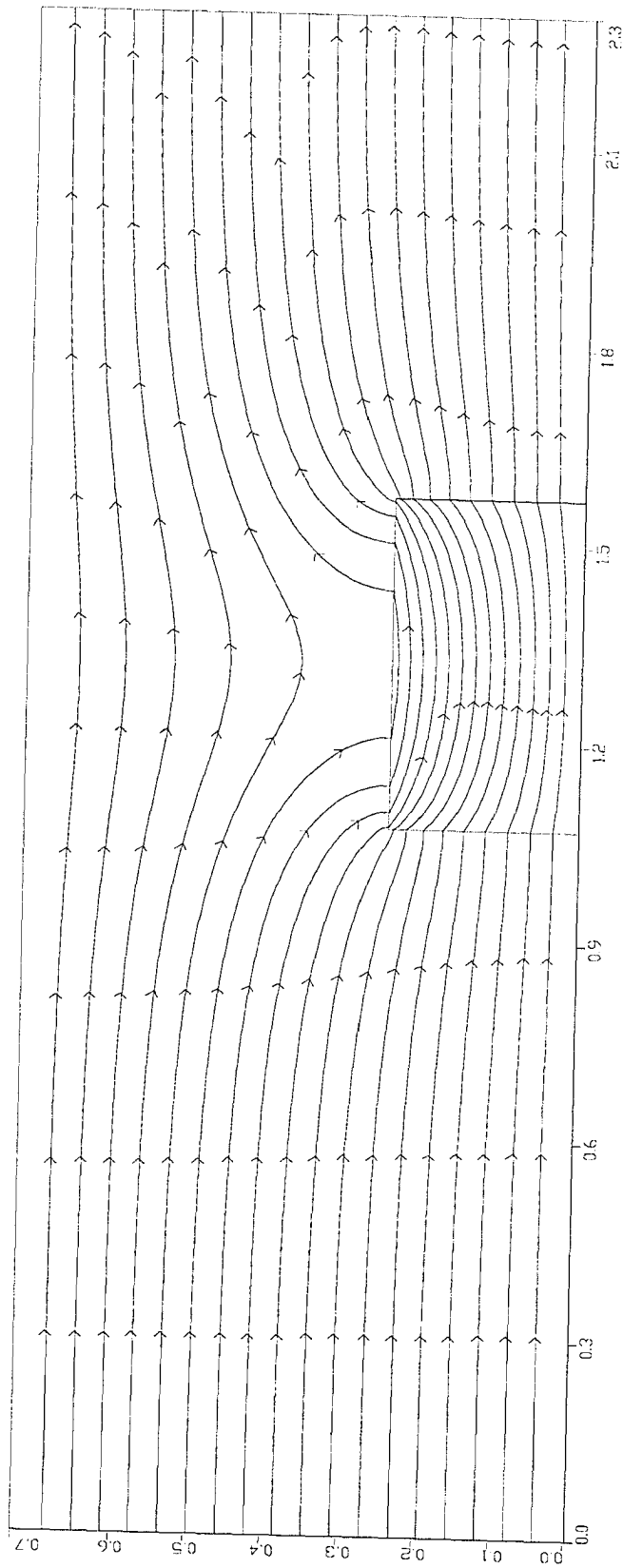


Fig. 6.6 Simulated flow lines for the 50 cm sand-gravel system.

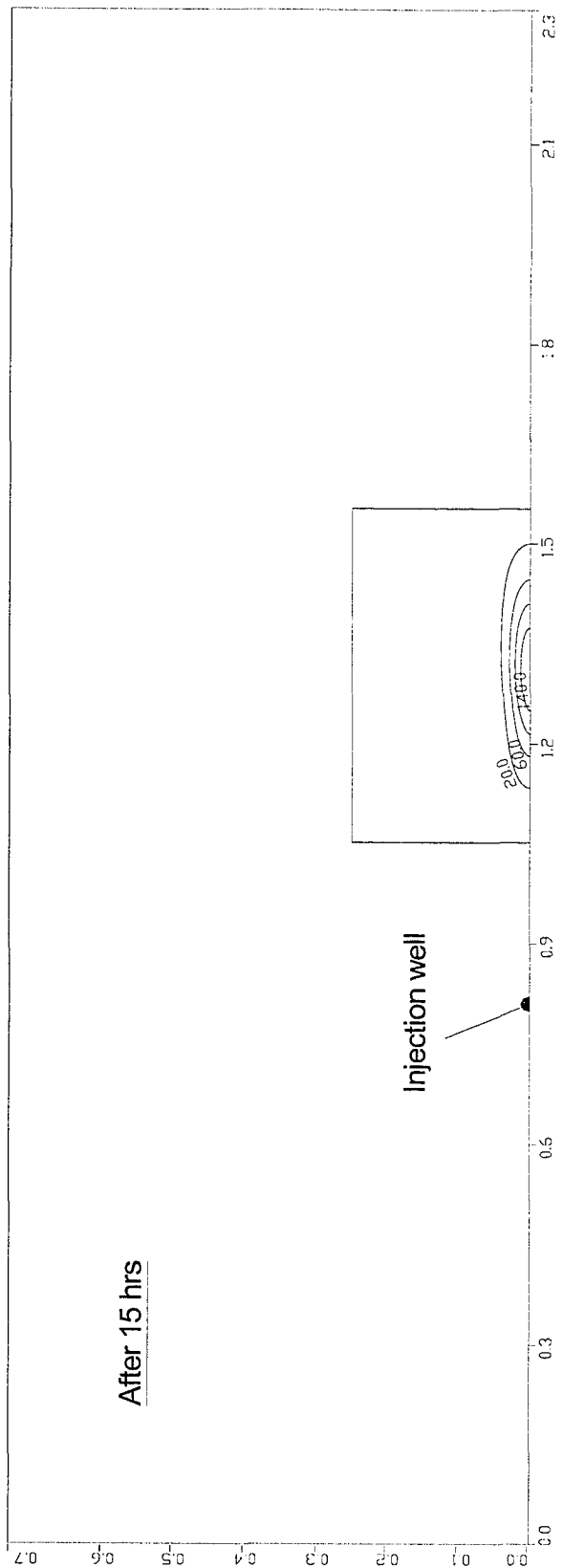


Fig. 6.7 Plume contours for the 50 cm sand-gravel system after 15 hrs.

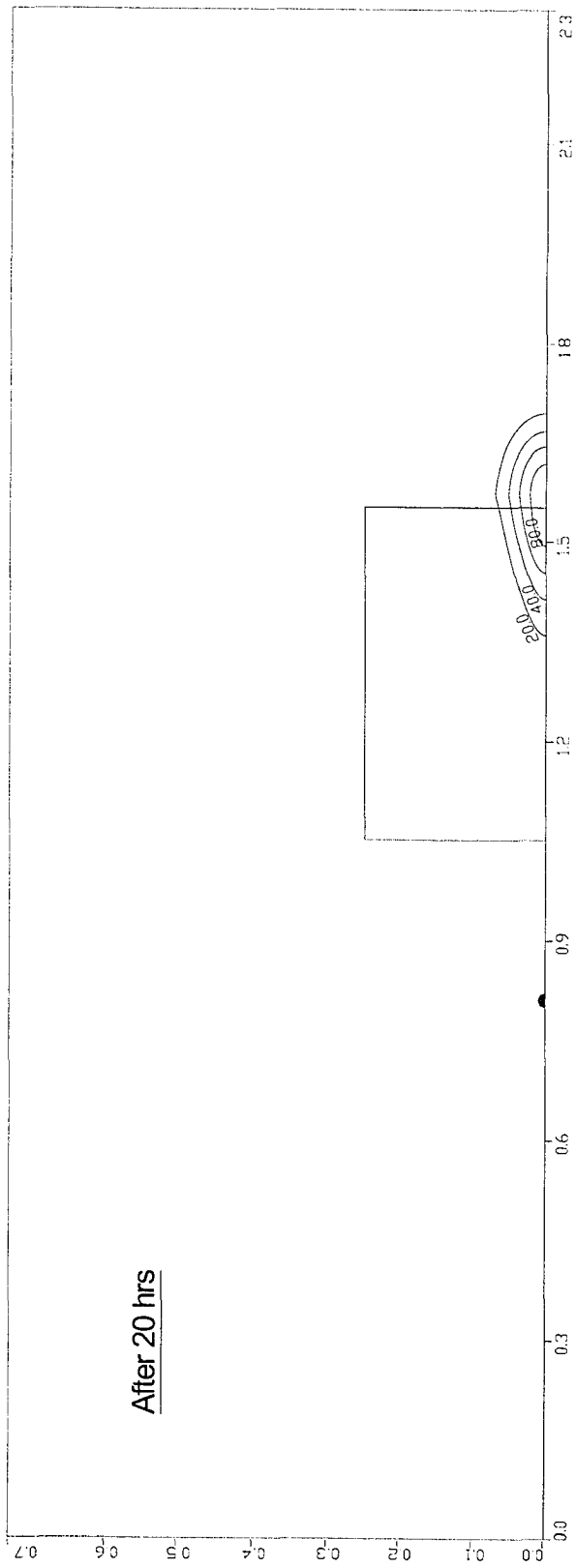


Fig. 6.8 Plume contours for the 50 cm sand-gravel system after 20 hrs.

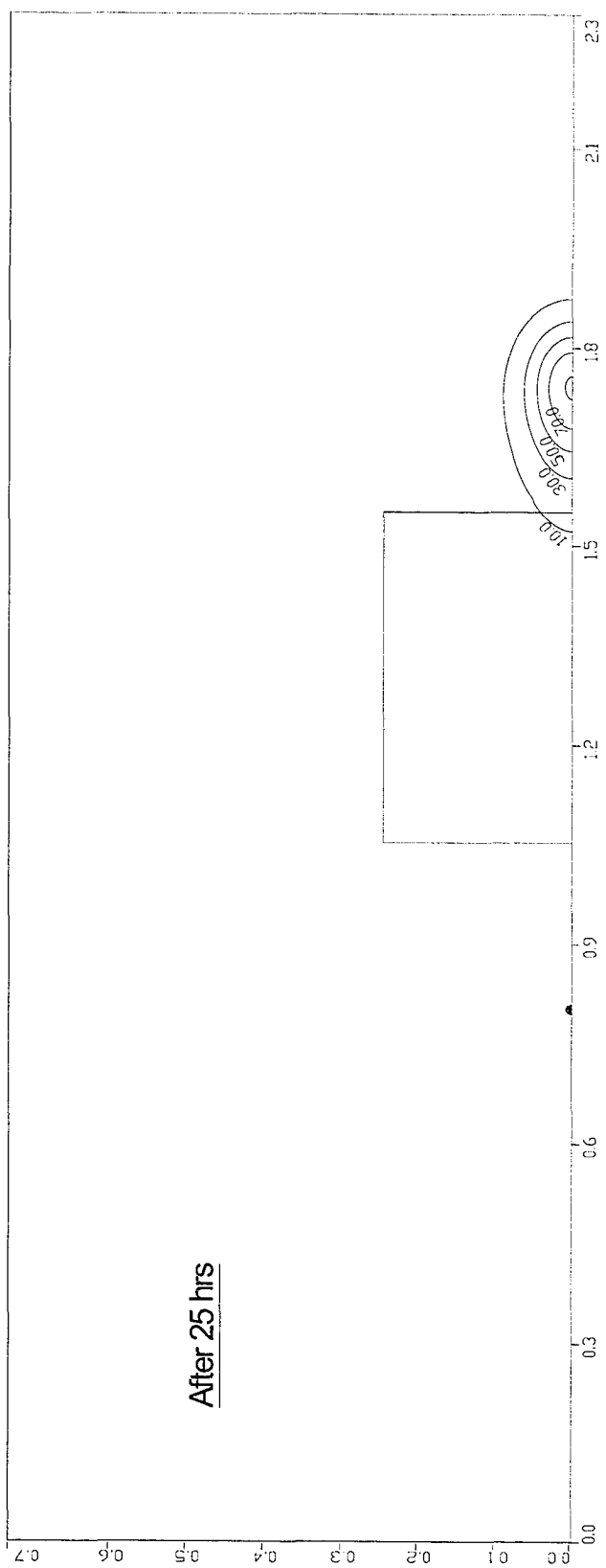


Fig. 6.9 Plume contours for the 50 cm sand-gravel system after 25 hrs.

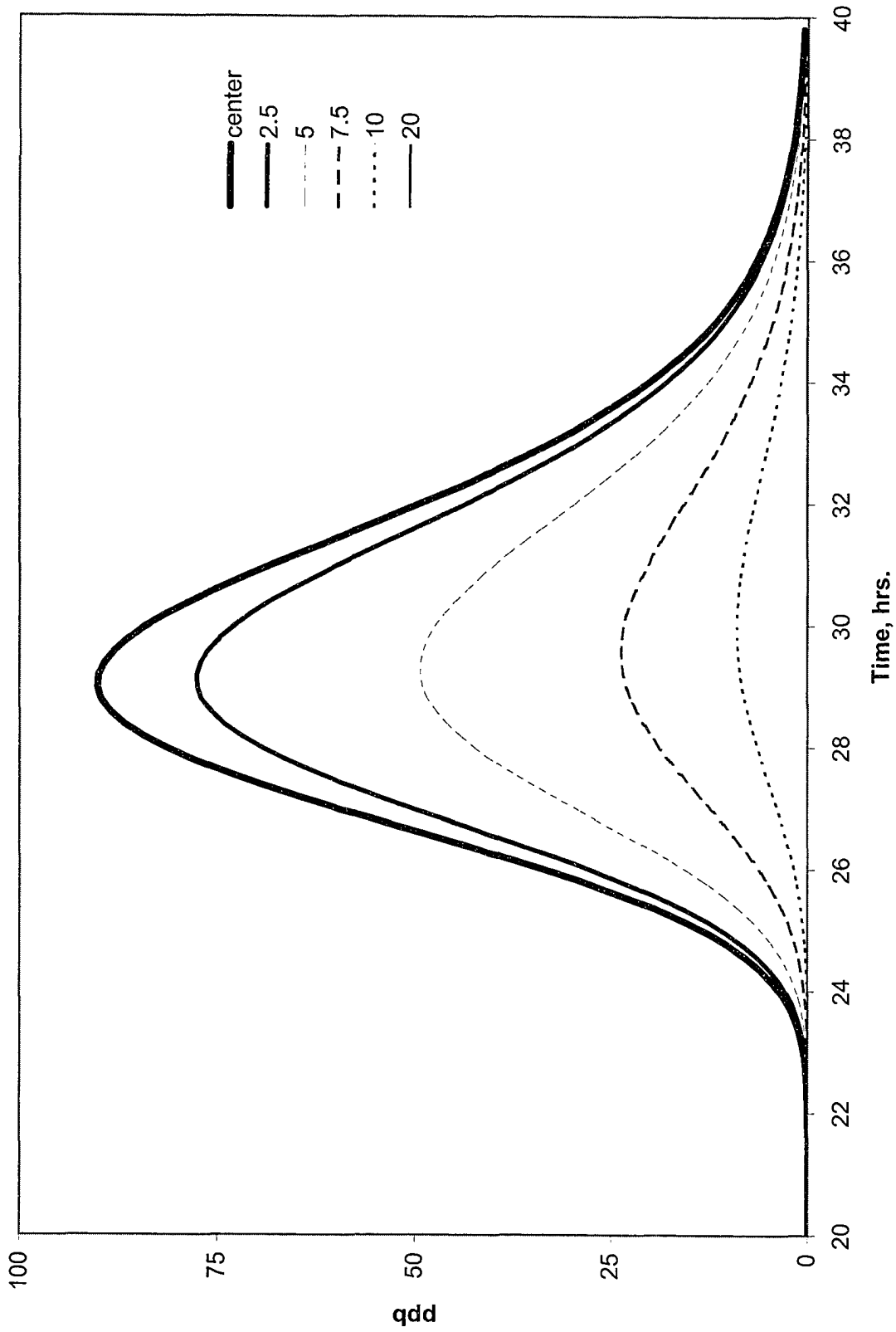


Fig. 6.10 Simulated concentration profiles with time at different measuring points.

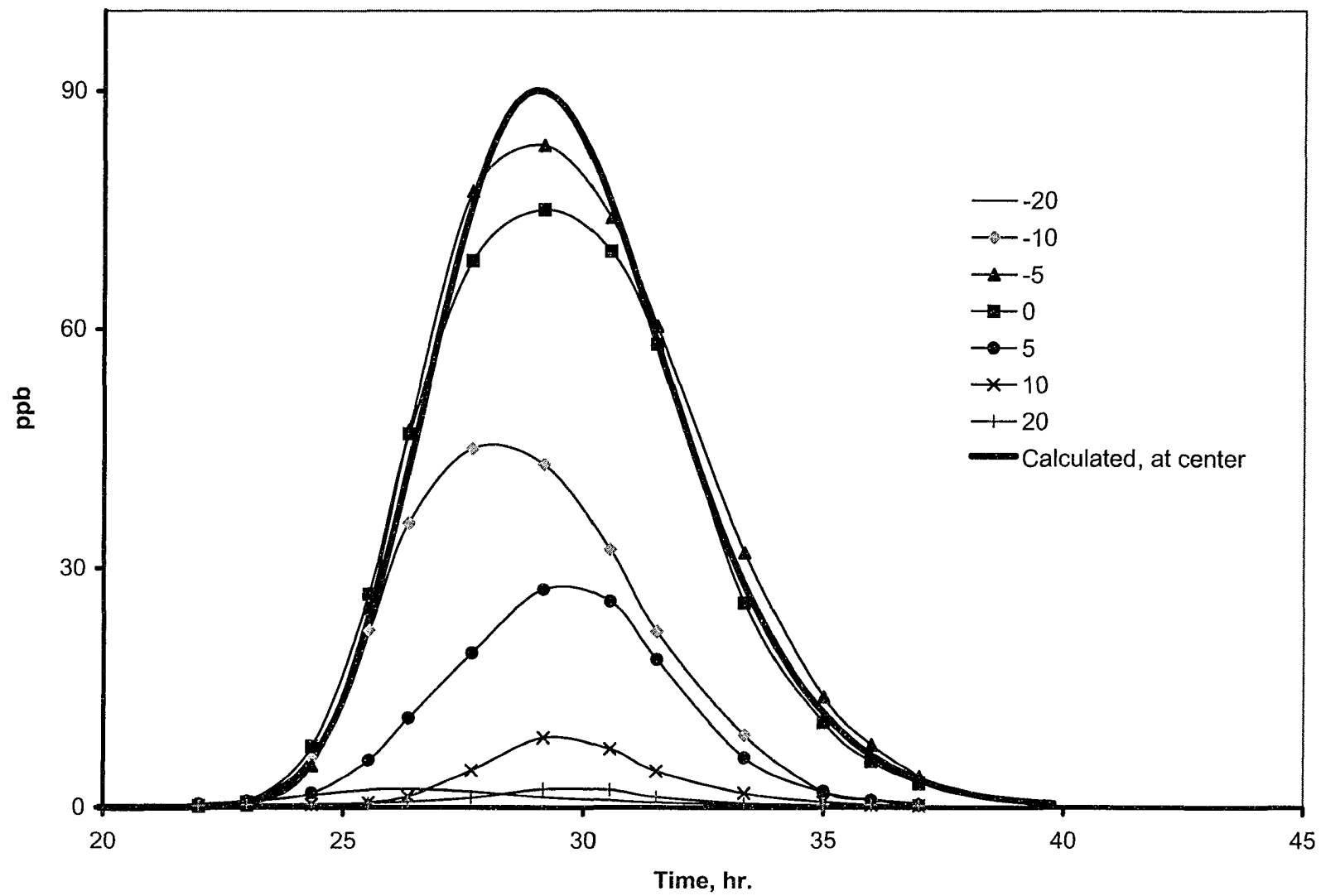


Fig. 6.11 Concentration profiles with time at different measuring points with the calculated at the center.

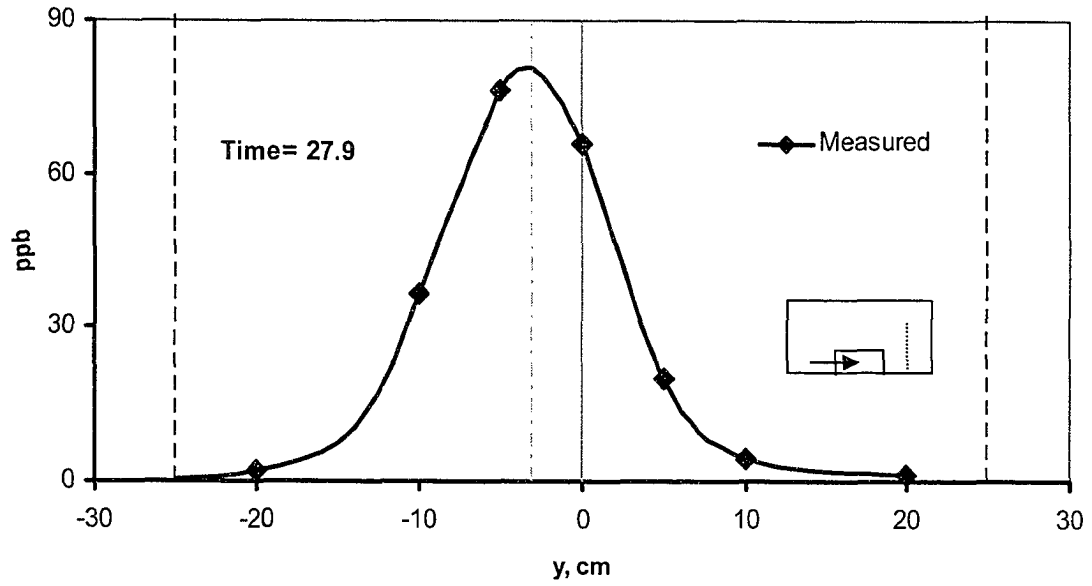


Fig. 6.12 Traverse concentration profile shows the plume is sifted to the left.

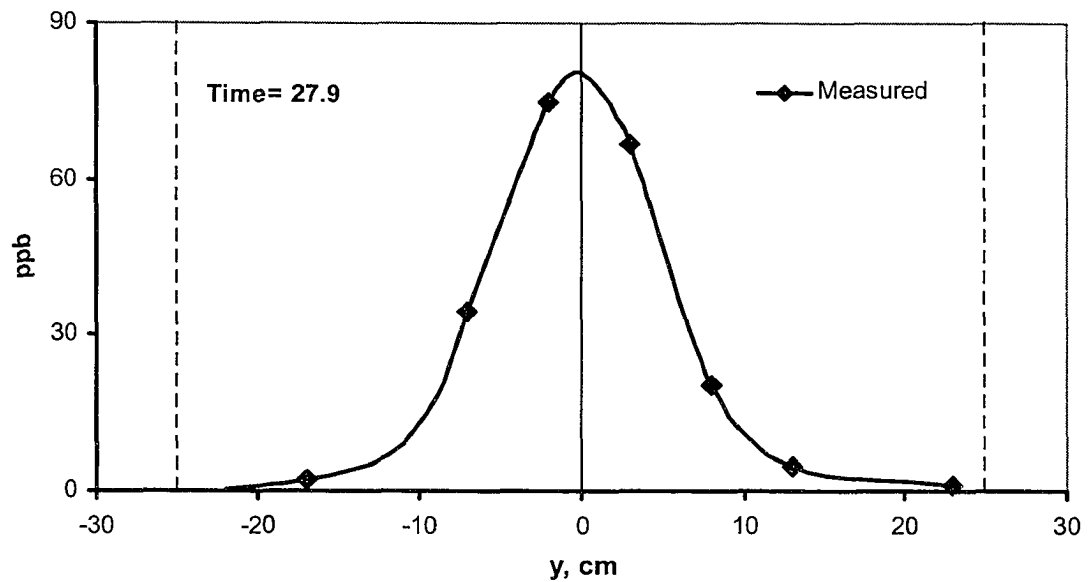


Fig. 6.13 Traverse concentration profile with plume adjusted to the center.

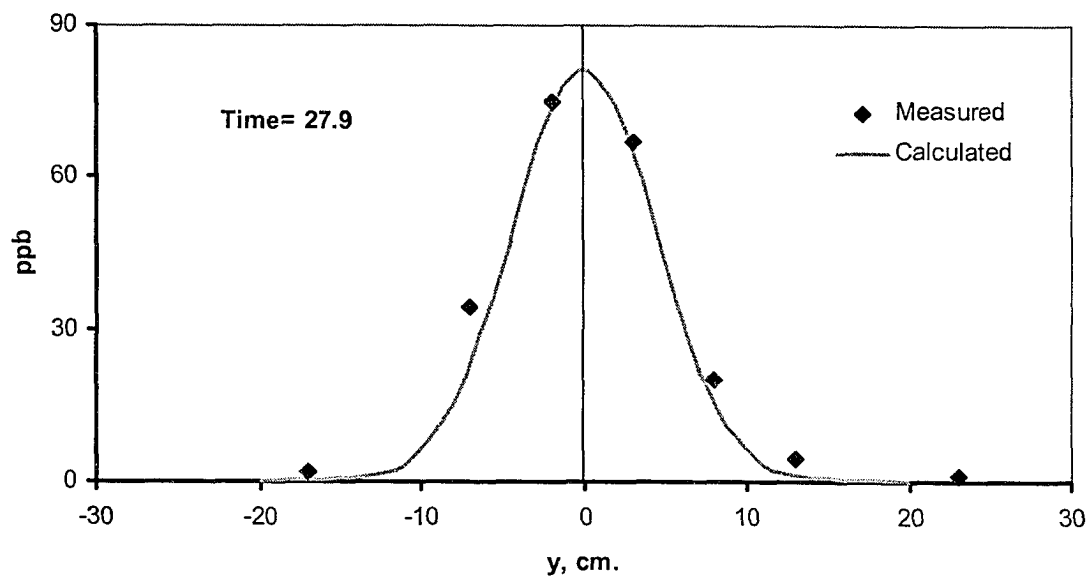


Fig. 6.14 Comparison of measured and calculated transverse concentration profile after 27.9 hours.

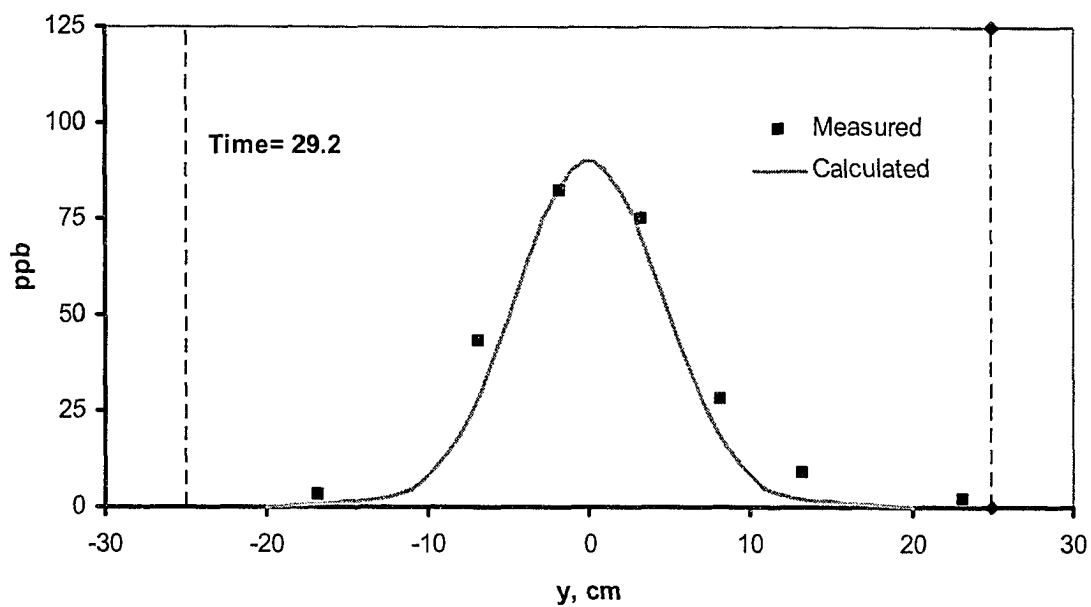


Fig. 6.15 Comparison of measured and calculated transverse concentration profile after 29.2 hours.

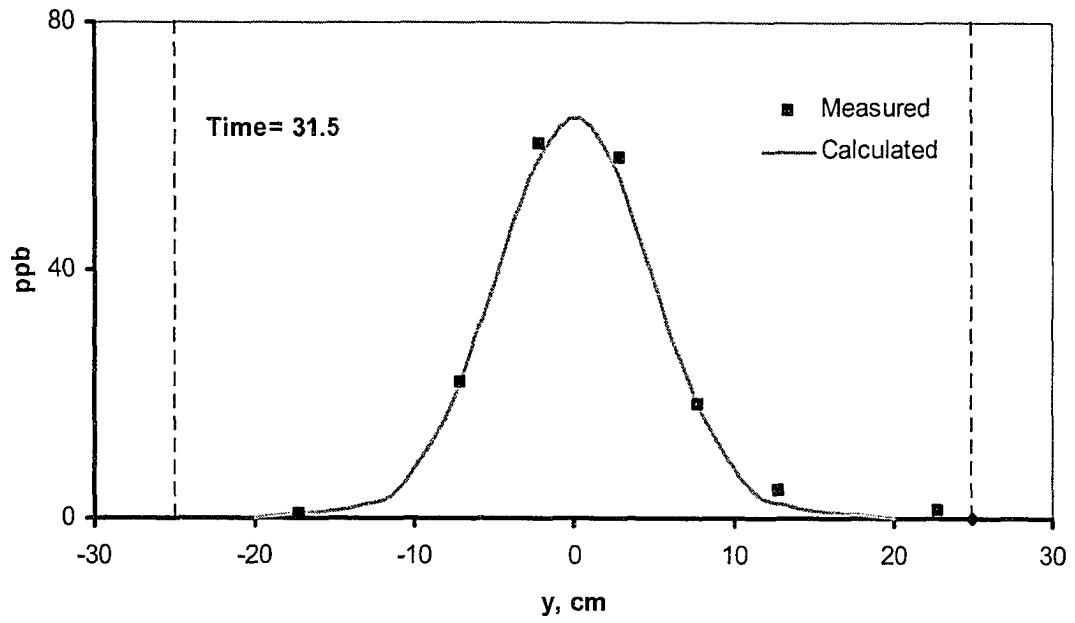


Fig. 6.16 Comparison of measured and calculated transverse concentration profile after 31.5 hours.

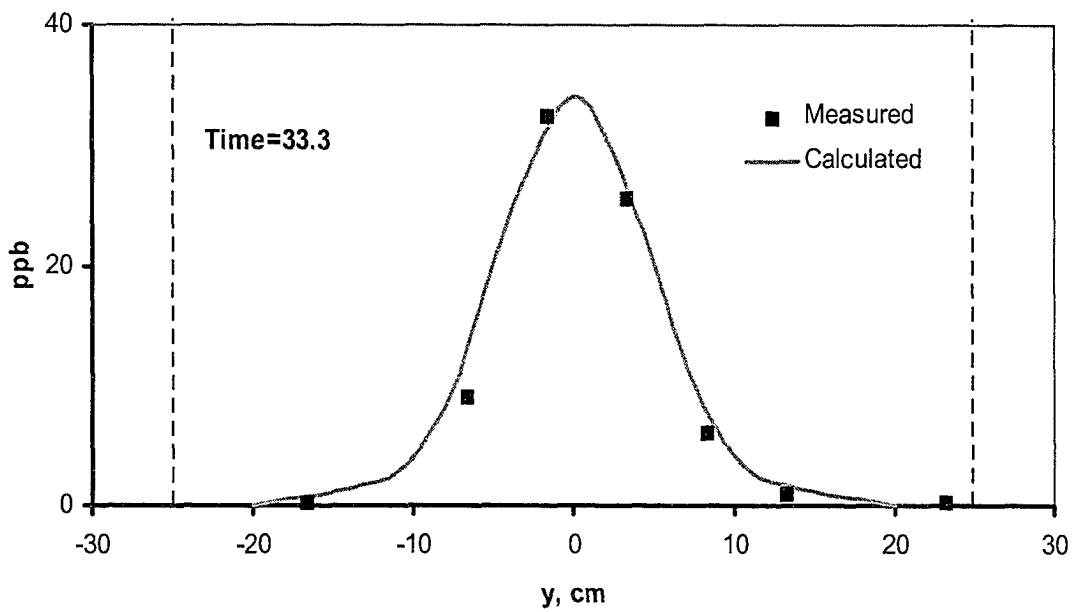


Fig. 6.17 Comparison of measured and calculated transverse concentration profile after 33.3 hours.

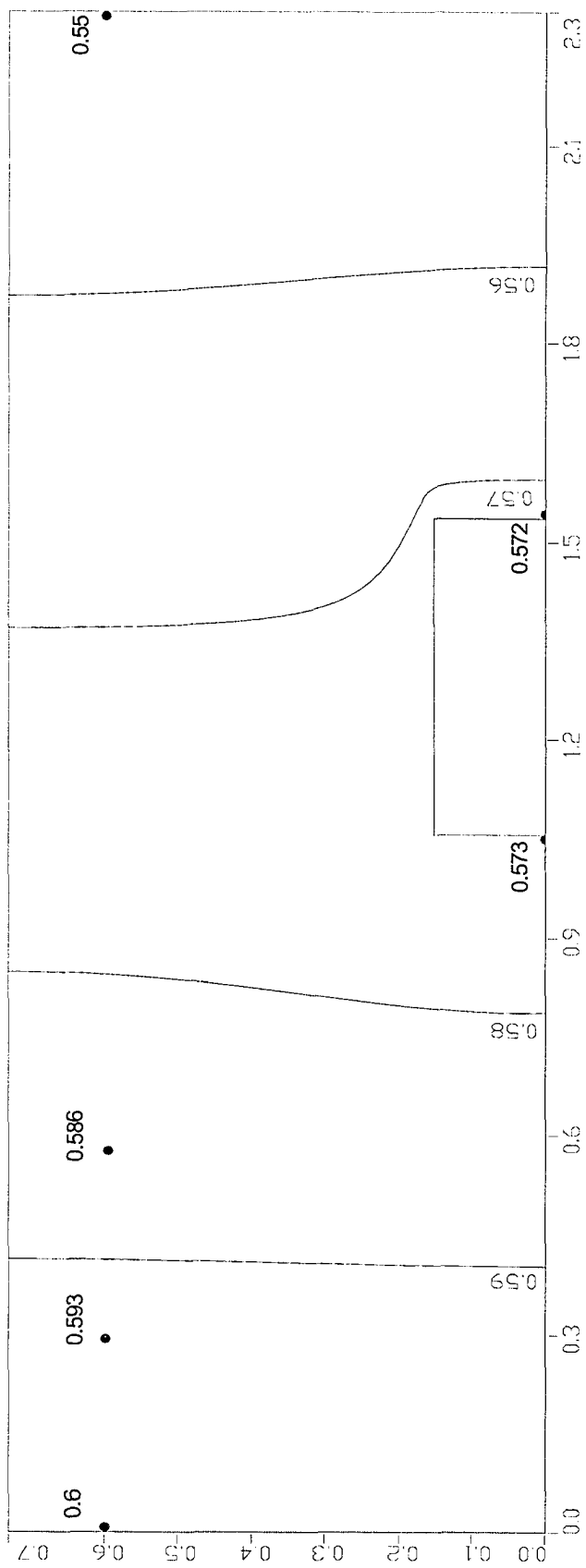


Fig. 6.18 Hydraulic heads distribution for the 30 cm sand-gravel system.

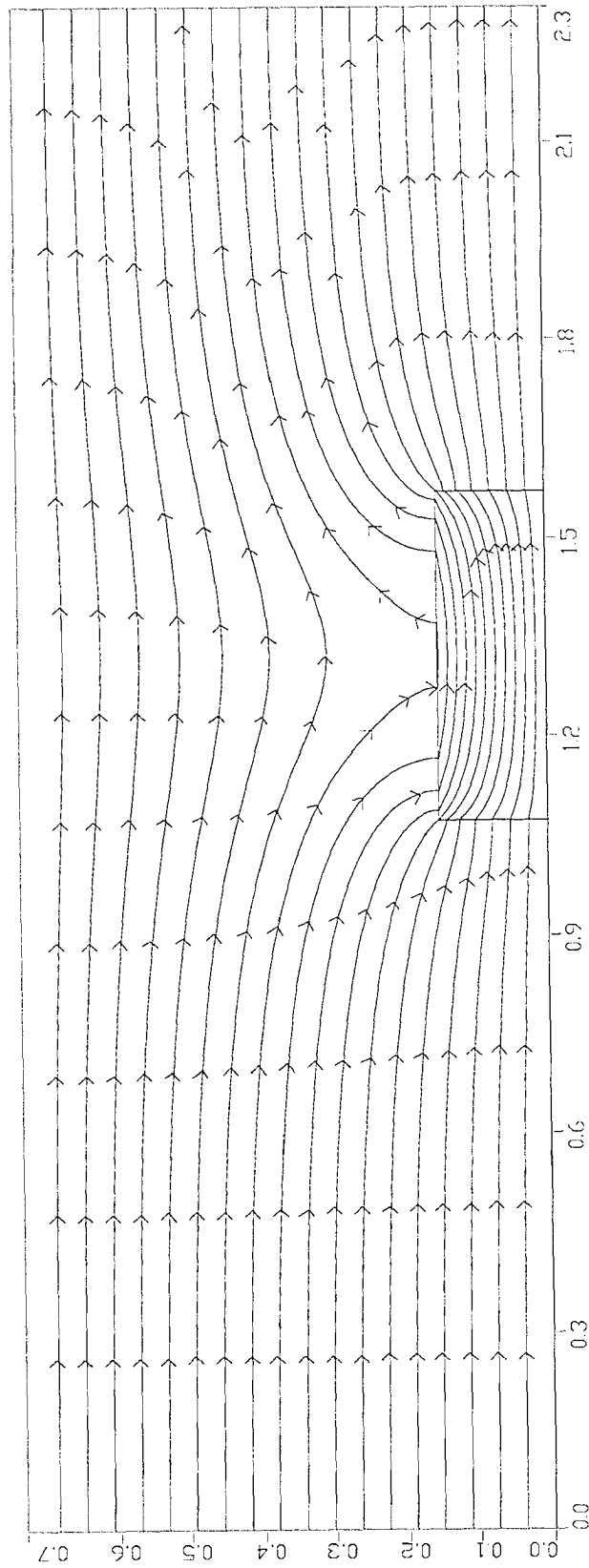


Fig. 6.19 Flow lines for the 30 cm sand-gravel system.

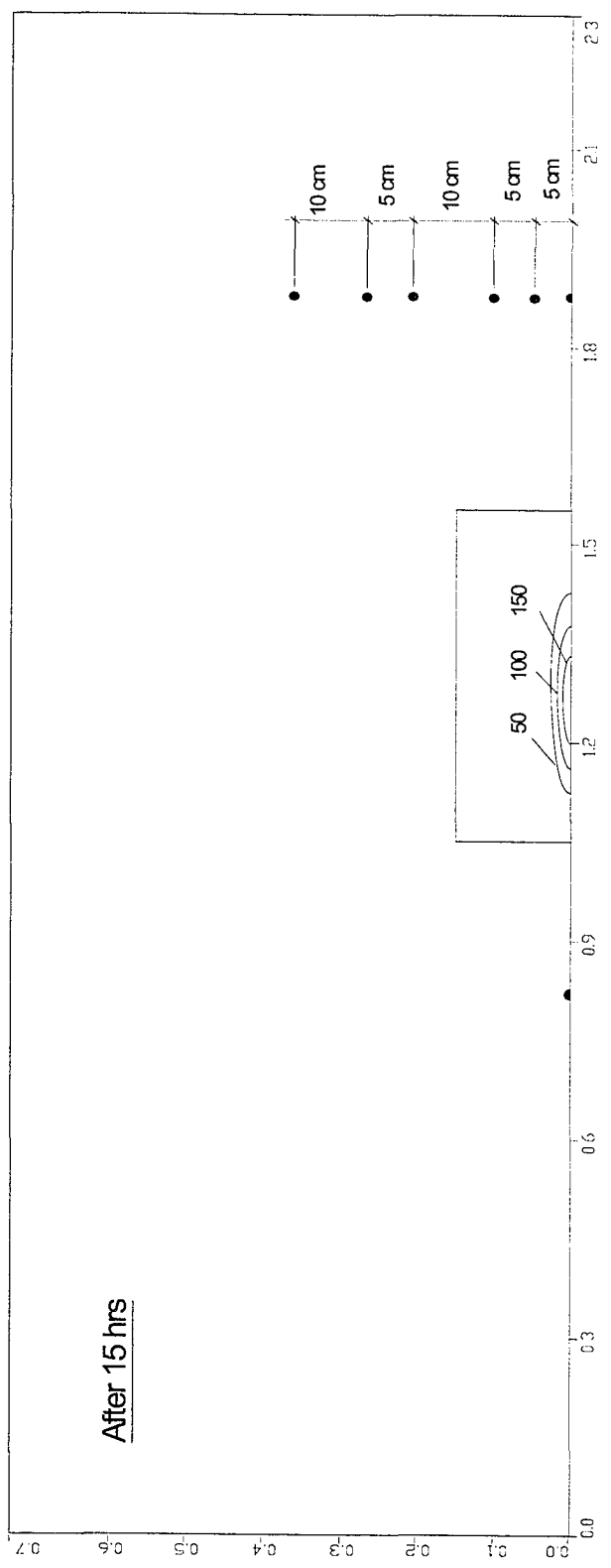


Fig. 6.20 Plume contours for the 30 cm sand-gravel system after 15 hrs.

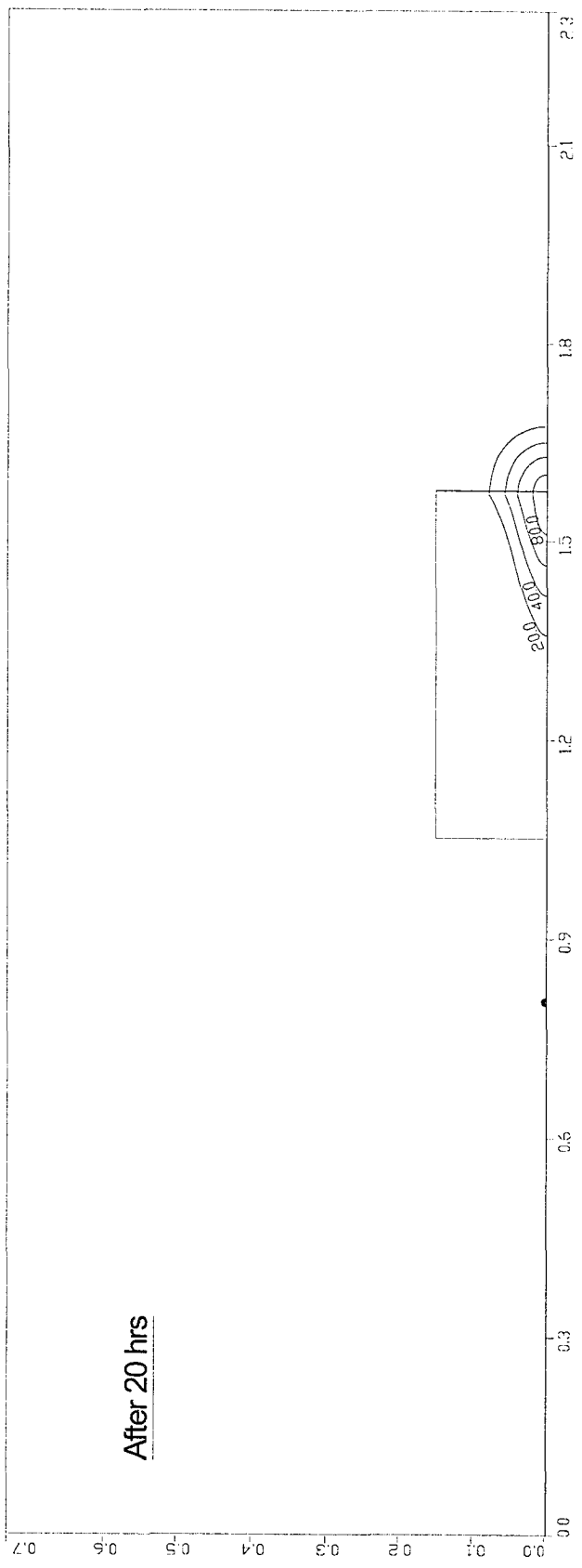


Fig. 6.21 Plume contours for the 30 cm sand-gravel system after 20 hrs.

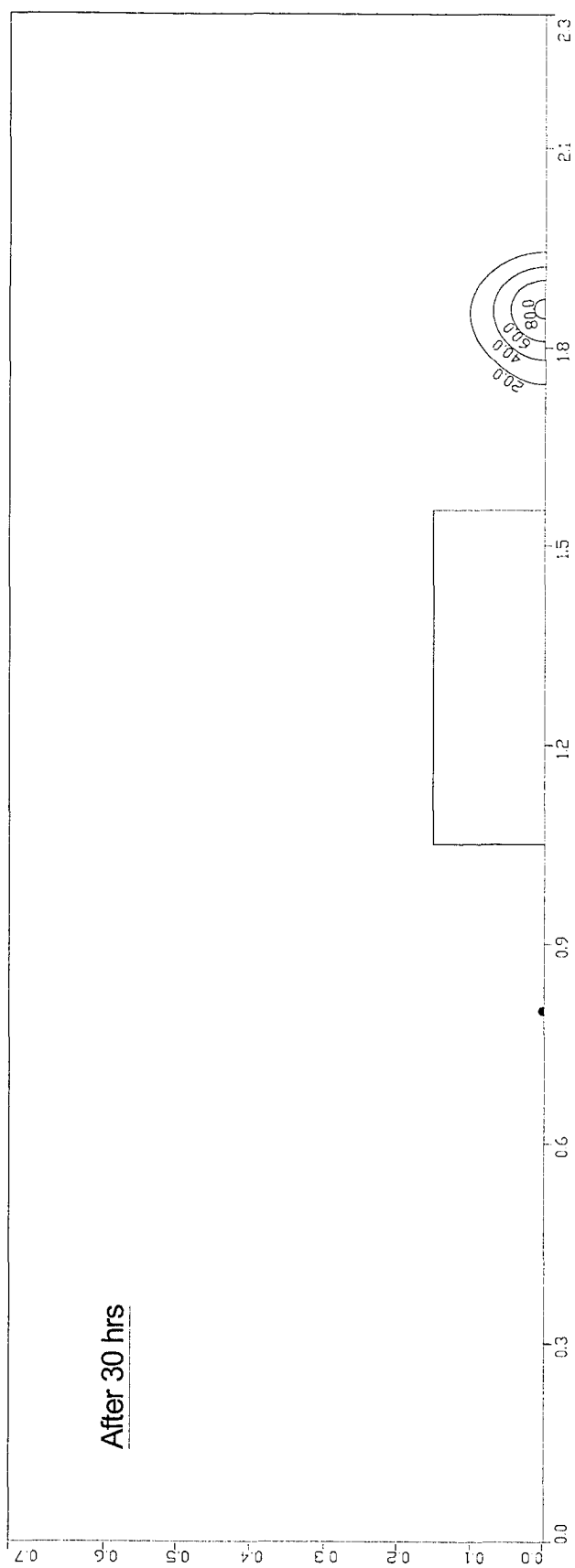


Fig. 6.22 Plume contours for the 30 cm sand-gravel system after 30 hrs.

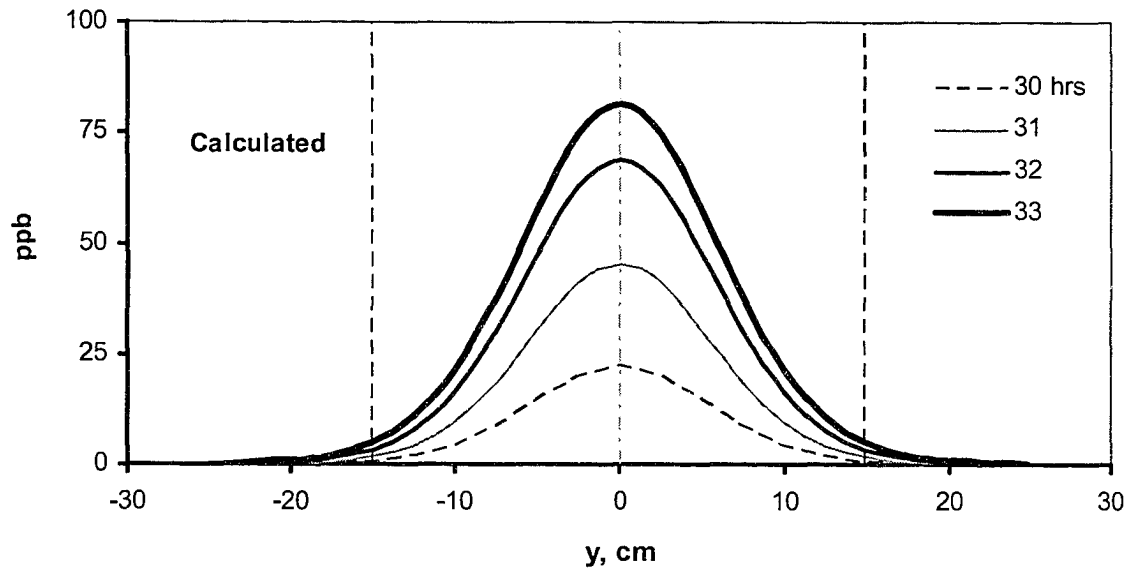


Fig. 6.23 Simulated transverse concentration profile.

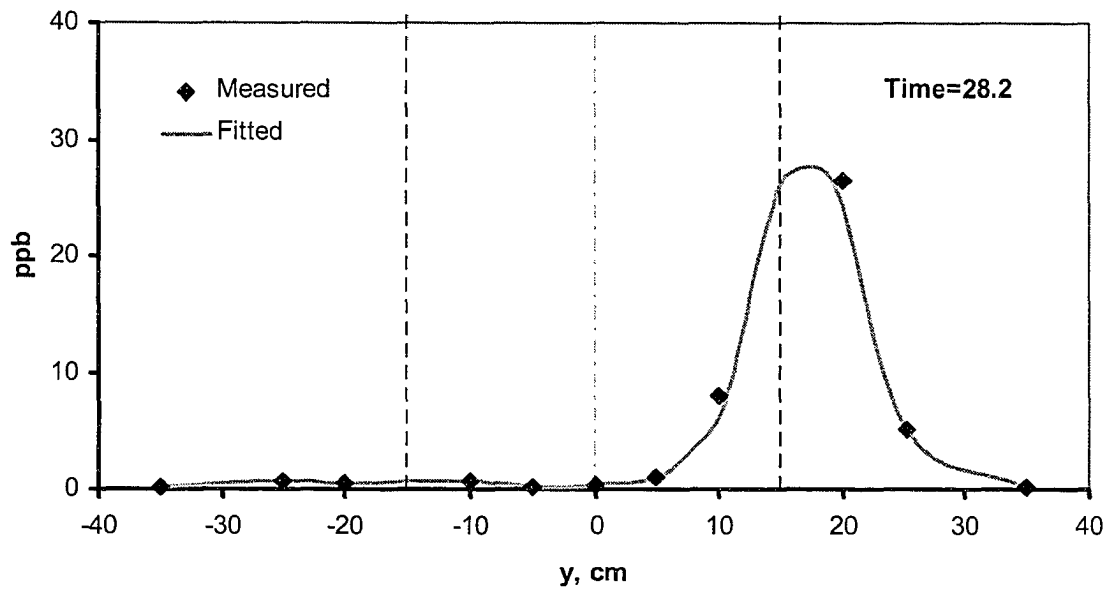


Fig. 6.24 Measured concentration profile after 28.2 hours for the 30 cm sand-gravel system.

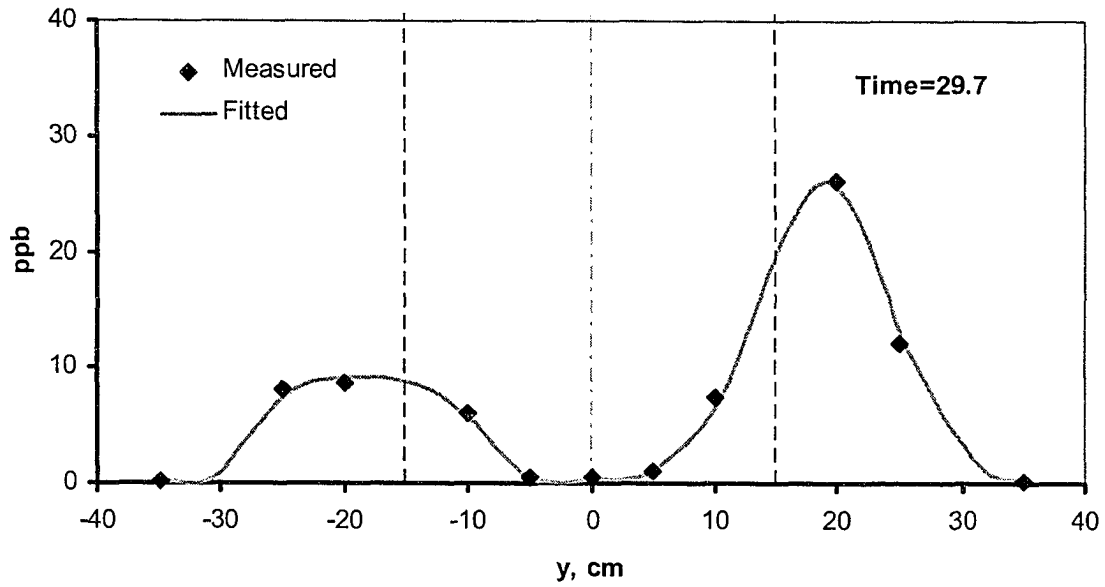


Fig. 6.25 Measured concentration profile after 29.7 hours for the 30 cm sand-gravel system.

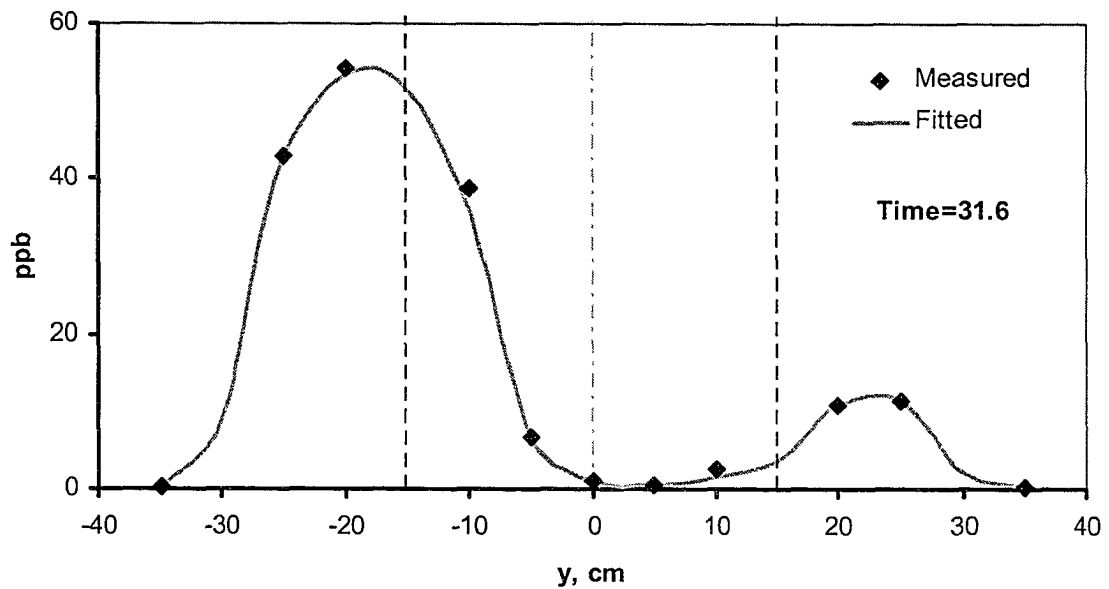


Fig. 6.26 Measured concentration profile after 31.6 hours for the 30 cm sand-gravel system.

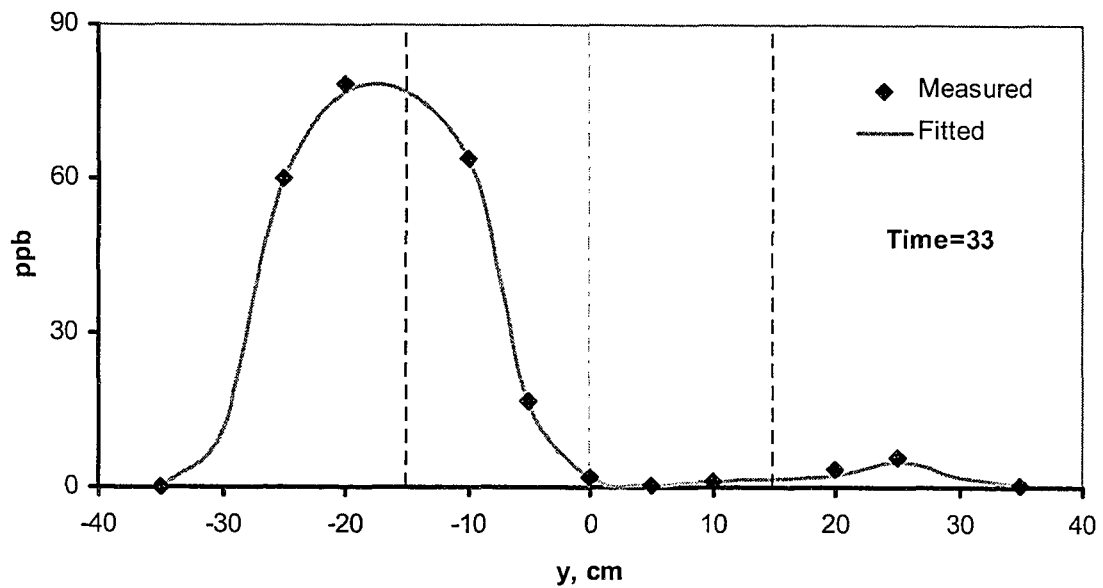


Fig. 6.27 Measured concentration profile after 33 hours for the 30 cm sand-gravel system.

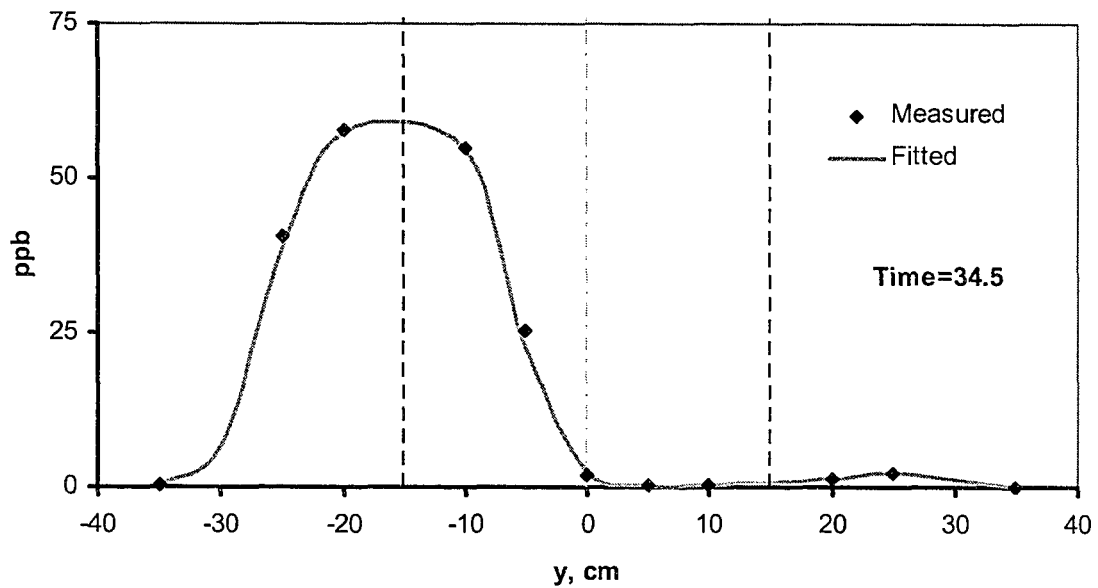


Fig. 6.28 Measured concentration profile after 34.5 hours for the 30 cm sand-gravel system.

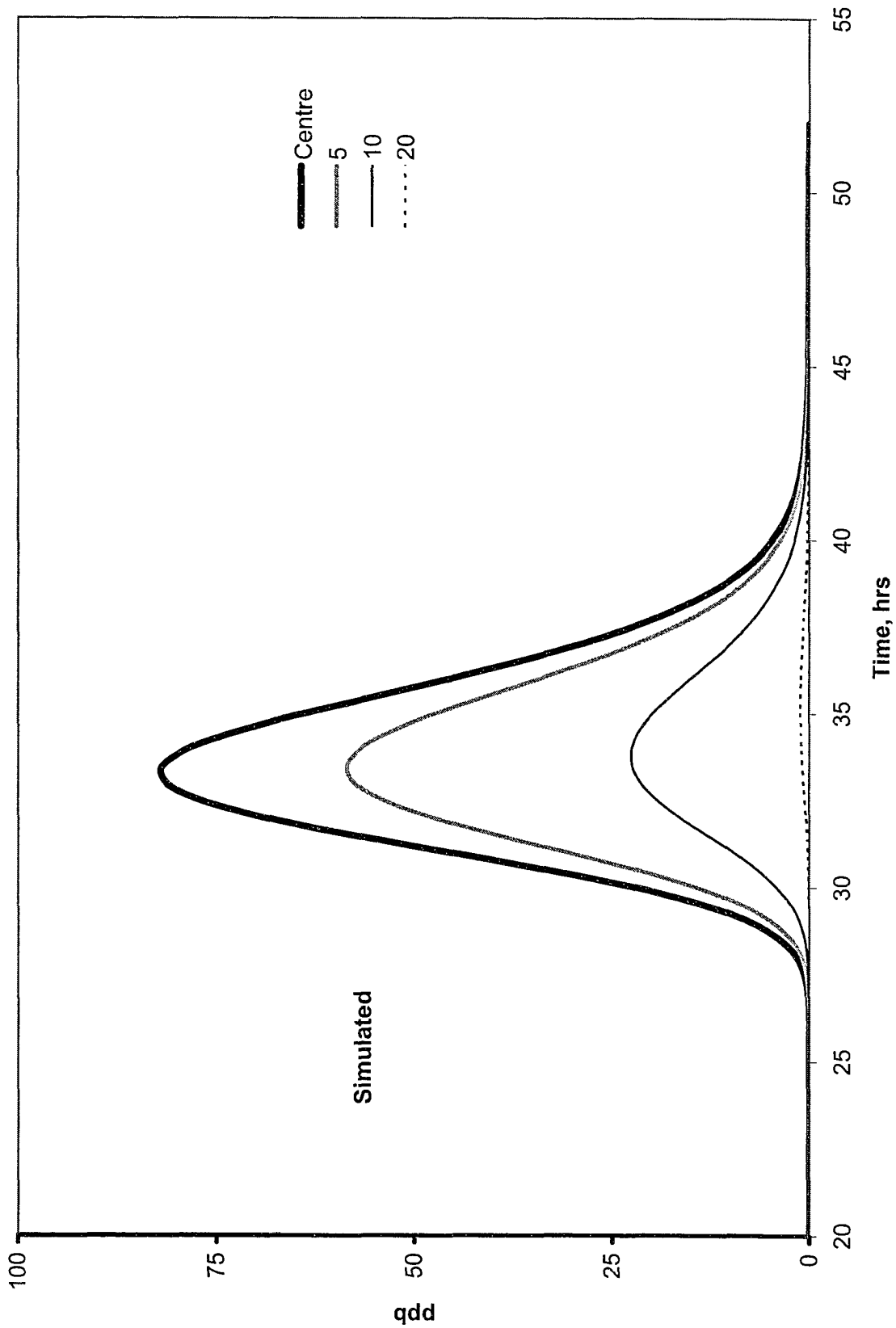


Fig. 6.29 Simulated concentration history at measuring ports for the 30 cm scenario.

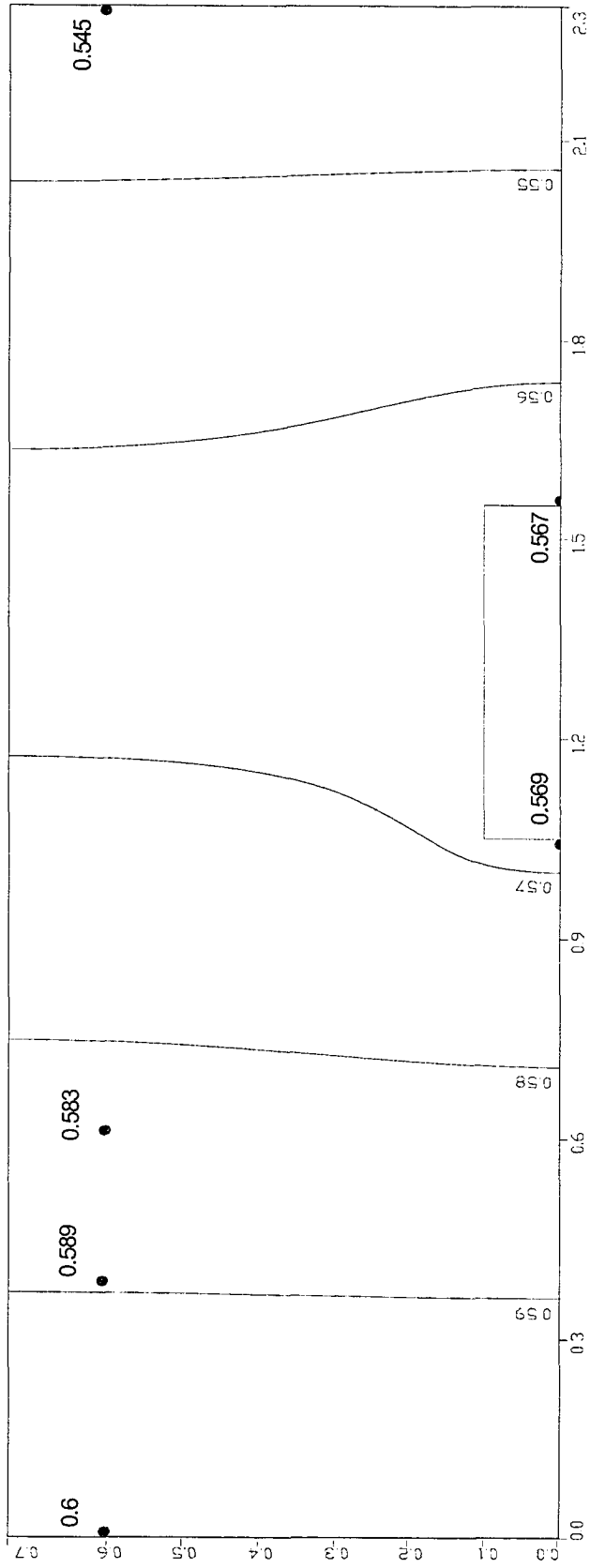


Fig. 6.30 Hydraulic heads distribution for the 20 cm sand-gravel system.

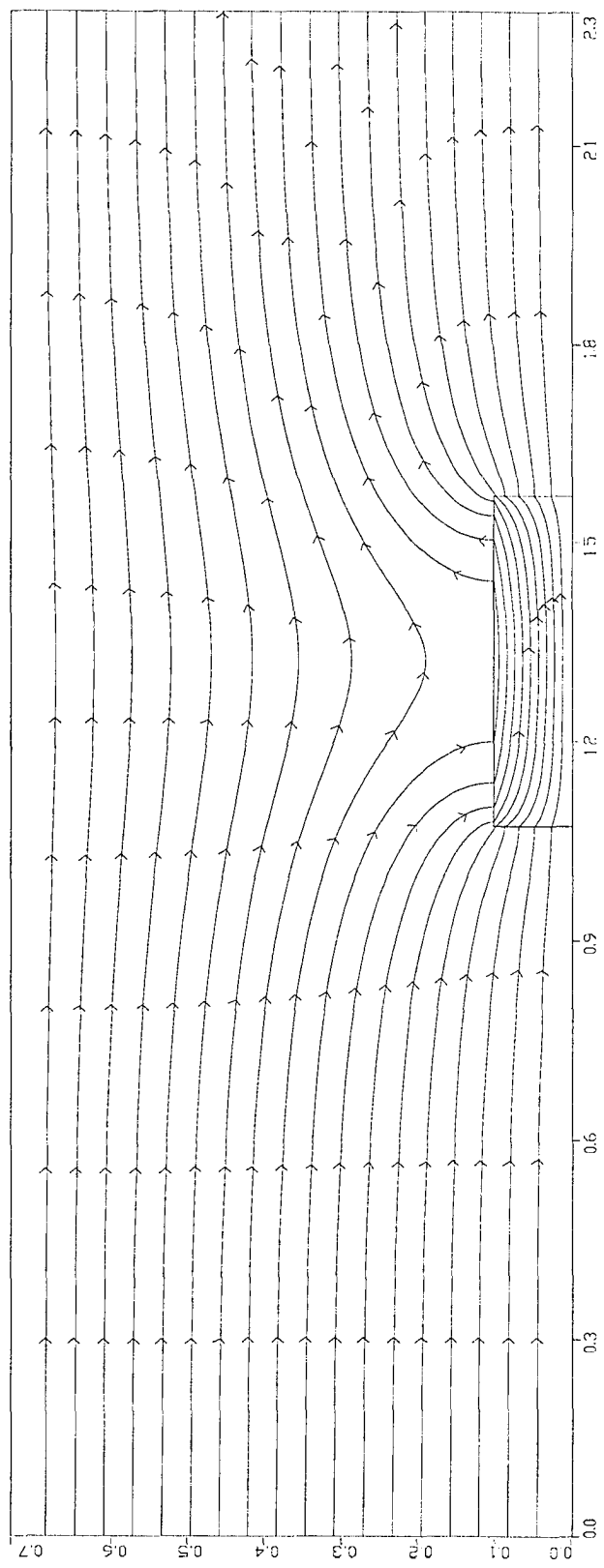


Fig. 6.31 Flow lines for the 20 cm sand-gravel system.

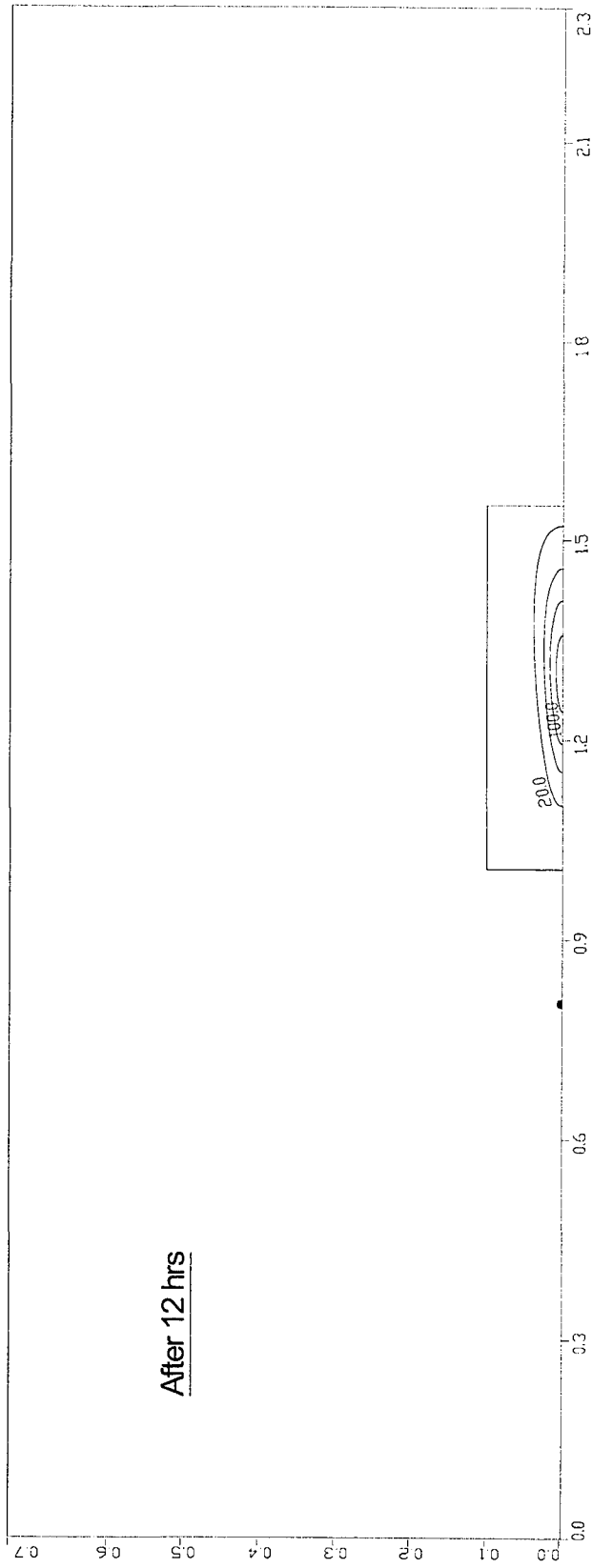


Fig. 6.32 Plume contours for the 20 cm sand-gravel system after 12 hrs.

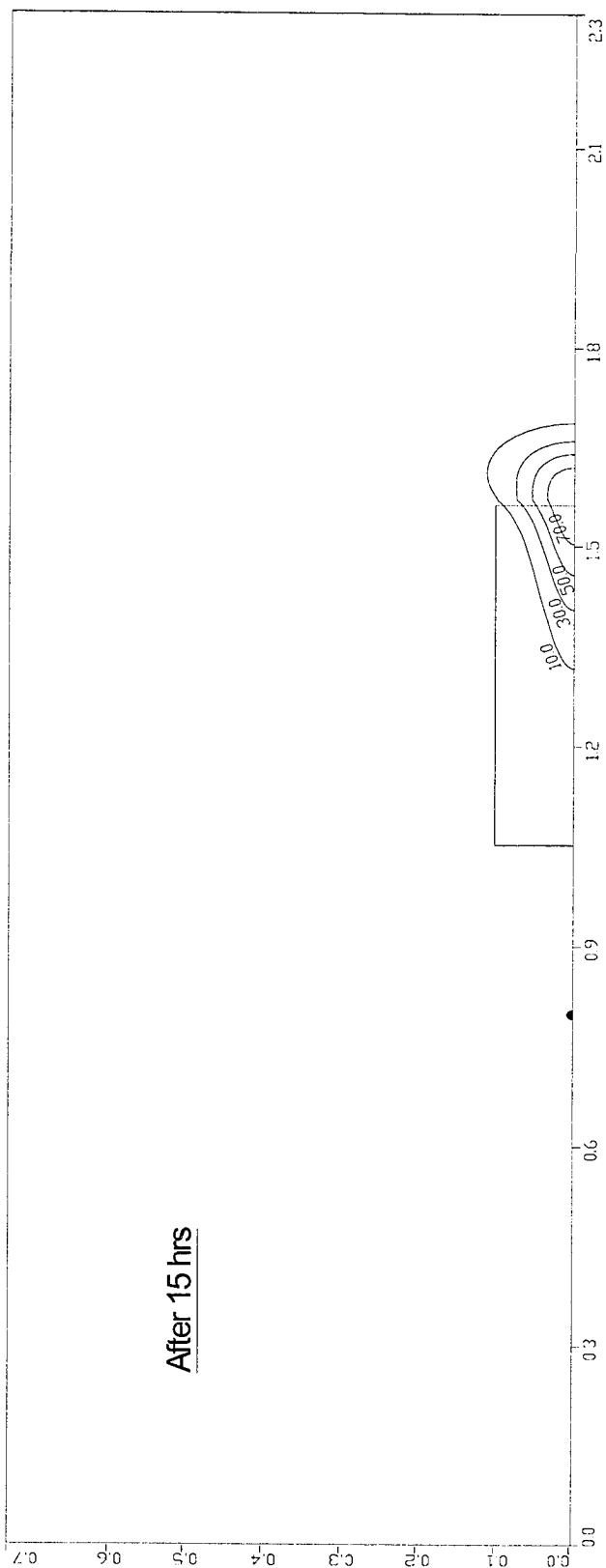


Fig. 6.33 Plume contours for the 20 cm sand-gravel system after 15 hrs.

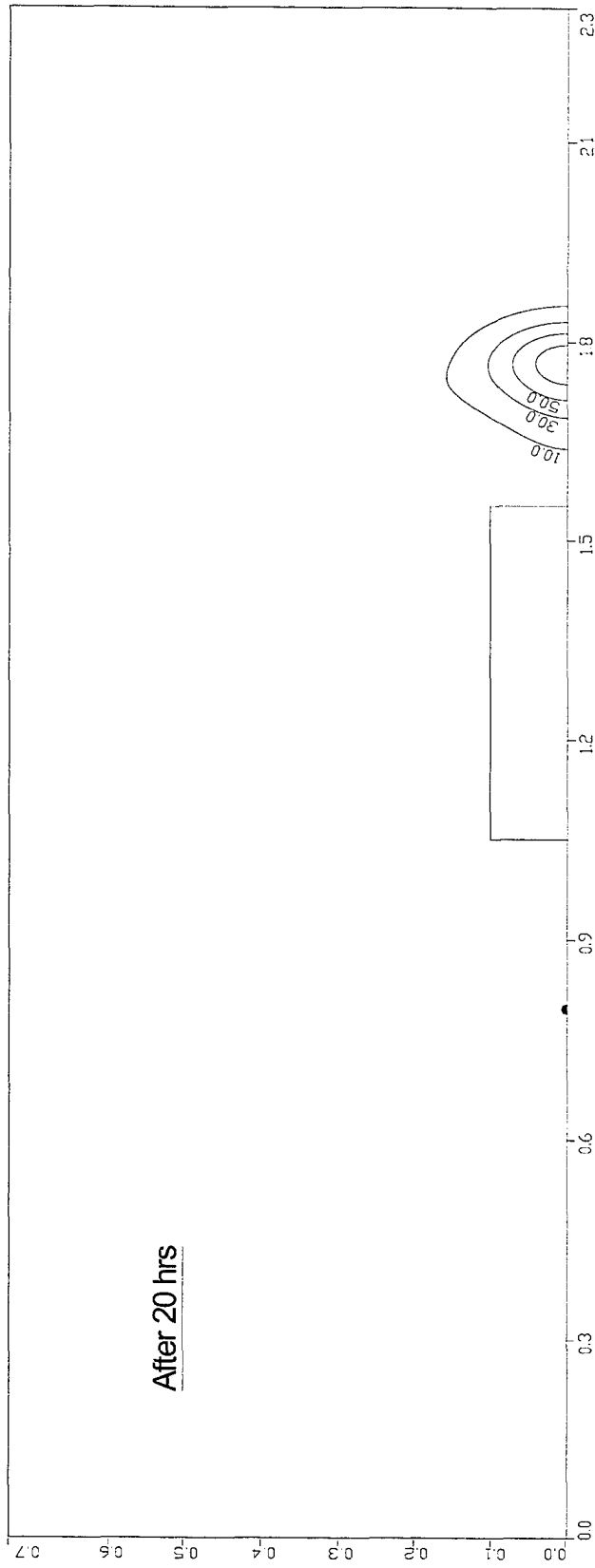


Fig. 6.34 Plume contours for the 20 cm sand-gravel system after 20 hrs.

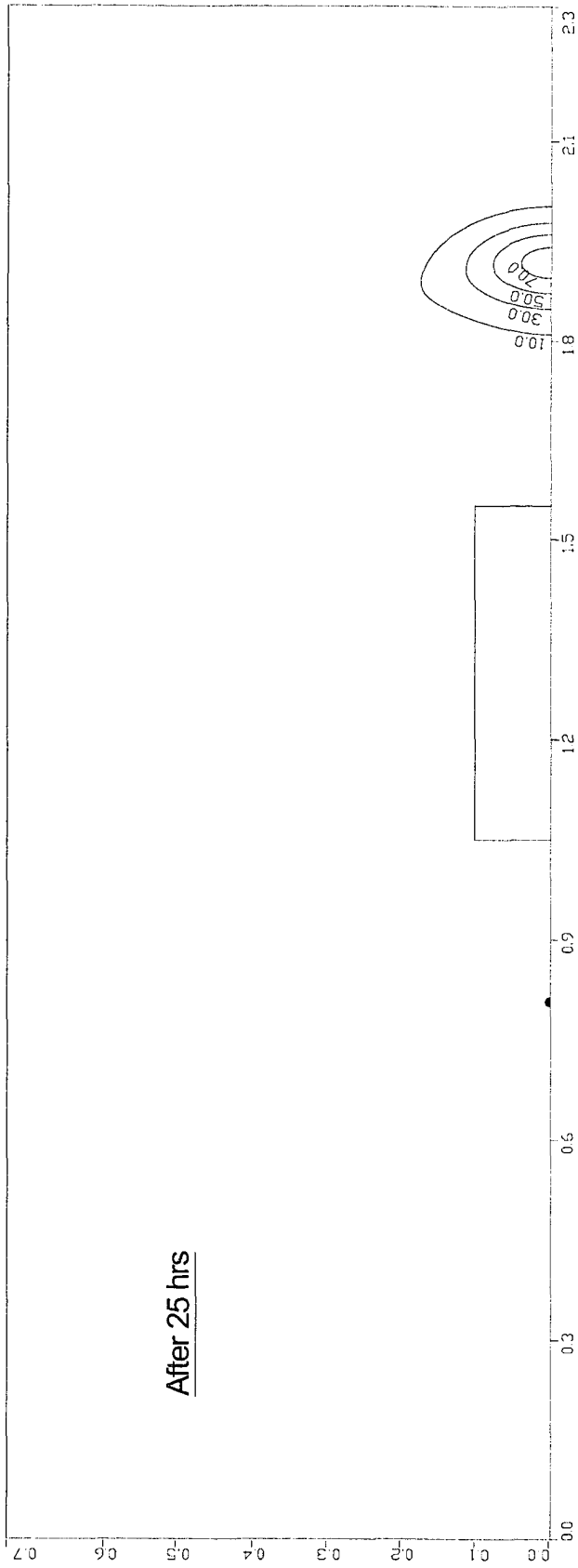


Fig. 6.35 Plume contours for the 20 cm sand-gravel system after 25 hrs.

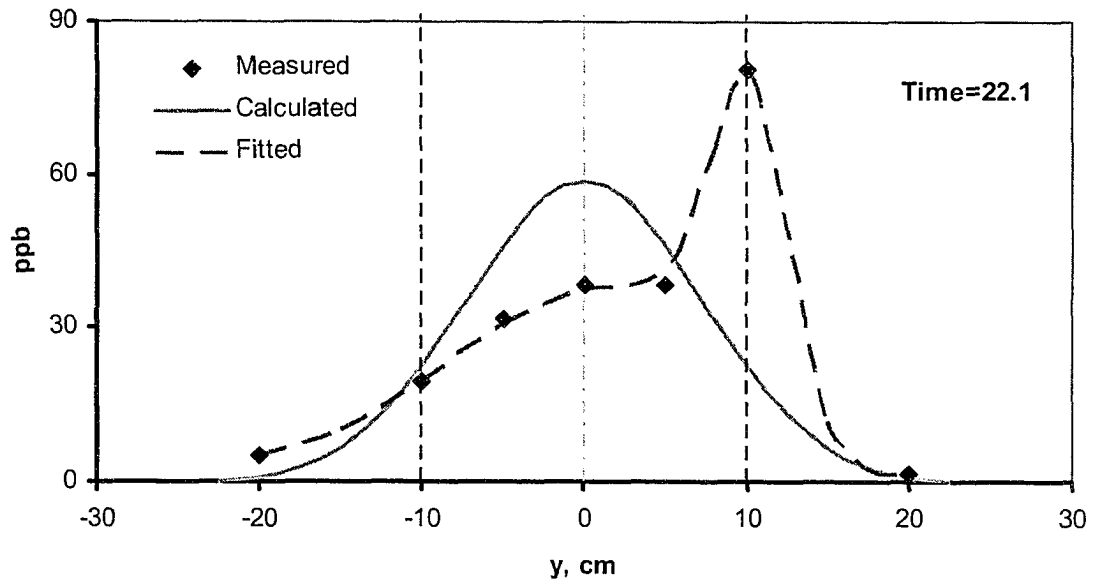


Fig. 6.36 Comparison of measured and simulated transverse concentration profile after 22.1 hours for the 20 cm scenario.

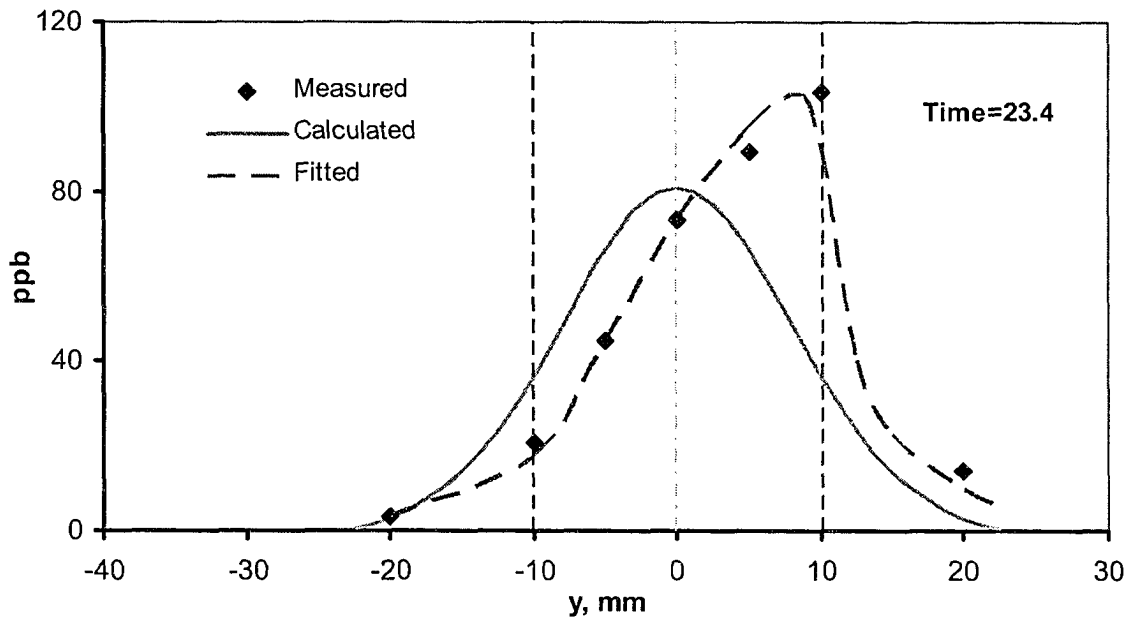


Fig. 6.37 Comparison of measured and simulated transverse concentration profile after 23.4 hours for the 20 cm scenario.

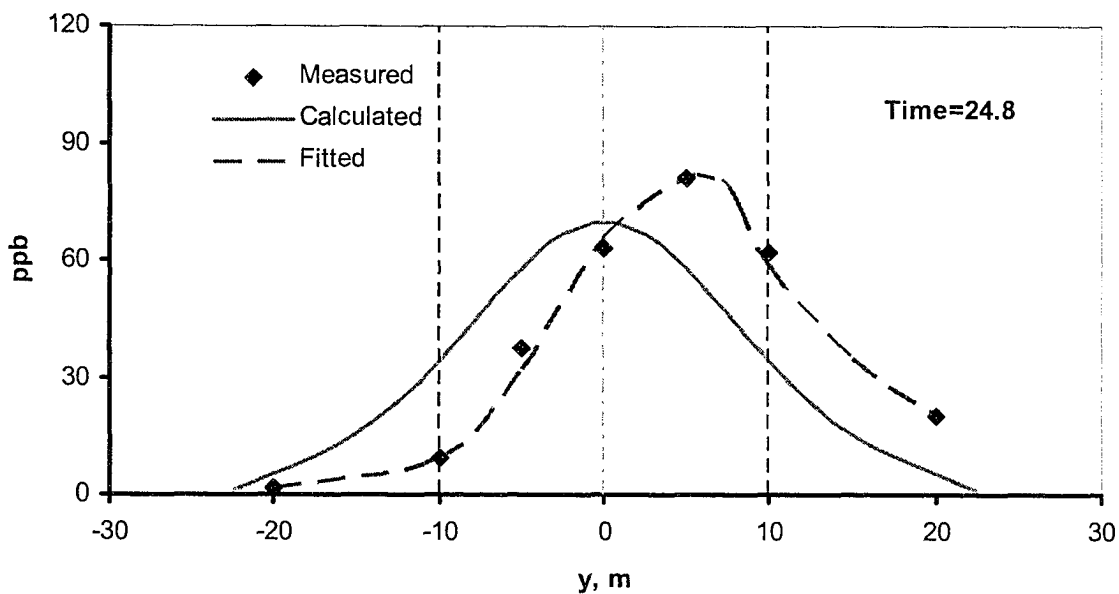


Fig. 6.38 Comparison of measured and simulated transverse concentration profile after 24.8 hours for the 20 cm scenario.

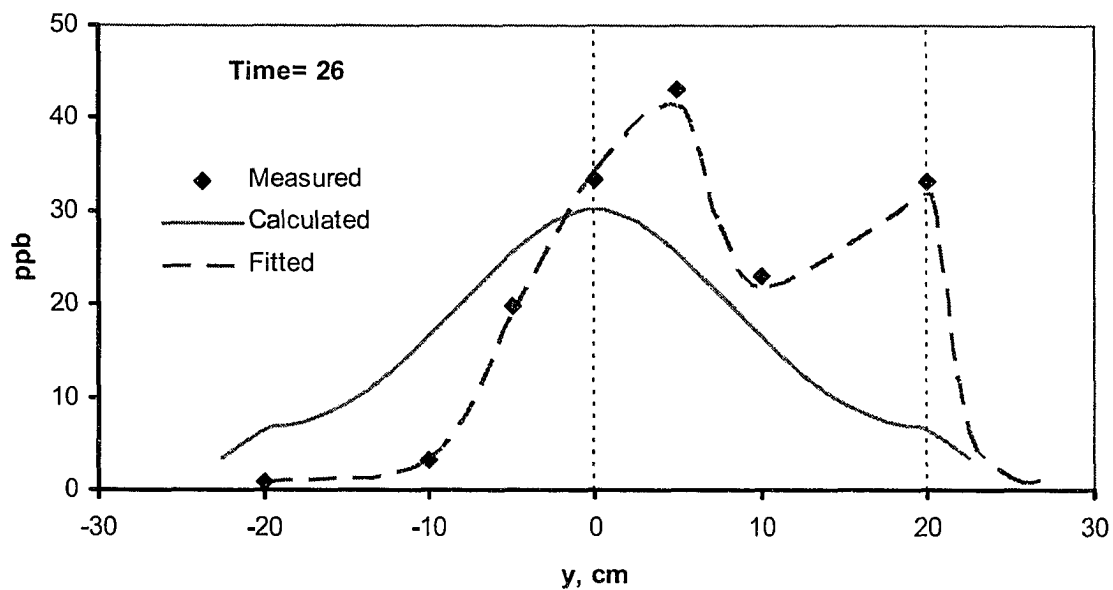


Fig. 6.39 Comparison of measured and simulated transverse concentration profile after 26 hours for the 20 cm scenario.

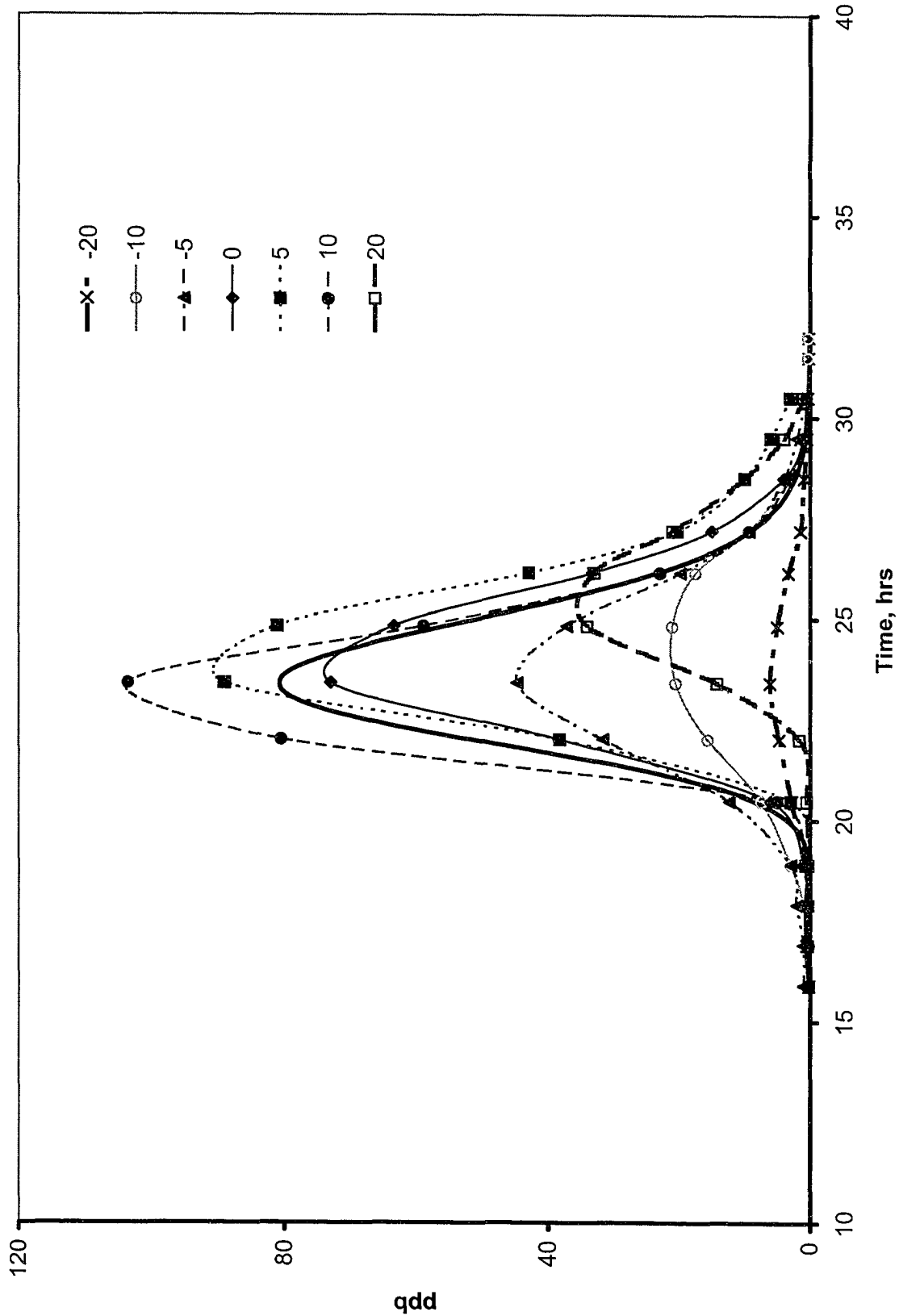


Fig. 6.40 Plume history at the measuring ports as well as that calculated at the center for the 20 cm sand-gravel system.

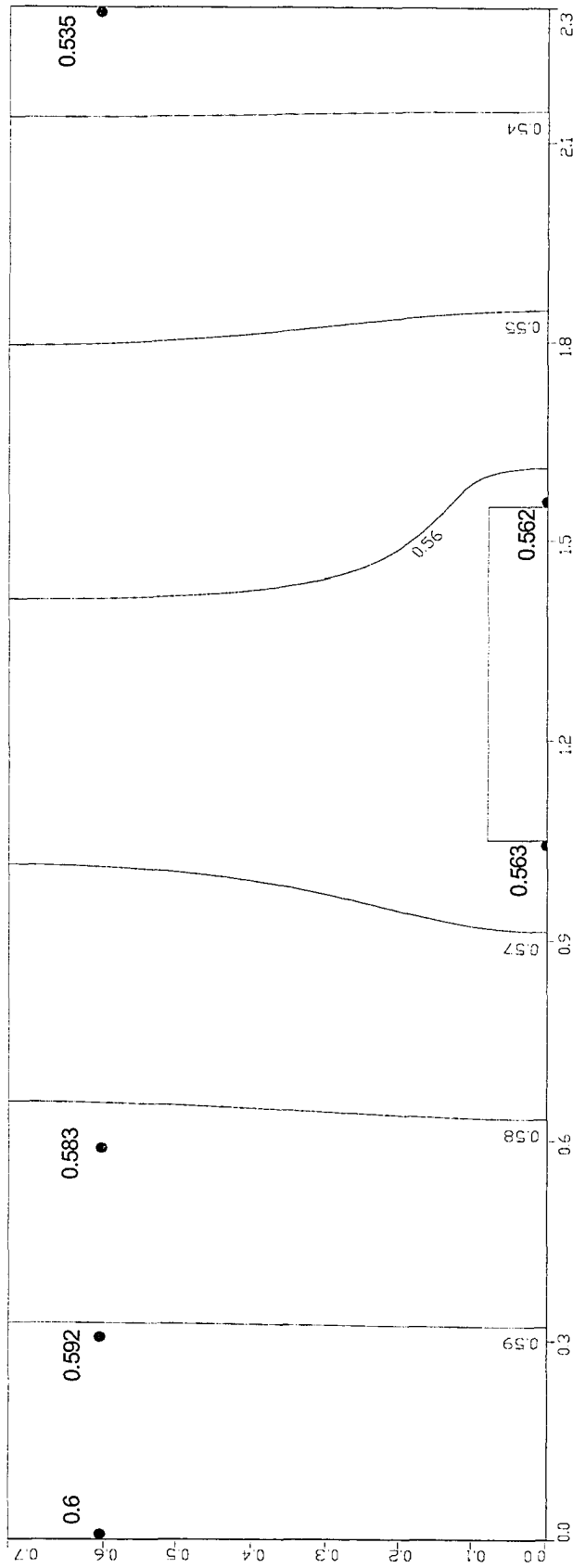


Fig. 6.41 Hydraulic heads distribution for the 15 cm sand-gravel system.

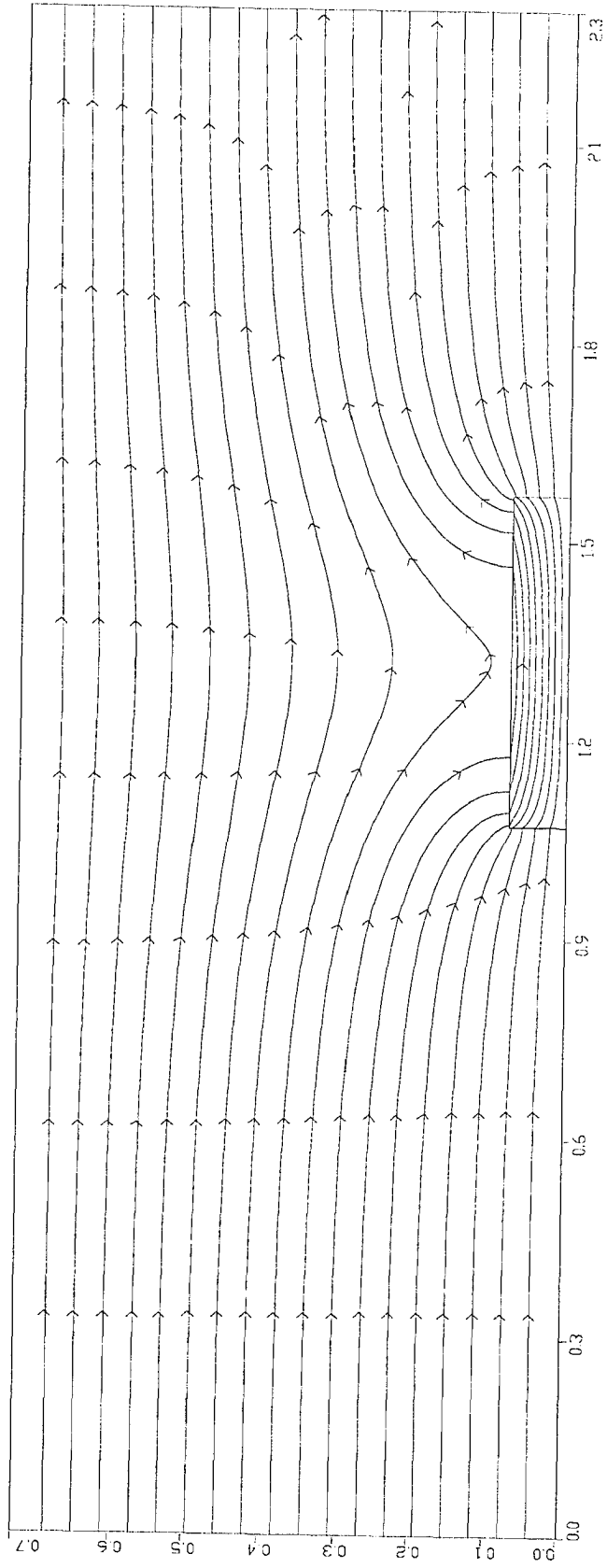


Fig. 6.42 Flow lines for the 15 cm sand-gravel system.

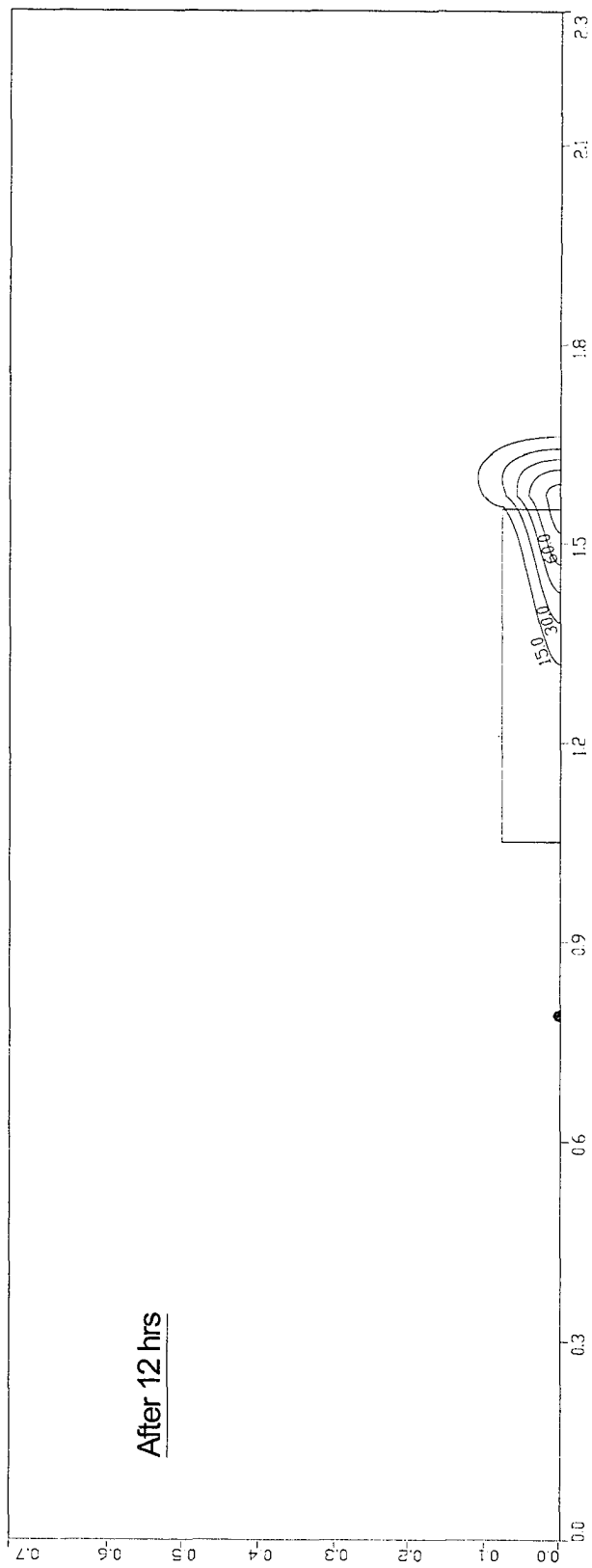


Fig. 6.43 Plume contours for the 15 cm sand-gravel system after 12 hrs.

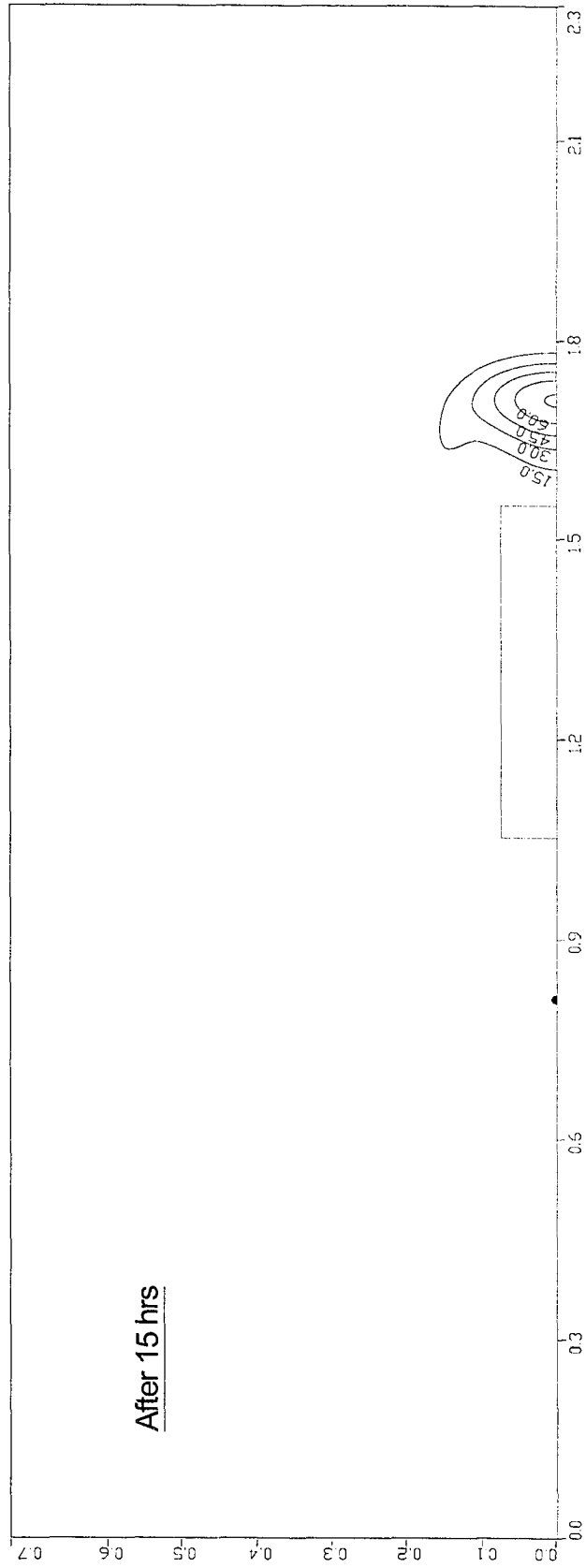


Fig. 6.44 Plume contours for the 15 cm sand-gravel system after 15 hrs.

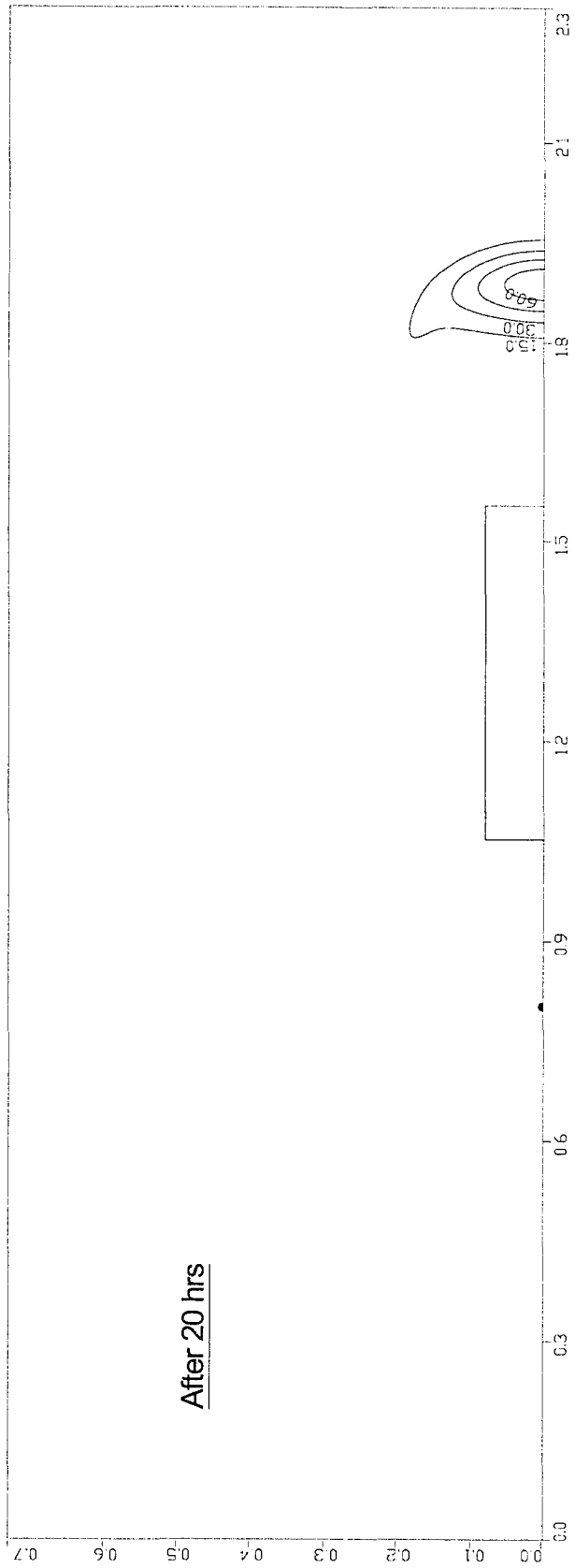


Fig. 6.45 Plume contours for the 15 cm sand-gravel system after 20 hrs.

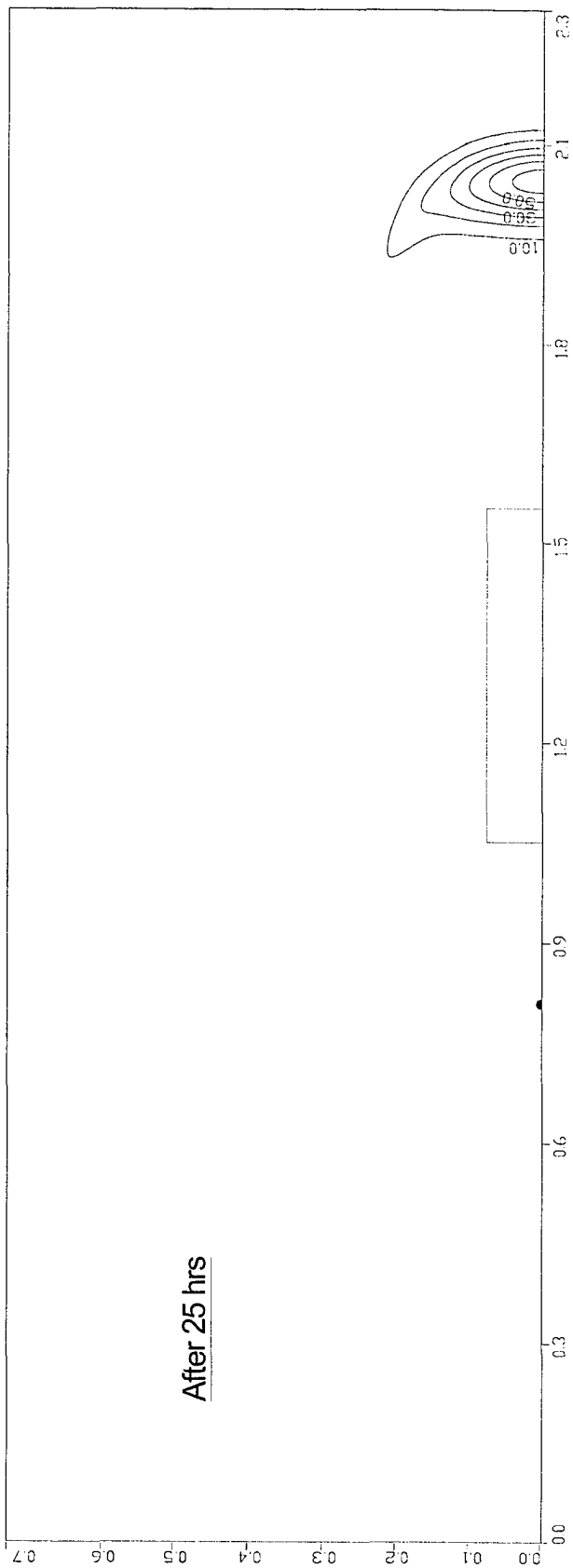


Fig. 6.46 Plume contours for the 15 cm sand-gravel system after 25 hrs.

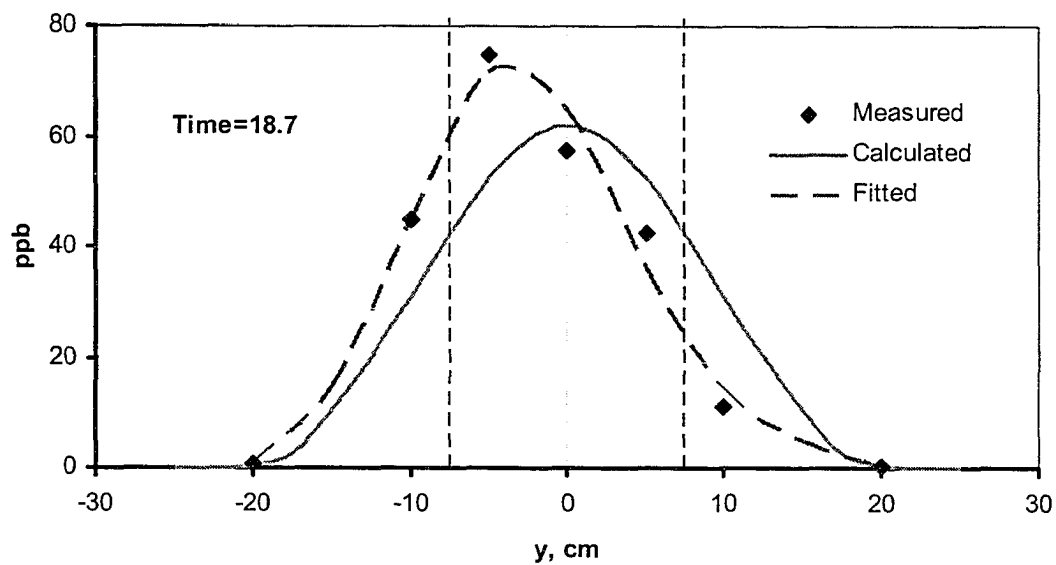


Fig. 6.47 Comparison of measured and simulated transverse concentration profile after 18.7 hours for the 15 cm sand-gravel system.

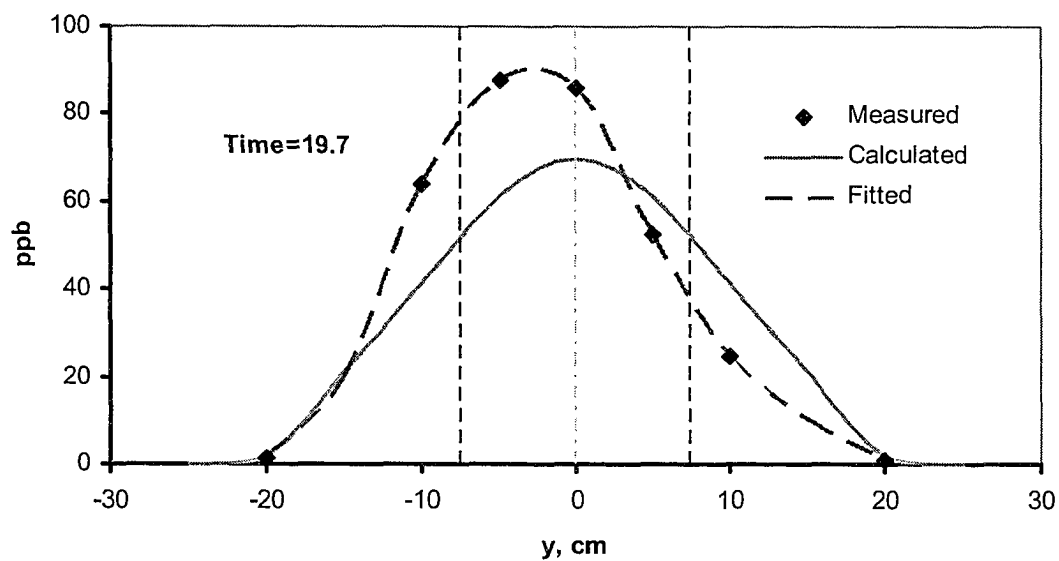


Fig. 6.48 Comparison of measured and simulated transverse concentration profile after 19.7 hours for the 15 cm sand-gravel system.

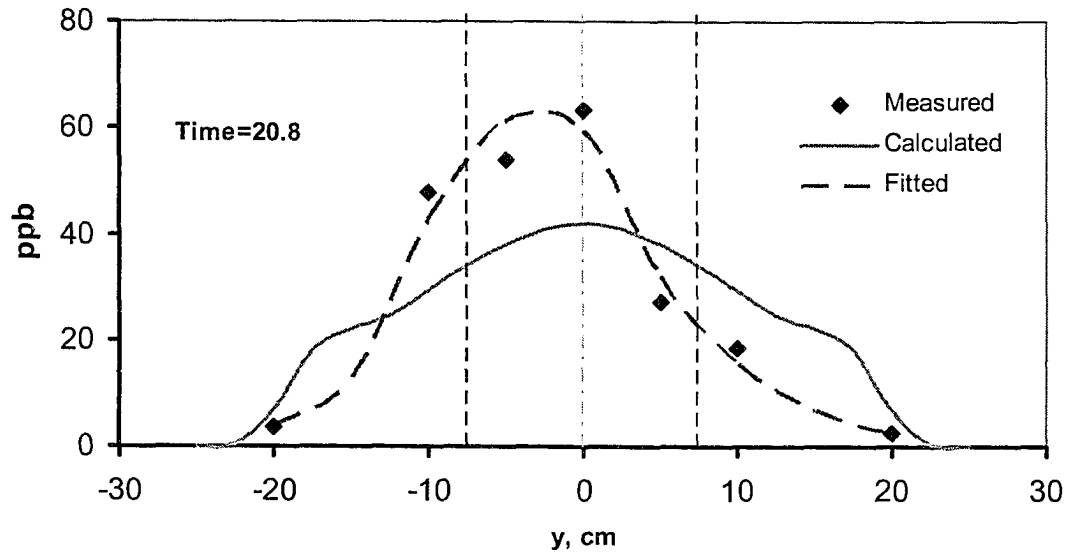


Fig. 6.49 Comparison of measured and simulated transverse concentration profile after 20.8 hours for the 15 cm sand-gravel system.

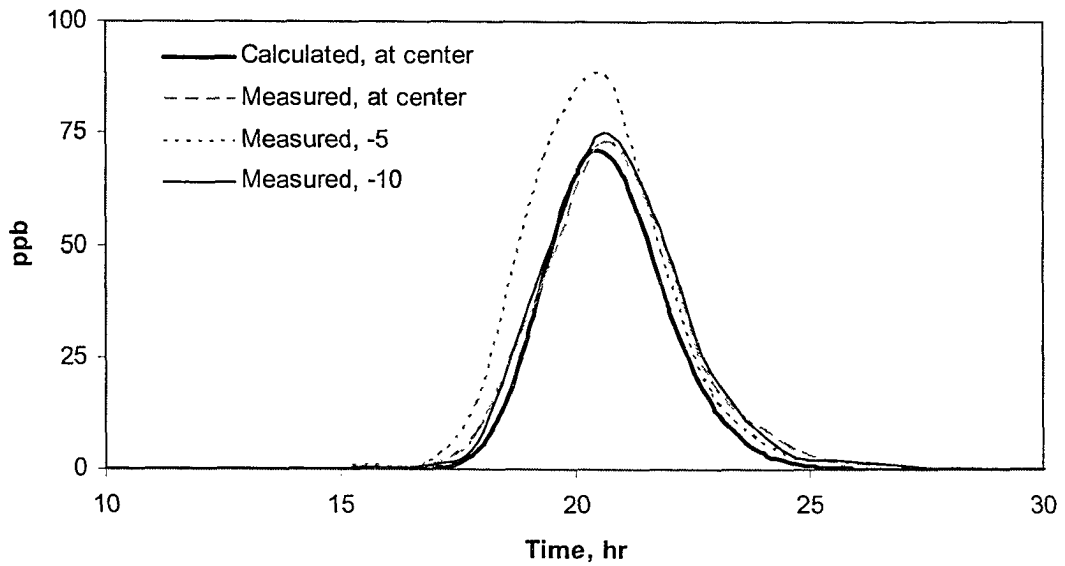


Fig. 6.50 Measured concentration history at some measuring ports and the simulated at the center for the 15 cm sand-gravel system.

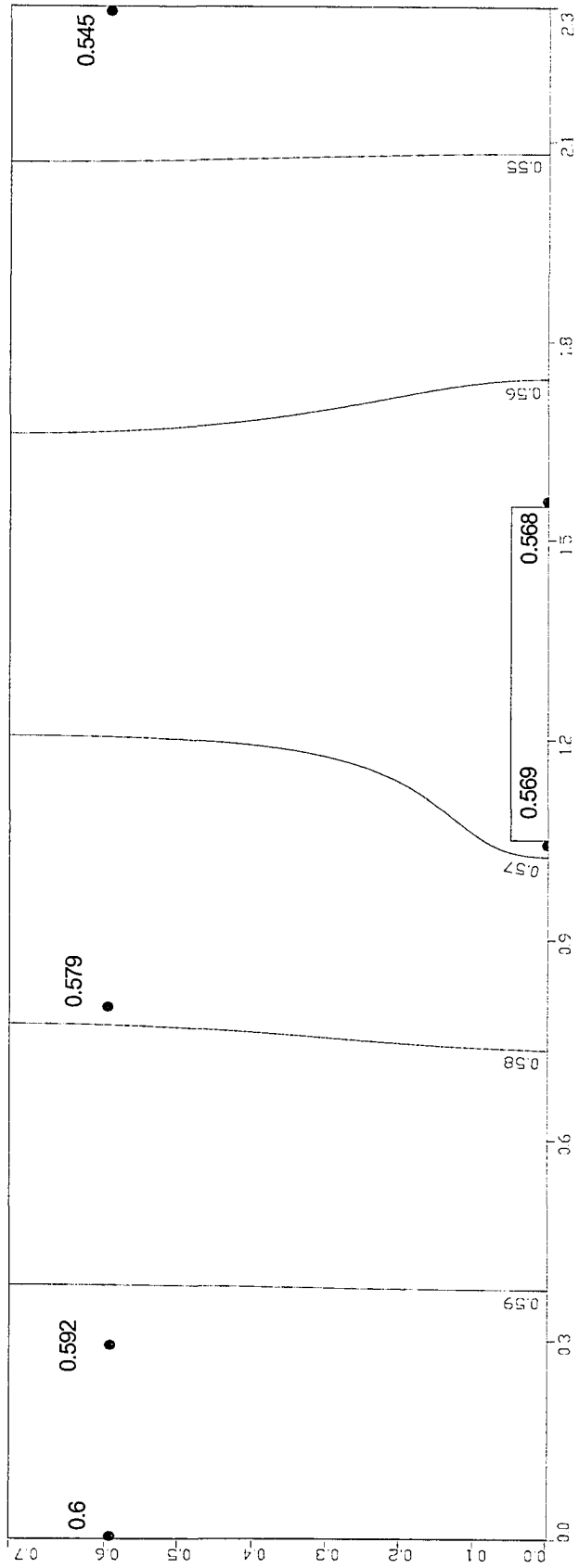


Fig. 6.51 Hydraulic heads distribution for the 10 cm sand-gravel system.

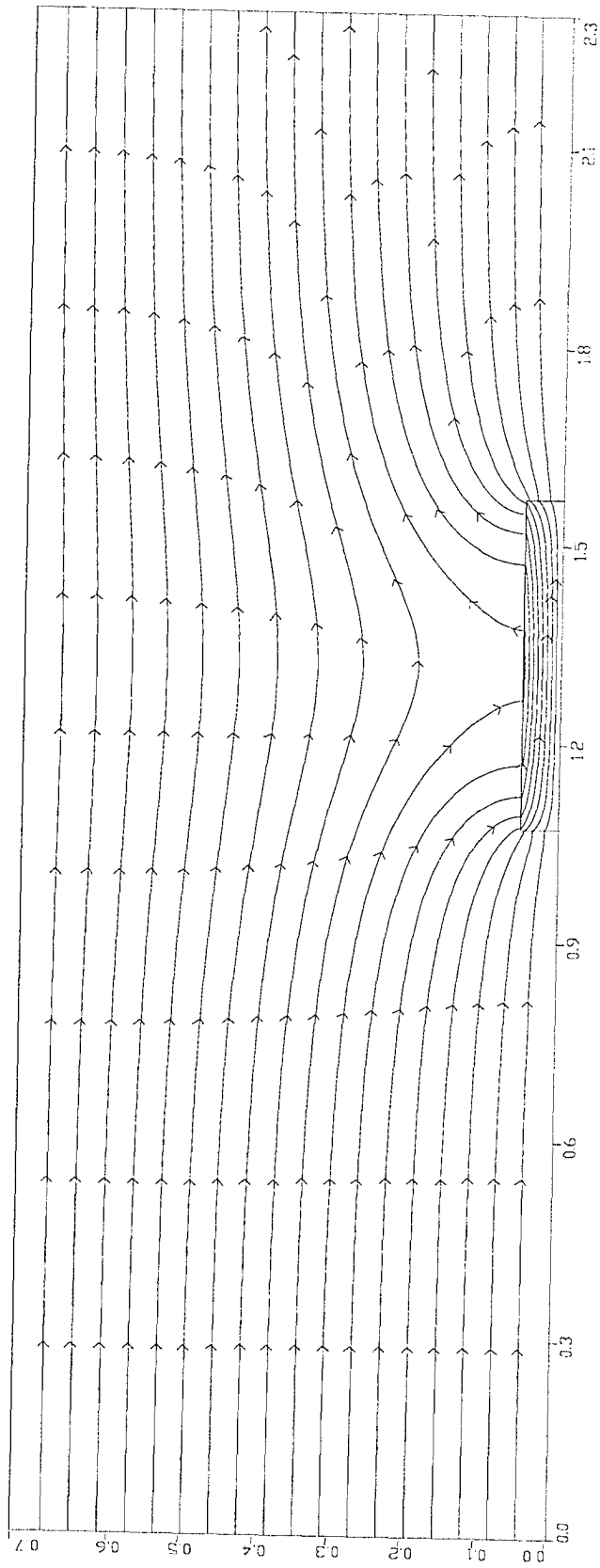


Fig. 6.52 Flow lines for the 10 cm sand-gravel system.

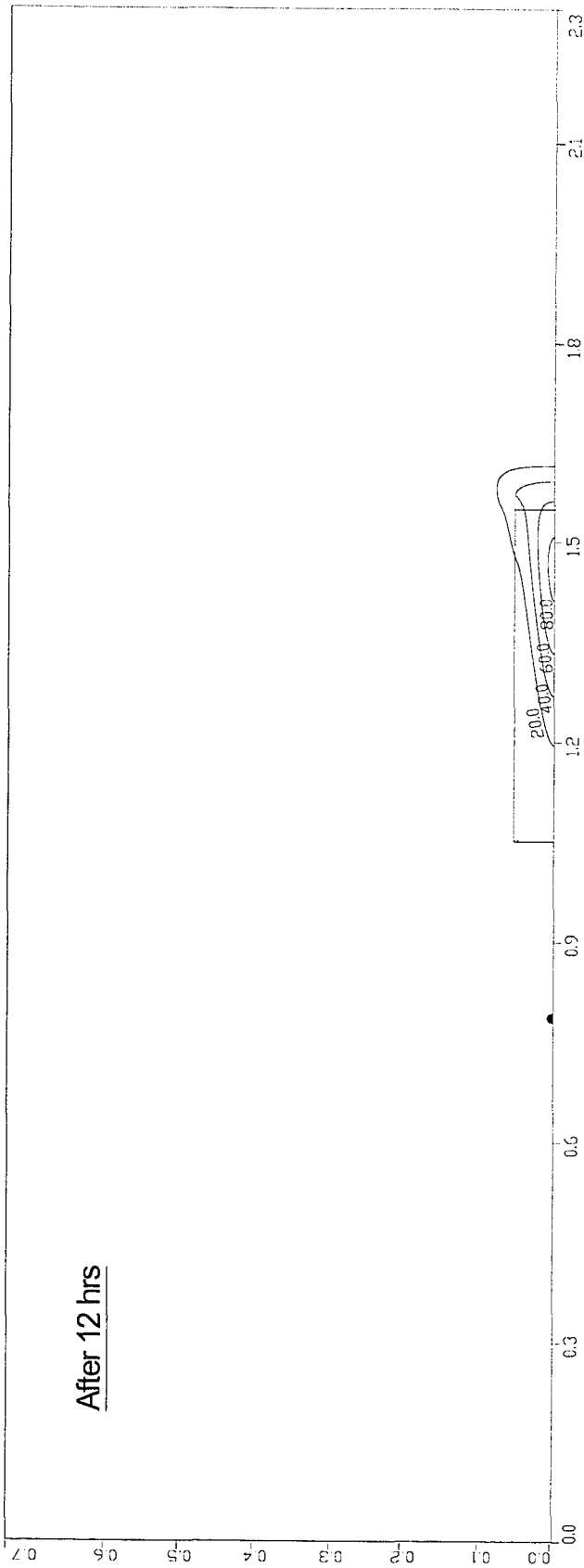


Fig. 6.53 Plume contours for the 10 cm sand-gravel system after 12 hrs.

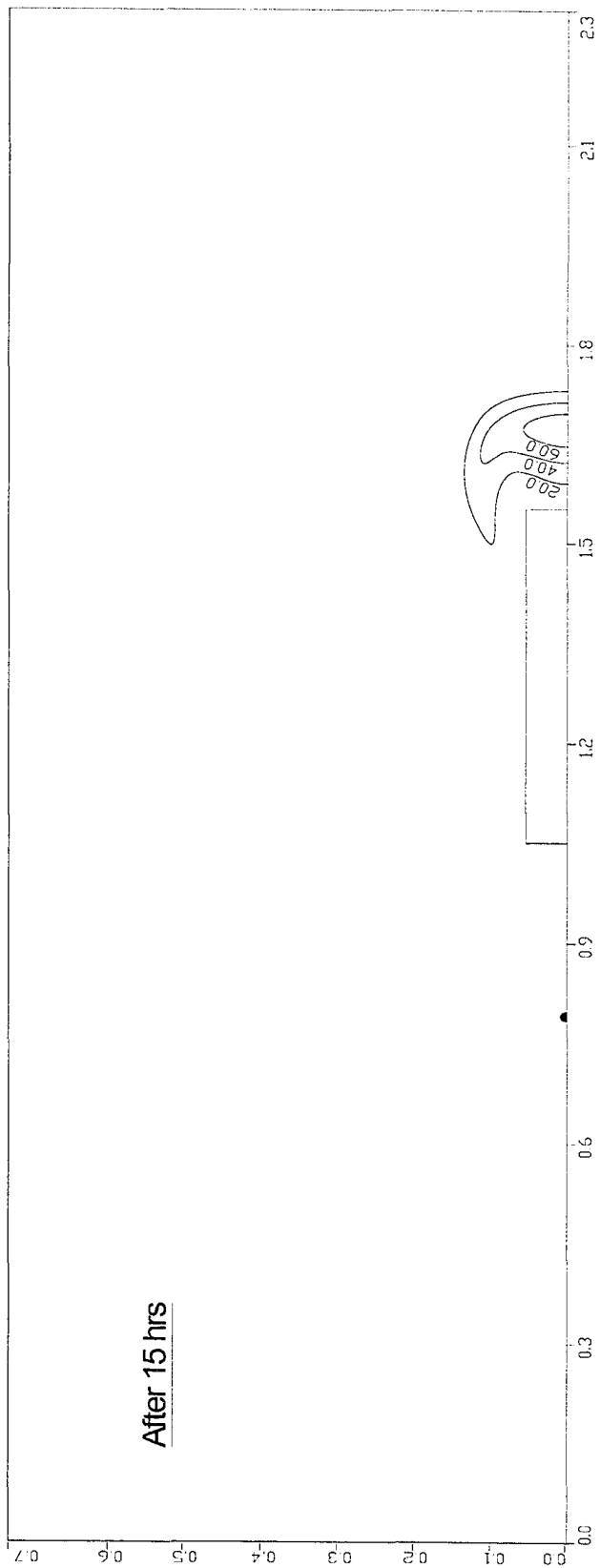


Fig. 6.54 Plume contours for the 10 cm sand-gravel system after 15 hrs.

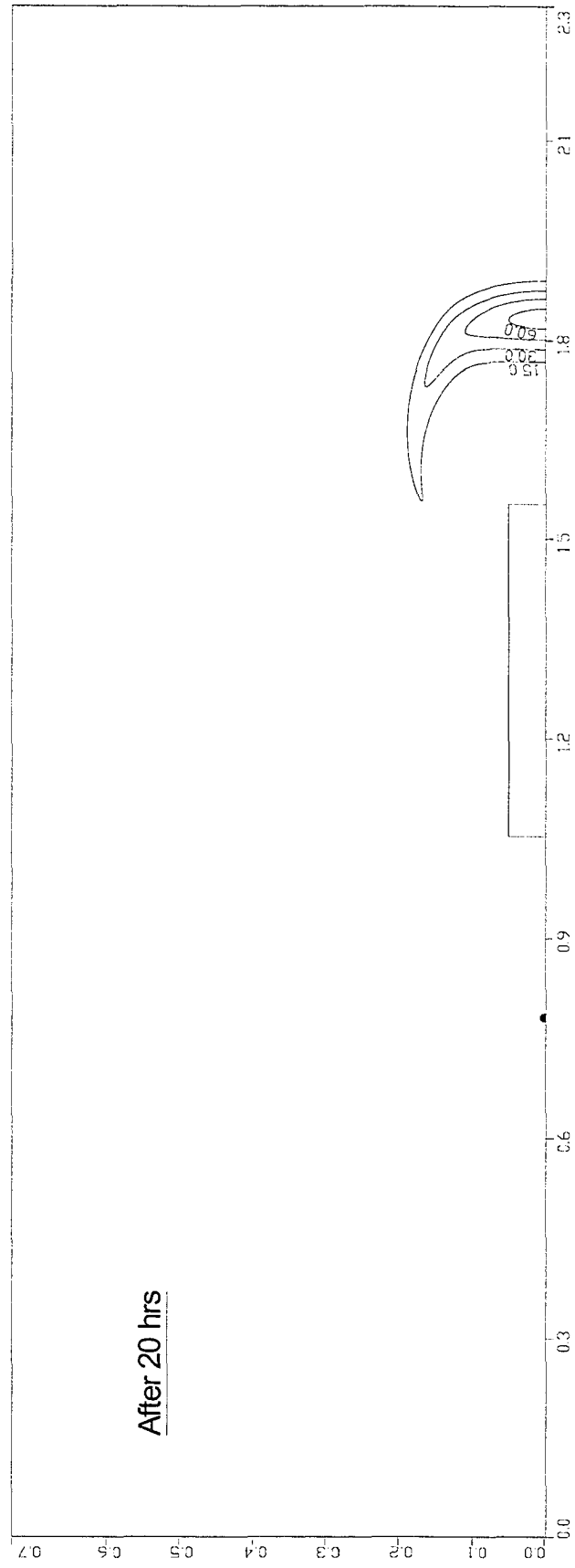


Fig. 6.55 Plume contours for the 10 cm sand-gravel system after 20 hrs.

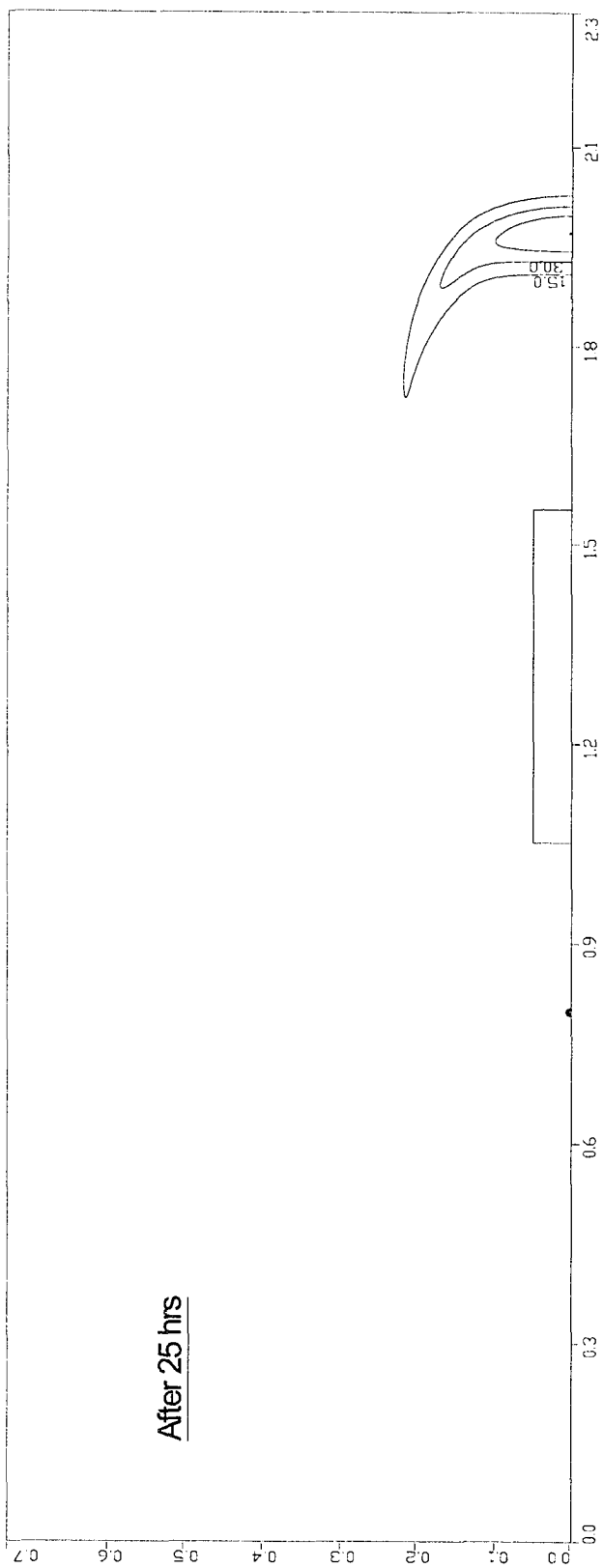


Fig. 6.56 Plume contours for the 10 cm sand-gravel system after 25 hrs.

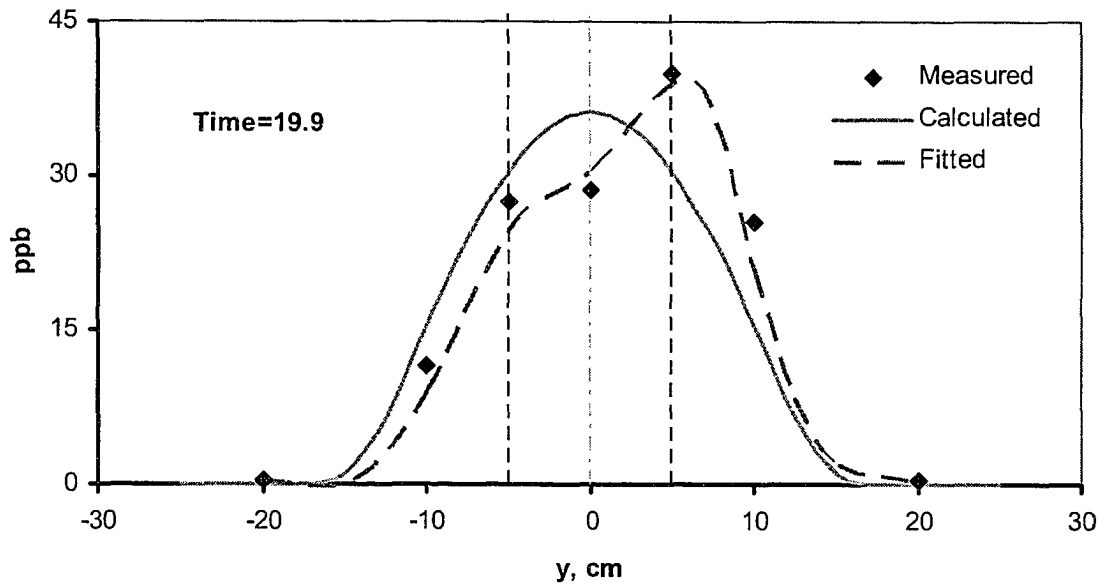


Fig. 6.57 Comparison of measured and simulated transverse concentration profile after 19.9 hours for the 10 cm gravel scenario.

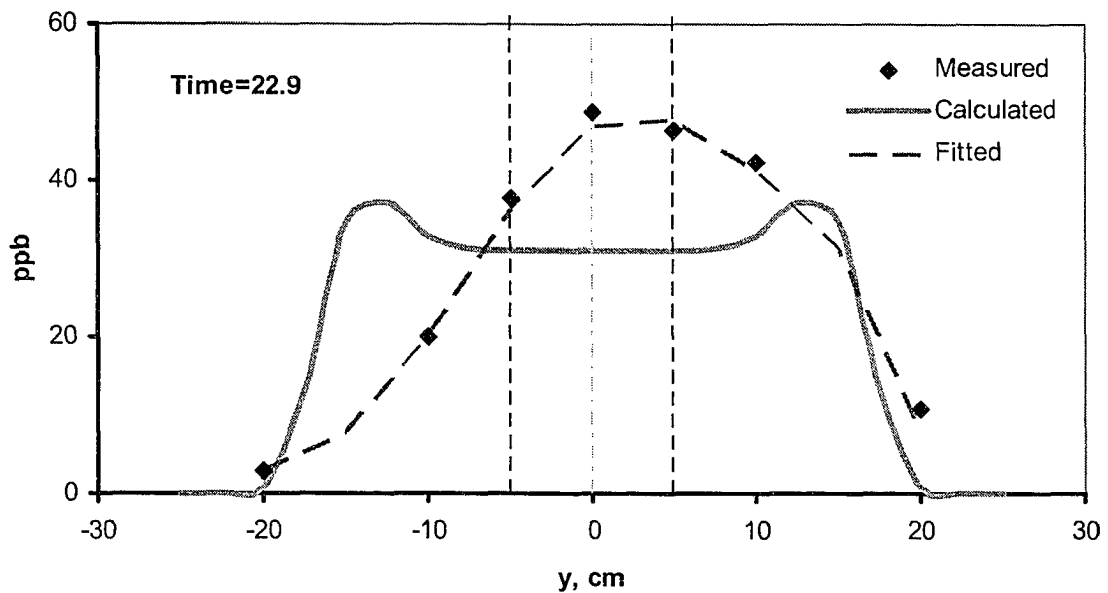


Fig. 6.58 Comparison of measured and simulated transverse concentration profile after 22.9 hours for the 10 cm sand-gravel system.

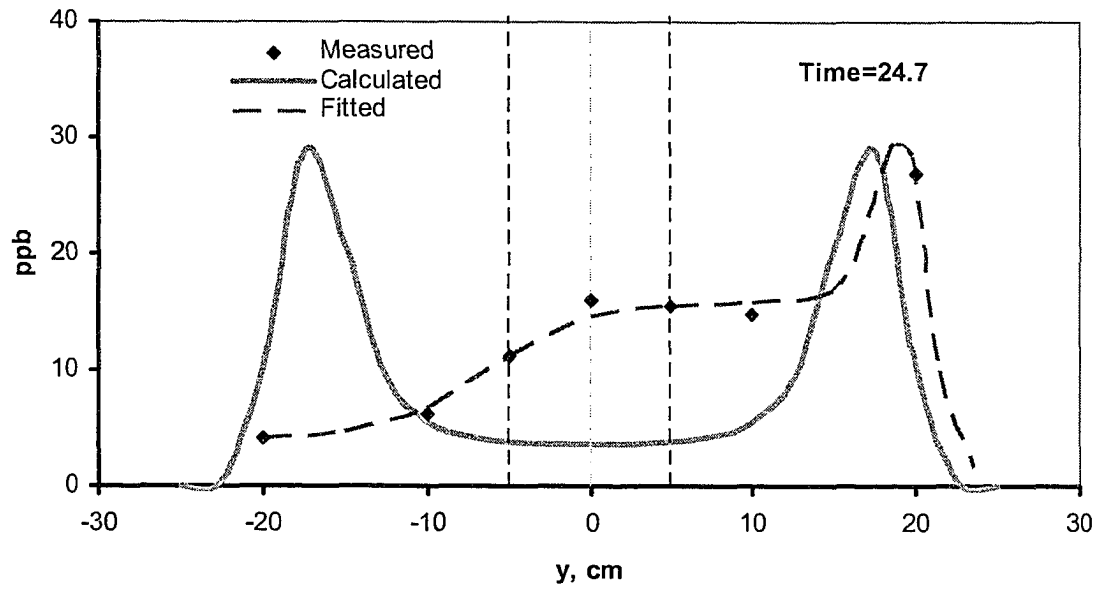


Fig. 6.59 Comparison of measured and simulated transverse concentration profile after 24.7 hours for the 10 cm sand-gravel system.

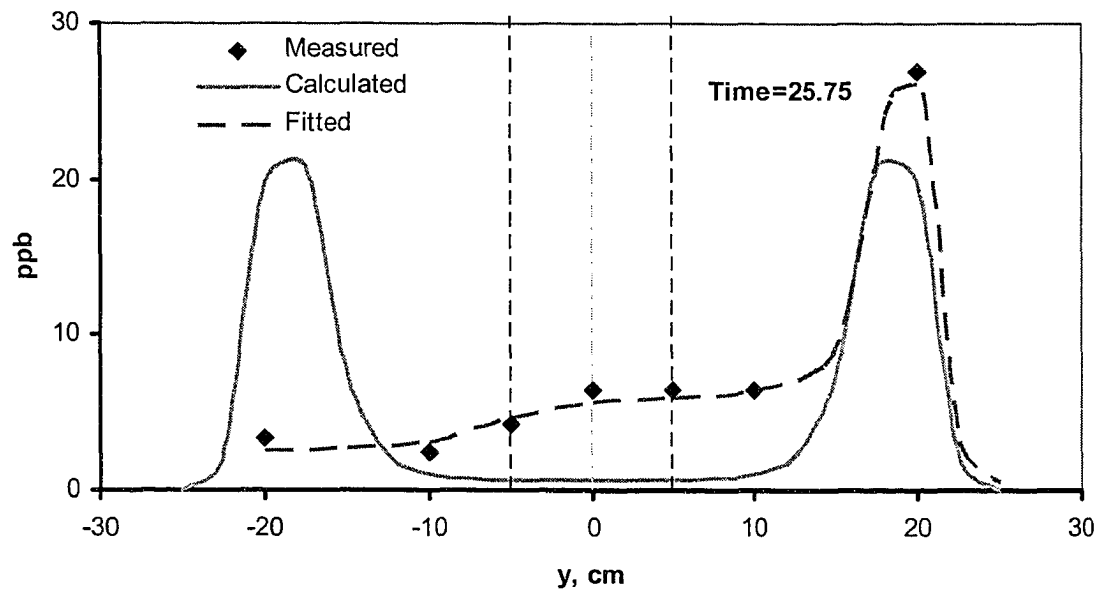


Fig. 6.60 Comparison of measured and simulated transverse concentration profile after 22.75 hours for the 10 cm sand-gravel system.

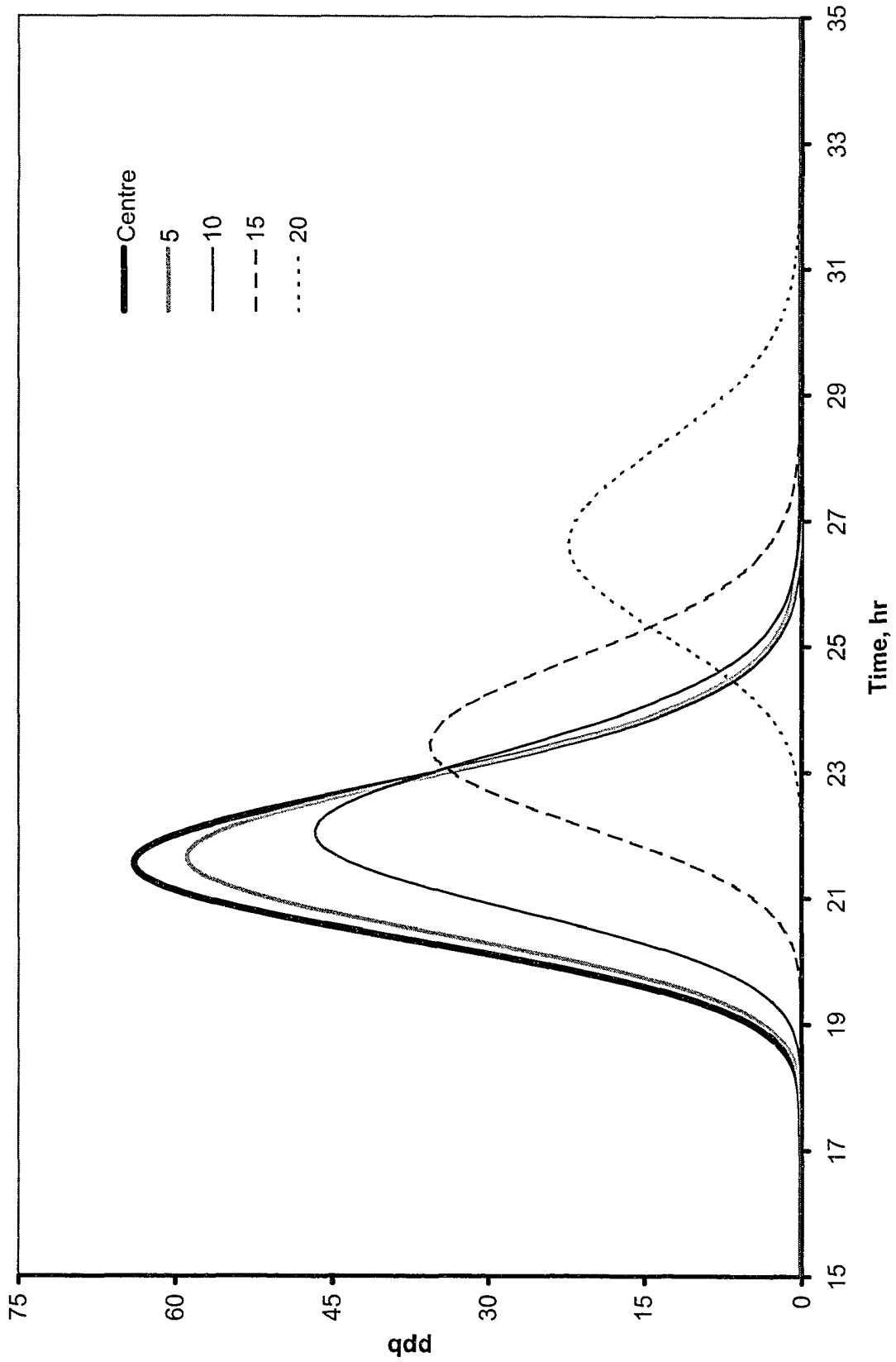


Fig. 6.61 Calculated concentration history at measuring ports for the 10 cm sand-gravel system.

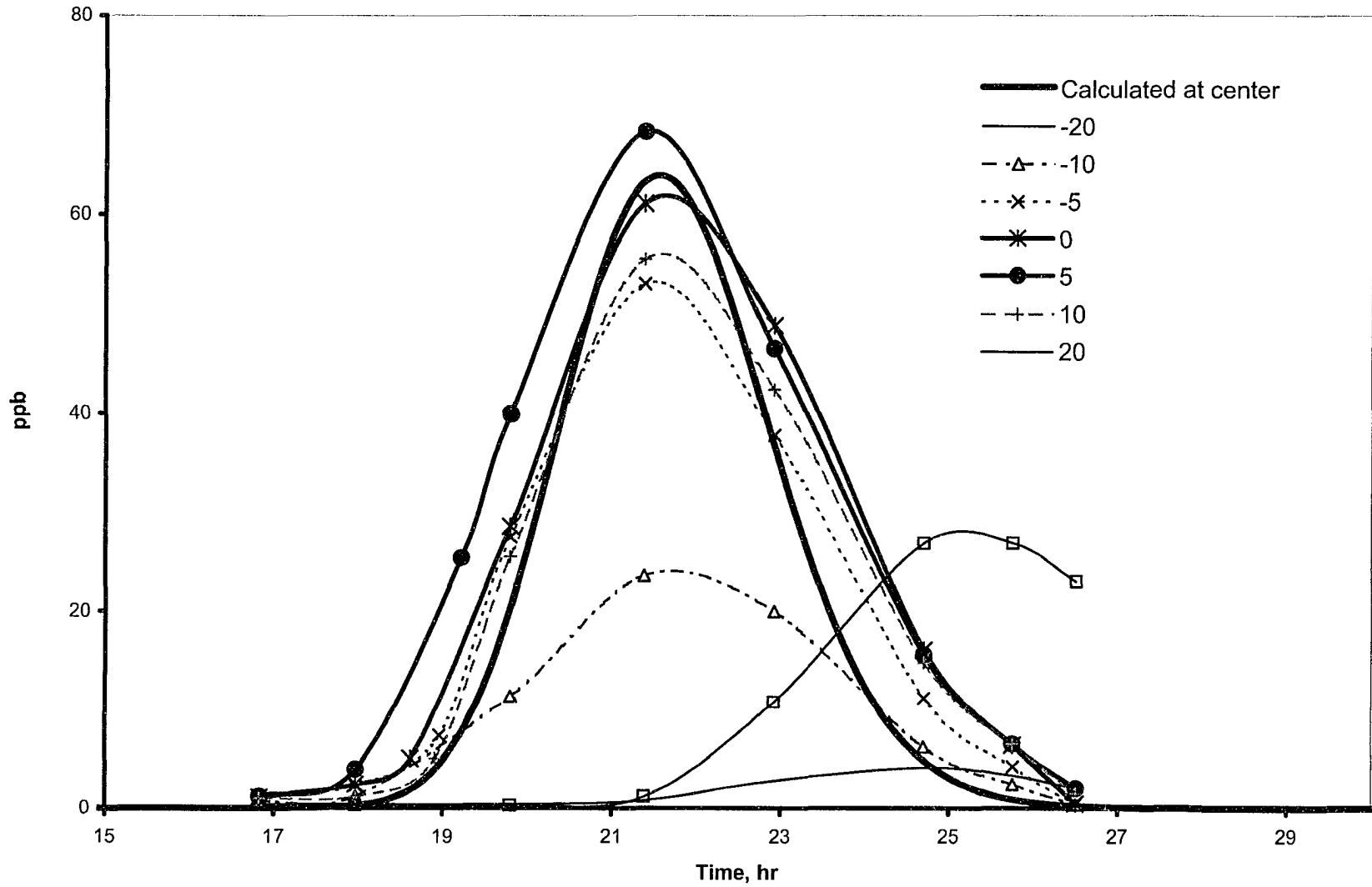


Fig. 6.62 Measured concentration history at measuring ports as well as that calculated at center for the 10 cm sand-gravel system.

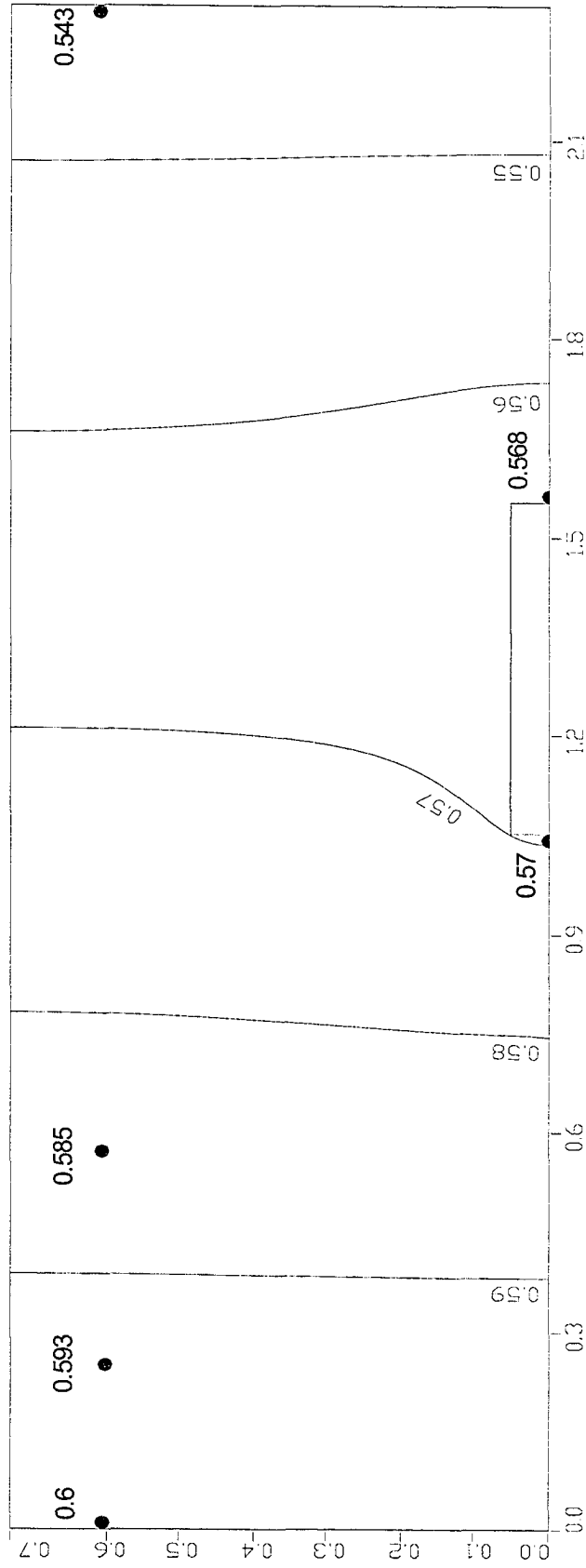


Fig. 6.63 Hydraulic heads distribution for the 5 cm sand-gravel system.

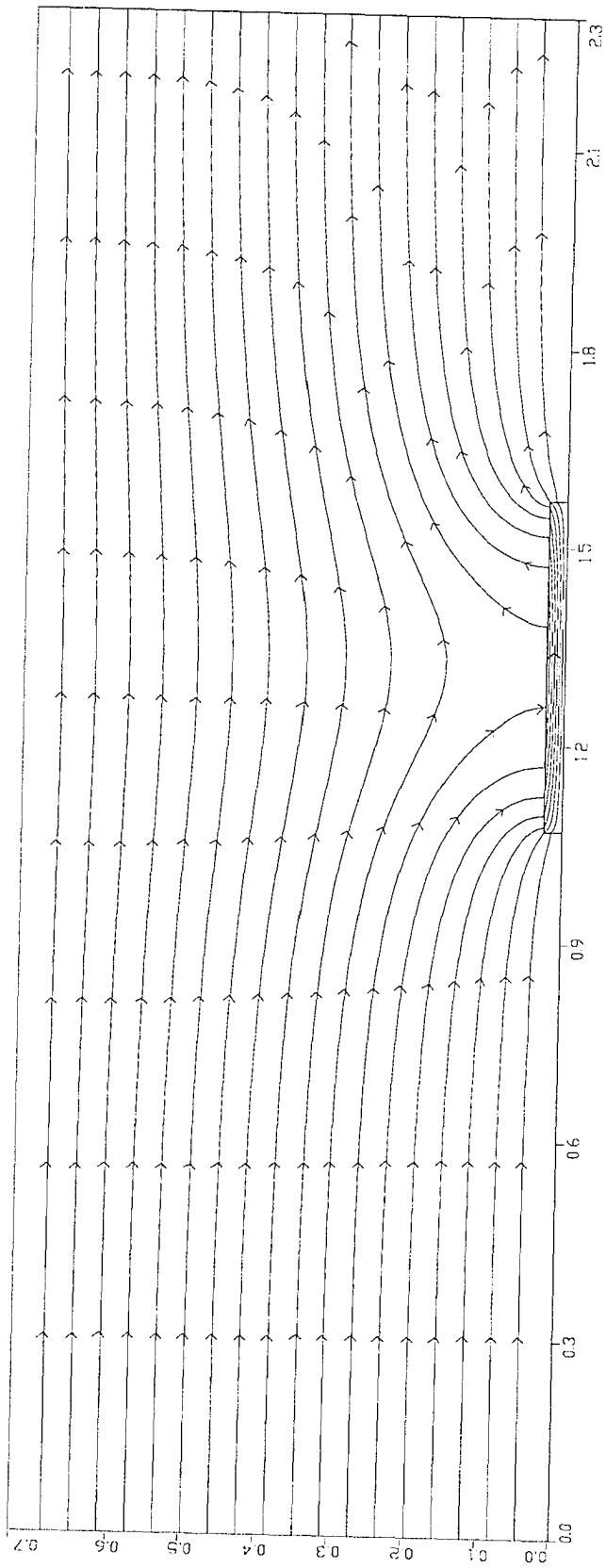


Fig. 6.64 Flow lines for the 5 cm sand-gravel system.

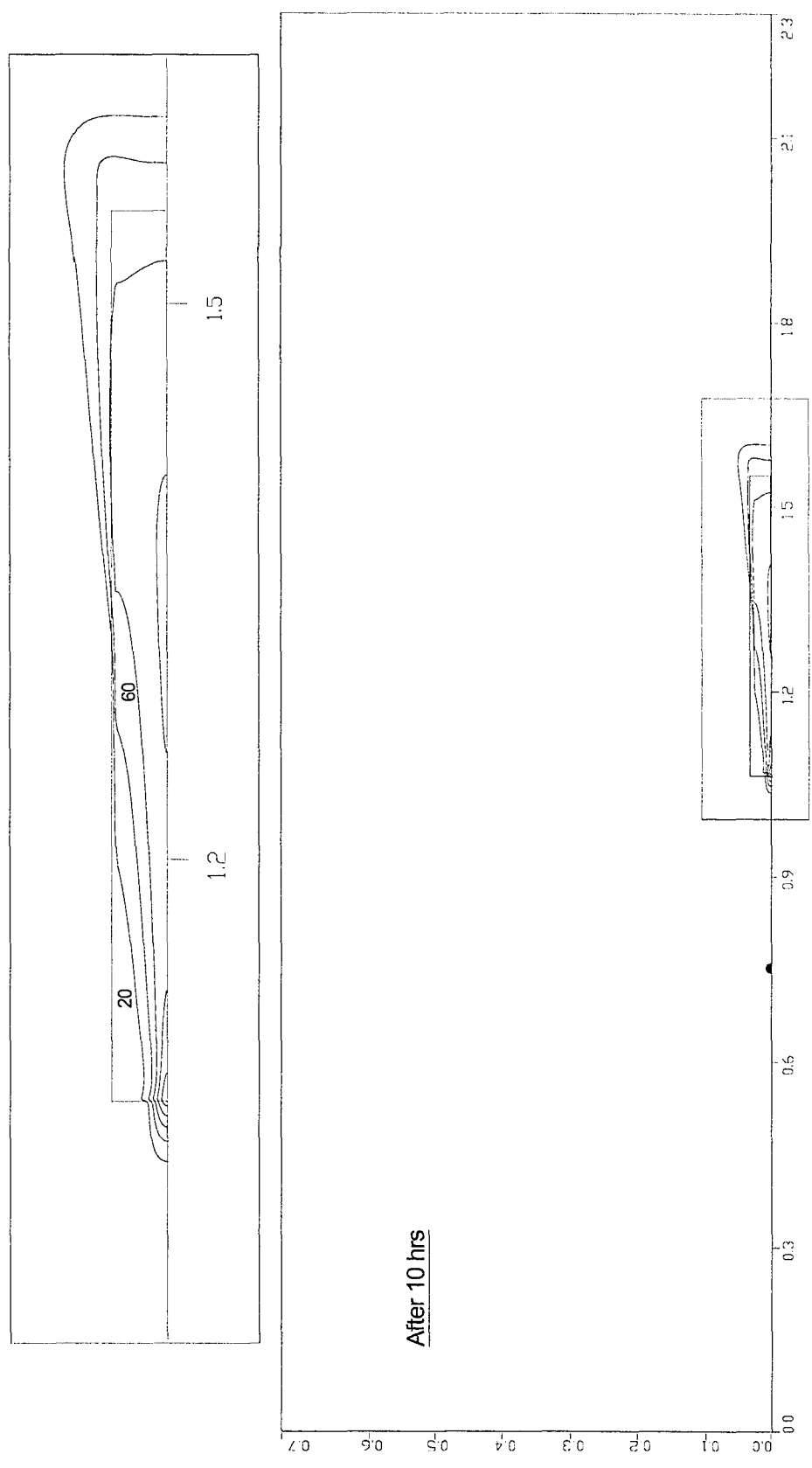


Fig. 6.65 Plume contours for the 5 cm sand-gravel system after 10 hrs.

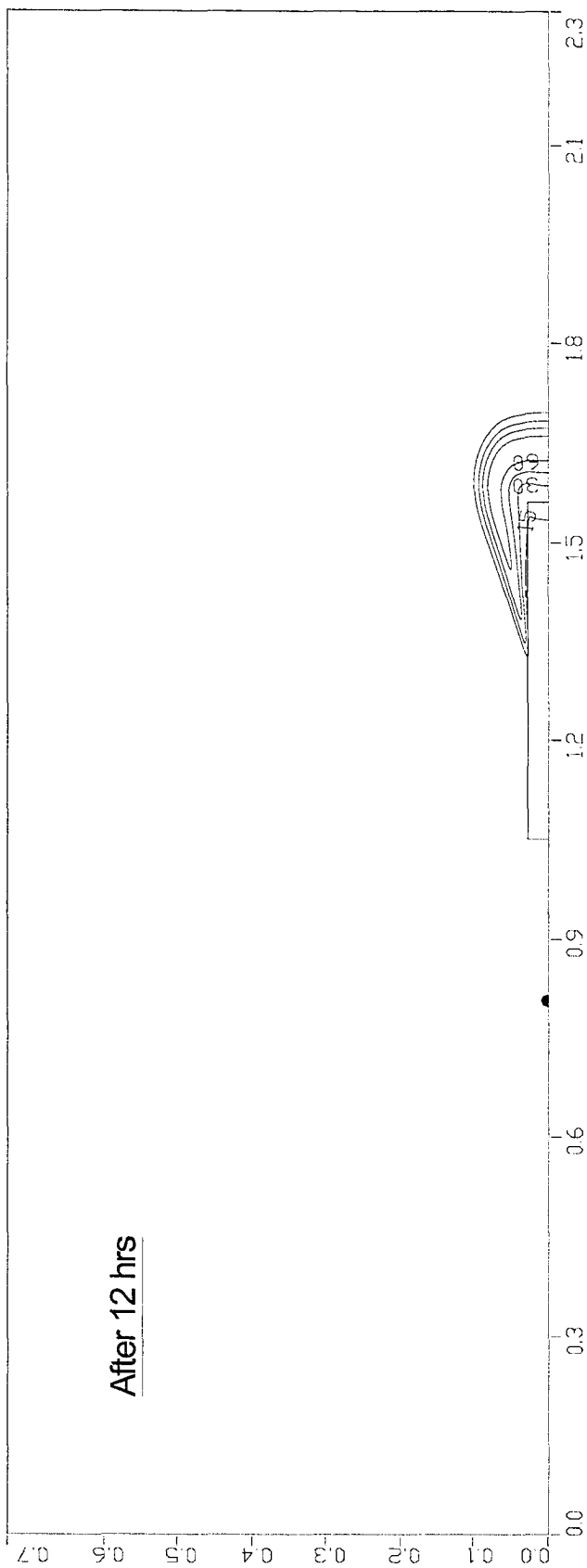


Fig. 6.66 Plume contours for the 5 cm sand-gravel system after 12 hrs.

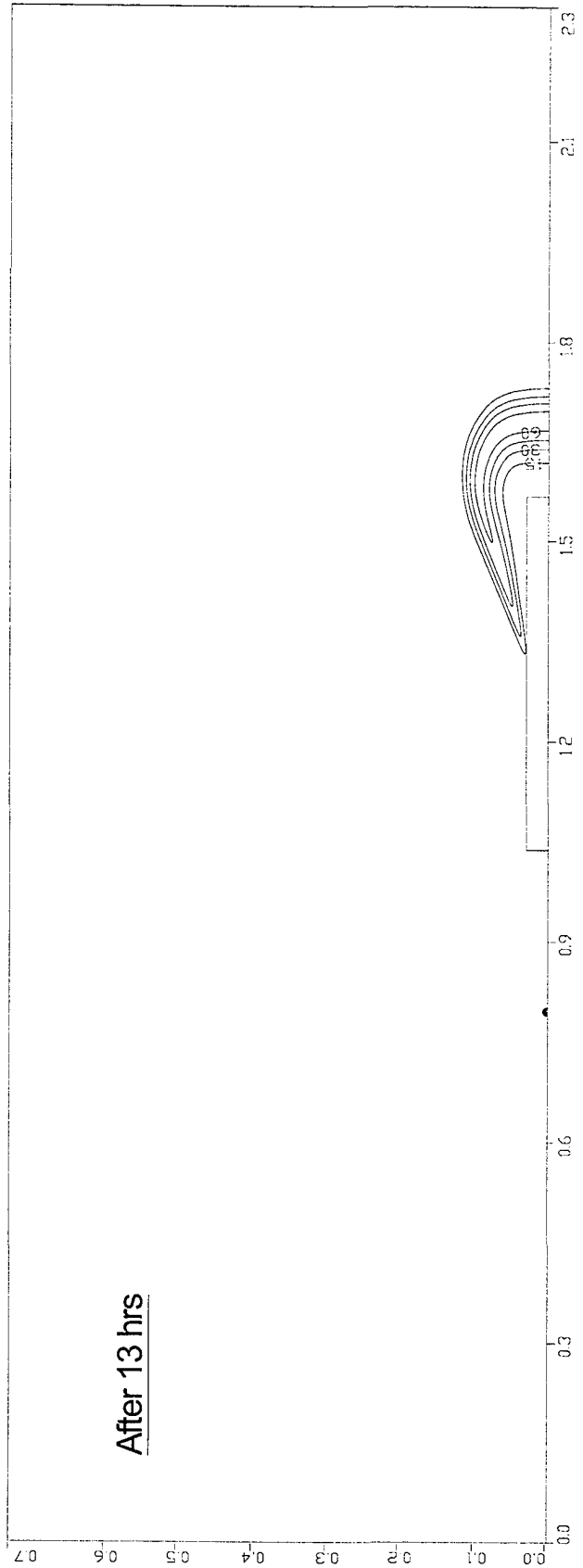


Fig. 6.67 Plume contours for the 5 cm sand-gravel system after 13 hrs.

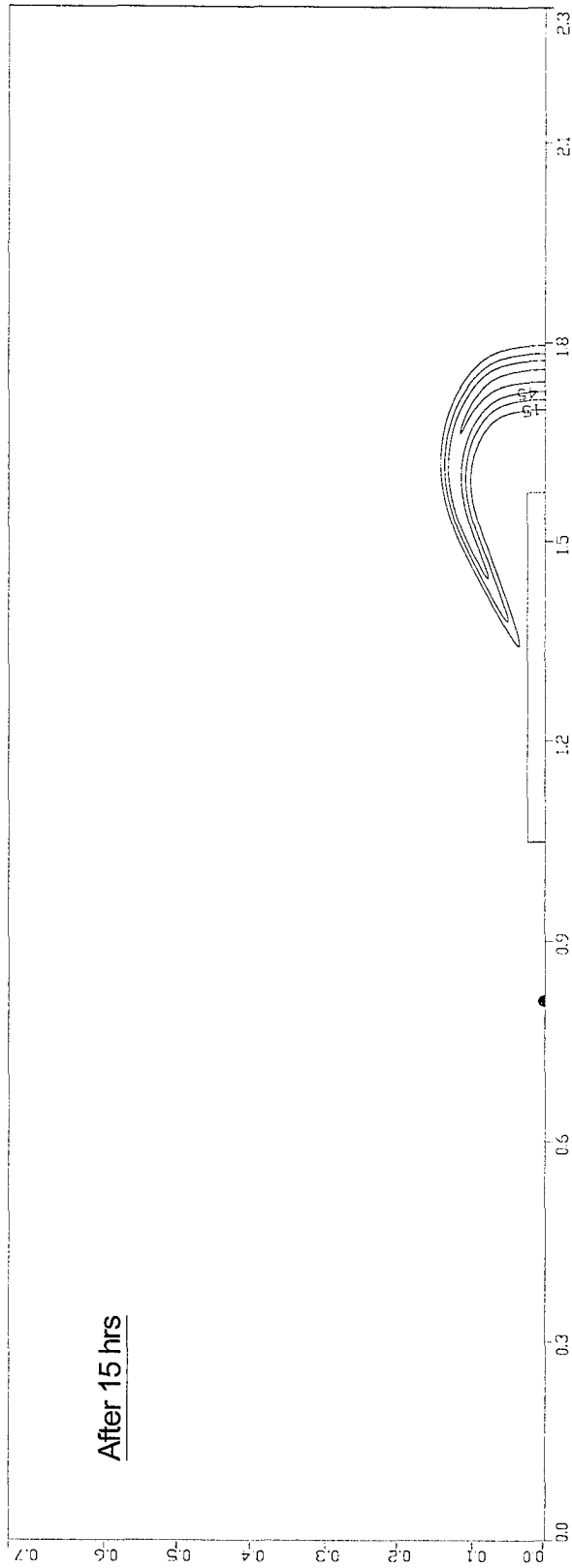


Fig. 6.68 Plume contours for the 5 cm sand-gravel system after 15 hrs.

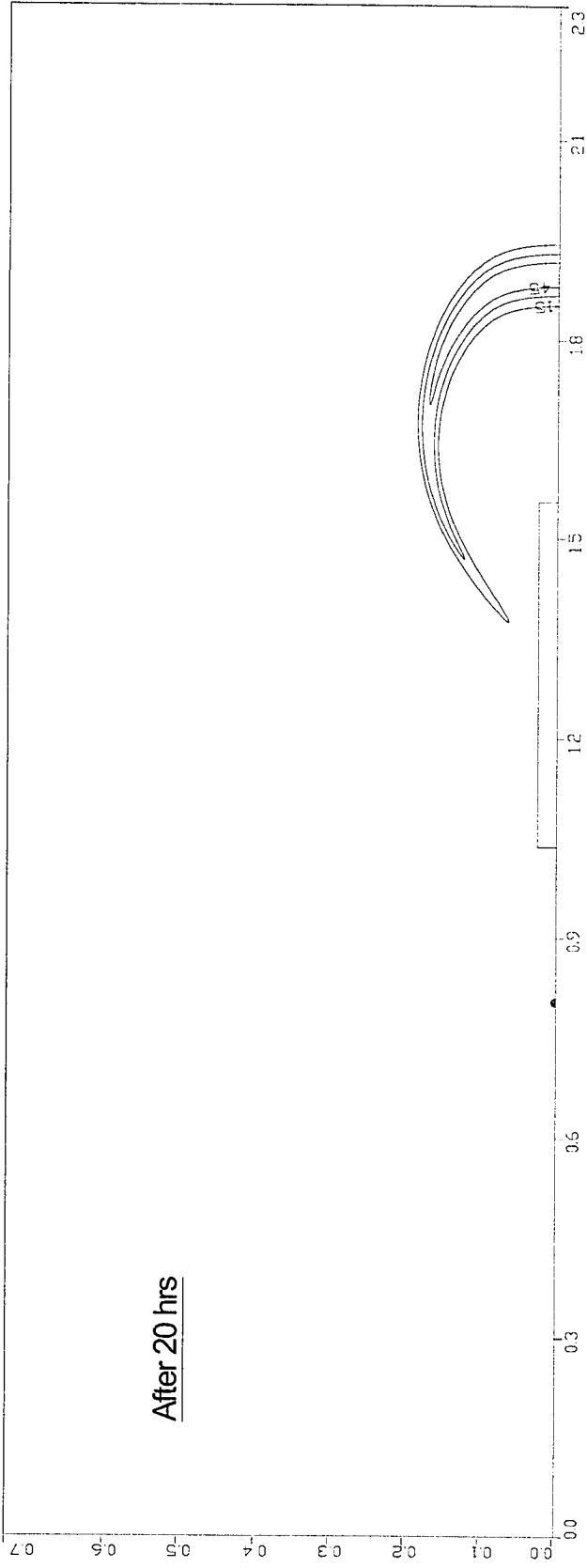


Fig. 6.69 Plume contours for the 5 cm sand-gravel system after 20 hrs.

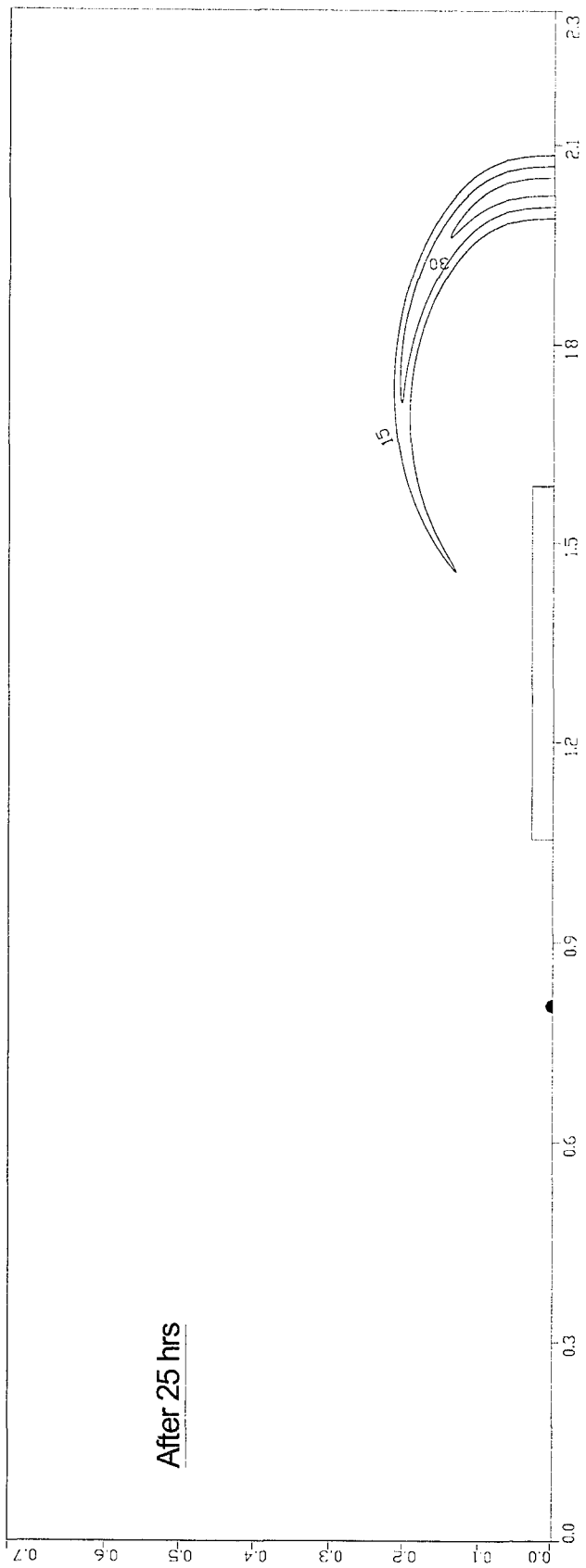


Fig. 6.70 Plume contours for the 5 cm sand-gravel system after 25 hrs.

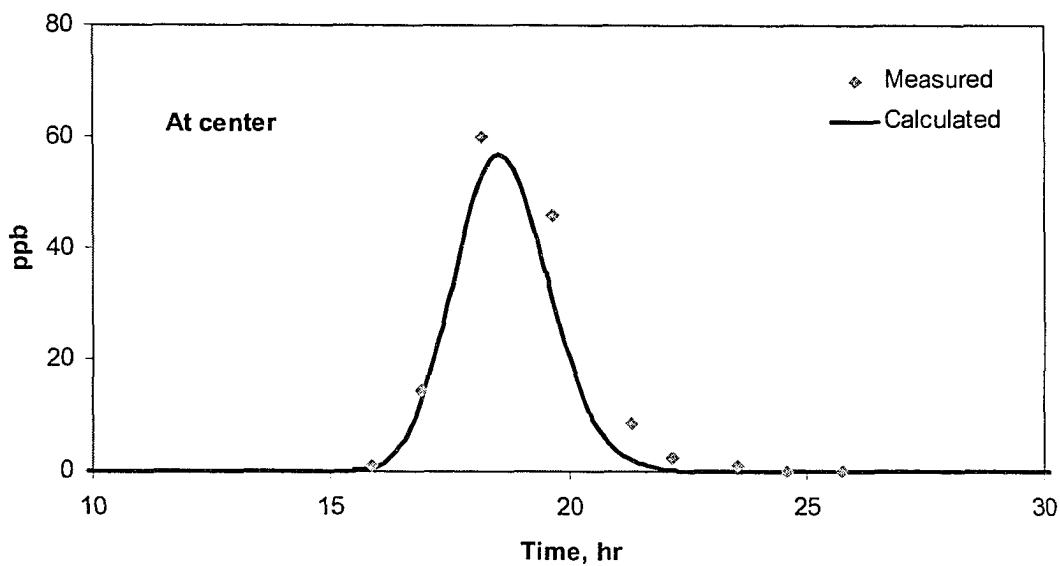


Fig.6.71 Comparison of measured and simulated concentration history at center for the 5 cm gravel scenario.

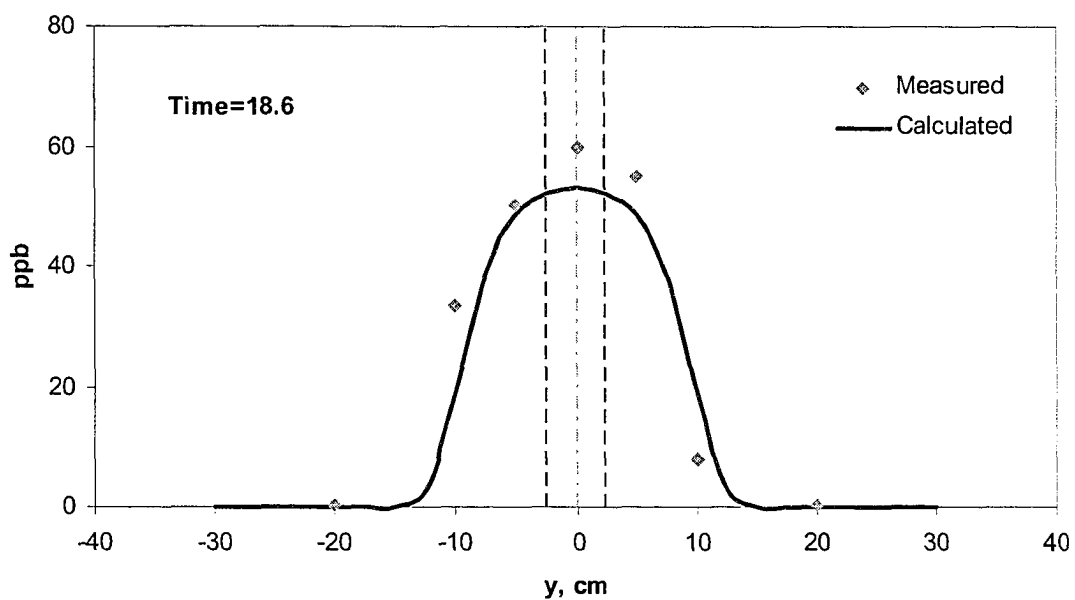


Fig. 6.72 Comparison of measured and simulated transverse concentration profile after 18.6 hours for the 5 cm gravel scenario.

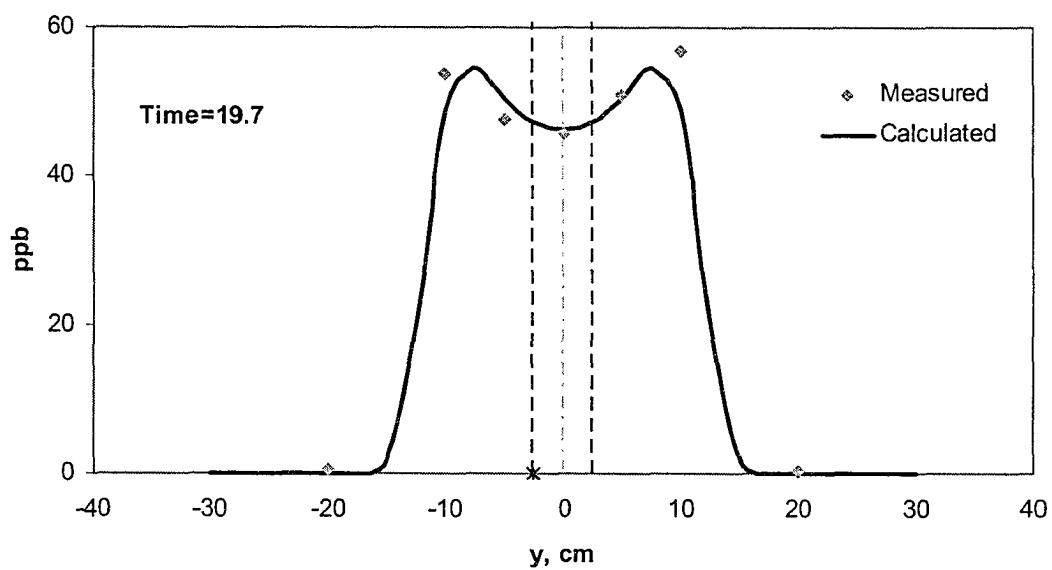


Fig. 6.73 Comparison of measured and simulated transverse concentration profile after 19.7 hours for the 5 cm gravel scenario.

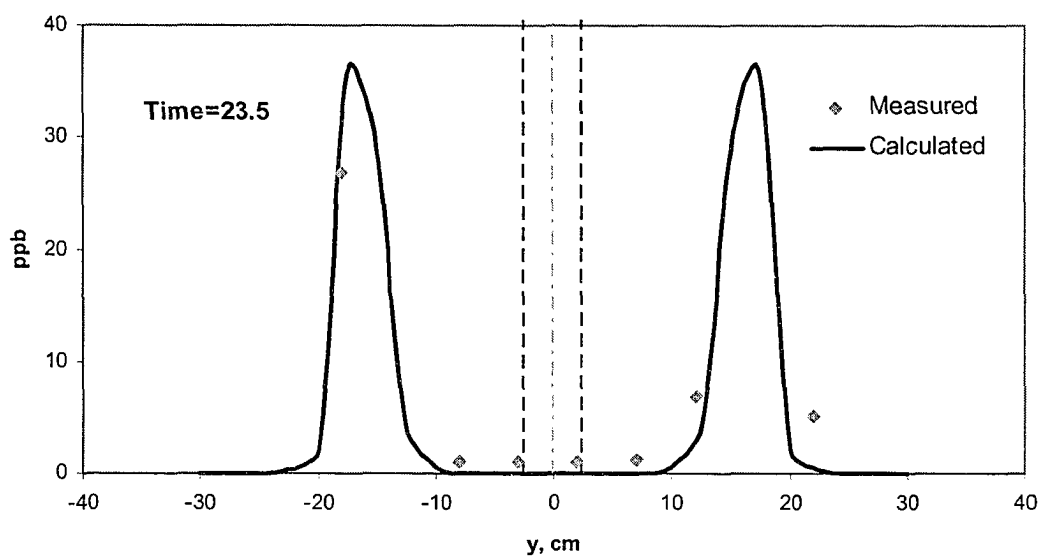


Fig. 6.74 Comparison of measured and simulated transverse concentration profile after 23.5 hours for the 5 cm gravel scenario.

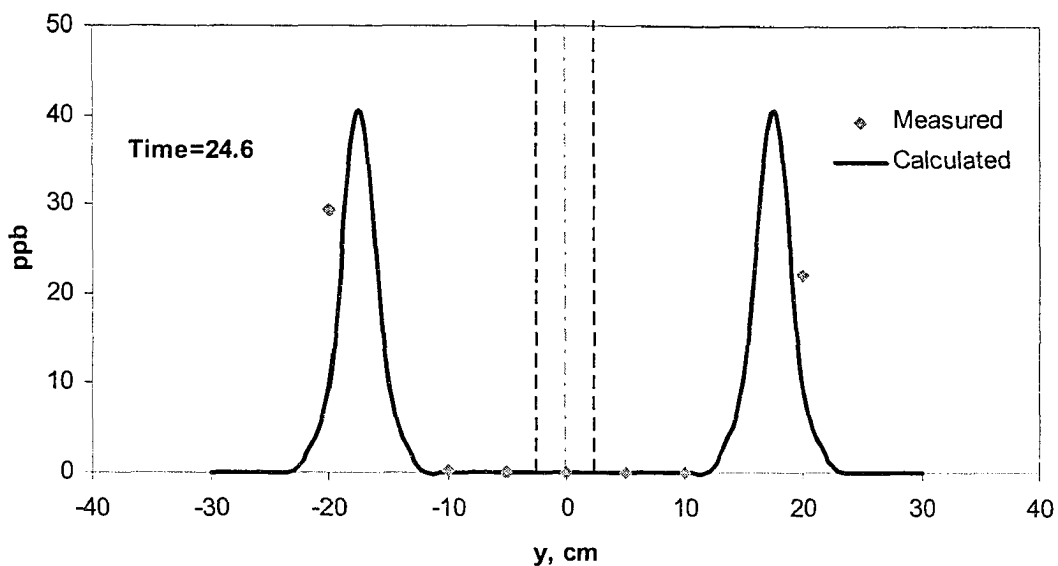


Fig. 6.75 Comparison of measured and simulated transverse concentration profile after 24.6 hours for the 5 cm gravel scenario.

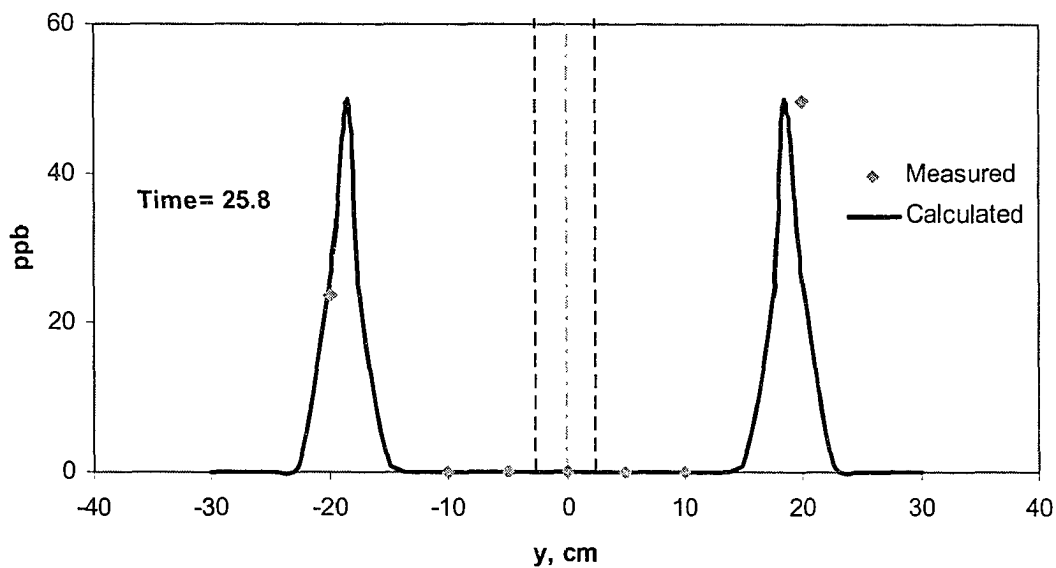


Fig. 6.76 Comparison of measured and simulated transverse concentration profile after 25.8 hours for the 5 cm gravel scenario.

## CHAPTER 7

### CONCLUSIONS AND CONTRIBUTIONS

The findings of this work may be categorized into two main themes. The first one describes the main output of the parametric study that was conducted to study issues related to TMF in northern Saskatchewan. And the second emphasizes the main findings of the experimental and numerical work to address the significance of violating the continuum hypothesis on model simulation.

#### 7.1 On the Parametric Study.

The parametric study has shown the complexity of the TMF system. Groundwater flow and solute transport have been shown to be impacted by permeability contrast between the different zones. The main findings of the parametric study may be summarized as:

- It has been shown that the initial solute concentration profile at the tailings/sand interface needs to be accurately modeled in order to correctly predict the downgradient concentration and mass flux. The need for a finer mesh, especially in the vicinity of the interface boundaries between different zones, has been demonstrated.
- The pervious surround was shown to reduce solute concentrations downgradient the TMF as well as the mass flux out of the domain in comparison to a no surround scenario. By providing groundwater with a

path of low resistance around the tailings, advection through the tailings is minimized and hence the rates of solute release are minimized.

- The permeability of the sand layer has shown to impact groundwater flow and solute transport. The main feature of the sand layer permeability is the flushing that occurs due to the initial mass within this layer upon decommissioning. The peak concentration downgradient of the TMF is a function of the initial rate at which the mass in the sand layer is transported by advection out of this layer. The flushing is more pronounced when the sand layer permeability is higher. As the permeability of the sand layer decreases, the flushing effect in this layer gets smaller resulting in lower downgradient concentrations and mass flux. Previous studies on this issue have ignored the sand layer.

## **7.2 On the Continuum Hypothesis.**

It has been established that in order to apply the continuum hypothesis to different phenomena occurring in porous media, certain length scale constraints need to be satisfied. Three major length scale constraints were defined such that proper macroscopization may result. The first of which ensures that pore scale heterogeneity is no longer influencing the macroscopic quantities. The second ensures that the extent of the domain is large enough such that the boundary effects may not be significant. And the third length scale constraint ensures that the variations of the averaged conservative quantities within the averaging volume be linear. Although other authors introduced this constraint during their

mathematical manipulations to generate averaged conservation laws, it has been introduced in this work in another context. In this work, it has been introduced as a requirement for proper macroscopization not as a consequence of certain mathematical manipulations.

In situations where there exist parts of a given porous medium domain with different properties, length scale constraints need to be satisfied for each zone. Recognizing the difficulties in satisfying these constraints in the vicinity of interface boundaries separating different regions, it has been recommended to extend the properties of the different regions to where the interfaces exist. The errors generated in doing so are expected to be insignificant to the overall behavior of the system. Measurements in the vicinity of the interface boundaries, however, are inappropriate and will not reveal any useful information regarding the behavior of the system.

In situations when there exist regions in the porous medium domain where length scale constraints are not satisfied, then the most appropriate technique would be to average over the thickness of this region and to deal with it as a two-dimensional domain encompassed in a three dimensional region as suggested by Hassanzadieh and Gray. However, this technique has several disadvantages in determining some of the parameters suggested when conducting the averaging.

This study is unique in the sense that no previous experimental work has been proposed for the sole purpose of determining the behavior of a system

when violating the continuum hypothesis for porous media. Moreover, it has far reaching conclusions, which may be summarized in the following points:

1. When the thickness of the pervious layer was small, on the order of 5 mean grain diameters or less, and the length scale constraints violated, reasonable agreement was obtained when comparing the measured downgradient concentrations with simulated values when the macroscopic properties were used for the simulation. This of course does not imply that the length scale constraints are irrelevant. The reason for the good match was twofold. First, the experimental and model results indicated that the solute spread across the entire thickness of the pervious layer even though the processes may have differed between the experiment and the model (i.e., channeling and dispersion towards the centre of the pervious layer for the experiment and dispersion from the centre of the layer to the edges of the pervious layer for the simulation). Second, the sampling location was at a sufficient downgradient distance such that sufficient mixing/dispersion occurred between the exit of the pervious layer and the sampling location.
2. As the thickness of the pervious layer was increased, no reasonable match was obtained between measurements (30 cm downgradient the gravel zone) and simulation based on macroscopic properties of the pervious layer due to the violation of the length scale constraints in this layer. For this particular system, it was found that channeling of flow along the interface boundaries was a significant factor. This revealed the fact

that when the extent of the domain was not large enough, the second length scale constraint was violated. The match between the experimental data and the model simulations may also be a function of the sampling location. Had the sampling location been further downgradient, such that the impact of channeling on the measured concentrations was reduced due to mixing/dispersion that occurs between the exit of the pervious layer and the sampling points, the match between the experimental data and the model simulations may have been better.

3. In line with the two previous conclusions, one may state that there exists a region downgradient or surrounding the pervious region where the impacts of violating the length scale constraints are pronounced and where one should expect that there may not be good agreement between measured and simulated data. Beyond this region, the impacts of violating the length scale constraints are reduced as sufficient averaging/mixing has occurred between the pervious layer and the sampling location and hence one can expect a better match. The size of this region may be a function of the ratio of the length to the width of the pervious layer. As the width decreases and the length increases, complete mixing across the layer occurs and the region impacted by the violation of the length scale constraints is reduced.
4. The impacts of channeling are case dependent in the sense that for different configurations or setups, channeling may not be very severe. As a matter of fact, in natural systems where gradation in the structure of the

material at the interface boundaries is likely to occur, channeling may not be significant. From the point of view of modeling systems where channeling may be significant, one may need to introduce a high hydraulic conductivity layer (many order of magnitudes of that of the pervious layer for our system) to allow for this effect in the simulations. However, it is difficult to estimate the flow and transport parameters needed to represent the interface and the applicability of the continuum approach across this interface is questioned.

5. Even with the presence of channeling, the downgradient peak concentrations measured in all the scenarios were not significantly different (within 14%) than that suggested by simulation. This point is important, in a sense, because the peak concentrations are often used as a design criteria based on the allowable concentrations determined by licensing authorities.
6. This study has been based on the assumption of a conservative contaminant for which the source term was well defined. Within the vicinity of the pervious layer, the processes were limited to advection, dispersion and diffusion. For a complex field scenario with a reactive tracer and a variable or uncertain source term, the number of processes within the vicinity of the pervious layer that impact the downgradient concentrations is large. In this study for a conservative tracer, it was found that the processes in the vicinity of the pervious layer were not well represented and the detail at the local scale was lost. In the case of a complex field

scenario, these processes will have a significant impact on the source concentrations, etc. and hence the impacts of violating the length scale constraints may be increased.

### **7.2.1 Conclusions related to the TMFs in Northern Saskatchewan.**

It is clear that the length scale constraints defined for the continuum approach to be applicable are violated in the vicinity of the pervious surround. However, based on the results presented in this thesis, the following general conclusions can be drawn with respect to the impacts of these violations on the simulated flow and transport at a TMF.

1. Channeling may occur at the host rock/surround interface or the sand/surround interface. One way to address this may be to increase the hydraulic conductivity of the pervious layer to include the impact of channeling. Another alternative is to include a thin zone of higher permeability at the interface. In both cases, it is not clear how to adjust these parameters, it is case dependent, and the length scale constraints are still violated. A parametric study or sensitivity analysis is required to address the uncertainty in these parameters. The worse case or conservative scenario should be considered and the model calibrated as field data become available.
2. The sampling locations used for model calibration are important. Calibrating to concentrations measured in the immediate vicinity of the pervious surround would be inappropriate given the variability one should

expect in the regions where the length scale constraints are violated. The experimental results presented in this study indicate that the impacts of any violations in the length scale constraints are reduced as you move further downgradient of the pervious layer. Hence, concentrations measured at distances significantly downgradient of the TMF should be used to calibrate a model.

3. In regions where the length scale constraints are violated, one should not compare measured and simulated data as the processes are not well represented in this region. In the case of the TMF, the processes occurring within the pervious surround may have a significant impact on the mobility and fate of contaminants contained in the tailings. For this scenario, one's confidence in the numerical model's ability to simulate these processes based on the continuum approach is reduced. Given that the alternatives are limited, one should consider a worst case or conservative scenario.
4. It is also important to note that in dealing with a more complex field scenario, there are many uncertainties related to the soil parameters, the thickness of the pervious surround and sand layers, the presence of heterogeneities, etc. Hence, the errors associated with violating the length scale constraints may only represent a small fraction of the errors or uncertainties related to the overall model. This reinforces the need to consider the worst case or conservative scenario in the absence of field data.

### 7.3 Contributions.

The contributions of this work to science and engineering may be categorized into three main areas that represent the first three words in thesis title: theoretical, experimental and numerical investigations of flow and solute transport in saturated porous media subjected to violation of the continuum hypothesis.

1. Contribution on the theoretical basis of applying the continuum hypothesis to transport phenomena in porous media.
  - In this regard a thorough investigation of the continuum hypothesis was given. Length scale constraints defined to justify the applicability of the continuum approach in porous media were introduced.
  - The third length scale constraint was introduced and justified based on a thorough investigation of the requirements for proper averaging. This approach has not been presented in the literature. It does appear in the literature as a result of the mathematical manipulations performed in the averaging process.
  - The problems associated with the interface boundaries were identified. The available alternatives in the literature were introduced. The difficulty in dealing with intermediate regions where the continuum hypothesis may not be adopted was highlighted. The available techniques in the literature to dealing with this situation are insufficient

and even difficult to handle. This led to the experimental work presented herein to shed more light on this issue.

- Identifying the potential violation to the continuum hypothesis when modeling the TMF in northern Saskatchewan utilizing the pervious surround concept.

## 2. Contributions made by the experimental study.

- Experimental work was performed to investigate the behavior of systems under the situation when the continuum hypothesis is violated. Six, carefully designed, experimental setups were used for this purpose. The properties of the media used were carefully estimated and modeled. This experimental work is unique. To the author's knowledge, no detailed and accurate experimental work was done before for the purpose of defining the behavior of porous media systems violating the continuum hypothesis.
- Highlighting the significance of the interface boundary when length scale constraints are violated.
- Providing a recommendation in simulating similar systems when the continuum approach may not be adopted.

## 3. Contributions made by the numerical study.

- Conducting a numerical parametric study on a two-dimensional conceptual model simulating a real scale TMF in northern Saskatchewan. The parametric study highlighted the effect of the

pervious surround properties on the performance of the TMF and highlighted the role of the sand layer that is constructed between the tailings and the pervious surround and the impact of its initial concentration at decommissioning. To the author's knowledge, this has not been evaluated in any other study.

- Highlighting the need for finer mesh in the vicinity of interface boundaries where a sharp contrast in properties exists. In addition, identify the presence of excess solute mass due to discretization at the interface boundary and highlighting its effect on the downgradient concentration profile.
- Highlighting the inappropriateness of simple finite difference and finite element schemes when modeling advection dominated problems. In this case it is better to use higher order elements or method of characteristics.

## CHAPTER 8

### RECOMMENDATIONS FOR FUTURE WORK

Several ideas may be introduced for a comprehensive overview of this subject. The ideas that need to be further investigated include studying the followings:

1. The effect of grain size of the gravel layer.

This study has been based on a certain mean grain size. Different sizes are expected to affect the behavior of this system, which needs to be further investigated.

2. The effect of the interface boundary.

The interface boundary, in this experimental work, has shown to have significant impact on the behavior of the system by providing channeling to the flow. However, as was mentioned earlier, in naturally occurring geologic formations gradation of properties is likely to occur and the resistance of the interface region may be higher. Experimentally this may be achieved by adding resistance to the interface boundary (corrugated interface for example).

3. The effect of complex interfaces.

This study was also based on two media that were largely homogeneous. In cases of more complex systems, e.g. the interface between highly fractured rock system (that may be dealt with as an equivalent porous medium) and a

homogeneous porous medium where the REV in the two regions may be very different, other sophisticated theoretical as well as experimental techniques need to be explored for the study of fluid flow and contaminant transport in this complex system.

4. The effect of local heterogeneity arising during the emplacement and compaction of the gravel. This may be done by generating a stochastic realization of the permeability field.
5. Simulating the system assuming a higher permeability to the interface to mimic channeling and to correctly predict the location of the plume.
6. Consider analogues studies in which the continuum hypothesis was violated. For example, in chemical engineering reactor design.
7. Consider modeling the pervious layer as a two-dimensional domain encompassed within a three-dimensional region as suggested by Hassanizadeh and Gray. In this case one may utilize planar elements similar to those used when modeling fractures. It should be mentioned, however, that the parameters introduced by this approach may be used as fitting parameters.
8. Consider glass bead experiments to visualize the impacts of channeling, dispersion, etc., and to further assess the impacts of violating the length scale constraints.

# **Appendix A**

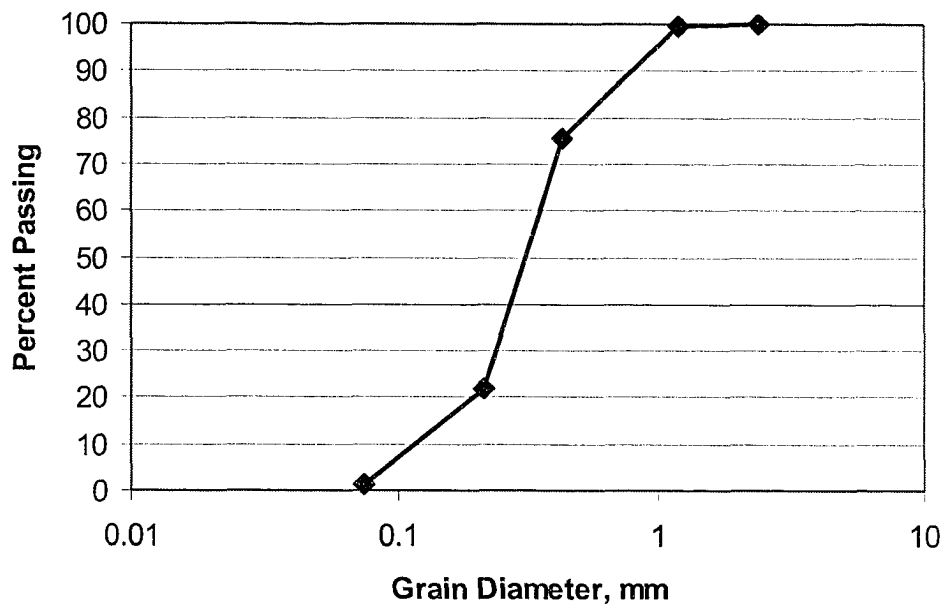
## **Estimating Sand and Gravel Properties**

## Sieve Analysis on Mortar Sand

From West (2000)

	Tare Mass	Tare + Sand	Sample	Hole Size	% passing
Big	318.76	598.61	279.85		100
8	108.56	108.75	0.19	2.38	99.93
16	106.35	107.85	1.5	1.19	99.39
40	129.19	129.23	66.65	0.425	75.36
70	119.9	268.26	148.36	0.212	21.87
<200	127.71	185.03	57.32	0.075	1.2
	324.43	327.78	3.35		0
			277.37		

Grain Size Analysis - Mortar Sand



**In-Situ porosity Measurements - Sand**

Mass of Dry Soil, g	Volume of hole, ml	Porosity
1650	997.8	0.376
1793	1098.4	0.384
1233	750.5	0.38
1542	935.5	0.378

Average porosity	0.3795
Std	0.0034

## In-Situ Hydraulic Conductivity Testing, Sand

Height= 0.6 m

Width= 1.45 m

ml/min	Head difference, cm	K, m/s
92	4.5	9.01E-05
102	5	8.99E-05
112	5.5	8.97E-05
123.5	6	9.07E-05
132.5	6.4	9.12E-05

Average K	9.03E-05	m/s
Std	6.23E-07	

### Effect of lowering upgradient reservoir water level on plume arrival time.

Volume injected	1	ml
Conc.	9000	ppb
Porosity	0.38	
Volume of water	2.94E-06	m <sup>3</sup> /s

Upstream	0.5	m
Av. Height	0.465	
Area	0.6789	m <sup>2</sup>
Darcy's Vel.	4.32919E-06	
Average Vel.	1.11005E-05	m/s

hr	min	s	Time, hrs	ppb
15	1	0	15.017	104.47
15	13	0	15.22	192.03
15	23	20	15.39	274.62
15	34	20	15.57	344.62
17	1	55	17.03	454.55
17	29	45	17.5	311.5
17	44	40	17.74	185.53
18	0	20	18.01	113.35
18	18	35	18.31	67.71
18	36	5	18.60	37.02
18	57	10	18.95	20.15

## Dispersivity in sand

### Point Source Experiments

#### Setup #1

Width, m	1.46
Height, m	0.7
Area, m <sup>2</sup>	1.022
Porosity	0.38
Darcy Vel, m/s	2.46276E-06
Seepage Vel, m/s	6.27454E-06
Volume injected, ml	1
Conc.	10000

#### Measurements @ 50 cm

hr	min	Time	ppb
18	8	18.13	10.1
18	43	18.717	31.5
19	3	19.05	73.8
19	37	19.62	175.5
20	3	20.05	273.7
20	36	20.6	369.5
21	0	21	463
21	20	21.33	526
22	55	22.92	473.6
23	10	23.17	385.1
23	53	23.88	266.8
24	23	24.38	183.6
25	3	25.05	120.2
25	42	25.7	73.4
26	27	26.45	37.1

#### Measurements @ 61.5 cm Run#1

hr	min	Time, hr	ppb
21	44	21.73	1
23	30	23.5	3.3
24	4	24.07	23.6
24	44	24.73	79.2
25	25	25.42	223
26	4	26.07	411.7
27	0	27	498.5
27	28	27.47	463.9
28	51	28.85	220.4
30	0	30	73.1
31	11	31.18	23

## Measurements @ 61.5 cm Run#2

hr	min	Time, hr	ppb
22	51	22.85	4.9
23	44	23.73	6.2
24	9	24.15	20.6
24	46	24.77	78.1
25	27	25.45	200
26	4	26.07	374
26	58	26.97	477.6
28	5	28.08	362.9
28	45	28.75	230

## Measurements @ 80 cm

hr	min	Time, hr	ppb
29	6	29.1	1.9
29	53	29.88	3.2
30	33	30.55	10
31	13	31.27	24.3
32	8	32.13	62.9
32	32	32.53	90.4
33	30	33.5	165.1
34	3	34.05	230
36	30	36.5	262.5
36	47	36.78	247

## Measurements @ 100 cm

hr	min	Time, hr	ppb
39	25	39.42	71.2
39	43	39.72	83.4
40	11	40.18	94.4
40	42	40.7	106.3
41	16	41.27	125.4
41	52	41.87	128
42	36	42.6	115.2
43	36	43.6	76.9
43	55	43.92	60.6
45	19	45.32	23.8
46	32	46.53	10
47	44	47.73	5

## Setup #2

Volume	1	ml
Conc.	9000	ppb
Mass	0.000000009	kg
Q, water	3.28122E-06	m <sup>3</sup> /s
Upstream height	0.64	m
Area	0.9344	m <sup>2</sup>
Porosity	0.38	

## @ 50 cm from the source

hr	min	s	Time, hrs	ppb
11	42	30	11.71	1.64
12	0	30	12.01	1.38
12	28	45	12.48	1.27
12	46	5	12.77	2.69
13	12	15	13.20	19.38
13	35	50	13.6	97.45
13	58	10	13.97	263.05
14	6	40	14.11	328.65
15	54	10	15.9	270.18
16	14	45	16.25	132.8
16	27	20	16.46	79.78
16	52	25	16.87	29.09
17	25	40	17.43	12.73

## @ 75 cm from the source

hr	min	s	Time, hr	ppb
20	14	40	20.24	1.13
20	32	45	20.55	3.64
20	45	50	20.77	8.12
21	3	20	21.06	16.47
21	32	30	21.55	44
21	49	30	21.8	94.62
22	15	45	22.26	197.35
22	39	30	22.66	304.51
23	4	40	23.08	344.91
23	25	5	23.42	318.36
23	47	10	23.78	261.13
24	2	40	24.04	186.37
24	23	45	24.4	130.91
24	55	30	24.95	70.07
25	17	20	25.29	30.43
25	30	50	25.52	20
26	0	20	26.01	10.91

## Line Source Experiments

At Level "0"

Width	1.46	m
Height	0.475	m
Area	0.6935	m <sup>2</sup>
Porosity	0.38	
Darcy Vel.	2.29017E-06	m/s
Seepage Vel.	6.03E-06	m/s
Area	0.000176715	m <sup>2</sup>
Conc.	2000	ppb

Run # 1

Measurements @ 1.17 m from source

 $R^2=0.935$ 

hr	min	Time, hr	ppb, centre	R	L
46	40	46.67	0	0	0
48	0	48	0	0	0
50	6	50.1	20	0.4	0.1
51	6	51.1	67	1.1	0.5
52	45	52.75	164.4	4	2.1
53	26	53.43	168.1	4.2	2.4
54	46	54.77	114.4	3.1	1.7
55	36	55.6	56.2	2	0.9
57	11	57.18	15.3	0.3	0.3
58	45	58.75	4.2	0.1	0

Run # 2

hr	min	Time, hr	ppb, centre	R	L
48	29	48.48	0		
49	32	49.53	5		
50	31	50.52	15	0.6	
51	44	51.73	71.8	2.2	0.8
52	46	52.77	155.3	3.8	1.7
54	8	54.13	171.1	4.4	2.5
55	8	55.13	121.3	3.3	1.9
56	18	56.3	56.7	1.2	0.9
57	15	57.25	26.2	0.5	
58	0	58.0	15.3	0.3	

At Level "-1"

Run#1

$R^2=0.95$

hr	min	Time, hrs	ppb @ centre	ppb, R
48	29	48.48	2	0
49	32	49.53	12	0
50	31	50.517	35.5	2
51	44	51.73	81.3	6
52	30	52.5	117.6	10
54	8	54.13	128.5	13.7
55	8	55.13	99.3	12.5
56	18	56.3	59.3	9
57	15	57.25	30.2	5
58	0	58	18	3

Run# 2

hr	min	Time, hrs	ppb @ centre	ppb, R
48	15	48.25	3.6	0
50	30	50.5	44.8	1
51	31	51.517	87.4	4.3
52	40	52.67	135.5	10.5
53	41	53.68	141.8	13.8
54	42	54.7	110.1	12.8
55	50	55.83	69.5	9.6
57	11	57.18	24.1	4.6
58	45	58.75	7.9	1.7

## Sieve Analysis on Gravel

#1

Hole size	Sample	% Passing
15	0	100
12.7	0	100
9.51	1762	69.6
6.3	600	23.7
4.76	150	5.9
2.38	20	0.8
Total	2532	

#2

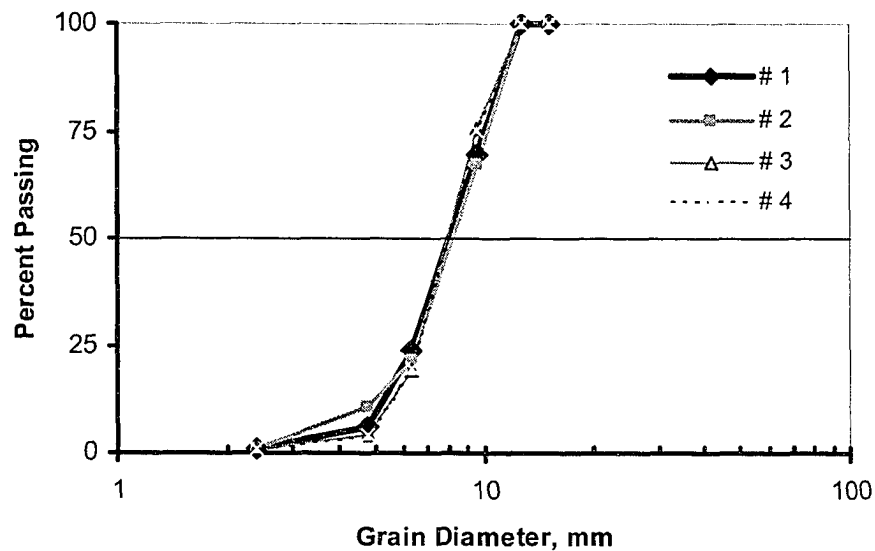
Hole size	Sample	% Passing
15	0	100
12.7	0	100
9.51	1420	67.17
6.3	450	21.3
4.76	229	10.8
2.38	15	0.71
Total	2114	

#3

Hole size	Sample	% Passing
15	0	100
12.7	0	100
9.51	1670	75.91
6.3	420	19.1
4.76	90	4.1
2.38	20	0.91
Total	2200	

#4

Hole size	Sample	% Passing
15	0	100
12.7	0	100
9.51	1762	69.6
6.3	600	23.7
4.76	150	5.9
2.38	20	0.79
Total	1921	



Average grain size,  $d_{50} = 8.15$  mm.

Std = 0.141.

## Gravel Porosity

Total Volume, L	20
-----------------	----

Volume of water, L	Porosity
7.64	0.382
7.45	0.372
7.4	0.3696
7.78	0.389
7.7	0.385
7.78	0.389

Average porosity	0.3811
Std	0.008437

### Hydraulic Conductivity measurements of the gravel.

Height	0.55	m
width	1.45	m
Area	0.7975	m <sup>2</sup>
Length	2.35	M
d-grain	0.00815	m
$\mu$ -water	0.001	Pa.s
$\rho$ -water	1000	kg/m <sup>3</sup>

Volume, m <sup>3</sup>	Average time, s	Std	V-Darcy, m/hr	Re	Average head difference, m	Std	dh/dx
0.004	35.375	0.52	0.510429	1.06	0.001175	0.046	0.0005
0.004	40.6	0.55	0.44474	0.93	0.00103	0.027	0.000438
0.004	57	0.5	0.316779	0.66	0.000751	0.04	0.00032
0.004	79.4	0.55	0.227411	0.47	0.000545	0.014	0.000232
0.004	99	-	0.182388	0.38	0.000417	0.026	0.000177
0.004	100	-	0.180564	0.38	0.00042	-	0.000179

## Gravel Dispersivity Measurements.

### Point Source Experiments

#### Run #1

Co, ppb	9,000.0
Volume injected, m3	1.00E-06
Porosity	0.38
Width	1.45
Depth	0.54
Area	0.783

Volume-water, m3	4.00E-03
Time, s	100
V-Darcy, m/s	5.11E-05
V-Average, m/s	1.345E-04

#### Measurements @ 75 cm of the injection point

Time			Time, min.	ppb @ 75 cm of the injection point
hr	min	sec		
0	36	5	36.08	0
0	45	10	45.17	0.1124
0	55	10	55.167	1.296
1	5	9	65.15	5.696
1	15	0	75	11.96
1	20	50	80.8	14.288
1	29	50	89.83	15.856
1	36	42	96.7	13.276
1	46	0	106	8.984
1	56	50	116.8	4.608
2	8	0	128	2.0104
2	20	35	140.58	0.912
2	30	0	150	0.4696

## Measurements @ 125 cm of the injection point

Time, min	ppb
35.1	0
45.1	0.07
55	0.28
65	1.7
75.1	5.6
82.0	8.96
87.1	10.76
92.8	11.71
97.5	11.19
104.9	9.68
112.1	7.16
117.2	5.2
128.5	2.65
145.3	0.8

## Point Source Experiments

### Run #2

Measurements @ 75 cm of the injection point

Co	9.00E-03	kg/m <sup>3</sup>
Vo	1.00E-06	m <sup>3</sup>
Porosity	0.38	
Width	1.45	m
Depth	0.54	m
Area	0.783	m <sup>2</sup>

Volume-water	4.00E-03	m <sup>3</sup>
Time	103	s
V-Darcy	4.96E-05	m/s
V-Average	1.27E-04	m/s

Time			Time, min.	ppb @ 75 cm of the injection point
hr	min	sec		
0	35	5	35.08	0
0	45	5	45.08	0.0676
0	55	0	55	0.2784
1	5	0	65	1.6992
1	15	5	75.08	5.6424
1	21	59	81.98	8.9584
1	27	5	87.08	10.7584
1	32	50	92.83	11.7104
1	37	30	97.5	11.1944
1	44	53	104.88	9.6784
1	52	5	112.08	7.1624
1	57	10	117.167	5.2024
2	8	28	128.47	2.6512
2	25	20	145.33	0.7868

## **APPENDIX B**

### **Sand-Gravel Experiments**

**S-G-50, Run # 1 (included in thesis text)**

- 0.5 ml of 800,000 ppb uranine dye was mixed with 72.5 ml of pure water and injected in an injection well located 31 cm upgradient the gravel.
- Water flow rate = 0.00212 l/s.
- Water height in the upgradient reservoir= 58 cm. (p.s. the upgradient head boundary condition for all the scenarios was assumed 60 cm and the measured head difference were used for the downgradient BC).

Table B1 Concentration measurements 30 cm downgradient the gravel.

hr	min	Time, hr	-20	-10	-5	0	5	10	20
22	0	22.0	0.3	0.25	0.02	0.11	0.4	0.2	0.2
23	0	23.0	0.7	0.89	0.3	0.68	0.8	0.3	0.3
24	21	24.35	1.6	6.2	5.2	7.6	1.8	0.4	0.4
25	32	25.53	2.2	22.1	24.9	26.7	5.9	0.6	0.5
26	21	26.35	2.3	35.7	47.3	46.8	11.1	1.4	0.7
27	40	27.67	2.0	45.0	77.3	68.6	19.3	4.6	1.2
29	10	29.17	1.3	43.0	83.2	75	27.3	8.7	2.3
30	33	30.55	0.9	32.4	74.0	69.8	25.8	7.3	2.2
31	31	31.52	0.6	22.0	60.4	58.1	18.5	4.5	1.3
33	21	33.35	0.4	9.0	32.0	25.6	6.2	1.8	0.5
35	0	35.0	0.3	2.0	13.8	10.6	2.0	0.7	0.3
36	0	36.0	0.3	1.0	7.8	5.7	0.9	0.3	0.3
37	0	37.0	0.2	0.5	3.8	3.0	0.3	0.2	0.2

Table B2 Head measurements.

Manometer	#2	#3	#4	#5	#6	#7
X-coordinate, cm (From upgradient reservoir)	0	35	60	107	157	230
Y -coordinate, cm (From the center)	55	55	55	0	0	55
Head, cm	60	59.0	58.3	56.8	56.7	54.4

**S-G-50, Run # 2**

- 0.5 ml of 800,000 ppb uranine dye was mixed with 75 ml of pure water and injected in an injection well located 31.5 cm upgradient the gravel.
- Water flow rate = 0.00218 l/s.

Table B3 Concentration measurements 31 cm downgradient the gravel.

hrs	min	Time, hrs	-20	-10	-5	0	5	10	20
23	45	23.75	0.4	0.2	0.2	1.2	0.6	1.4	7
24	57	25	0.6	0.5	1.1	6.3	5.3	6.6	7.2
25	58	26	0.5	1.1	3.7	20.3	18.6	10.7	3.7
26	57	27	0.4	1.2	9.3	43.3	40.4	17.2	1.6
28	5	28.1	0.5	3.1	18	66.7	64.4	27.2	1.1
29	0	29	0.8	5.2	20.7	71.7	68.7	32.2	1.4
30	57	31	0.7	5	14.3	48.3	38	18.6	1
32	10	32.2	0.5	2.5	7.8	29.2	17.9	7.9	0.5
33	1	33	0.4	1.2	5	17.7	9.2	3.8	0.3

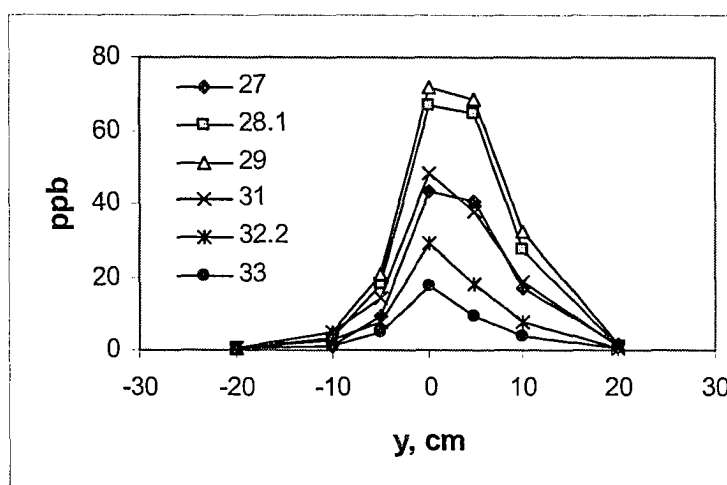


Fig. B1 Measured solute concentration at measuring points for the 50 cm sand-gravel system.

Table B4 Head measurements.

Manometer	#2	#3	#5	#6	#7
X-coordinate, cm (From upgradient reservoir)	0	34	108	157	203
Y-coordinate, cm (From the center)	50	50	0	0	50
Head, cm	60	59	56.2	56.1	53.3

**S-G-30, Run # 1 (included in thesis text)**

- 0.5 ml of 800,000 ppb uranine dye was mixed with 72.5 ml of pure water and injected in an injection well located 31 cm upgradient the gravel.
- Water flow rate = 0.0017 l/s.
- Water height in the upgradient reservoir= 52.5 cm.

Table B5 Concentration measurements 31 cm downgradient the gravel.

hr	min	Time, hrs	-35	-25	-20	-10	-5	0	5	10	20	25	35
25	32	25.53	0.4	0.3	1.1	0.3	0.2	0.2	0.1	0.5	1.6	0.2	0.1
26	49	26.82	0.1	0.2	0.2	0.3	0.21	0.2	0.5	3.3	11.2	1	0.1
28	10	28.17	0.1	0.7	0.5	0.6	0.2	0.3	1	8.1	26.5	5.1	0.1
29	41	29.68	0.2	8.2	8.6	6	0.5	0.6	1.1	7.5	26.2	12.1	0.1
31	37	31.62	0.2	42.9	54.2	38.7	6.7	1.1	0.6	2.5	10.8	11.3	0.2
33	2	33.03	0.1	59.9	78.5	64	16.8	1.9	0.4	1	3.5	5.7	0.2
34	30	34.5	0.2	40.7	57.7	55	25.3	2	0.2	0.4	1.2	2.2	0.1
36	38	36.63	1.3	10	15.1	18.6	16.6	1.2	0.1	0.2	0.4	0.5	0.1

Table B6 Head measurements.

Manometer	#2	#3	#4	#5	#6	#7
X-coordinate, cm (From upgradient reservoir)	0	30	65	107	157	230
Y -coordinate, cm (From the center)	57	57	57	0	0	57
Head, cm	60	59.3	58.4	57.3	57.2	54.9

**S-G-30, Run # 2**

- 0.5 ml of 800,000 ppb uranine dye was mixed with 72.5 ml of pure water and injected in an injection well located 30 cm upgradient the gravel.
- Water flow rate = 0.00173 l/s.

Table B7 Concentration measurements 32 cm downgradient the gravel.

hrs	min	Time, hrs	-35	-25	-20	-10	-5	0	5	10	20	25	35
25	33	25.6	0.4	20	1.5	0.7	0.2	0.2	0.1	0	0	0	0.1
27	20	27.3	0.1	36	17.7	16.7	0.4	0.2	0.5	0	0	0	0.1
30	18	30.3	0.1	86.6	106.8	86.4	18	6.1	0.7	0.2	0.2	0.2	0.1
32	57	33	1.5	48.6	54.3	102	54.4	8.2	0.3	0.1	0.1	0.2	0.1
34	43	34.7	8.9	18.2	23.5	55	45	2.6	0.1	0.1	0.1	0.1	0.2
35	50	35.8	11	10	12	25	24	1.6	0.1	0.1	0.1	0.1	0.2

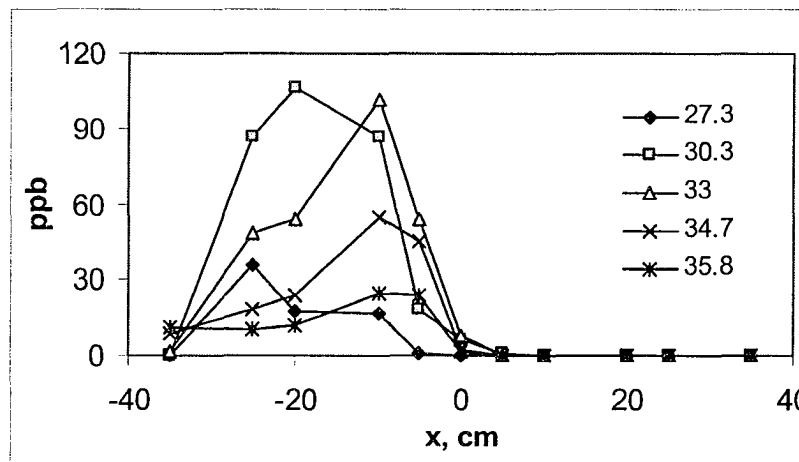


Fig. B2 Measured solute concentration at measuring points for the 30 cm sand-gravel system.

### Measurements in the gravel, the 30 cm scenario

#### 1 ml samples

Table B8 Measurements at the entrance of the gravel

hrs	min	Time, hrs	-10	-5	0	5	10
7	57	7.95	0	0	0.2	0.2	0.1
9	00	9	0	0	1.2	0.1	0.1
9	58	9.95	0.1	0.1	90.3	0.1	0
10	58	10.95	0.7	0.7	349	3.6	0
11	55	11.92	0.2	0.2	271.1	32.2	0
12	21	12.35	0.1	0.2	170.3	49.3	0.2
12	47	12.78				45.6	

Table B9 Measurements at the mid of the gravel

hrs	min	Time, hrs	-15	-7.5	0	7.5	15
12	55	12.92	0.8	42.2		11.4	2.8
13	21	13.35	1.1	50		20.7	3.9
13	47	13.78	5.6	62.1		33.1	6.4

Table B10 Measurements at the end of the gravel

hrs	min	Time, hrs	-15	-7.5	0	7.5	15
15	47	15.78	0.6	2.6	6.2	21	2
16	45	16.75	1	3.5	6.3	28.5	2
17	43	17.72	2.4	6.7	5.3	17.1	1.6
18	24	18.4	6.4	9.9	4.2	8.7	1.2
19	24	19.4	14.4	16	3.1	2.6	0.6
20	35	20.6	24.7	21.4	3.2	1.1	1.2
21	31	21.5	22.5	24.2	3.8	0.4	0.3
22	55	22.92	13.3	20.6	3.5	0.3	0.2

**S-G-20, Run # 1 (included in thesis text)**

- 0.5 ml of 800,000 ppb uranine dye was mixed with 72.5 ml of pure water and injected in an injection well located 29 cm upgradient the gravel.
- Water flow rate = 0.00183 l/s.
- Water height in the upgradient reservoir= 50 cm.

Table B11 Concentration measurements 29 cm downgradient the gravel.

hr	min.	Time, hrs	-20	-10	-5	0	5	10	20
15	50	15.83	0.2	0.3	1	0.4	0.2	0.2	0.2
16	54	16.9	0.5	0.5	1	0.7	0.3	0.2	0.3
17	54	17.9	0.5	1	2	0.8	0.4	0.4	0.3
18	54	18.9	0.7	2.9	2.9	1	0.6	0.9	0.3
20	28	20.47	2.8	7.4	12.4	6	2.9	5	0.5
22	0	22	4.7	15.7	31.7	38.4	38.3	80.5	1.6
23	24	23.4	6.1	20.6	44.8	73	89.1	103.7	14.3
24	49	24.82	5	21.1	37.2	63.3	81.1	58.8	34.1
26	8	26.13	3.3	17.6	19.9	33.3	43	23	33.1
27	11	27.18	1.5	9.4	9.3	15.1	20.4	9.4	21.1
28	30	28.5	0.9	3.3	4	4	10	3	10
29	28	29.5	0.5	1.2	2	1	6	1	4
30	33	30.5	0.3	0.6	0.7	0.5	3	0.5	1
31	31	31.5	0.2	0.3					
32	0	32	0.2	0.3					

Table B12 Head measurements.

Manometer	#2	#3	#4	#5	#6	#7
X-coordinate, cm (From upgradient reservoir)	0	40	62	107	157	230
Y -coordinate, cm (From the center)	57	57	57	0	0	57
Head, cm	60	58.9	58.3	56.9	56.7	54.5

**S-G-20, Run # 2**

- 0.5 ml of 800,000 ppb uranine dye was mixed with 70 ml of pure water and injected in an injection well located 30 cm upgradient the gravel.

Table B13 Concentration measurements 30 cm downgradient the gravel.

hrs	min	Time, hrs	-20	-10	-5	0	5	10	20
19	2	19	2.9	2.9	2.9	5	1.1	1.1	0.5
20	12	20.2	9.2	7.4	12.4	31	7.3	0.4	0.3
21	28	21.5	10	15.7	31.7	80	58.6	3.8	0.5
22	39	22.7	12	20.6	44.8	83.9	122	35	4.1
24	12	24.2	15	21.1	37.2	41.2	95.5	109.5	23.5
25	43	25.7	7	17.6	19.9	12.4	31.6	90	33.7
27	12	27.2	3	9.4	9.3	3.4	8.2	32.5	17.1
29	36	29.6	1.1	2	3	1	1.5	3.8	2.9

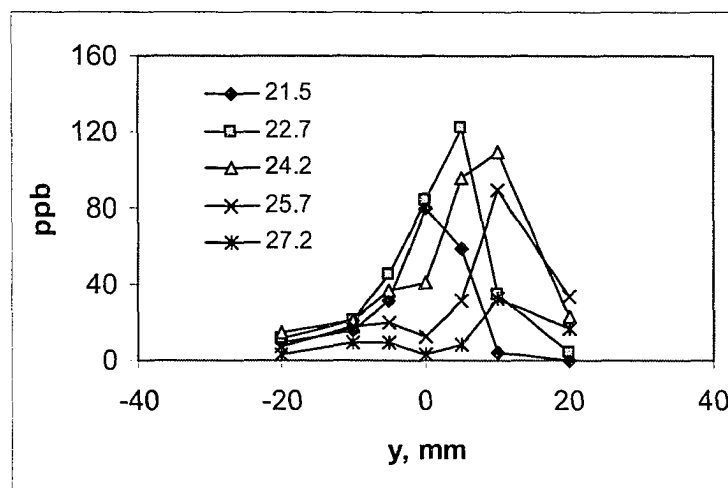


Fig. B3 Measured solute concentration at measuring points for the 20 cm sand-gravel system.

**S-G-15, Run # 1 (included in thesis text)**

- 0.5 ml of 800,000 ppb uranine dye was mixed with 72.5 ml of pure water and injected in an injection well located 30 cm upgradient the gravel.
- Water flow rate = 0.0023 l/s.
- Water height in the upgradient reservoir= 55 cm.

Table B14 Concentration measurements 30 cm downgradient the gravel.

hr	min	Time, hr	-20	-10	-5	0	5	10	20
16	0	16	0.3	1.2	1.5	0.5	0.7	0.5	0.2
17	7	17.12	0.7	12.2	29.8	9.5	9.9	1.1	0.3
18	36	18.6	0.6	44.8	74.8	57.5	42.5	11.2	0.4
19	42	19.7	1.2	63.8	87.5	85.9	52.3	24.5	0.9
20	52	20.867	3.8	47.8	54.1	63.5	27.3	18.6	2.4
21	57	21.95	5.9	22	21.7	27.3	9.2	7	4.1
22	58	22.97	5.6	4.6	4.2	8.9	2.9	2	2.6
24	35	24.58	2.4	1	2	2	1.1	0.8	1

Table B15 Head measurements.

Manometer	#2	#3	#4	#5	#6	#7
X-coordinate, cm (From upgradient reservoir)	0	28	60	107	157	230
Y -coordinate, cm (From the center)	56	56	56	0	0	56
Head, cm	60	59.2	58.3	56.3	56.2	53.5

**S-G-15, Run # 2**

- 0.5 ml of 800,000 ppb uranine dye was mixed with 72.5 ml of pure water and injected in an injection well located 30 cm upgradient the gravel.
- Water flow rate = 0.0022 l/s.

Table B16 Concentration measurements 30 cm downgradient the gravel.

hrs	min	Time	-20	-10	-5	0	5	10	20
16	18	16.3	0.4	0.8	0.5	0.4	0.7	0.4	0.3
17	55	17.9	4.1	4.5	0.7	1.2	1.1	2.8	0.3
18	52	18.9	7.6	26.5	5.9	8.2	6.2	6.5	0.3
19	58	20	11.5	62.8	27	30	21.7	19.5	0.4
21	20	21.3	17.5	90.8	67.2	63.1	43.1	16	1.2
22	30	22.5	16.7	70.9	81.9	56.8	35	7.2	1.6
23	33	23.5	9.3	28.3	55	32.7	18.5	2.8	1.6
24	31	24.5	4.5	11.2	28	16.3	9.3	1.4	0.7

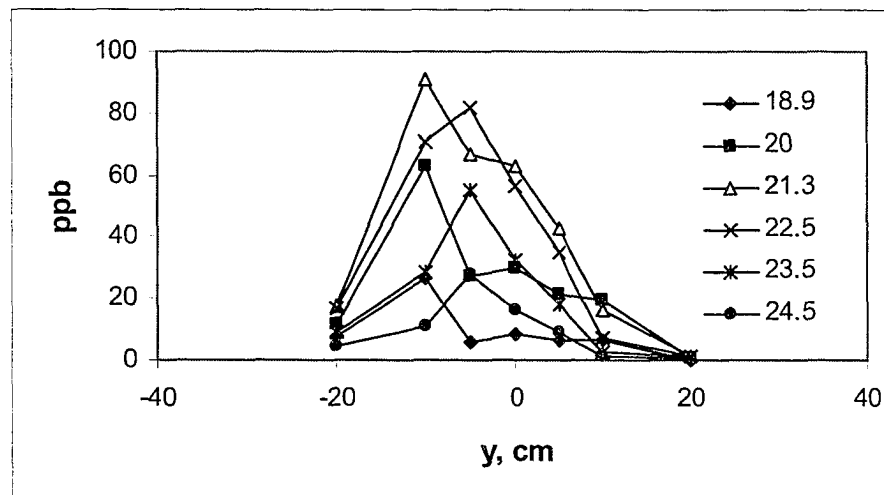


Fig. B4 Measured solute concentration at measuring points for the 15 cm sand-gravel system.

**S-G-15, Run # 3**

- 0.5 ml of 800,000 ppb uranine dye was mixed with 71.5 ml of pure water and injected in an injection well located 29 cm upgradient the gravel.
- Water flow rate = 0.002 l/s.

Table B17 Concentration measurements 30.5 cm downgradient the gravel.

hrs	min	Time, hrs	-20	-10	-5	0	5	10	20
15	14	15.2	0.6	1.2	1.2	0.8	0.7	0.5	0.2
16	52	16.9	0.5	0.9	1.6	8.2	7.4	1.3	0.3
17	54	17.9	0.5	5.8	15.1	34.1	23.6	4.7	0.4
19	22	19.4	1.5	46.7	71	72.9	37.1	15.2	0.9
20	36	20.6	6.3	75.2	88.1	52	20.7	13.5	1.1
21	49	21.8	10.8	53.8	48.4	19.8	6.7	5.3	1.6
22	55	22.9	9.7	21.9	17.3	6.2	2.3	1.7	1.3
24	25	24.4	3.5	4.1	3.3	1.5	1.5	0.8	1

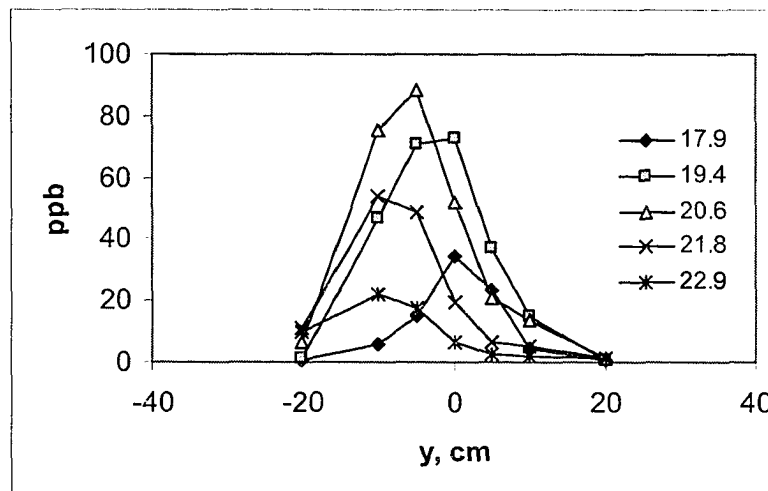


Fig. B5 Measured solute concentration at measuring points for the 15 cm sand-gravel system.

**S-G-10, Run # 1 (included in thesis text)**

- 0.5 ml of 800,000 ppb uranine dye was mixed with 75 ml of pure water and injected in an injection well located 29 cm upgradient the gravel.
- Water flow rate = 0.002 l/s.
- Water height in the upgradient reservoir= 51 cm.

Table B18 Concentration measurements 30 cm downgradient the gravel.

hr	min	Time, hrs	-20	-10	-5	0	5	10	20
16	50	16.83	0.4	0.7	1.2	1.1	1.2	1	0.3
17	58	17.97	0.4	1.2	2.3	2.4	3.9	1.2	0.3
19	48	19.8	0.4	11.4	27.5	28.6	39.9	25.5	0.3
21	23	21.38	0.8	23.6	53	61.1	68.3	55.5	1.2
22	55	22.92	2.8	20	37.8	48.8	46.5	42.4	10.8
24	42	24.7	4.1	6.2	11.2	16.1	15.6	14.8	26.9
25	45	25.75	3.3	2.4	4.2	6.4	6.5	6.5	26.9
26	30	26.5	2	0.4	0.4	0.5	2	1.5	23

Table B19 Head measurements.

Manometer	#2	#3	#4	#5	#6	#7
X-coordinate, cm (From upgradient reservoir)	0	30	80	107	157	230
Y -coordinate, cm (From the center)	56	56	56	0	0	56
Head, cm	60	59.2	57.9	56.9	56.8	54.5

**S-G-10, Run# 2**

- 0.5 ml of 800,000 ppb uranine dye was mixed with 71 ml of pure water and injected in an injection well located 30 cm upgradient the gravel.
- Water flow rate = 0.0019 l/s.

Table B20 Concentration measurements 30 cm downgradient the gravel.

hrs	min	time	-20	-10	-5	0	5	10	20
16	3	16	0.8	1.3	1.3	4.1	1.5	1.4	
17	32	17.5	0.5	11.3	10.3	53.3	6.8	1.7	0.4
19	8	19.1	0.3	38.4	56.4	73.8	61.6	33.9	0.2
20	39	20.6	4.7	35	54.9	33.9	61.9	58.5	0.4
21	57	22	16.9	16.4	24.2	9	27.8	34.7	0.3
23	55	24	18.7	2.4	3.4	1.4	3.9	5.5	3.2
24	52	24.9	4.6	1.5	1	1	1	3	22.9
25	41	25.7	1.5	.25	.5	1	.6	1	29

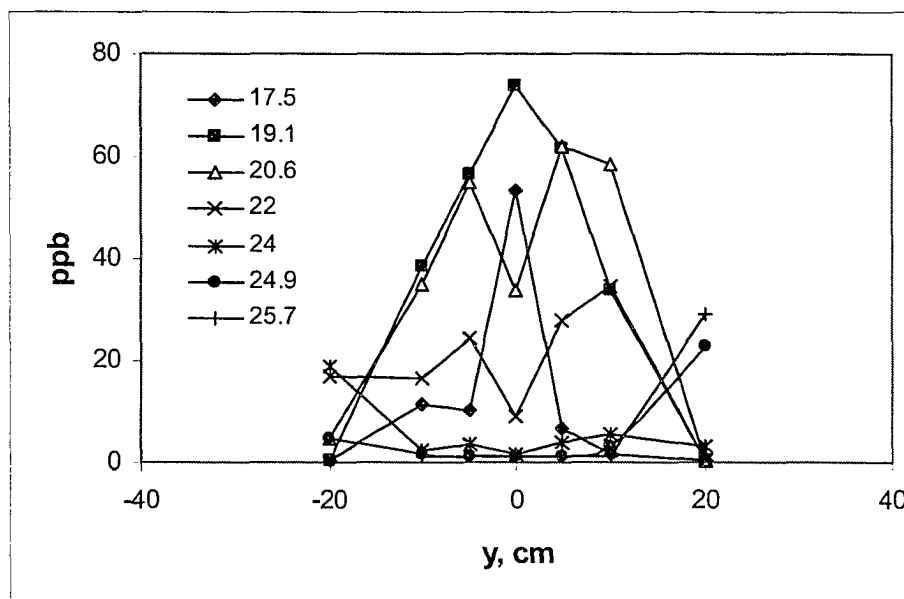


Fig. B6 Measured solute concentration at measuring points for the 10 cm sand-gravel system.

**S-G-10, Run # 3**

- 0.5 ml of 800,000 ppb uranine dye was mixed with 75 ml of pure water and injected in an injection well located 29 cm upgradient the gravel.
- Water flow rate = 0.002 l/s.
- Water height in the upgradient reservoir= 51 cm.

Table B21 Concentration measurements 30 cm downgradient the gravel.

hrs	min	Time, hrs	-20	-10	-5	0	5	10	20
13	40	13.7	0.6	0.4	0.5	0.5	0.5	0.5	1
16	18	16.3	0.5	0.5	0.5	1.2	0.5	0.4	0.4
17	38	17.6	0.4	3	2.7	22.9	1.5	0	0.5
19	32	19.5	1.1	23.5	33.2	57.4	35.2	17.4	0.6
21	12	21.2	13	32	37.8	32	45	41.7	0.5
22	39	22.7	19.7	17.8	20.1	10.7	27.4	33	1
23	43	23.7	14	4	5	7	5	10	6

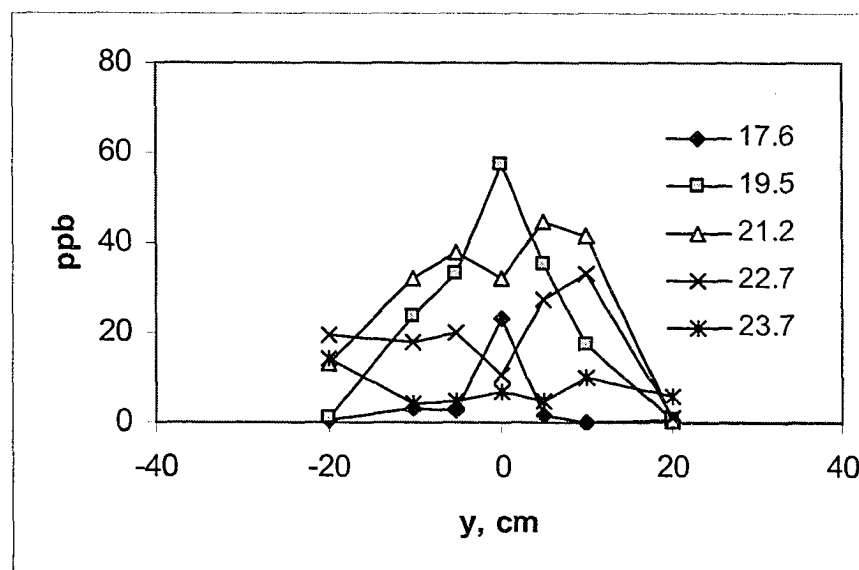


Fig. B7 Measured solute concentration at measuring points for the 10 cm sand-gravel system.

**S-G-5, Run # 1 (included in thesis text)**

- 0.5 ml of 800,000 ppb uranine dye was mixed with 72.5 ml of pure water and injected in an injection well located 29 cm upgradient the gravel.
- Water flow rate = 0.0017 l/s.
- Water height in the upgradient reservoir= 51 cm.

Table B21 Concentration measurements 29 cm downgradient the gravel.

hr	min	Time, hrs	-20	-10	-5	0	5	10	20
16	18	16.3	0.3	0.4	0.7	1.0	1.2	0.8	1.1
17	25	17.42	0.4	4.1	10.9	14.5	13.6	0.5	0.4
18	40	18.67	0.4	33.6	50.3	60	55	8.1	0.4
20	9	20.15	0.4	53.8	47.5	45.7	51	56.8	0.3
21	47	21.78	4.4	20	10.4	8.6	12.6	56.4	0.4
22	40	22.67	13	4.9	3.2	2.5	4.1	29.5	0.4
24	2	24.03	26.8	1.1	1.0	1.0	1.2	6.9	5.2
14	6	25.1	29.3	0.2	0.1	0.1	0.1	0.1	22.2
16	13	26.22	23.6	0.1	0.1	0.1	0.1	0.1	49.7

Table B22 Head measurements.

Manometer	#2	#3	#4	#5	#6	#7
X-coordinate, cm (From upgradient reservoir)	0	28	80	107	157	230
Y -coordinate, cm (From the center)	56	56	56	0	0	56
Head, cm	60	59.3	58.5	57.0	56.8	54.6

**S-G-5, Run # 2**

- 0.5 ml of 800,000 ppb uranine dye was mixed with 71 ml of pure water and injected in an injection well located 30 cm upgradient the gravel.
- Water flow rate = 0.0018 l/s.

Table B23 Concentration measurements 30.5 cm downgradient the gravel.

hrs	min	Time, hrs	-20	-10	-5	0	5	10	20
12	10	12.2	0.6	0.6	0.3	0.3	0.9	0.4	0.6
14	27	14.5	0.4	0.3	0.3	0.3	0.3	0.4	0.4
15	35	15.6	0.3	0.3	0.3	0.3	0.3	0.3	0.5
17	28	17.5	0.2	3.2	13	14.8	8.4	0.3	0.2
18	36	18.6	0.2	29.2	52.4	62.5	49	2.1	0.4
20	25	20.4	0.4	60.9	49.2	47.1	59.6	48.3	0.3
21	25	21.4	1	32.6	20.2	16.2	29.1	73	0.4
22	36	22.6	4.5	9.4	5.1	3.5	8.7	52.4	0.2
24	3	24.1	20.3	1.9	1.2	0.9	1.7	13.7	1.4
24	55	24.9	31.8	0.5	0.1	0.2	0.5	2	8
26	3	26	20	0.2	0.1	0.2	0.5	1	20

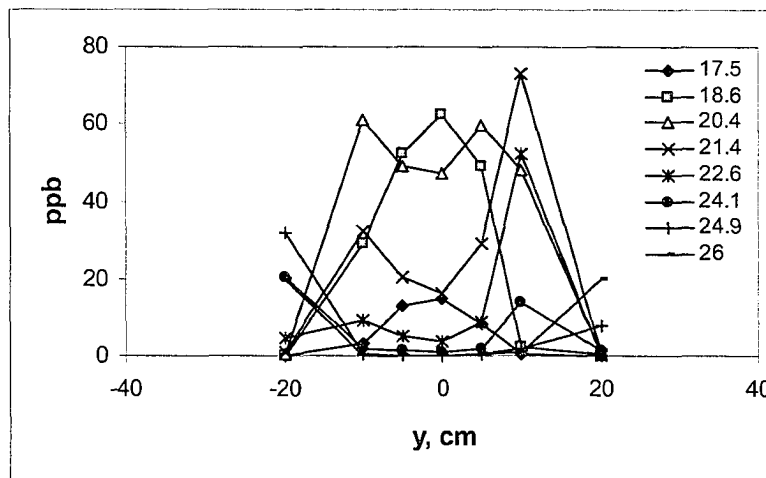


Fig. B8 Measured solute concentration at measuring points for the 5 cm sand-gravel system.

Table B24 Head measurements.

Manometer	#2	#3	#4	#5	#6	#7
X-coordinate, cm (From upgradient reservoir)	0	30	75	107	157	230
Y -coordinate, cm (From the center)	56	56	56	0	0	56
Head, cm	60	59.3	58.2	56.9	56.7	54.6

## REFERENCES

Abdelouas, A., Lutze, W. and Nuttal, H. 1999, Uranium contamination in the subsurface: characterization and remediation, in Uranium: mineralogy, geochemistry and the environment, edited by Burns, P. and Finch, R., Reviews in Mineralogy, V. 38, pp.433-473.

Anderson, T.B. and Hackson, R. 1967, A fluid mechanical description of fluidized beds, Ind. Eng. Chem. Fundam. V. 6, pp. 527-538.

Bachmat, Y. and Bear, J. 1986, Macroscopic modeling of transport phenomena in porous media. 1: The continuum approach, Transport in Porous Media, v. 1, pp. 213-240.

Baetsle, L.H., 1969, Migration of radionuclides in porous media, Progress in nuclear energy series XII, health physics, A.M.F. Duhamel, ed., Pergamon Press, Elmsford, NY, pp. 707-730.

Baveye, P. and Sposito, G. 1984, The operational significance of the continuum hypothesis in the theory of water movement through soils and aquifers, Water Resources Research, v. 20, No. 5, pp. 521-530.

Bear, J. 1972, Dynamics of Fluids in Porous Media, Elsevier, Amsterdam.

Bear, J., 2002, Personal communications.

Beavers, G.S., and Joseph, D.D. 1967, J. Fluid Mech., v. 30, pp. 197.

Benenati, R.F., and Brosilow, C.B., 1962, AIChE J. v. 8, No. 3, pp. 359-361.

Cameco Corporation, 1994, Key Lake Operation-Deillmann In-Pit Tailings Management Facility, Environmental Impact Statement, February.

Cameco, 1998, Review of Hydrology in the Vicinity of the Rabbit Lake In-Pit TMF, March.

Chattot, J-J, 2002, Computational aerodynamics and fluid dynamics: an Introduction, Springer.

Cogema Resources Inc., 1997, McClean Lake Project JEP Tailings Management Facility, December.

Carbonell, R.G. and Whitaker, S., 1984, Heat and mass transfer in porous media. In Fundamentals of transport phenomena in porous media (edited by J. Bear and M.Y. Corapcioglu), pp. 123-198. Martinus Nijhoff, Dordrecht, The Netherland.

Cioranescu, D., Donato, P., and Cioraneascu, D. 2000, An Introduction to Homogenization, Oxford University Press.

Courant, R., Friedrichs, O., and Lewy, H., 1967, On the partial difference equations of mathematical physics, *IBM Journal*, 11, pp. 215-234.

Cushman, J.H. 1982, Proofs of the volume averaging theorems for multiphase flow, *Advances in water resources*, v. 5, pp. 248-253.

Cushman, J.H. 1983, Multiphase transport equations I: General equation for macroscopic local space-time homogeneity, *Trans. Theory and Stat Physics* 12, 35-71.

Cushman, J.H. 1984, On unifying concepts of scale, instrumentation, and stochastic in the development of multiphase transport theory, *Water Resour. Res.* 20, 1668-1672.

Cushman, J.H. and Ginn, T.R., 1993, Non-local dispersion in media with continuous evolving scales of heterogeneity, *Transport in Porous Media*, v. 13, pp. 123-138.

Dominique-Janine, 1993, McClean project, and Midwest joint venture, report of the joint federal-provincial panel on uranium mining developments in northern Saskatchewan, Regina.

Donahue R., (2000), *Geochemistry of Arsenic in Uranium Mill Tailings, Saskatchewan, Canada*, PhD. Thesis, University of Saskatchewan.

Donahue, R., Hendry, M.J., and Landine, P., 2000, Distribution of arsenic and Nickel in uranium mill tailings, Rabbit Lake, Saskatchewan, Canada, *Appl Geochem*, 15 (8), 1097-1119.

Eidsath, A.B. 1981, Flow and dispersion in spatially periodic porous media: A finite element study, MS Thesis, Department of Chemical Engineering, University of California at Davis.

Ergun, S., 1952, Fluid flow through packed columns, *Chemical Engineering Progress*, v. 48, No. 2, pp. 89-94.

Finch, R., and Murakami, T. 1999, Systematics and paragenesis of uranium minerals, in Uranium: mineralogy, geochemistry and the environment, edited by Burns, P. and Finch, R., Reviews in Mineralogy, V. 38, pp.91-179.

Freeze, A.R. and Cherry, J.A., 1979, Groundwater, Prentice Hall; 1 edition.  
Grathwohl, P., 1998, Diffusion in Natural Porous Media: Contaminant Transport, Sorption/Desorption and Dissolution Kinetics (Topics in Environmental Fluid Mechanics, 1), Kluwer Academic Publishers; 1st edition.

Gray, W.G., 1975, A derivation of the equations for multiphase transport, Chem. Engng. Sci. 30, 229-233.

Gray, W.G. and Lee, P.C.Y. 1977, On the theorems for local volume averaging of multiphase systems, Int. J. Multiphase Flow 3, 333-342.

Gray, W.G., 1982, Derivation of vertically averaged equations describing multiphase flow in porous media, Water Resources Research, v. 18, No. 6, pp. 1705-1712.

Gray, W.G., Leijnse, A., Kolar, R.L. and Blain, C.A. 1993, Mathematical Tools for Changing Spatial Scales in the Analysis of Physical Systems, CRC Press, Boca Raton, Florida.

Gulf Minerals, 1981, Environmental Impact Statement Collins Bay B-Zone Development, Second Addendum.

Haber, S., and Mauri, R., 1983, Boundary conditions for Darcy's flow through porous media, Int. J. Multiphase Flow, v. 9, pp. 561-574.

Hassanizadeh, M. and Gray, W., 1979, General conservation equations for multiphase systems: 1. Averaging procedure, Advances in water resources, v.2, pp. 131-144.

Hassanizadeh, M. and Gray, W., 1979, General conservation equations for multiphase systems: 2. Mass, momenta, energy, and entropy equations, Advances in water resources, v.2, pp. 191-203.

Hassanizadeh, M. and Gray, W., 1979, General conservation equations for multiphase systems: 3. Constitutive theory for porous media flow, Advances in water resources, v.3, pp. 25-40.

Hassanizadeh, M. and Gray, W., 1989 [a], Derivation of conditions describing transport across zones of reduced dynamics within multiphase systems, Water resources research, v. 25, No. 3, pp. 529-539.

Hassanizadeh, M. and Gray, W., 1989 [b], Boundary and interface conditions in porous media, *Water resources research*, v. 25, No. 7, pp. 1705-1715.

Hedstrom, G. 1975, Models of difference schemes for  $u_t + u_x = 0$  by partial differential equations, *Math. Comp.*, 29, pp. 969-977.

Hoagland, D.R., 1981, Application of the Method of Spatial Averaging to Fluid Flow in Nonuniform Porous Media, M.S. Thesis, Department of Chemical Engineering, University of California at Davis, 1981.

Hubbert, M. K., 1956, "Darcy's law and the field equations of the flow of underground fluids", *Petroleum Trans.*, AIME, v. 207, pp. 222-239.

Hornung, U. 1997, *Homogenization and Porous Media*, Springer-Verlag.

Idelchik, 2001, *Handbook of Hydraulic Resistance*, Begell House.

International Atomic Energy Agency booklet, 2000, *Climate Change and Nuclear Power*, IAEA/PI/A72E, 00-02779.

Inventory of Radioactive Waste in Canada, Low-Level Radioactive Waste Management Office, Ottawa, Canada, 1999.

IPCC Third Assessment Report, *Climate Change 2001: The Scientific Basis*, Cambridge University Press.

Jeulin, D., and Ostoja-Starzewski, M., Editors, 2001, *Mechanics of Random and Multiscale Microstructures*, CISM Courses and Lectures, Springer Wien.

Koch, D.L. and Brady, J.L., 1987, A non-local description of advection-diffusion with application to dispersion in porous media, *J. Fluid Mech.*, v. 180, pp. 387-403.

Lange, K., Van Geel, P.J., and Nguyen, T.S. 2003, Physical and Numerical Modelling of a Dual Porosity Fractured Rock Surrounding an In-Pit Uranium Tailings Management Facility, *Proceedings of the 56<sup>th</sup> CGS-IAH Conference*, Winnipeg, Sept. 28-Oct.1,2003.

Lautermilch, E., 2000, *Saskatchewan: New Mines for the New Millennium*, the Uranium Institute 25<sup>th</sup> Annual Symposium, London.

Lebedev, V.L. 1958, *Random Processes in Electrical and Mechanical Systems*, the state publishing house of physical and mathematical literature, Moscow.

Marle, C.M., 1982, On macroscopic equations governing multiphase flow with diffusion and chemical reactions in porous media, *Int. J. Engng. Sci.*, v. 20, No. 5, pp. 643-662.

Mehta, D., and Hawley, M.C., 1969, Wall effect in packed columns, *Industrial & Engineering Chemistry Progress Design and Development*, v. 8, No. 2, pp. 280-282.

Misfeldt, G.A., Loi, J.I., Herasymuik, G.M., and Clifton, A.W., 1999, Comparison of tailings containment strategies for in-pit and above ground tailings management facilities. *Proceedings of the 52<sup>nd</sup> Canadian Geotechnical Conference*, Oct. 25-27, Regina, Saskatchewan, pp 279-286.

Nield, D.A., and Bejan, A. 1992, *Convection in Porous Media*, Springer-Verlag, New York.

Nuclear Energy Agency, 2001, *Uranium 2001: Resources, production and demand*, A joint report by the OECD Nuclear Energy Agency and the IAEA.

Ochoa-Tapia, J.A., Stroeve, P. and Whitaker, S. 1995a, Momentum transfer at the boundary between a porous medium and a homogeneous fluid I: Theoretical development, *Int. J. Heat Mass Trans.* 38, 2635-2646.

Ochoa-Tapia, J.A and Whitaker, S. 1995b, Momentum transfer at the boundary between a porous medium and a homogeneous fluid II: Comparison with experiment, *Int. J. Heat Mass Trans.* 38, 2647-2655.

Ochoa-Tapia, J.A and Whitaker, S. 1998b, Momentum transfer at the boundary between a porous medium and a homogeneous fluid: Inertia effects, *J. porous Media* 1, 201-217.

Pitchler, T., Hendry, M.J., and Hall, G.E.M., 2001, The mineralogy of arsenic in uranium mine tailings at the Rabbit Lake In-pit Facility, northern Saskatchewan, Canada, *Environmental Geology*, 40, (4-5), 495-506.

Prat, M. 1989, On the boundary conditions at the macroscopic level, *Transport in Porous Media* 4, 259-280.

Prat, M. 1990, Modeling of heat transfer by conduction in a transition region between a porous medium and an external fluid, *Transport in Porous Media* 5, 71-95.

Prat, M. 1992, Some refinements concerning the boundary conditions at the macroscopic level, *Transport in Porous Media* 7, 147-161.

Propster, M. and Szekely, J., 1977, The porosity of systems consisting of layers of different particles, *Powder Technology*, v. 17, pp 123-138.

Quintard, M. and Whitaker, S., 1990a, Two-phase flow in heterogeneous porous media I: The influence of large spatial and temporal gradients, *Transport in Porous Media* 5, 341-379.

Quintard, M. and Whitaker, S., 1990b, Two-phase flow in heterogeneous porous media II: Numerical experiments for flow perpendicular to a stratified system, *Transport in Porous Media* 5, 429-472.

Quintard, M. and Whitaker, S., 1993a, Transport in ordered and disordered porous media: Volume averaged equations, closure problems, and comparison with experiment, *Chem. Engng. Sci.* 48, 2537-2564.

Quintard, M. and Whitaker, S., 1994a, Transport in ordered and disordered porous media I: The cellular average and the use of weighting functions, *Transport in Porous Media* 14, 163-177.

Quintard, M. and Whitaker, S., 1994b, Transport in ordered and disordered porous media II: Generalized volume averaging, *Transport in Porous Media* 14, 179-206.

Quintard, M. and Whitaker, S., 1994c, Transport in ordered and disordered porous media III: Closure and comparison between theory and experiment, *Transport in Porous Media* 15, 31-49.

Quintard, M. and Whitaker, S., 1994d, Transport in ordered and disordered porous media IV: Computer generated porous media, *Transport in Porous Media* 15, 51-70.

Quintard, M. and Whitaker, S., 1994e, Transport in ordered and disordered porous media V: Geometrical results for two-dimensional systems *Transport in Porous Media* 15, 183-196.

Reynolds, W. C. and Perkins, H. C., 1977. "Engineering Thermodynamics" 2<sup>nd</sup> ed. McGraw-Hill Book Company,

Richardson, S., 1971, A model for the boundary condition of a porous material. Part 2. *J. Fluid Mech.*, v. 49, 2, pp. 327-336.

Roblee, L., Baird, R. and Tierney, J., 1958, *AIChE*, v. 4, pp 460.

Scheidegger, A., 1974, *The physics of flow through porous media*, 3<sup>rd</sup> ed., University of Toronto Press.

Skagius, K., and Neretnieks, I., 1986, Porosities and diffusivities of some nonsorbing species in crystalline rocks. *Water Resources Research*, v. 22, No. 3, pp. 389-398.

Slattery, J.C., 1967, Flow of viscoelastic fluids through porous media, *AIChE Journal* 13, 1066-1071.

Smith, G.D., 1985, Numerical solution of partial differential equations: finite difference methods, *Oxford Applied Mathematics and Computing Science Series*, 3<sup>rd</sup> ed.

Somerton, C.W., and Catton, I., 1982, On the thermal instability of superposed porous and fluid layers, *Trans. ASME*, v. 104, pp. 160-165.

Strikwerda, J., 1989, Finite difference schemes and partial differential equations, *Wadsworth & Brooks/Cole Advanced Books & Software*.

Taylor, G.I., 1971, A model for the boundary condition of a porous material. Part 1. *J. Fluid Mech.*, v. 49, 2, pp. 319-326.

Therrien, R. and Sudicky, E.A., 1996, Three-dimensional analysis of variably-saturated flow and solute transport in discretely fractured porous media. *Journal of Contaminant Hydrology*, v. 23, pp. 1-44.

Toda, M., Kubo, R., and Saito, N., 1983, *Statistical Physics I: Equilibrium Statistical Mechanics* (Springer Series in Solid-State Sciences).

Total and Minatco Ltd, 1991, McClean Lake Project Environmental Impact Statement, Supporting Documents VI and VII, September.

Warming, R. and Hyett, 1974, the modified equation approach to the stability and accuracy analysis of finite-difference methods, *J. Comput. Phys.*, 14, pp. 159-179.

West A (2000), Physical and numerical modeling of an in-pit tailings management facility, M.Sc. thesis, Carleton University.

West, A., P.J. Van Geel, K. Raven, T.S. Nguyen, M.B. Belfadhel, and P. Flavelle (2003), Groundwater Flow and Solute Transport in a Laboratory Scale Analogue of a Decommissioned In-Pit Tailings Management Facility, *Canadian Geotechnical Journal*, 40(2), pp 326-341.

Wexler, E.J., 1992, Analytical solutions for one-, two-, and three-dimensional solute transport in ground-water systems with uniform flow: U.S. Geological Survey Techniques of Water-Resources Investigations, book 3, chap. B7, 190 p.

Whitaker, S., 1966, The equations of motion in porous media, Chemical engineering science, v. 21, pp. 291-300.

Whitaker, S., 1967, Diffusion and dispersion in porous media, AIChE Journal 13, 420-427.

Whitaker, S., 1969, Advances in the theory of fluid motion in porous media, Industrial and Engineering Chemistry Fundamentals, 14-28.

Whitaker, S., 1981, Introduction to Fluid Mechanics, R.E. Krieger Pub. Co., Malabar, Florida.

Whitaker, S., 1983, Fundamental Principles of Heat Transfer, R.E. Krieger Pub. Co., Malabar, Florida.

Whitaker, S., 1985, A Simple geometrical derivation of the spatial averaging theorem, Chem. Engr. Ed., 19, 18-21 and 50-52.

Whitaker, S., 1986, Flow in porous media I: A theoretical derivation of Darcy's law, Transport in Porous Media, 1, 3-25.

Whitaker, S., 1999, Method of Volume Averaging, 1<sup>st</sup> edition, Kluwer Boston, Inc.

Wilson, J.L., and Miller, P.J., 1978, Two-dimensional plume in uniform groundwater flow, J. Hydraul. Div. ASCE, v. 104, pp. 503-514.

World Energy Outlook 1998, International Energy Agency/OECD, Paris, 1998.

World information service on Energy, WISE Uranium Project: 2002, ([www.antenna.nl/wise/uranium/new02.html](http://www.antenna.nl/wise/uranium/new02.html)).

World Nuclear Association, World Nuclear Power Reactors 2003-05 and Uranium Requirements, January 2005, ([www.world-nuclear.org/](http://www.world-nuclear.org/)).

[www.uic.com.au/](http://www.uic.com.au/)

[www.gov.sk.ca/enermine/facts/semuran.htm](http://www.gov.sk.ca/enermine/facts/semuran.htm)

[www.nuclearsafety.gc.ca/eng/safety/pdf/0738\\_E1.pdf](http://www.nuclearsafety.gc.ca/eng/safety/pdf/0738_E1.pdf)

[http://www-pub.iaea.org/MTCD/publications/PDF/cnpp2003/CNPP\\_Webpage/PDF/2001/Documents/Documents/Canada%202001.pdf](http://www-pub.iaea.org/MTCD/publications/PDF/cnpp2003/CNPP_Webpage/PDF/2001/Documents/Documents/Canada%202001.pdf)